Droplet-Based Separation Tools for Multidimensional Biological Separations

Nuchutha Thamsumet

A thesis submitted in partial fulfilment of the requirement for the degree of Doctor of Philosophy

Department of Chemistry, Imperial College London

October 2015

Declaration of Originality

I hereby declare that this thesis is the product of my own work and to the best of my knowledge any parts contained in this thesis has not been submitted in any form for any other degree at any academic institution. Information derived from the published and unpublished work of others has been fully acknowledged in the text and references are given in the bibliography.

Nuchutha Thamsumet

Copyright Declaration

Abstract

Proteins have been extensively studied over the last decade as comprehensive understanding of the proteome can definitely lead to the discovery of novel biomarkers, early-stage disease diagnoses and the development of diagnostic tools and novel drug therapies. One of the crucial and fundamental processes in protein analysis is protein separation, which is usually performed as multidimensional separations to achieve high resolution and high peak capacity. However, high performance analyses are difficult to achieve due to the challenges involved in efficiently integrating different dimensions.

In this work, we present the development of a microfluidic device for the effective transfer of protein droplets into the second separation dimension. Consequently, the device provides a stable, reproducible, easy to operate, portable and flexible system to connect a first dimension separation to the downstream second dimension analysis via droplets. The droplets act to preserve the resolution during transfer between separation techniques.

In summary, a fluorescently labeled protein ladder serving as a representative of proteins separated from the first dimension is compartmentalized into droplets using the robotic droplet generator. These protein droplets are then transferred via the interfacing microdevice into the second dimension where the released proteins are further separated using capillary gel electrophoresis. Herein, several designs of interfacing microdevices were evaluated for the successful transfer of droplet contents (droplet injection) into the second dimension. The buffer for capillary gel electrophoresis was developed to achieve high-speed and high-resolution separations of proteins in droplet-based injection format. Several fluorescent dyes were also examined for protein labeling to achieve high fluorescent intensities necessary when using this droplet format. Successful droplet-based separation of proteins necessitates the seamless integration of all the developed components. This has been demonstrated here.

This interface automates the oil depletion process, minimizes dead volume, prevents dispersion of analyte bands and reduces sample loss at the interface between separation

dimensions. Furthermore, optimization of the entire system used in conjunction with the interfacing microdevice provided for ease of operation and more efficient droplet injections. Moreover, droplet injection into parallel separation channels was achieved, highlighting the interfaces capacity for high-throughput analyses.

Acknowledgements

I would like to gratefully thank many people for help and support throughout my study. Without these people this thesis would not be possible.

First of all, I would like to express my deepest gratitude to my supervisors Andrew deMello and John deMello for invaluable advice, encouragement and all the generous supports that both of you provided throughout this long journey of my study. It has been great opportunity to work with both of you.

I would also like to convey my sincere appreciation to Fiona Pereira for her expertise in capillary electrophoresis and for her time and devotion to closely support me all along during my project including reading through this thesis and to Xize Niu and his research group for beneficial ideas, wonderful advice and for all supports throughout this work.

Additionally, I would like to thank and acknowledge Tony Cass and Joshua Edel research groups for sharing the instruments and for all the kind support from people in the groups, especially for Sanjiv Sharma and Aleksandar Ivanov. I am also gratefully thank to Siva Krishnadasan, Adrian Nightingale, Thomas Phillips, James Bannock, Bruno Matarese, Steven Sim and members of John deMello research group for all help and wonderful supports that made my days at ICL meaningful, to Simon Berger for 3D printing, to Katherine Elvira, Xavier Casadevall I Solvas, Claire Stanley, Bartosz and Tomasz Koprowski, Jennifer Gassmann and members of Andrew deMello research group for advice, supports and accompanying me during visiting ETH.

Special thanks to Sirirat Panich and all of my friends in the UK for the support and friendship. I really had a good time in the UK with all of you guys.

I also gratefully acknowledge The Royal Thai Government for the financial support throughout my PhD study.

Finally, I am indebted for my beloved family for their endless love, support and encouragement. I am also very thankful to Yotsawat Pomyen for love, understanding and taking good care of me.

Table of Contents

List of Abbreviations

2D	Two Dimensional
3D	Three Dimensional
5/6-TAMRA, SE	5/6-Carboxytetramethylrhodamine, Succinimidyl ester
ABS	Acrylonitrile Butadiene Styrene
AMPD	2-Amino-2-methyl-1, 3-propanediol
APS	Ammonium peroxydisulfate
B	Buffer
BHT	Butylated hydroxytoluene
BME	β-mercaptoethanol
BSA	Bovine Serum Albumin
BW	Buffer Waste
CA	Carbonic Anhydrase
CACO	Cacodylic acid
CAD	Computer Aided Design
CCD	Charge-Coupled Device
CCK	Cholecystikinin flanking peptide
CE	Capillary Electrophoresis
CEC	Capillary Electrochromatography
CGE	Capillary Gel Electrophoresis
CHES	2-(Cyclohexylamino) ethanesulfonic acid
cIEF	Capillary Isoelectric Focusing
cITP	Capillary Isotachophoresis
CMC	Critical Micelle Concentration
CO	Concanavalin A
Cy3	Indocarbocyanine
Cy5	Indodicarbocyanine
CZE	Capillary Zone Electrophoresis
Da	Dalton
DI	Deionised Water
DIGE	Differential Gel Electrophoresis

DMSO	Dimethyl sulfoxide
DNA	Dioxyribonucleic acid
EOF	Electroosmotic Flow
ESI	Electrospray Ionization
F/P	Fluorophore/Protein
FC	Fluorescamine
FCS	Fetal Calf Serum
FITC	Fluorescein isothiocyanate
Fluorescein-MAL	Fluorescein-5-maleimide
FSCE	Free Solution Capillary Electrophoresis
GEMBE	Gradient Elution Moving Boundary Electrophoresis
GFP	Green Fluorescent Protein
GPC	Gel Permeation Chromatography
GST	General Separation Transform
HPA	*Helix Pomatia* Lectin
HPCE	High Performance Capillary Electrophoresis
HPFA+	High Purity Perfluoroalkoxy Plus
HPLC	High-Performance Liquid Chromatography
HSA	Human Serum Albumin
Hz	Hertz
I.D.	Inner Diameter
IDP	Indistinguishable Peaks
IEF	Isoelectric Focusing
IgG	Immunoglobulin G
IPG	Immobilized pH Gradient
LC	Liquid Chromatography
LE	Leading Electrolyte
LOC	Lab-on-a-chip
LPA	Linear Polyacrylamide
MALDI	Matrix-Assisted Laser Desorption/Ionization
MCE	Microchip Capillary Electrophoresis
MEEKC	Microemulsion Electrokinetic Chromatography
MEKC	Micellar Electrokinetic Capillary Electrophoresis

μ-RPLC	Micro Reverse Phase Liquid Chromatography
μTAS	Micro Total Analysis System
mRNA	Messenger Ribonucleic acid
MS	Mass Spectrometry
MW	Molecular Weight
MWCO	Molecular Weight Cut Off
NHS	N-Hydroxysuccinimide
NS	No Separation
NT	Not Tested
O.D.	Outer Diameter
OAT	Overall Analysis Time
OCEC	Open Channel Electrochromatography
OPA	*ortho*-Phthalaldehyde
OV	Ovalbumin
PC	Polycarbonate
PCR	Polymerase Chain Reaction
PDA	Photodiode Array
PDI	Polydispersity Index
PDMA	Polydimethyl acrylamide
PDMS	Polydimethylsiloxane
PEB	Post Exposure Bake
PES	Polyethersulfone
PET	Polyethylene terephthalate
pI	Isoelectric Point
PMMA	Poly(methyl methacrylate)
PNA	Lectin Peanut Agglutinin
PS	Polystyrene
PTFE	Polytetrafluoroethylene
PVC	Polyvinylchloride
RNA	Ribonucleic acid
S	Sample
S/N	Signal-to-noise ratio
SARS	Severe Acute Respiratory Syndrome

SDS	Sodium Dodecyl Sulfate
SDS-PAGE	Sodium Dodecyl Sulfate – Polyacrylamide Gel Electrophoresis
SEA	Staphylococcal Enterotoxin A
SEB	Staphylococcal Enterotoxin B
SGE	Slab Gel Electrophoresis
SW	Sample Waste
TBE	TRIS-Borate-EDTA
TE	Terminating Electrolyte
TEMED	N, N, N', N'-tetramethylenediamine
TNS	2-Toluidinonaphthalene-6-sulfonate
TRIS	Tris (hydroxymethyl) aminomethane
TRITC	Tetramethylrhodamine isothiocyanate
tRNA	Transfer Ribonucleic acid
UV	Ultraviolet
WG	Wheat Germ Agglutinin

List of Symbols

σ_{ads}^2	Adsorption of analytes on the capillary wall variance
σ_{det}^2	Detection volume variance
σ_{diff}^2	Longitudinal diffusion of analyte molecules variance
σ_G^2	Geometry of the channel variance
σ_{inj}^2	Injection volume variance
σ_P^2	Pressure drop variance
σ_T^2	Capillary temperature variance
c	Polymer concentration
c^*	Polymer threshold concentration
d	Characteristic dimension or tube diameter
D	Molecular diffusion coefficient
E	Electric field strength
H	Plate height
L_c	Capillary length
L_s	Separation length
N	Theoretical plate number
N_A	Avogadro number
r	Axial radius of the curvature along the channel direction
R	Resolution
R_g	Radius of gyration of the polymer
t	Migration time
V	Voltage applied across the channel
W	Peak width
γ	Surface tension
ΔP	Differential pressure across liquid surface
$\Delta\mu_{ep}$	Difference in electrophoretic mobility
ε	Dielectric constant
ζ	Zeta potential
η	Viscosity
μ_{eo}	Electroosmotic mobility

μ_{ep}	Electrophoretic mobility
ν	Fluid velocity
ν_{eo}	Electroosmotic flow velocity
ν_{ep}	Electrophoretic velocity
ξ	Average pore size
ρ	Density of fluid

List of Figures

Chapter I

Figure 1.7: A Schematic showing concentration-gradient droplets formed in a T-junction geometry by varying sample (red) and diluent (light grey) flow rates in which the magnitude of flow rates are indicated by the size of the arrows. The dark grey represents the oil phase. Image reproduced from reference 53.

Figure 1.8: Microdroplet formation using a flow-focusing geometry (a) Water flows from the middle channel and is sandwiched by oil flowing from the two side channels into an orifice. Water-in-oil droplets are formed downstream of the orifice; (b) Droplets are generated when the aqueous and oil phases pass through the orifice. In the absence of surfactants, small droplets may merge and form larger droplets after generation. Image reproduced from reference 55.

Figure 1.9: (a) Mixing in droplets flowing in a straight channel (b) Mixing in droplets flowing in a winding channel. Images reproduced from reference 28.

Figure 1.10: Droplet manipulations (a) Passive merging of two adjacent droplets[60] (b) Sequential splitting of droplets[61] (c) Dielectrophoretic sorting[62] (d) Droplet trapping arrays[63]

Figure 1.11: Schematics of (a) Differential centrifugation and (b) Isopycnic centrifugation. For differential centrifugation, subcellular contents are fractionated based on their sizes. At low speeds and shorter centrifugation times, larger particles are precipitated at the bottom of the tube, while smaller particles remain in a supernatant. Repeated centrifugations at higher speeds and for longer times allow fractionation of the remaining subcellular contents. For isopycnic centrifugation, subcellular contents are fractionated based on their densities. Components migrate along a sucrose density gradient and stop moving when they reach a location in the gradient that matches its density. Images reproduced from reference 2.

Figure 1.12: Dialysis. Only small molecules can penetrate through a membrane of a dialysis bag or tube, while proteins are retained inside the dialysis bag or tube. Image reproduced from reference 66.

Figure 1.13: (a) Ion-exchange chromatography (b) Size-exclusion chromatography (c) Affinity chromatography. Images reproduced from reference 25.

Figure 1.14: Slab gel electrophoresis. Smaller proteins can pass through the pores of a gel with ease and will, therefore, elute faster than larger proteins. Image reproduced from reference 25.

Figure 1.15: Instrumental setup of a standard capillary electrophoresis system consists of a capillary connecting two buffer reservoirs, a sample reservoir which can be replaced with one of the buffer reservoirs, two electrodes placed at each buffer reservoir to apply an electric field across the capillary using a high-voltage power supply, and a detector.

Figure 1.16: Schematics of a cross-piece microchip with normal injection mode (a) During loading step; (b) During separation step

Figure 1.17: (a) Sample loading during pinched injection; (b) Sample dispensing during pinched injection; (c) Gated injection (i) Applied voltage for sample (S) = 700 V, buffer (B) = 1000 V, sample waste (SW) and buffer waste (BW) = 0 V, (ii) prior to injection: S = 700 V, B, BW and SW = 0 V, (iii) sample dispensing: voltages were shifted back to the same as those of (i). Image (a) and (b) reproduced from reference 108, while image (c) reproduced from reference 34.

Figure 1.18: Two-dimensional gel electrophoresis. Proteins are separated by isoelectric focusing in the first dimension and by SDS gel electrophoresis in the second dimension. Image reproduced from reference 124.

Figure 1.19: Images of microchips containing two intersecting channels as valves (V1 and V2) for the 2D separation of (a) a tryptic digest of BSA having MEKC as the first dimension and CZE as the second dimension, and (b) a tryptic digest of β-casein having OCEC coupled with CZE. Both microchips consist of a sample reservoir (S), two sample waste reservoirs (SW1 and SW2), two buffer reservoirs (B1 and B2) and one buffer waste reservoir (BW). The separated analytes are detected at the point D illustrated in Figure 1.18a and at the points x and y as shown in Figure 1.18b. Image (a) is reproduced from reference 119 and image (b) is reproduced from reference 120.

Figure 1.20: An image of a PMMA microchip with intersecting channel geometries as interfaces between CGE (1^{st} dimension) and MEEKC (2^{nd} dimension) for the separation of cytosolic proteins of *E. coli.* The reservoirs shown in the image are sample reservoir (A), sample waste reservoir (B), CGE buffer reservoir (C), CGE sample waste reservoir (D), MEEKC buffer reservoir (E) and MEEKC buffer waste reservoir (F). Detection is performed at the point d_1 as shown in the image. Image reproduced from reference 139.

Figure 1.21: Schematics of simple cross-intersection geometries for protein separations by IEF coupled with CZE. A sample is first separated by IEF and when the analyte bands reach the intersection, they are then separated by CZE. The direction of IEF in the first dimension separation is from reservoir A to reservoir C in (a) and from reservoir 1 to reservoir 2 in (b). The direction of CZE is from reservoir B (buffer) to reservoir W (waste) in (a) and from reservoir 3 to reservoir 4 in (b). The dashed box D in part (a) shows the detection area. Schematics (a) and (b) reproduced from references 140 and 141, respectively.

Figure 1.22: IEF coupled with CGE using a variety of interfaces between the two separation dimensions. (a) A 2D-separation microchip incorporating a PDMS membrane as an interface (i) A protein mixture is first separated in a composite PDMS membrane serving as an IEF channel (red line). The composite PDMS membrane is then assembled to the other two PDMS pieces: parallel green lines represent the channels in the top PDMS piece and parallel blue lines represent the channels in the bottom PDMS piece. Together they form a single PDMS device for CGE. The separated analytes from the IEF channel are transferred to parallel vertical channels to perform CGE in the second dimension, (ii) The separated fluorescein-conjugated bovine serum albumin (BSA^F) and Texas-red-conjugated ovalbumin (Ov^{TR}) bands are obtained using different filters for the detection of fluorescein and Texas Red. (b) A staggered-channel network within a planar PC microchip for 2D separations (i) A schematic of the microchip shows a horizontal channel for IEF separation traversing vertical channels for performing CGE, (ii) Shows

IEF focusing of a protein mixture, (iii) The focused proteins are transferred electrokinetically to the second dimension, (iv) CGE is then performed in the vertical channels. (c) Schematics of 2D separation processes utilizing microvalves as interfaces between IEF and CGE separations (i) During CGE buffer loading, right valves connected to an IEF channel are closed, (ii) IEF buffer loading, left valves connected to a CGE channel are closed, (iii) All valves are closed after IEF focusing, (iv) Left valves are opened again for CGE separation. (d) An IEF-CGE microchip employing *in situ* polymerized gel as valves (i) A micrograph of the stained polymerized gel within vertical channels, (ii) The enlargement of (i) shows an IEF channel and an array of CGE channels containing polymerized gel. Image (a) reproduced from reference 142, image (b) reproduced from reference 143, image (c) reproduced from reference 144 and image (d) reproduced from reference 146.

Figure 1.23: (a) A schematic of a microchip for IEF coupled with μ-RPLC using microvalves as interfaces. The microvalves are manually turned off after separation in an IEF channel. The analytes are then further separated using μ-RPLC. (b) 2D separation by IEF coupled with DIGE (i) An illustration of a microchip having an IEF channel laying across an array of DIGE channels, (ii) The connection between the IEF channel (horizontal channel) and DIGE channels (vertical channels) using very small channels that prevent gel buffer from dispersing into the IEF channel during the focusing operation, (iii) The gel buffer fills all channels, (iv) The IEF channel is cleared by applying a vacuum at one end and water at the other end, (v) IEF buffer is then introduced into the clean IEF channel. (c) Illustrations of GEMBE coupled with CZE separation. The microdevice consists of a sample reservoir, a CZE buffer reservoir, a buffer waste reservoir, a GEMBE channel connected to a CZE channel via an intersection geometry. By varying the bulk solution counterflow velocity in GEMBE, analytes are allowed to enter the channel at different times. The analyte bands from GEMBE are periodically injected into a CZE channel for further separation by turning on/off a computer-controlled relay. Image (a) reproduced from reference 150, image (b) reproduced from reference 151, image (c) reproduced from reference 122.

Chapter II

Figure 2.1: A schematic illustrating the process of chromium mask fabrication consisting of four steps. The pattern on a film mask is transferred to a chromium coated glass wafer by exposure to the UV light. The exposed photoresist and the chromium layer are then removed to reveal the pattern on the chromium mask.

Figure 2.2: A chemical structure of Bisphenol A Novolak epoxy oligomer containing 8 epoxy groups provide for high degree of cross-linking after photoactivation. Image reproduced from reference 5.

Figure 2.3: Flow chart showing the process of SU-8 master fabrication and surface treatment by silanization.

Figure 2.4: An image and schematics of a robotic droplet generator (a) An image showing the entire system of the robotic droplet generator consisting of a PTFE tube inserted into a metal hook, an oil-filled carousel, a camera, a glass syringe and a syringe

pump; (b) An enlargement of the oil-filled carousel part showing the carousel that can move forward and backward as illustrated by the arrows and the hook that can be in the "up" and "down" position under the control of a solenoid. Fifteen samples can be held by holes on a metal ring for this model of the robotic droplet generator; (c) A schematic illustrating droplet generation from two samples using the robotic droplet generator (i) The carousel moves until the tip of the hook is in the oil phase beneath the first sample (red), (ii) The hook is in the "up" position and withdraws the sample (red), (iii) The hook is in the "down" position and withdraws the oil, (iv) The carousel moves again towards the second sample (blue) until the tip of the hook is underneath the sample, (v) The same process as that of (ii) occurs to achieve a droplet of the second sample (blue), (vi) The process in (iii) is repeated. Image (b) and (c) reproduced from reference 9.

Figure 2.5: Schematics illustrating overall instrumentation of Peregrine (a) Outside of the machine showing main cover, status panel and carousel cover; (b) Inside the machine showing main cover interlock, lamp cover and main electrophoresis compartment/ optical rail components inside the main cover, carousel cover interlock inside the carousel cover and power switch at the side of the machine. Images reproduced from reference 10.

Figure 2.6: Schematic depicting the components inside the main cover of Peregrine. Image reproduced from reference 10.

Figure 2.7: Schematics illustrating outside and inside of the capillary block used with Peregrine machine (a) Overview of the capillary block; (b) Capillary track (red line) of 20.2 cm input capillary length; (c) Illustrating a fused silica capillary with 1.25 cm detection window. Images reproduced from reference 10.

Figure 2.8: An example of (a) raw data obtained from 1-pixel detector showing transmittance vs. time (scan count) and (b) GST processed electropherogram in which the axes are absorbance vs. time (min).

Figure 2.9: Equiphase map (a) An example of equiphase map; (b) Schematic illustrating how the equiphase map is generated. Image (a) reproduced from reference 10 and (b) adapted from reference 12.

Chapter III

Figure 3.1: Diagram showing the process of buffer development for protein separations.

Figure 3.2: Microfluidic devices used to perform protein gel electrophoresis (a) A cross-piece PDMS microdevice; (b) A cross-piece PDMS microdevice with an enlarged channel for the insertion of a glass capillary; (c) Aluminium platform for holding either a cross-piece PDMS microdevice or a cross-piece PDMS microdevice coupled to a glass capillary. S = sample reservoir, SW = sample waste reservoir, B = buffer reservoir and BW = buffer waste reservoir.

Figure 3.3: The separation of a 3-protein mixture in Beckman buffer using the CE machine (a) GST processed electropherograms of lysozyme (1), CA (2), BSA (3) and a mixture of these proteins performed in Beckman buffer using a 34 cm long capillary having an effective length of 20 cm, at 25°C and using electric field strength of 441.18

V/cm (Note: Y-axes are offset due to overlaying). All samples were prepared in Beckman sample buffer with the addition of 2-mercaptoethanol (BME); (b) An equiphase map obtained from the separation of the mixture.

Figure 3.4: The separation of a 3-protein mixture in Beckman buffer in which samples were prepared in (a) 10 mM TRIS-HCl, 0.1% SDS, pH 6.6; (b) 5 mM SDS, 5 mM sodium tetraborate buffer, pH 8.5; (c) 5 mM SDS, 5 mM sodium tetraborate buffer, pH 8.8. For (a), (b) and (c), (i) Showing GST processed electropherograms of lysozyme (1), CA (2), BSA (3) and a mixture of these proteins performed in Beckman buffer using the CE machine that employed a 34 cm long capillary having an effective length of 20 cm, at 25°C (Note: Y-axes are offset due to overlaying), (ii) Showing the equiphase map from the separation of the mixture. The electric field strength used in (a) was 300 V/cm and used in (b) and (c) was 450 V/cm.

Figure 3.5: Effect of pH of samples on protein separation. (a) A plot of mobility versus molecular weight of proteins; (b) A plot of resolution versus molecular weight. Two sets of a 3-protein mixture (lysozyme, CA and BSA) prepared in 5 mM borate buffer, 5 mM SDS at pH 8.5 and pH 8.8 were separated in Beckman buffer using the CE machine that employed a 34 cm long capillary having an effective length of 20 cm, at 25°C and using separation field strength of 450 V/cm.

Figure 3.6: The separation of a 3-protein mixture in an 80/20 mixture of Beckman buffer and 5 mM SDS in 5 mM sodium tetraborate buffer, pH 9.0 using the CE machine (a) GST processed electropherograms of lysozyme (1), CA (2), BSA (3) and a mixture of these proteins performed using a 34 cm long capillary having an effective length of 20 cm, at 25°C and using electric field strength of 462.4 V/cm. Thiourea peaks (4) are also observed in these electropherograms (Note: Y-axes are offset due to overlaying); (b) The equiphase map from the separation of the mixture.

Figure 3.7: Electropherogram of a fluorescently labeled protein ladder (20-200 kDa fluorescent molecular weight marker, Sigma Aldrich, UK) performed in Beckman buffer solution in a cross-piece PDMS microdevice using electric field strength of 135 V/cm. Detection was done at 0.5 cm from the intersection. Note: The injection time was at 120 seconds according to the electropherogram.

Figure 3.8: Electrophoresis of BSA and thiourea in various concentrations of diluted Beckman buffer using the CE machine. (a) GST processed electropherograms of BSA and thiourea performed in Beckman diluted in DI water at concentrations of 0.2x (green line), 0.25x (pink line), 0.33x (blue line) and 0.5x (red line) using a 34 cm long capillary having an effective length of 20 cm, at 25°C and using electric field strength of 441.18 V/cm. The peaks shown in these electropherograms are thiourea injected from the opposite end of the capillary to BSA, which is not observed (Note: Y-axes are offset due to overlaying); (b) An equiphase map shows the opposite direction of migration of thiourea due to high EOF.

Figure 3.9: Electropherograms of protein ladder (20-200 kDa fluorescent molecular weight marker, Sigma Aldrich, UK) performed in 0.2x Beckman mixed with EOTrol buffer on a cross-piece PDMS microdevice using electric field strength of 121.67 V/cm. The separations were observed at two detection points: 0.5 cm (black line) and 1.0 cm

(blue line) measured from the intersection. Note: The actual injection time was not recorded and y-axes are offset due to overlaying.

Figure 3.10: An electropherogram of protein ladder (20-200 kDa fluorescent molecular weight marker, Sigma Aldrich, UK) electrophoresed in dialysed Beckman against DI water on a cross-piece PDMS microdevice coupled to a glass capillary using electric field strength of 88.75 V/cm. The cross-piece PDMS microdevice contained 0.1x TBE solution, while the 7-cm glass capillary contained dialysed Beckman buffer. Note: The actual injection time was not recorded.

Figure 3.11: Electropherograms of protein ladder (20-200 kDa fluorescent molecular weight marker, Sigma Aldrich, UK) performed in (a) dialysed Beckman against 0.1x TBE and (b) dialysed Beckman against 0.1x TBE added 0.5% SDS on a cross-piece PDMS microdevice coupled to a glass capillary using electric field strength of 88.75 V/cm. The cross-piece PDMS microdevice contained 0.1x TBE mixed with EOTrol solution, while the 7-cm glass capillary contained dialysed Beckman buffer. Note: Time shown in the electropherograms was not the actual time from the injection.

Figure 3.12: Electropherograms of fluorescein (1 and 2) and BSA-FITC (3) separated in (a) 1.5% PDMA in 0.085 M, 0.1% SDS, pH 9.3 using separation field strength of 133 V/cm (detection at 0.5 cm) and (b) 3% PDMA in 0.085 M, 0.1% SDS, pH 9.3 using separation field strength of 200 V/cm (detection at 2 cm). The sample was prepared in 0.2% SDS.

Figure 3.13: Possible existing structures of fluorescein. Image reproduced from reference 49.

Figure 3.14: Effect of polymer concentration and effect of adding glycerol in running buffer. (a) Electropherograms of a protein mixture separated in 3% PEO 100 kDa (green line) and 5% PEO 100 kDa (pink line) in 0.1 M TRIS-CHES, 0.1% SDS, pH 8.7 and 3% PEO 100 kDa (blue line) and 5% PEO 100 kDa (red line) in 0.1 M TRIS-CHES, 0.1% SDS, 5% glycerol, pH 8.7 (Note: Y-axes are offset due to overlaying); (b) Plot of mobility vs. molecular weight; (c) Plot of resolution vs. molecular weight. The separations of a protein mixture (lysozyme (1), CA (2) and BSA (3)) were performed using a 34 cm long capillary having an effective length of 20 cm, at 25°C and using electric field strength of 441.18 V/cm. All samples were prepared in 1x TBE buffer, 0.1% SDS, pH 7.56. Note: CA peak (2) in 5% PEO 100 kDa buffer containing 5% glycerol (red line) is indistinguishable. Therefore, mobility for CA and resolution results for this buffer are not available.

Figure 3.15: Effect of polymer concentration of mixed polymer molecular weight. (a) Electropherograms of a protein mixture separated in 3% PEO 100 kDa mixed with 2% PEO 200 kDa (green line), 5% PEO 100 kDa mixed with 1.5% PEO 200 kDa (pink line), and 6% PEO 100 kDa mixed with 0.5% PEO 200 kDa (red line) in 0.1 M TRIS-CHES, 0.1% SDS, 2% glycerol, pH 8.5 (Note: Y-axes are offset due to overlaying); (b) Plot of mobility vs. molecular weight; (c) Plot of resolution vs. molecular weight. The separations of a protein mixture (lysozyme (1), CA (2) and BSA (3)) were performed using a 34 cm long capillary having an effective length of 20 cm, at 25°C and using

electric field strength of 441.18 V/cm. All samples were prepared in 1x TBE buffer, 0.1% SDS, pH 7.56. Note: Lysozyme peak (1) is not shown in 3% PEO 100 kDa mixed with 2% PEO 200 kDa buffer. Therefore, mobility for lysozyme and resolution between lysozyme and CA are not available.

Figure 3.16: Effect of buffer pH. (a) Electropherograms of a protein mixture separated in 3% PEO 100 kDa mixed with 2% PEO 200 kDa in 0.1 M TRIS-CHES, 0.1% SDS, 2% glycerol, pH 8.3 (red line) and pH 8.5 (green line) (Note: Y-axes are offset due to overlaying); (b) Plot of mobility vs. molecular weight; (c) Plot of resolution vs. molecular weight. The separations of a protein mixture (lysozyme (1), CA (2) and BSA (3)) were performed using a 34 cm long capillary having an effective length of 20 cm, at 25°C and using electric field strength of 441.18 V/cm. All samples were prepared in 1x TBE buffer, 0.1% SDS, pH 7.56. Note: Lysozyme peak (1) is not shown in buffer pH 8.5. Therefore, mobility for lysozyme and resolution between lysozyme and CA are not available.

Figure 3.17: Comparison of the current during electrophoresis in 3% PEO 100 kDa mixed with 2% PEO 200 kDa in 0.1 M TRIS-CHES, 0.1% SDS, 2% glycerol, pH 8.3 and pH 8.5. (a) Plots between current and voltage of buffer pH 8.3 (red line) and buffer pH 8.5 (black line). Plots of current and time during separation in (b) buffer pH 8.3 and (c) buffer pH 8.5.

Figure 3.18: Electrophoretic separation of a fluorescently labeled protein ladder (11-155 kDa Benchmark fluorescent protein standard) performed in a cross-piece PDMS microdevice. (a) An electropherogram showing the fluorescein peak in the front followed by 7 protein bands of protein ladder separated in 5% PEO (100 kDa) in 0.05 M TRIS-CHES 0.1% SDS, pH 8.5 using electric field strength of 208.33 V/cm. Detection was done at 1.3 cm from the intersection; (b) A plot of mobility versus molecular weight of 11-155 kDa protein ladder; (c) A plot of resolution versus molecular weight. Note: The injection time was at 80 seconds according to the electropherogram.

Figure 3.19: Electrophoretic separation of a fluorescently labeled protein ladder (11-155 kDa Benchmark fluorescent protein standard) performed in a cross-piece PDMS microdevice. (a) An electropherogram showing the fluorescein peak in the front followed by 7 protein bands of protein ladder separated in 6% PEO (100 kDa) in 0.05 M TRIS-CHES 0.1% SDS, pH 8.5 using electric field strength of 167.5 V/cm. Detection was done at 1.0 cm from the intersection; (b) Showing three repetitions of protein separations; (c) A plot of mobility versus molecular weight; (d) A plot of resolution versus molecular weight. Note: The injection time was at 120 seconds according to the electropherogram.

Figure 3.20: Electropherograms comparing between BSA peak in fluorescently labeled protein ladder (11-155 kDa Benchmark fluorescent protein standard) and the injected BSA-FITC. The separations were performed in a cross-piece PDMS microdevice using 6% PEO (100 kDa) in 0.05 M TRIS-CHES, 0.1% SDS, pH 8.5 at separation field strength of 167.5 V/cm and were detected at 1.0 cm from the injection point (Note: Y-axes are offset due to overlaying).

Figure 3.21: Electrophoretic separation of a fluorescently labeled protein ladder (11-155 kDa Benchmark fluorescent protein standard) performed in a cross-piece PDMS microdevice coupled to a glass capillary. (a) An electropherogram showing the

fluorescein peak in the front followed by 7 protein bands of protein ladder separated in 6% PEO (100 kDa) in 0.05 M TRIS-CHES 0.1% SDS, pH 8.5 using electric field strength of 188 V/cm. Detection was done at 2.0 cm from the intersection; (b) A plot of mobility versus molecular weight; (d) A plot of resolution versus molecular weight. Note: The injection time was at 120 seconds according to the electropherogram.

Chapter IV

Figure 4.1: The reaction of protein conjugated with FITC.

Figure 4.2: The reaction of protein conjugated with NHS-Fluorescein.

Figure 4.3: Absorption spectra of (a) lysozyme conjugated FITC and (b) BSA conjugated FITC. Both protein conjugates were prepared in DI water.

Figure 4.4: Electrophoresis performed in 6% PEO 100 kDa in 0.05 M TRIS-CHES, 0.1% SDS, pH 8.5 using a cross-piece PDMS microdevice. The electric field was applied at ~168 V/cm and the detection was made at 1 cm. The electropherograms of (a) lysozyme-FITC prepared in 0.1% SDS buffer and heated at 95 °C for 5 min and (b) 38.5 μM FITC dissolved in DI water.

Figure 4.5: Possible forms of FITC in an aqueous solution (a) neutral species (p-quinoid); (b) neutral species (lactone); (c) neutral species (zwitterion); (d) cation; (e) anion (carboxylate); (f) anion (phenolate) and (g) dianion

Figure 4.6: The reaction of free FITC with TRIS containing in 6% PEO buffer.

Figure 4.7: Absorption spectra of (a) lysozyme conjugated NHS-Fluorescein and (b) BSA conjugated NHS-Fluorescein. Both protein conjugates were prepared in DI water.

Figure 4.8: The electropherogram of NHS-Fluorescein performed in 6% PEO 100 kDa in 0.05 M TRIS-CHES, 0.1% SDS, pH 8.5 using a cross-piece PDMS microdevice. The electric field was applied at ~168 V/cm and the detection was made at 1 cm. 0.5 mM NHS-Fluorescein was prepared in 0.1x TBE buffer

Figure 4.9: The reaction of NHS-Fluorescein in 6% PEO buffer (a) The hydrolysis of NHS-Fluorescein and (b) The reaction between NHS-Fluorescein and TRIS.

Figure 4.10: The electropherograms of lysozyme-NHS-Fluorescein electrophoresed in 6% PEO 100 kDa in 0.05 M TRIS-CHES, 0.1% SDS, pH 8.5 using a cross-piece PDMS microdevice (a) First injection of lysozyme-NHS-Fluorescein; (b) Second injection of lysozyme-NHS-Fluorescein; (c) First addition of 4 μl 0.1 mM NHS-Fluorescein to the depleted lysozyme-NHS-Fluorescein and (d) Second addition of 4 μl 0.1 mM NHS-Fluorescein to the depleted lysozyme-NHS-Fluorescein. The electric field was applied at ~168 V/cm and the detection was made at 1 cm. Lysozyme-NHS-Fluorescein was prepared in 0.1% SDS buffer and heated at 95 °C for 5 min, while 0.1 mM NHS-Fluorescein was prepared in 0.1x TBE buffer.

Figure 4.11: Effect of SDS concentration on the fluorescence intensity of protein conjugated NanoOrange. (a) The background intensity of 0.05 M TRIS-CHES, pH 8.5 buffer containing various concentrations of SDS (i) 0% SDS, (ii) 0.01% SDS and (iii) 0.1% SDS; (b) 10 µl of 0.01 mg/ml lysozyme conjugated 1x NanoOrange was added to 0.05 M TRIS-CHES, pH 8.5 buffer containing (i) 0% SDS, (ii) 0.01% SDS and (iii) 0.1% SDS; (c) A graph translating the fluorescence intensity from the images in Figure 4.11a and Figure 4.11b into the values in which the blue columns show the intensity of the background buffer containing 0-0.1% SDS and the red columns show the intensity of the buffer added 10 µl of 0.01 mg/ml lysozyme conjugated NanoOrange.

Figure 4.12: Fluorescence intensity of protein conjugated NanoOrange. (a) Lysozyme conjugated NanoOrange droplet and (b) BSA conjugated NanoOrange droplet. The concentration of the proteins conjugated dye used to generate droplets were 0.5 mg/ml.

Figure 4.13: An electropherogram of BSA conjugated NanoOrange obtained from the injections of five droplets into 6% PEO 100 kDa in 0.05 M TRIS-CHES, 0.1% SDS, pH 8.5 using the interfacing droplet-based microdevice "Design 6". The electrophoresis was performed at the electric field strength of ~ 333 V/cm and detected at 1.0 cm.

Chapter V

Figure 5.1: Compartmentalization of analyte bands into droplets (a) A schematic showing separated analyte bands from a first dimension being compartmentalized into droplets that are transferred downstream for further analysis; (b) A mixture of fluorescent dyes was injected at the cross-channel part of a microdevice shown in the inset (color images). The mixture was separated using CGE and the separated bands moved along the straight channel to a T-junction where droplets could be generated. Schematics are reproduced from reference 34 and 35.

Figure 5.2: Droplet-based interfacing microdevices employing surface modification. (a) A droplet generated at a hydrophobic T-junction channel moves towards a hydrophilic separation channel where it fuses with an immiscible boundary allowing the droplet contents to be injected into the separation channel; (b) A schematic showing a sample plug moving along a segmented flow channel prior to merging with a virtual wall at a K-shaped interface. Here, only small amount of the sample is injected into the separation channel; (c) A parallel electrophoretic analysis on a microdevice employing K-shaped interfaces for the transfer of sample plugs; (d) A schematic and images showing the transfer of sample plugs obtained from a microdialysis probe (not shown) into a separation channel using a hydrophilic extraction bridge. Schematics and images reproduced from reference 36, 37, 38 and 39, respectively.

Figure 5.3: Droplet-based interfacing microdevices coupled to mass spectrometry analysis (a) A micrograph showing an analyte plug being transferred into an aqueous stream employing an array of apertures as an interface for pressure control; (b) An integrated platform for protein analysis consisting of a droplet generation part, which compartmentalizes eluted bands from HPLC, and an electrospray ionization emitter for mass spectrometry analysis of proteins in droplets. Schematics and image reproduced from reference 40 and 41, respectively.

Figure 5.4: Droplet-based interfacing microdevices developed by *Niu* and co-workers (a) A schematic showing the compartmentalization of eluted bands from the first separation dimension into droplets (left) and droplet injection into the second dimension employing a pillar-structured microdevice to eliminate oil surrounding droplets (right); (b) Schematics of the Nano LC-MALDI-MS droplet-based interfacing microdevice (i) Separated analyte bands from Nano-LC are compartmentalized into droplets, (ii) Droplet contents are collected at the tip of the probe prior to the deposition onto the MALDI stage, whilst oil is absorbed into an oleophilic film; (c) Schematics illustrating the interfacing microdevices utilizing an oleophilic membrane as an oil depletion unit (i) An entire microdevice made of PDMS (left) and a PDMS microdevice coupled to a glass capillary (right), (ii) A schematic depicting the injection of a droplet through an open channel, while oil is depleted via the oleophilic membrane. Schematics reproduced from reference 31, 32 and 33, respectively.

Figure 5.5: Schematics and an image illustrating the structure of the initial interface design used to perform single or multiple separations (a) A schematic of the entire microdevice consisting of a top layer (black solid lines) and a bottom layer (black and red dashed lines) of PDMS. The top PDMS layer contains two parallel separation channels with reservoirs at each end (the left reservoir is the "buffer reservoir" and the right reservoir is the "buffer waste reservoir"), two channels with enlarged ends to allow insertion of the droplet delivery tubes and four oil depletion units (with a pillar in each unit). The bottom PDMS layer consists of four open circles at the same positions as the oil depletion units in the top layer; (b) An enlargement of the oil depletion units.

Figure 5.6: (a) A schematic showing the separated top and bottom PDMS layers: (i) Top layer, (ii) Bottom layer; (b) An image showing a separation channel connected to two sides of pillar-structured oil depletion units and a channel for delivering droplets.

Figure 5.7: A top view schematic of the microdevice during droplet injection experiment. One end of the droplet delivery tube is inserted into a side channel of the microdevice, while the other end is connected to the syringe pump to drive droplets towards a separation channel. An electric field is applied across the separation channel by placing a cathode in the buffer reservoir and an anode in the buffer waste reservoir.

Figure 5.8: Illustration of the droplet injection process. (a) The injection of a mixture of a fluorescent dye and a food dye. (i) The microdevice prior to injection at t = 0 s, (ii) The first sample plug is injected into the separation channel (t = 50 s) and moves towards the anode, (iii) The first sample plug stops being injected at t = 53 s, (iv) The next sample plug is injected at t = 54 s (v) A sample plug is injected at t = 63 s, whilst the previous one is still being injected. Buffer solution leakage can be observed at the right oil depletion unit in each image; (b) A dead volume exists at the connection between the droplet delivery tube and the droplet delivery channel. Oil surrounding the droplets is thus accumulated and causes droplets merge prior to injection; (c) Diffusion of the sample into the oil depletion units. Experiments were performed at an infusing flow rate of 0.12 μl/min and an electric field strength of 85.7 V/cm.

Figure 5.9: Schematics illustrating the structure of "Design 2" for single or multiple separations (a) A schematic of the entire microdevice consisting of a top layer (solid lines) and a bottom layer (dashed lines) in PDMS. The top PDMS layer consists of two

parallel separation channels with reservoirs at each end (the left reservoir is the "buffer reservoir" and the right reservoir is the "buffer waste reservoir"). The bottom PDMS layer is cut into two pieces and placed 2-3 mm apart beneath the top layer; (b) Schematics showing the separated top and bottom PDMS layers: (i) Top layer, (ii) Bottom layer before being cut and (iii) Bottom layer cut after oxygen plasma treatment.

Figure 5.10: Schematics showing the experimental setup used for droplet injection using the interfacing microdevice "Design 2". (a) The interfacing microdevice placed on droplet delivery tubes. Both tubes are on a PTFE membrane. The open channels are aligned to the mouths of the two droplet delivery tubes cut at 30° to the edge. The other ends of the tubes are connected to precision syringe pumps; (b) A platform to hold the microdevice during the experiments consists of two acrylic plates: a top plate and a bottom plate. The microdevice along with the tubes and the PTFE membrane is placed on the bottom plate of the platform, whilst the top plate is put on the microdevice to secure everything in place. There is a square cavity on the top plate at the position of the buffer reservoir so that a Pt electrode can be immersed into the buffer reservoir through the cavity.

Figure 5.11: Droplet injections in parallel channels. (a) The injection of an analyte mixture droplet into the upper separation channel. (i) The droplet prior to injection at t = 0 s, (ii) The droplet is injected at t = 1 s, (iii) The whole droplet is successfully injected and moves along the separation channel towards the anode at t = 2 s; (b) The injection of the analyte mixture droplet into the lower separation channel. (i) The droplet prior to injection at t = 107 s, (ii) The droplet is injected at t = 110 s, (iii) The whole droplet is successfully injected into the separation channel at t = 111 s. Some of the analyte mixture moves towards the anode (right arrow) but some moves in the opposite direction towards the cathode (left arrow). The arrows indicate the direction of the analyte mixture movement; (c) Droplet injection in the lower channel (right), while a droplet in the other tubing (left) moves towards the upper channel.

Figure 5.12: Schematics illustrating the third generation interfacing microdevice with two open-channel structures. (a) Separated top layer and bottom PDMS layers (i) Top layer consisting of a T-junction droplet delivery channel with an expansion at the left and right sides to allow insertion of droplet delivery tube and a glass capillary, respectively. A buffer reservoir is placed at one end of the channel, whilst a buffer waste reservoir (not shown) is placed at the end of the capillary, (ii) Initial design of the bottom layer. A flat PDMS layer is cut and placed 2-3 mm separately after oxygen plasma treatment, (iii) Second design of the bottom layer. A rectangular, thin PDMS layer is removed after oxygen plasma treatment; (b) Entire microdevices after bonding the top and bottom layers (i) The top layer of microdevice bonded with the first design of the bottom layer "Design 3.1", (ii) The top layer of microdevice bonded with the second design of the bottom layer "Design 3.2".

Figure 5.13: Schematics illustrating the experimental set up used for droplet injection using the third generation interfacing microdevices. (a) "Design 3.1" with the separated bottom layer; (b) "Design 3.2" with the open, rectangular bottom layer. Both microdevices are configured in the same manner, i.e. droplet delivery tube and a glass capillary are inserted into the left and the right enlarged channels, respectively, and the open channel is placed on a PTFE membrane for oil depletion. A cathode is placed at a

buffer reservoir, while an anode is placed at a buffer waste reservoir for application of an electric field.

Figure 5.14: Images showing the injection of droplets and the migration of droplet content towards the separation channel performed in microdevice "Design 3.1". (a) A droplet leaves the mouth of the droplet delivery tube and moves into the droplet delivery channel; (b) The droplet content is accumulated at the mouth of the tube and its movement ceases; (c) After a period of time, the droplet contents start moving again.

Figure 5.15: Schematics illustrating the fourth interfacing microdevices containing two similar open-channel designs. (a) Separated top and bottom PDMS layers: (i) Top layer of "Design 4.1" consisting of a round U-shaped droplet delivery channel, (ii) Top layer of "Design 4.2" consisting of a square U-shaped droplet delivery channel. Both designs consist of an enlarged channel in the middle of the U-shaped channel for insertion of droplet delivery tube, a buffer reservoir and the other enlarged channel for the insertion of a glass capillary at each end of the U-shaped channel, (iii) Bottom layer of both "Design 4.1" and "Design 4.2" consisting of a rectangular open space on a PDMS sheet, which is cut after oxygen plasma treatment; (b) The entire microdevices after bonding: (i) "Design 4.1", (ii) "Design 4.2".

Figure 5.16: Schematics illustrating the process of droplet injection using the fourth generation of interfacing microdevices. (a) "Design 4.1" with a round U-shaped PDMS channel; (b) "Design 4.2" with a square U-shaped PDMS channel. Both microdevices are operated in the same manner. A droplet delivery tube is inserted into the enlarged channel at the middle of the U-shaped channel, while a glass capillary is inserted into the other enlarged channel. The entire microdevice is placed on a PTFE membrane, which serves as an oil depletion unit. A cathode is placed at a buffer reservoir, while an anode is placed at a buffer waste reservoir.

Figure 5.17: Images showing the injection of a droplet in "Design 4.1". The red dashed lines indicate the open PDMS channel of the microdevice. (a) A droplet moves towards the mouth of the droplet delivery tube; (b) The droplet contents form a spherical plug when the droplet reaches the open PDMS channel, while the oil is absorbed into the PTFE membrane underneath; (c) The droplet content migrates towards a glass capillary placed downstream (the movement direction indicated by a yellow arrow).

Figure 5.18: An electropherogram of fluorescein obtained from droplet injections performed in the microdevice "Design 4.1". Three fluorescein droplets were injected and detected inside a glass capillary. Each droplet was injected as single injection. The electric field used in this experiment was ~ 253 V/cm.

Figure 5.19: Images showing the injection of a droplet performed using "Design 4.2". The red dashed lines indicate the open PDMS channel of the microdevice. (a) A droplet enters the PDMS channel of the microdevice; (b) The droplet contents form a spherical plug; (c) The droplet content migrates along the PDMS channel and then into a glass capillary (with movement direction indicated by a yellow arrow).

Figure 5.20: Images showing multiple injection of a droplet performed using Design 4.2. The red dashed lines indicate the open PDMS channel of the microdevice. (a) A part of a

droplet is injected into the PDMS channel; (b) The injected droplet content migrates along the PDMS channel, with material being left at the mouth of the tube; (c) Most of the droplet content migrates towards a glass capillary (the movement direction indicated by a yellow arrow), while a small portion of the droplet diffuses at the top and the bottom edges of the tube (blue arrows).

Figure 5.21: An electropherogram of fluorescein obtained from droplet injections performed in a "Design 4.2" microdevice. Five fluorescein droplets were injected and detected inside a glass capillary. Each droplet was injected as multiple injections.

Figure 5.22: Schematics and images depicting the structure of the fifth generation interfacing microdevices made of acrylonitrile butadiene styrene or ABS (a) Separated top and bottom layer: (i) Modified top layer from "Design 4.2" with four holes, (ii) Bottom layer with four post, (iii) A photograph showing the back of the top layer of the 3D-printed microdevice, (iv) A photograph of the front of the top layer showing a 4 mm I.D. buffer reservoir, (v) A photograph of the bottom layer; (b) The entire microdevice after assembling: (i) A schematic showing inside the microdevice, (ii) A photograph of the assembled microdevice showing the buffer reservoir and the side channel for the insertion of a droplet delivery tube, (iii) A photograph of the assembled microdevice showing the buffer reservoir and the side channel for the insertion of glass capillary.

Figure 5.23: A schematic showing the experimental set up of droplet injection using the fifth generation interfacing microdevice developed from "Design 4.2". A PTFE membrane is cut into a small piece, folded and placed into the square hole of the bottom layer prior to being assembled with the top layer. Droplet delivery tube is inserted into the enlarged channel at the middle of the U-shaped channel, while a glass capillary is inserted into the other enlarged channel. A cathode is placed at a buffer reservoir, while an anode is placed at a buffer waste reservoir, which is a microcentrifuge tube (not shown) for the application of an electric field.

Figure 5.24: Images showing hydrophilic testing on the surface of 3D-printed pieces of microdevices (a) Red food dye was dropped onto the surface of each 3D-printed piece. Before (right) and after (left) surface treatment with 10% SDS at 70°C for 2 hours; (b) Red food dye filled up the entire channel of the microdevice.

Figure 5.25: Schematics depicting the structure of the sixth design of interfacing microdevices. (a) A schematic of the entire microdevice consisting of a top (solid lines) and a bottom (dashed lines) layer of PDMS; (b) Schematics showing the separated top and bottom PDMS layers: (i) The top layer consisting of a straight channel connected to a buffer reservoir at one end and an enlarged channel for the insertion of a glass capillary at the other end, (ii) The 2-3 mm separated PDMS bottom layer after plasma treatment.

Figure 5.26: Schematics showing the experimental setup of droplet injection experiment using the sixth design of the interfacing microdevices. (a) A droplet delivery tube cut a 30° angle at one end was placed onto a PTFE membrane, while the other end of the tube was connected to a syringe pump. The microdevice with an inserted glass capillary was then placed on the tube by aligning the PDMS channel onto the mouth of the tube; (b) An acrylic platform used to hold the microdevice consisting of two plates. The microdevice along with the tube, the glass capillary and the PTFE membrane is placed on the bottom

plate of the platform. The top plate is then put on the microdevice to secure everything in place. One Pt electrode is immersed into a buffer reservoir through a square cavity on the top acrylic plate, while the other Pt electrode is immersed into a buffer waste reservoir (a microcentrifuge tube which is not shown) placed at the end of the capillary.

Figure 5.27: Images showing the injection of a fluorescein droplet. (a) A fluorescein droplet moves towards the mouth of the tube at the flow rate of 0.3 µl/min; (b) The oil surrounding the droplet is absorbed into a PTFE membrane, whilst fluorescein released from the droplet forms a spherical shape at the mouth of the tube; (c) Fluorescein is successfully injected into the PDMS channel (red dashed lines) and migrates under an electric field (333.33 V/cm) towards an anode.

Chapter VI

Figure 6.1: Illustrations of (a) one-piece and (b) two-piece droplet delivery tube.

Figure 6.2: A photograph showing the assembly of the interfacing droplet-based microdevice on the old platform.

Figure 6.3: Diagram showing the problems occurred in each part of the experiment.

Figure 6.4: Images showing the leakage of a droplet due to the imperfect joining of two tubes (a) The leakage of a whole droplet (i) A droplet reaches the connection between two tubes, (ii) The droplet starts to leak into the sleeve, (iii) The rest of the droplet is leaking out; (b) The leakage of a part of a droplet. The droplet designated as "1" has the normal shape, while the shape of droplets designated as "2" and "3" is deformed after they pass the connection between two tubes.

Figure 6.5: The injection of nine fluorescein droplets using "Design 6" interfacing microdevice. (a) An electropherogram of nine injected fluorescein droplets (designated from 1 to 9). In this experiment, the droplets were delivered to the mouth of the tube at the flow rate of 0.3 µl/min and injected to the open channel containing 0.1% SDS. Fluorescein released from droplets migrated into the 5-cm long glass capillary containing 6% PEO 100 kDa in 0.05 M TRIS-CHES, 0.1% SDS, pH 8.5. The applied electric field during this experiment was 333.33 V/cm. The detection was performed at 1 cm from the injection point; (b) A scatterplot between the droplet volume and the fluorescence intensity of nine injected droplets with the correlation coefficient (r) of 0.9752 and the p-value of 7.7×10^{-6}.

Figure 6.6: An electropherogram obtained from the injection of BSA-FITC droplets using "Design 6" interfacing microdevice. In this experiment, the droplets were delivered to the mouth of the tube at the flow rate of 0.3 µl/min and injected to the open channel containing 0.005 M TRIS-CHES, 0.1% SDS, pH 8.5. BSA-FITC released from droplets migrated into the 5-cm long glass capillary containing 6% PEO 100 kDa in 0.05 M TRIS-CHES, 0.1% SDS, pH 8.5. The applied electric field during this experiment was 333.33 V/cm. The detection was performed at 1 cm from the injection point.

Figure 6.7: Electropherograms showing fluorescent protein standard (11-155 kDa) mixed with 0.18 µM fluorescein separated in 6% PEO 100 kDa in 0.05 M TRIS-CHES, 0.1%

SDS, pH 8.5 using the interfacing droplet-based microdevice "Design 6". The droplets were delivered to the interfacing PDMS microdevice containing 0.005 M TRIS-CHES, 0.1% SDS, pH 8.5 at the flow rate of 0.08 μl/min. The detection was around 2.5 cm from the injection point, while the total length of the system was 8.0 cm. The applied separation fields were (a) 81.25 V/cm; (b) 118.75 V/cm; (c) 125 V/cm and (d) 150 V/cm. Fluorescein peak was designated as (1) and protein ladder was designated as (2).

Figure 6.8: A photograph showing the new platform to facilitate the assembly of interfacing droplet-based separation unit. Note: the PDMS microdevice shown in the photo was not the actual size used in the experiment.

Figure 6.9: The overlay of electropherograms of fluorescein droplets injected in parallel channels of the interfacing droplet-based microdevice "Design 6". Fluorescein peaks obtained from the above channel and from the below channel were illustrated as black line and red line, respectively. The droplets were delivered to the interfacing PDMS microdevice containing 0.005 M TRIS-CHES, 0.1% SDS, pH 8.5 at the flow rate of 0.1 μl/min. The detection was around 1.3 cm from the injection point, while the total length of the system was 6.0 cm. The applied electric field was ~ 217 V/cm. The detection was performed at 1.3 cm from the injection point.

List of Tables

Chapter I

Chapter II

Chapter III

Chapter IV

Chapter V

Chapter I

Introduction

1.1 Importance of studying cells and cellular contents (i.e. proteins)

All living organisms can be categorized as being either unicellular (single-celled) or multicellular. Unicellular organisms are the simplest organisms consisting of only one cell (e.g. bacteria and protozoa), while multicellular organisms (e.g. plants and animals) are far more complex[1,2]. A typical human, for example, contains around 37 trillion cells that work in a concerted manner to support life[3]. All biological processes in both unicellular and multicellular organisms are known to occur at the cellular level[1]. By differentiating between cell types and understanding how cells work and respond to different environments, advanced biological sciences that accelerate medical diagnoses and improve medical therapies can be more easily developed[4]. Studies of both cells and their contents are therefore important in providing a more comprehensive understanding of biological functions and mechanisms occurring throughout an organism.

Table 1.1: Estimated gross molecular contents of a typical 20-micron human cell[5]

Molecule	Mass %	MW (daltons)	Number of Molecules	Molecule %	Number of Molecular Types
Water	65%	18	1.74×10^{14}	98.73%	1
Other Inorganic	1.5%	55	1.31×10^{12}	0.74%	20
Lipid	12%	700	8.4×10^{11}	0.48%	50
Other Organic	0.4%	250	7.7×10^{10}	0.04%	~200
Protein	20%	50,000	1.9×10^{10}	0.01%	~5,000
RNA	1%	1×10^{6}	5.0×10^{7}	3×10^{-5} %	----
DNA	0.1%	1×10^{11}	46	3×10^{-11} %	----
TOTALS	**100%**	**----**	**1.76×10^{14}**	**100%**	**----**

A generic human cell (a few tens of microns in diameter) consists of water (98.73%), other inorganics (0.74%), lipid molecules (0.48), organics (0.04%), proteins (0.01%), RNA (3×10^{-5}%) and DNA (3×10^{-11}%)[5]. Of all the cell components, proteins exhibit the widest variety in their molecular identity (**Table 1.1**) despite only comprising 0.01% of

the total molecular composition. Such a large diversity of protein types suggests the distinct and varied functions they play. The importance of proteins in cells can also be confirmed by inspection of the system interaction map between proteins in a fruit fly cell (**Figure 1.1**)[1]. This map pictorially shows how each protein relates or interacts with other cellular proteins and how a change in one protein affects others.

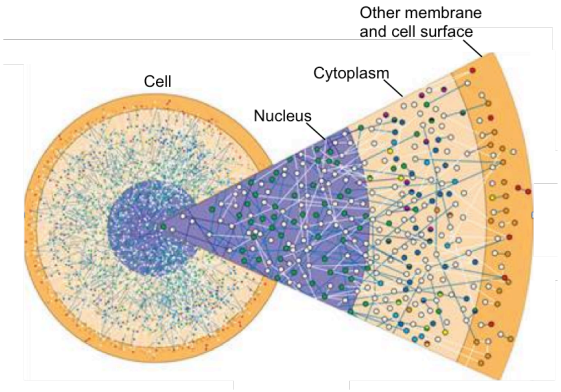

Figure 1.1: A system map illustrating the interactions between proteins in a fruit fly cell constructed from databases of known proteins and their interactions. The map shows 3,500 proteins (dots) located at different cellular positions with their interaction network (lines). Image reproduced from reference 1.

Proteins are widely recognized as one of the most important classes of biomarkers for many diseases including bladder cancer[6], breast cancer[7,8], colorectal cancer[8], esophageal cancer[8,9], liver cancer[10], lung cancer[8,11], leukemia[8], kidney cancer[12], ovarian cancer[13], prostate cancer[8,14], pancreatic cancer[13], cardiovascular disease[15], Alzheimer's disease[16], tuberculosis[17] and severe acute respiratory syndrome (SARS)[17]. Variations in the amount, structure and function of proteins associated with a disease can be used to discriminate between healthy and diseased individuals and may be effective at identifying the presence of the disease at an early stage[18,19]. Moreover, studies of proteins can be used to elucidate disease mechanisms and predict the response of patients to treatments or side effects that might occur[13]. In recent years, proteins have also become central figures in the process of drug development by serving as therapeutic targets used to monitor the efficacy of medical treatments[20]. Accordingly, the study of proteins expressed in cells, tissues or organisms (proteomics) has attracted increasing attention in recent years since a

comprehensive understanding of proteomes (the entire protein compliment in a cell, tissue or organism expressed by a genome[21]) will almost certainly lead to the discovery of novel biomarkers and the development of diagnostic tools and novel drug therapies[22, 23,24].

1.2 Proteins

Proteins are biological macromolecules found in every cell in a living organism. Thousands of different proteins have been identified and characterized. They range from low to high molecular weight and exhibit a diversity of biological functions. These include catalytic proteins (or enzymes), regulatory proteins (or hormones), antibodies, structural proteins (such as muscle fibres, hair, horn, wool, nails and feathers) and proteins involved in cell-cell recognition etc[1,2,18] (**Figure 1.2a**). Proteins are polymeric molecules formed from a linear chain of amino acid residues. Standard amino acids can be categorized into five groups based on their chemical properties. Members of the first group contain a nonpolar, uncharged aliphatic *R* group and consist of glycine, alanine, proline, valine, leucine, isoleucine and methionine. Members of the second group possess an aromatic *R* group and consist of phenylalanine, tyrosine and tryptophan. Molecules in the third contain a polar, uncharged *R* group and consist of serine, threonine, cysteine, asparagine and glutamine. The fourth group consists of lysine, arginine and histidine, where each contains a basic polar and positively charged *R* group, whereas the final group consisting of aspartate and glutamate contains a negatively charged *R* group[2].

Proteins normally exhibit four distinct aspects of structure, termed primary structure, secondary structure, tertiary structure, and quaternary structure (**Figure 1.2b**). The primary structure of a protein consisting of a linear polypeptide chain simply refers to the linear sequence of amino acids in the chain. The secondary structure of a protein is established by the formation of hydrogen bonds between amino groups (NH) and carbonyl groups (CO) on the same polypeptide chain (yielding an alpha helix or a rod-like structure) or on different polypeptide chains (yielding a beta sheet structure). In an aqueous system, when an alpha helix or a beta sheet polypeptide chain arranges itself so that its hydrophobic side chains point inside to form a non-polar core and its hydrophilic side chains point outside towards the solution, a tertiary structure (a globular compact three-dimensional structure) forms. In addition to the tertiary, multiple-subunit proteins

possess a quaternary structure. A dimer consisting of two identical subunits is the simplest form of quaternary structure[25].

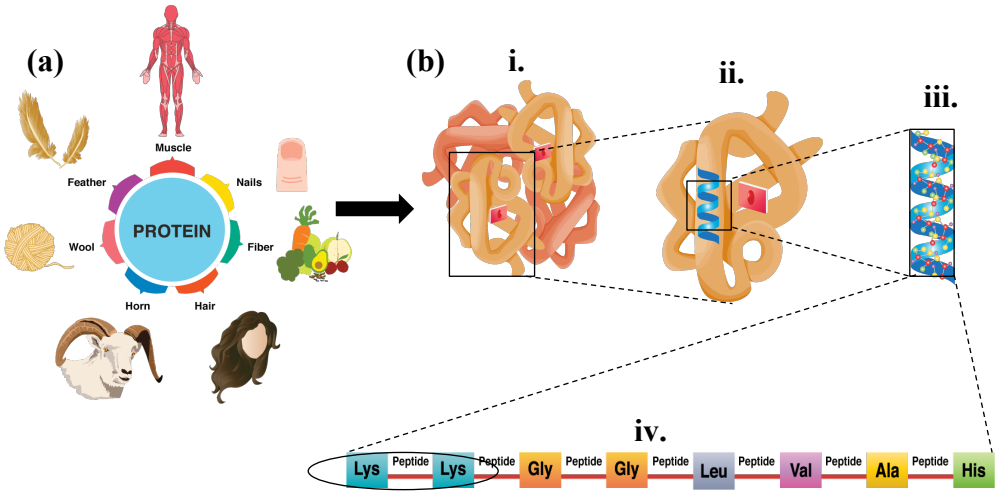

Figure 1.2: (a) Examples of proteins as functional components in nature; (b) Hierarchy of protein structure from the most complicated to the simplest structures (i) Quaternary structure consisting of 4 subunits called a tetramer, (ii) Tertiary structure defining the compact globular structure of a protein, (iii) An alpha helix describing secondary structure of a protein, (iv) Primary structure defined by the sequence of a linear polypeptide chain. Image (b) adapted from reference 2.

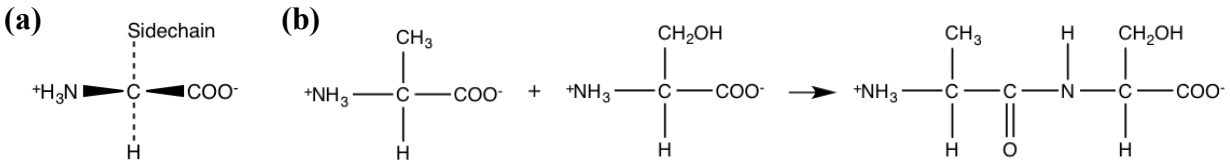

Figure 1.3: (a) General structure of an amino acid; (b) Formation of a peptide bond between two amino acids (i.e. alanine and serine). Images reproduced from reference 18.

Two amino acid residues (**Figure 1.3a**) can be covalently joined via a peptide bond (between a carboxylate group on one amino acid and an amino group on the other amino acid) to form a dipeptide (**Figure 1.3b**)[2,18]. When a large number of amino acid residues are joined, a polymer chain of amino acids known as a polypeptide forms. Although

proteins may consist of one or more polypeptides spontaneously folded into a specific conformation, only polypeptides having molecular weights of more than 10,000 are classified as proteins[1,2].

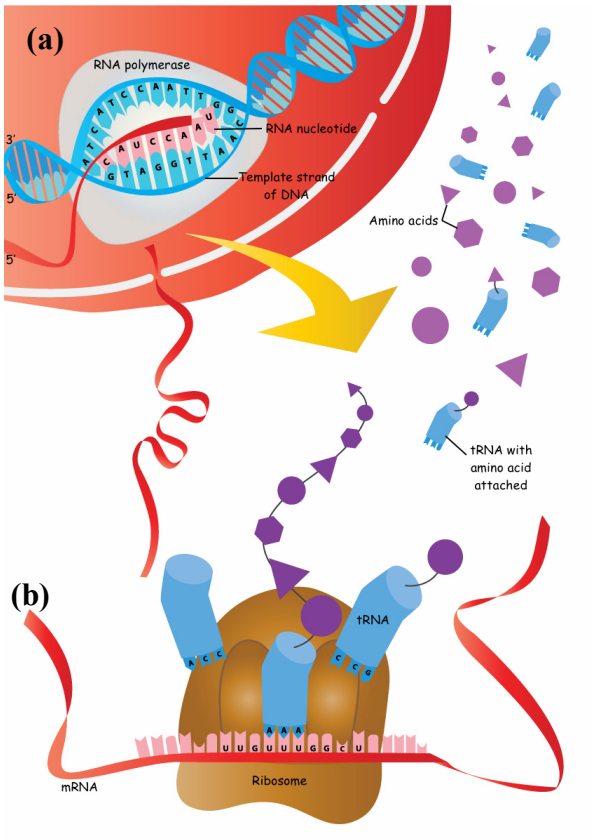

Figure 1.4: Protein synthesis (a) *Transcription*: A DNA double helix comprises a coding strand (read from the 5' end to 3' end) and a template strand (read from the 3' end to 5' end). During transcription, RNA polymerase finds a promoter sequence on the coding strand and attaches to the DNA. It then unwinds a short length of the double stranded DNA and separates the two DNA strands. The new RNA strand is then constructed by adding a new nucleotide that complements the nucleotide on the template strand at the 3' end. This process is repeated as the RNA polymerase moves along the template strand and stops when the enzyme reaches a termination sequence. The generated mRNA then migrates to the cytoplasm[26]; (b) *Translation*: First, a small ribosomal subunit attaches to the mRNA at the 5' end and then moves along the mRNA strand to find a start codon - a set of three bases. The first tRNA carrying the amino acid (methionine) with an anticodon pairs the anticodon with the start codon on the mRNA strand. In the meantime, a large ribosomal subunit joins the small ribosomal subunit and the first tRNA. Another tRNA molecule with an amino acid will bind its anticodon to the next matched codon inside the ribosome. When a peptide bond is formed between two amino acids, the first amino acid (methionine) leaves its attached tRNA. The process repeats again and again until the ribosome reaches a stop codon and the produced protein is then released[27]. Image (a) and (b) adapted from reference 1.

Each protein is constructed from a specific sequence of amino acids that is controlled by genetic information. Protein synthesis occurs via the processes of transcription and translation. During transcription, genetic information encoded from a template strand of deoxyribonucleic acid (DNA) is transferred to a messenger ribonucleic acid (mRNA). This process occurs in the nucleus of a cell (**Figure 1.4a**). The mRNA migrates from the nucleus into the cytoplasm where translation takes place. Protein translation involves four main components; mRNA, transfer RNA (tRNA), amino acids and ribosomes, that decode and translate the genetic information from the mRNA to a protein chain (**Figure 1.4b**)[26,27].

1.3 Conventional methods for high-throughput biological analysis

In biological research, the ability to assay or screen small volumes of analytes in an automated and rapid fashion is of critical importance. Conventionally, high-throughput analysis of biological samples is performed by parallel compartmentalization (e.g. using a well plate) or serial compartmentalization (e.g. by flow injection analysis).

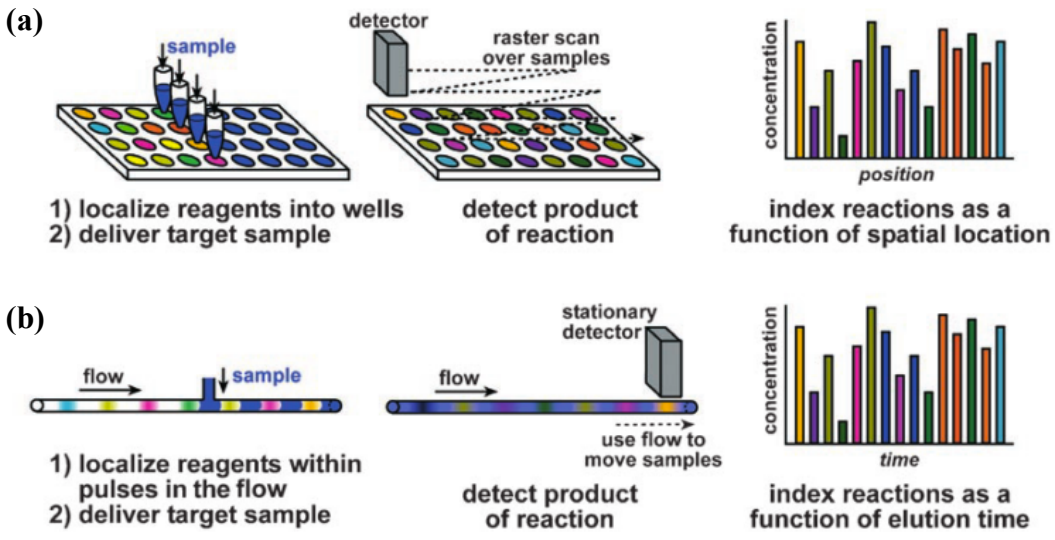

Figure 1.5: (a) Parallel compartmentalization using a well plate; (b) Serial compartmentalization using flow injection analysis. Images reproduced from reference 28.

In a well plate format, a sample is pipetted using a multichannel pipette into each well containing different reagents or different analytical conditions. Reaction products can be assayed using a plate reader in which an (optical) detector scans over or images (**Figure 1.5a**)[28]. Commercially available well plates are normally limited to 3456 wells with a minimum volume of ~1 μl[29,30]. In flow injection analysis, the sample is introduced into different reagent plugs (separated by a buffer solution) as the reagent flows along a length of tube. Reaction products are assayed when they pass through a downstream detector and signals as a function of elution times are extracted (**Figure 1.5b**)[28]. The use of well plates requires precise control of both fluid handling and is limited by potential evaporation of sample when using small well volumes. On the other hand, flow injection analysis encounters different problems. For example, dispersion has the potential to cause cross contamination between adjacent reagent zones and also presents difficulties in controlling reaction times and sample dilution[28]. In addition, complete automation of the analytical process when operating at high-throughput is difficult to achieve when conventional compartmentalization is utilized. To address these problems, the use of microfluidic systems for these analyses has been increasingly investigated in recent years.

1.4 Microfluidics: a new tool for biological analysis

Microfluidics defines the transportation and manipulation of ultra small volumes of fluid (typically between 10^{-9} to 10^{-15} litres)[31] within closed conduits having cross-sectional dimensions most conveniently measured in microns[31,32]. Such closed channels are generally constructed in substrates such as silicon, quartz, glass, and polymers (e.g. polydimethylsiloxane or PDMS and poly (methyl methacrylate) or PMMA)[33]. When functional processes such as sample introduction, sample pre-treatment, chemical reaction, product separation, and detection are integrated within a single microfluidic device, a micro total analysis system (μTAS) or Lab-on-a-Chip (LOC) is formed[34]. The miniaturization and integration of such processes within a single device affords short analysis times[32,35], portability[34,35,36], system automation[31,37], parallelization and high analytical throughput[37,38], minimal usage of sample and reagents[32,36], minimal waste generation[31], superior heat and mass transfer[32] and low-cost mass production[39]. Some of the key advantages of using microfluidic devices are a result of the vastly reduced diffusion lengths (and hence reduced mixing times when operating under laminar flow

conditions) and the huge increase in the reactor densities, which in turn increases the amount of chemical or biological information that can be extracted per unit time (**Table 1.2**).

Table 1.2: Some key device characteristics at three values of a characteristic length *d* [35]

Length *d*	**1 mm**	**100 µm**	**10 µm**
Volume	10^{-6} L	10^{-9} L	10^{-12} L
No. of molecules at 1 µM	6×10^{11}	6×10^{8}	6×10^{5}
Diffusion time	15 min	10 s	100 ms
Arrangement	25 volumes/cm^2	2500 volumes/cm^2	25×10^{5} volumes/cm^2
Arbitrary information density	1.5 values/min•cm^2	250 values/s•cm^2	2.5×10^{6} values/s•cm^2

Due to the advantages that microfluidic systems offer, an enormous number of applications ranging from chemical synthesis and analysis[40,41], high-throughput screening[42,43,44,] clinical diagnostics[41,45,46], DNA analysis[41,47] and cell-based assays[48,49] have been reported over the past two decades. Although microfluidic systems offer significant advantages when compared to macroscale platforms, single phase flows are still limited in some respects, e.g. in terms of sample dilution, cross contamination of reagent zones, difficulty in controlling reaction times, adsorption of reagents onto channel walls[28]. To eliminate these problems and to increase the potential of microfluidic technology in biological analysis, the compartmentalization of reagents in droplets dispersed in an immiscible carrier fluid has recently been used to good effect[28,39].

1.5 Droplet-based microfluidics

Droplets produced in microchannels, so-called microdroplets, typically have dimensions of a few microns[39] and volumes ranging from femtolitres to nanolitres[50]. Microdroplets are formed within microfluidic channels when a continuous phase (which normally wets

the microchannel walls) encloses a dispersed and immiscible phase. Droplets can be generated by various means but the most common methods that allow production of highly monodisperse droplets (<1-3% dispersity)[50] at high formation rates (up to several kHz)[51] involve the use of T-junctions and flow-focusing geometries[39,50].

For a T-junction geometry (**Figure 1.6**), a dispersed phase (normally aqueous) is injected perpendicularly to a continuous immiscible phase resulting in droplet generation through shear force and interfacial tension at the interface between the two fluids[28,39]. By changing fluid flow rates, channel widths or the relative viscosity between the two fluids, the size of droplets can be controlled[52].

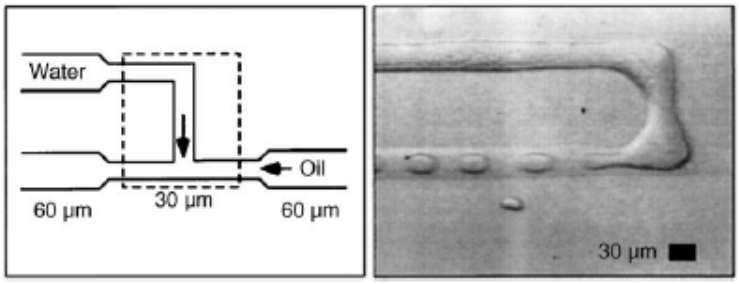

Figure 1.6: Microdroplet formation using a T-junction. In this case, an aqueous phase (i.e. water) is injected into a continuous oil phase. Image reproduced from reference 54.

Varying droplet contents or achieving concentration gradients using T-junction geometries can be accomplished with some limitations. For example, concentration gradients obtained by varying flow rates of sample and diluent as shown in **Figure 1.7** are limited by the need to adjust flow rates at each step to achieve serial concentration-gradient droplets, which in turn significantly lengthens the entire process[53].

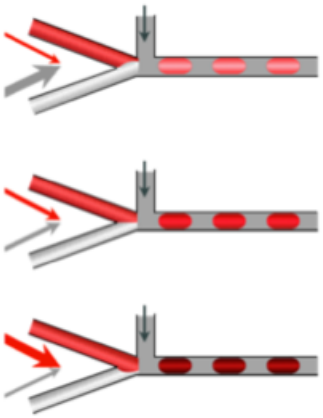

Figure 1.7: A Schematic showing concentration-gradient droplets formed in a T-junction geometry by varying sample (red) and diluent (light grey) flow rates in which the magnitude of flow rates are indicated by the size of the arrows. The dark grey represents the oil phase. Image reproduced from reference 53.

In the case of a flow-focusing geometry, a dispersed phase flows through a central channel that is sandwiched by a continuous phase flowing through two flanking channels. Both phases are then forced to flow through a small orifice, which is placed downstream as shown in **Figure 1.8**. The formation of droplets in or beyond the orifice occurs due to pressure and viscous stresses provided by the outer continuous phase[28,39]. Although the configuration of the flow-focusing is marginally more complicated than that of the T-junction, it allows the production of small or viscous droplet populations exhibiting low size dispersions[28,39].

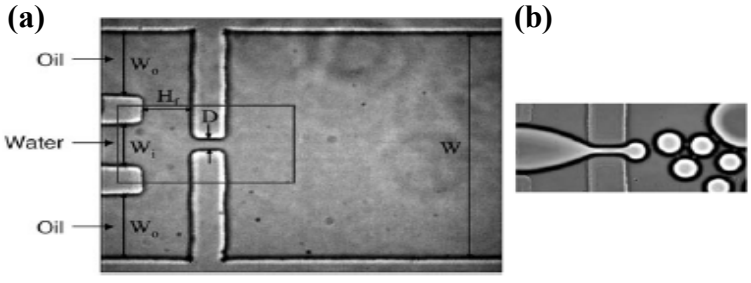

Figure 1.8: Microdroplet formation using a flow-focusing geometry (a) Water flows from the middle channel and is sandwiched by oil flowing from the two side channels into an orifice. Water-in-oil droplets are formed downstream of the orifice; (b) Droplets are generated when the aqueous and oil phases pass through the orifice. In the absence of surfactants, small droplets may merge and form larger droplets after generation. Image reproduced from reference 55.

In a channel containing continuous and miscible microflows, liquid typically moves under laminar flow, which can be characterized by the dimensionless Reynolds number (*Re*). *Re* defines the ratio of inertial and viscous forces and can be calculated according to **Equation 1.1** as

$$Re = \frac{\rho v d}{\eta} \tag{1.1}$$

where ρ is the density of the fluid (kg/m^3), v is the fluid velocity (m/s), d is characteristic dimension or tube diameter (m) and η is the dynamic viscosity of the fluid (kg/m·s)[40].

Laminar flow normally occurs when *Re* values are significantly below 2000[56]. Under laminar flow conditions, the mixing of reagents only occurs through diffusion of fluid elements orthogonal to the flow direction. On the other hand, reagent mixing within a segmented flow may be accelerated by chaotic advection[28]. Here, a droplet consisting of multiple reagents moving along a straight channel exhibits convection within each half of the droplet (two symmetrical halves form on the left and the right of the droplet with respect to the flow direction), with diffusion only occurring across the interface between the two halves (**Figure 1.9a**). However, the movement of a droplet along a winding channel allows for chaotic advection in which reorientation at the interface of the two halves as well as the stretching and folding of the contained striations leads to an exponential reduction in diffusional distances and thus mixing times (**Figure 1.9b**)[28].

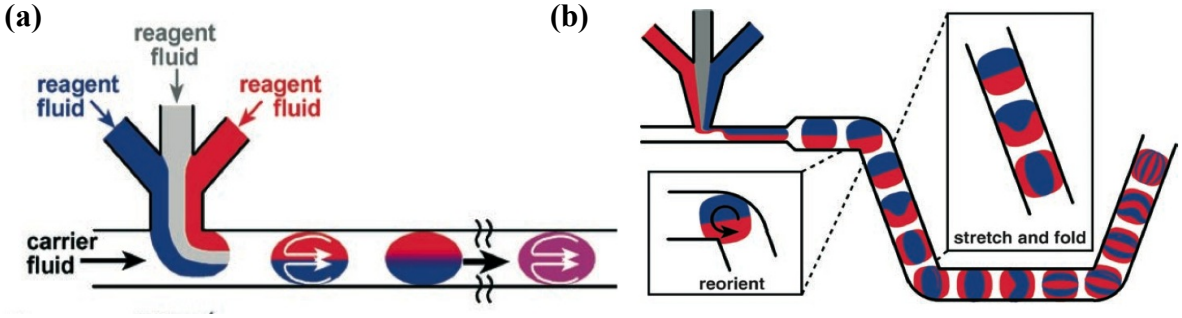

Figure 1.9: (a) Mixing in droplets flowing in a straight channel (b) Mixing in droplets flowing in a winding channel. Images reproduced from reference 28.

Droplets formed within microchannels can be manipulated in many ways to fulfill a range of unit operations. Various concentration gradients in droplets can be achieved by controlling the flow rates of either the sample or reagent streams[28,53]. Importantly, to examine multiple reaction conditions against a single sample, a cartridge technique can be used, where the sample is introduced via a T-junction into pre-formed droplets containing various reagents[28,53]. Droplet contents can also be varied by directly introducing reagents to droplets via side channels[28]. Furthermore, serial dilution of droplet contents can be performed by adding diluent droplets to a large 'mother droplet' to generate diluted 'daughter' droplets[57]. Different sample or reagent droplets can also be sequentially generated using automated droplet generators that provide for droplet-on-demand platforms[53,58,59]. Other droplet-based manipulations that enable complex chemical and biological experimentation include droplet merging, splitting, sorting, and trapping[28,39,51].

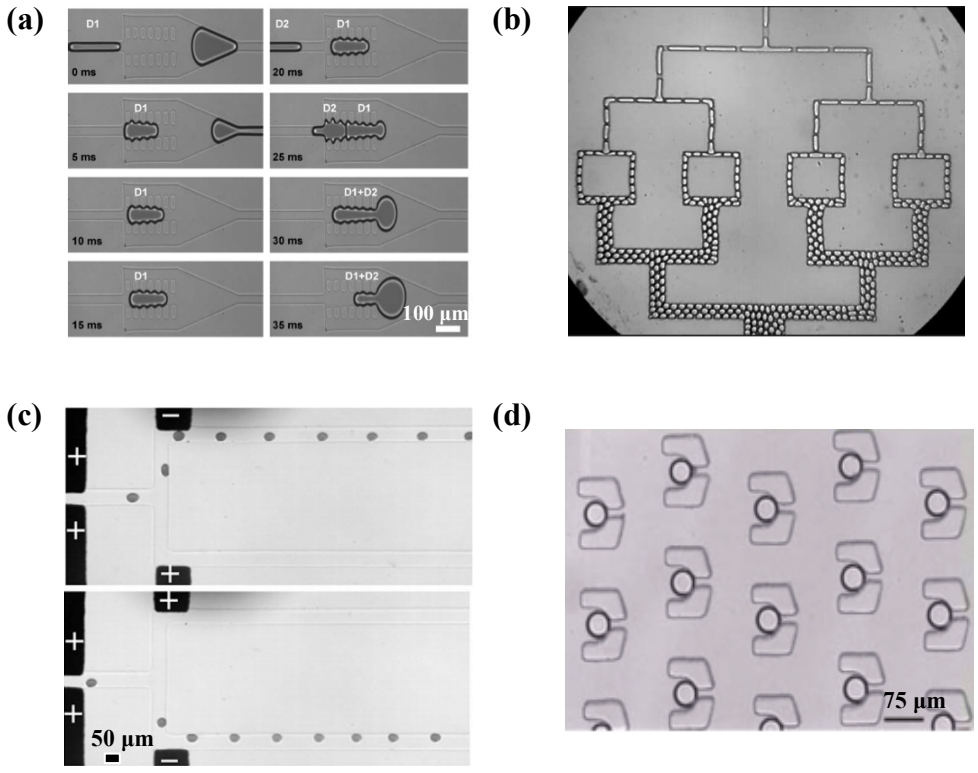

Figure 1.10: Droplet manipulations (a) Passive merging of two adjacent droplets[60] (b) Sequential splitting of droplets[61] (c) Dielectrophoretic sorting[62] (d) Droplet trapping arrays[63]

Droplet merging and splitting operations allow multi-step reactions to be performed with significant operational and configurational flexibility[28] since the initiation and termination of reactions can be controlled with precision. For example, **Figure 1.10a** shows the passive merging of two adjacent droplets using a pillar-array device developed by *Niu* and co-workers[60]. In addition, *Link* and co-workers[61] reported the use of a hierarchical T-junction device to facilitate the sequential splitting of droplets, as shown in **Figure 1.10b**. Another key droplet manipulation operation is droplet sorting. This allows the separation of the droplet of interest from a larger droplet population[52]. **Figure 1.10c** shows droplet sorting by means of dielectrophoresis. In this case, droplets migrate into one of two branches depending on the electrode charge[62]. Moreover, droplet trapping is very useful for the investigation of chemical and biological experiments that need extended times to proceed, such as cell incubation and protein expression[50]. **Figure 1.10d** shows an example of droplet trapping in which each droplet is localized and stored inside a trap for further investigation prior to being released[63].

In conclusion, the utilization of droplet-based formats not only provides for the same advantages as continuous-flow microfluidic systems, but crucially prevents the dilution, dispersion and cross-contamination of the analytes. Furthermore, an extraordinary large number of different reaction conditions can be screened in ultra-short times. This provides for a novel and direct route to high-throughput screening of biological samples.

1.6 Protein analysis

Proteins represent only about 0.01% of the molecular population contained within a human cell, but can be categorized into approximate variants (**Table 1.1**)[5]. This means that most protein types are present in a cell at very low analytical concentrations. For this reason, proteins of interest normally must be separated and purified from cellular organelles and other proteins prior to analysis. Cells can be lysed by several methods (based on physical, chemical, optical, electrical and acoustic methods[64,65]) to release the contained materials into solution. Unfortunately, this almost always (on the macroscale) results in extreme dilution of the contained materials including proteins. The solution is then centrifuged to fractionate subcellular contents or organelles on the basis of size (**Figure 1.11a**). It is also possible to separate subcellular contents that differ in density by

means of isopycnic centrifugation in which subcellular contents migrate in a medium containing step gradients of density and stop when they reach a point where their density matches the density of the medium (**Figure 1.11b**).

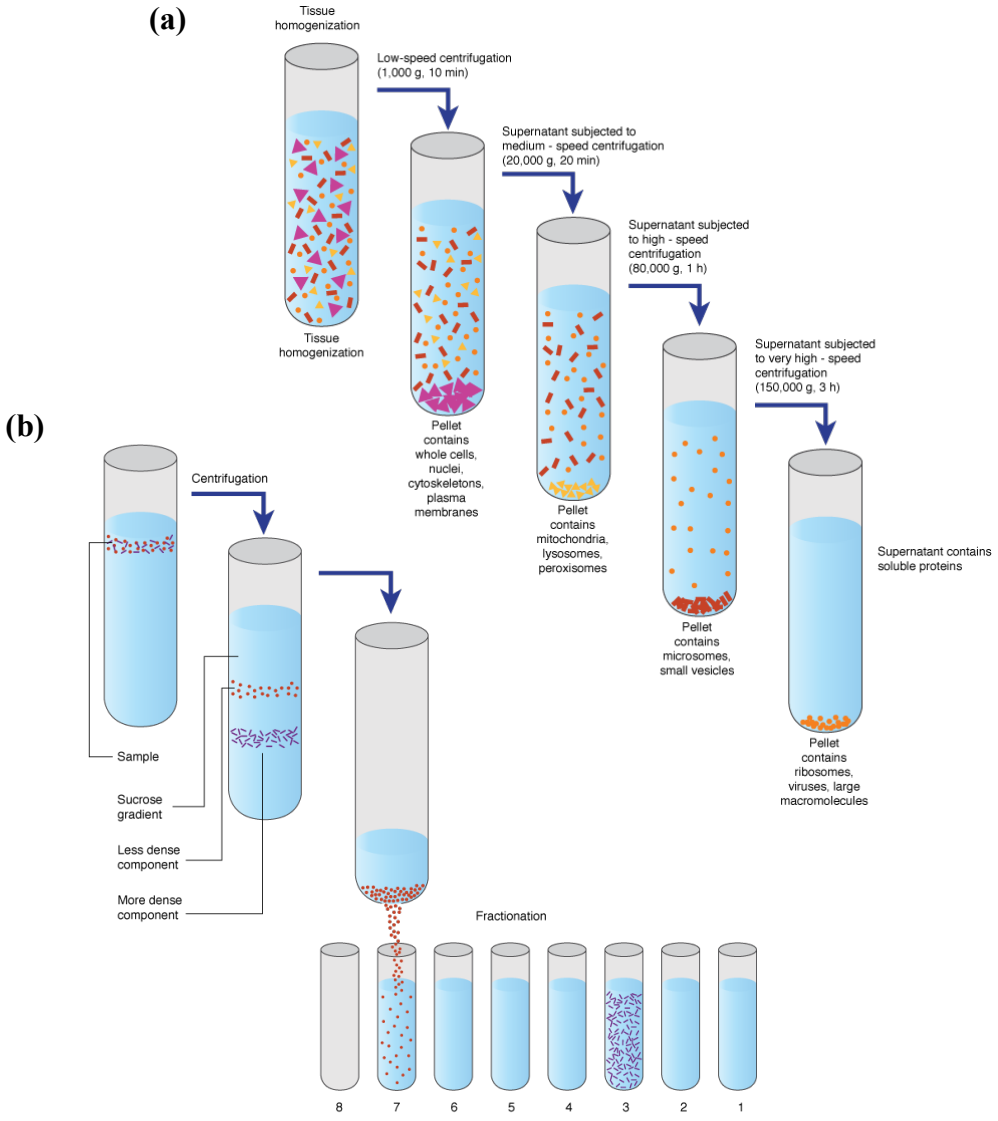

Figure 1.11: Schematics of (a) Differential centrifugation and (b) Isopycnic centrifugation. For differential centrifugation, subcellular contents are fractionated based on their sizes. At low speeds and shorter centrifugation times, larger particles are precipitated at the bottom of the tube, while smaller particles remain in a supernatant. Repeated centrifugations at higher speeds and for longer times allow fractionation of the remaining subcellular contents. For isopycnic centrifugation, subcellular contents are fractionated based on their densities. Components migrate along a sucrose density gradient and stop moving when they reach a location in the gradient that matches its density. Images reproduced from reference 2.

To extract proteins of interest from fractionated cellular components, salt (ammonium sulfate) is added to precipitate the proteins out of solution. The solution containing proteins of interest is then dialysed to remove other particulates (**Figure 1.12**). Proteins remaining in the dialysis bag or tube can then be further fractionated using column chromatography.

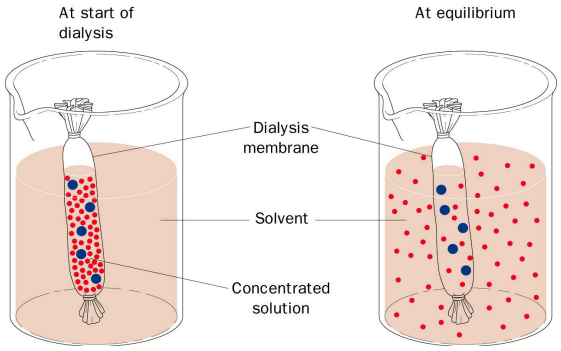

Figure 1.12: Dialysis. Only small molecules can penetrate through a membrane of a dialysis bag or tube, while proteins are retained inside the dialysis bag or tube. Image reproduced from reference 66.

The primary chromatographic methods used in protein separation are ion-exchange chromatography (**Figure 1.13a**), size-exclusion chromatography (**Figure 1.13b**) and affinity chromatography (**Figure 1.13c**). Ion-exchange chromatography is used to separate proteins based on differences in charge. In this method, a column is packed with charged polymer particles, called cation exchangers if polymer particles are negatively charged and anionic exchangers if polymer particles are positively charged. **Figure 1.13a** illustrates a column packed with negatively charged polymer beads. In this case, negatively charged proteins will migrate faster and elute earlier than positively charged proteins since the latter will bind with the negatively charged beads within the column, which in turn retards their migration rate. Size-exclusion chromatography separates proteins on the basis of their sizes. In this method, larger proteins elute faster than smaller ones because the smaller proteins are able to enter pores of polymer beads packed in a column (and thus spend some time in the pores prior to elution), whilst larger proteins cannot enter these pores and thus take less time to pass through the column as shown in **Figure 1.13b**. In affinity chromatography, the stationary phase consists of polymer beads

bound by a particular chemical group (or ligand). Proteins having a binding affinity for the ligand will bind to the polymer beads, while other proteins are washed out. The ligand-bound proteins are then eluted by adding ligand solution (**Figure 1.13c**)[2]. All the above methods separate proteins on the basis of differences in charge, size and binding affinity. Proteins can also be separated using electrophoresis[2,25].

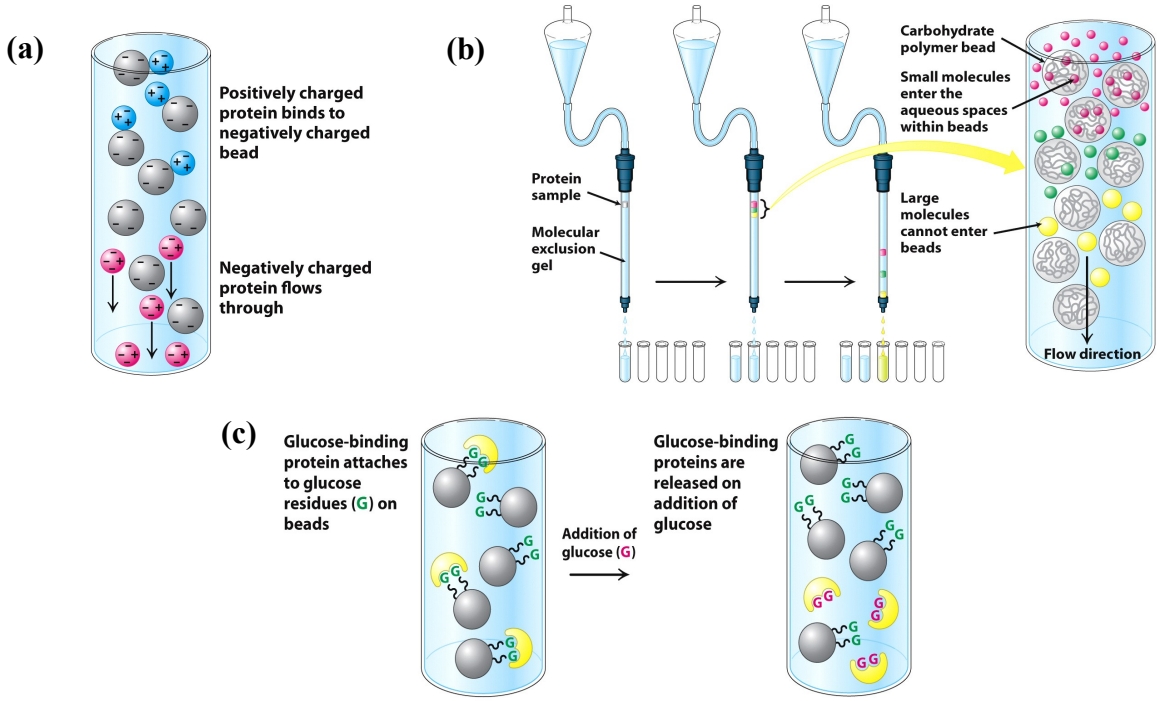

Figure 1.13: (a) Ion-exchange chromatography (b) Size-exclusion chromatography (c) Affinity chromatography. Images reproduced from reference 25.

1.7 Electrophoresis

Electrophoresis is a well-established separation technique that provides for the rapid and efficient separation of charged species[67]. When charged species migrate under an applied electric field, they separate based on the differences in their electrophoretic mobilities, which are controlled by the charge-to-mass ratio[68]. In simple terms, an ion of small size and high charge will move faster than an ion of large size and low charge[68]. Electrophoresis can be broadly categorized into three major experimental formats: slab

gel electrophoresis, capillary electrophoresis and microchip (or chip-based) capillary electrophoresis[69].

1.7.1 Slab Gel Electrophoresis (SGE)

Slab gel electrophoresis involves the use of a gel layered into a flat sheet as a support medium for electrophoresis. SGE has commonly been used to perform DNA analysis (due to the fact that DNA fragments of varying size will have essentially the same charge-to-mass ratio, and thus cannot be separated using free zone separations) and two-dimensional separations of proteins[70]. In the common vernacular slab gel electrophoresis usually refers to the separation of molecules in a polymer-based sieving medium. Typically, the gel is made from a cross-linked polyacrylamide or cellulose matrix, which acts as a molecular sieve[71]. To perform a separation, proteins are firstly linearized (or denatured) by heating in the presence of excess sodium dodecyl sulfate (SDS) and a reducing agent (such as β-mercaptoethanol or dithiothreitol)[71,72]. SDS hydrophobically and uniformly binds to linearized proteins. This binding interaction results in SDS-protein complexes with a net negative charge and with the charge-to-mass ratio of each SDS-protein complex being similar. SDS-protein complexes will, therefore, move under an applied electric field through a sieving matrix at a velocity defined by their molecular weight or size (**Figure 1.14**). For instance, a smaller protein will move more easily and more quickly through a sieving matrix than a larger one. Finally, separated proteins are stained with a dye such as Coomassie blue for visualization[2,72].

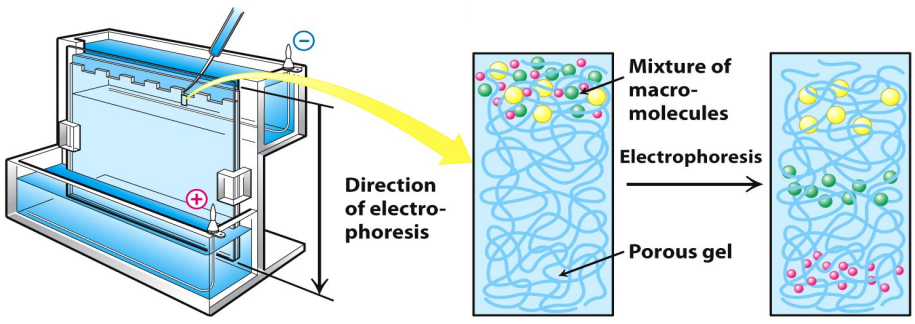

Figure 1.14: Slab gel electrophoresis. Smaller proteins can pass through the pores of a gel with ease and will, therefore, elute faster than larger proteins. Image reproduced from reference 25.

Another form of slab gel electrophoresis used in protein analysis is isoelectric focusing (IEF). Isoelectric focusing is a variant of electrophoresis utilized to separate amphoteric molecules containing both positively and negatively charged groups[73]. Amphoteric molecules, e.g. peptides and proteins, can exhibit a net positive or negative charge depending on the pH of the surrounding environment[74]. At a specific pH where positive and negative charges in an amphoteric molecule are balanced, an amphoteric molecule will be neutral; the specific pH being defined as the isoelectric point (pI) of the molecule[73,74].

In order to perform IEF, a mixture of carrier ampholytes (amphoteric molecules that are aliphatic, oligo-amino, oligo-carboxylic acid molecules[75,76] of varying length and branching and having molecular weight of around 200 to 1000[74,77]) is combined with an anti-convective polymer (e.g. polyacrylamide) and placed on a glass or plastic plate. This plate is placed between two electrodes, which are in contact with electrolyte solutions: an anode immersed in an anolyte (a low pH electrolyte solution) and a cathode immersed in a catholyte (a high pH electrolyte solution)[74]. When an electric field is applied, each ampholyte starts to move toward an appropriate electrode and will stop when a zero net charge is achieved (i.e. when the pH equals the pI). More acidic carrier ampholytes will migrate towards the anode, while more basic carrier ampholytes will migrate towards the cathode. When the system is in equilibrium and all ampholytes have stopped, the pH gradient (the arrangement of carrier ampholytes according to their pI) is established[73,74,78]. Subsequently, a protein mixture is added to the stable pH gradient gel. Proteins will migrate under the influence of an electric field until they reach a location where pH is equivalent to their pI and the separated zones visualized using dyes or stains after focusing[2,74].

Although both of the slab gel electrophoresis embodiments can be employed to separate proteins successfully, they are laborious, complex and time-consuming. Moreover, low voltages can only be used since heat dissipation in large volume systems is poor. Improvements in slab gel IEF have been realized by replacing the slab gel with an immobilized pH gradient (IPG) strip[24,79]. However, automatic operation and data acquisition are still difficult to achieve. Therefore, “capillary” electrophoresis formats have been introduced to solve these problems[74].

1.7.2 Capillary Electrophoresis (CE)

Capillary electrophoresis (CE) takes place in narrow-bore capillary tubes normally having an inner diameter (I.D.) between 20 and 100 μm[73]. Over the past 30 years, CE has emerged as a useful separation tool in chemical, biochemical and pharmaceutical applications due to distinct advantages over the conventional slab gel format[19,20]. For example, CE can provide for highly automated, rapid, and high-efficiency separations of either charged or neutral molecules using minute amounts of sample. In addition, heat dissipation in small-bore capillaries is far more efficient than in slab gel electrophoresis because of the significantly higher surface-to-volume ratios. This allows high applied potentials to be used, leading to faster and more efficient separations[19,67].

The evolution of capillary electrophoresis began in the late 19th century[67]. However, it was defined as free solution electrophoresis in capillaries in 1967 when *Hjertén*[80] performed the first free solution capillary electrophoresis in a tube having inner diameter of 3 mm. Later in 1979, *Mikkers et al.*[81] reported the use of polymer capillaries having inner diameters of 200 μm. In 1981, *Jorgenson* and *Lukacs*[82] introduced the standard theory and practical embodiment of glass capillary electrophoresis with capillary diameters less than 100 μm. Since then a wide range of applications that utilize CE as an analysis tool has been developed and reported[67].

1.7.2.1 Capillary electrophoresis formats

Capillary electrophoresis can be operated in various modes including capillary zone electrophoresis (CZE), capillary gel electrophoresis (CGE), capillary isoelectric focusing (cIEF), micellar electrokinetic capillary electrophoresis (MEKC), capillary isotachophoresis (cITP), and capillary electrochromatography (CEC)[67,73]. These modes are commonly used for the separation of biomolecules such as DNA, proteins, peptides and amino acids[19,20,83] and will therefore be introduced briefly.

Capillary zone electrophoresis (CZE), also known as free-solution capillary electrophoresis (FSCE)[84], is the simplest and most widely used form of CE used to separate charged molecules. Separation is simply based on differences in electrophoretic mobilities, which are governed by molecular size and charge. The velocity of charged

molecules travelling along a capillary filled with a conductive buffer solution and with an applied voltage across a channel is also defined in large part by electroosmotic flow or EOF[67,85].

Capillary gel electrophoresis (CGE) is a common mode of CE directly related to conventional slab gel electrophoresis. It makes use of a molecular sieving matrix, and results in the separation of compounds based on their molecular sizes. In simple terms, larger molecules can pass through the pores of the gel matrix less easily than smaller ones. As a result, larger molecules take more time to migrate to the detector. The molecular sieving matrix also helps to reduce broadening of analyte bands that occurs as a result of solute diffusion and convection currents caused by temperature gradients during electrophoresis[67,84]. The presence of a molecular sieving matrix has also been shown to minimize electroosmotic flow and to prevent the adsorption of solute onto capillary walls[67]. As mentioned in **Section 1.7.1**, slab gel and capillary gel electrophoresis have been extensively used in DNA sequencing[86,87]. For protein separations, *Karger et al.* introduced the use of cross-linked polyacrylamide gels containing SDS as a sieving medium for high-efficiency separation of proteins[88]. This technique is called capillary sodium dodecyl sulfate - polyacrylamide gel electrophoresis or capillary SDS-PAGE, and provides significant advantage in DNA, protein and polynucleotide analysis[72].

Due to the problems associated with conventional slab gel IEF described earlier, *Hjertén* and *Zhu*[89] first proposed the IEF separation of proteins in 200 μm I.D. glass capillaries. The separation principle in cIEF is similar to IEF. However, after focusing, separated zones can be removed from a capillary by establishment of a pressurized flow or by adding salt to the anolyte or catholyte. The latter results in a pH imbalance gradient that makes the focused analyte zones migrate. The utilization of cIEF allows for the use of high voltages, which in turn increases both resolution and decreases separation speed[67].

Micellar electrokinetic capillary electrophoresis or MEKC is one of the most useful CE modes for neutral biomolecular separations and was introduced by *Terabe* and co-workers[90] in 1984. This mode involves the addition of an ionic surfactant above its critical micelle concentration (CMC) into a buffer solution to form micelles that serve as a pseudostationary phase[91], while EOF acts as a mobile phase[92]. Commonly, SDS is used

as the surfactant since it forms anionic micelles with hydrophobic tails pointing into the centre of the micelles and hydrophilic heads pointing outwards into the buffer solution. The anionic SDS micelles are negatively charged on the surface and hence, they tend to move towards the anode. However, in a bare fused silica capillary at neutral or basic pH, the flow of EOF toward the cathode is much greater than the electrophoretic migration of the SDS micelles. Consequently, SDS micelles migrate towards the cathode at a slower velocity than the bulk solution. For example, when neutral molecules are separated by MEKC, each neutral molecule will interact differently with micelles depending on its hydrophobicity. In other words, highly hydrophobic, neutral molecules will spend more time inside the micelles and will migrate at the same rate, whereas highly hydrophilic, neutral molecules stay in a bulk solution and will migrate at the bulk solution flow rate. Thus, MEKC makes the separation of neutral molecules possible[67].

Capillary isotachophoresis (cITP) is an electrophoresis mode established through use of a discontinuous buffer system and separates ionic species based on differences in their electrophoretic mobilities[67]. An isotachophoretic separation has a leading electrolyte (LE) and a terminating electrolyte (TE) placed at different sides of the capillary. In this format the sample ions are placed between the LE and TE. The LE contains "leading ions" with the same charge as the sample ions but higher mobility, while the TE contains "terminating ions" of the same charge as the sample but lower mobility than all the sample ions[93,94]. During separation, a mixture of analytes is injected between the LE and TE and a constant electric field is applied. The polarity of the electric field is chosen depending on the charge of the leading ion. Application of the field will result in a low potential drop across the LE zone and a high potential drop in the TE zone. Analytes will migrate slowly in the LE zone and faster than the TE co-ions in the TE zone, resulting in a focusing of the analyte ions. The process of isotachophoresis, like IEF, can be divided into two steps. The first step involves the separation of the ions and the migration velocity of the individual ions in the mixed zones is different. In the second part a steady state is achieved, the ions have already separated from one other and all move with the same velocity. Consequently, once steady state is reached, the mixed zone disappears and the analyte components are completely separated between the LE and TE zones. Other buffer elements include counter ions, which aid in buffering and imaging (i.e. counter ions absorb more UV light compared to the sample ions enabling their detection). Detection is

performed downstream of separation and the length of each analyte band/zone can then be measured for quantitative analysis[93,94,95].

Capillary electrochromatography (CEC) is based on the marriage of capillary electrophoresis (CE) and high-performance liquid chromatography (HPLC). Here separation occurs in a small bore capillary packed with a particulate stationary phase, employing EOF to drive the mobile phase through the packed capillary. The order of elution depends on both the interaction of analytes with the stationary phase and electrokinetic migration velocities. Significantly, solute band dispersion is dramatically reduced in CEC, due to the plug flow profile, thus providing for exceptional separation efficiencies and peak resolution when compared to HPLC[96,97].

CE has been utilized in a wide range of applications over the past 30 years. For example, CZE, cIEF, MEKC and CEC (often coupled with mass spectrometry) have been used to determine a range of metal species such as selenium, arsenic, chromium, iron, mercury, aluminum, and zinc in biological and environmental systems[98]. In forensics, CE is commonly employed for illicit drug screening, the analysis of poisonous species in human fluid samples, toxicological analysis, the characterization of explosives and gunshot residues, and forensic investigations of DNA fingerprints[99]. Various modes of CE are used in food industries (e.g. cereals, fruit-based products, milk and dairy products, meat and fish products, soft drink, tea, alcoholic drink, vegetables, oils and sauces) for establishing food authenticity or adulteration, the analysis of nutrients in food, monitoring food processing and storage[100,101,102]. CE separations of a wide variety of mixtures such as organic compounds[86], inorganic ions[80,86], bases[80], nucleosides[80], nucleotides[80], nucleic acids[80,86], viruses, cells[80], subcellular particles[80], native and denatured DNA[80], DNA sequencing[86], amino acids[86], peptides[86] and proteins[80,86] are of critical importance in medical and pharmaceutical research[86,103,104].

1.7.2.2 Principle of separation in typical free zone CE

Figure 1.15 shows the basic instrumental setup used in capillary electrophoresis. The system consists of a capillary with both ends immersed in two buffer reservoirs, a cathode, an anode, a high-voltage supply, and a detector. The capillary is filled with

buffer solution prior to the introduction of a sample at one end of the capillary using either hydrodynamic or electrokinetic injection. A high voltage is then applied across the capillary causing two main phenomena: electrophoretic migration of analytes and electroosmosis (discussed in **Section 1.7.2.2**).

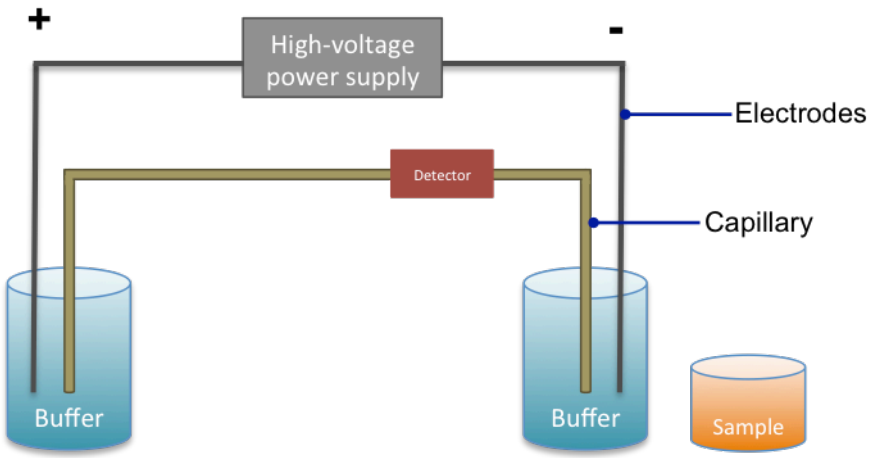

Figure 1.15: Instrumental setup of a standard capillary electrophoresis system consists of a capillary connecting two buffer reservoirs, a sample reservoir which can be replaced with one of the buffer reservoirs, two electrodes placed at each buffer reservoir to apply an electric field across the capillary using a high-voltage power supply, and a detector.

Analytes migrate based on their electrophoretic mobilities and on the magnitude and direction of electroosmotic flow and finally pass through the detector[67,68]. Various types of detectors can be used with CE such as UV-Visible absorbance detection, fluorescence detection, refractive index detection, surface-plasmon resonance detection, electrochemical detection and mass spectrometry detection[34]. The signal trace obtained from a fixed detector versus time is called an electropherogram[68]. Analytes separated in CE due to the differences in their electrophoretic velocities, v_{ep} (ms^{-1}), are present as peaks in an electropherogram. The electrophoretic velocity is defined as

$$v_{ep} = \mu_{ep} E \qquad (1.2)$$

where μ_{ep} is the electrophoretic mobility of an analyte ($m^2s^{-1}V^{-1}$) and E is the electric field strength (Vm^{-1})[67]. Besides the electrophoretic mobility, the migration of analytes also depends on electroosmotic flow, which describes the flow of a bulk solution in the presence of an applied electric field[85]. In a glass capillary at neutral or high pH, silanol groups on the capillary wall are deprotonated; thus, leaving an excess of negative charges on the wall. The negative charges are balanced to some extent by positive species from the bulk solution, and form an immobilized layer of ions. A second layer adjacent to the immobilized layer is termed the diffuse double layer, where positive charges accumulate but are still mobile[105]. When an electric field is applied, these mobile positive charges along with water molecules solvating them migrate toward a cathode. This causes a bulk electroosmotic flow with a velocity, v_{eo}, defined as

$$v_{eo} = \mu_{eo} E \tag{1.3}$$

$$\mu_{eo} = \frac{\varepsilon \zeta}{\eta} \tag{1.4}$$

Here μ_{eo} is the electroosmotic mobility ($m^2s^{-1}V^{-1}$), ε is the dielectric constant of the electrolyte, ζ is the zeta potential (V), and η is the viscosity ($kgm^{-1}s^{-1}$). Accordingly, the electroosmotic velocity can be defined using the Smoluchowski equation as

$$v_{eo} = \frac{\varepsilon \zeta}{\eta} E \tag{1.5}$$

According to the **Equation 1.5**, the electroosmotic flow velocity is directly proportional to the dielectric constant of the electrolyte, the zeta potential (defined as the potential gradient over the diffuse double layer[106]) and the electric field, while it is inversely proportional to the viscosity of the electrolyte solution. When the concentration of electrolyte increases, the zeta potential decreases due to compaction of the double layer[106] and the EOF decreases.

The total migration velocity of the analyte can then be defined as

$$\nu = \nu_{ep} + \nu_{eo} \tag{1.6}$$

Accordingly,

$$\nu = (\mu_{ep} + \mu_{eo})E = (\mu_{ep} + \mu_{eo})\frac{V}{L_C} \tag{1.7}$$

where V is the voltage applied across the channel, and L_c is the capillary length. The total mobility can also be determined by experimental measurement, i.e.

$$\mu = \frac{L_S L_C}{Vt} \tag{1.8}$$

where L_s is the separation length, and t is the migration time. The migration time is defined as the time that the analyte takes to travel from one end of the capillary to the other.

$$t = \frac{L_S}{\nu} = \frac{L_S L_C}{(\mu_{ep}+\mu_{eo})V} \tag{1.9}$$

The efficiency of separation is reduced by band broadening, which is caused by numerous factors including the finite injection volume (σ^2_{inj}), the detection volume (σ^2_{det}), adsorption of analytes on the capillary wall (σ^2_{ads}), longitudinal diffusion of analyte molecules (σ^2_{diff}), capillary temperature variations (σ^2_T), pressure drops (σ^2_P), and variations in the geometry of the channel (σ^2_G). In an ideal case, only longitudinal diffusion is appreciable. The longitudinal diffusion band variance is given by

$$\sigma^2_{diff} = \frac{2DL_S}{\nu} \tag{1.10}$$

where D is the molecular diffusion coefficient of the solute (m^2s^{-1}). The efficiency of a separation is described in simple terms by the theoretical plate number, N

$$N = \frac{L_S}{H} \tag{1.11}$$

where H is the plate height and defined by

$$H = \frac{\sigma_{diff}^2}{L_S} = \frac{2D}{(\mu_{ep}+\mu_{eo})E} \quad (1.12)$$

The efficiency of the separation is thus given by

$$N = \frac{L_S^2}{\sigma_{diff}^2} = \frac{(\mu_{ep}+\mu_{eo})VL_S}{2DL_C} \quad (1.13)$$

The resolution of the separation defines the ability to separate two adjacent peaks and is defined in the term of peak width and migration time as

$$R = \frac{2(t_2-t_1)}{W_1+W_2} \quad (1.14)$$

where t_1 and t_2 are the migration time of two adjacent separated peaks, w_1 and w_2 are the width at the base of each peak.

The relationship between resolution and efficiency is given by

$$R = \frac{1}{4}\frac{\Delta\mu_{ep}}{\mu_{eo}+\mu_{ep}}\sqrt{N} \quad (1.15)$$

where $\Delta\mu_{ep}$ is the difference in electrophoretic mobility between the two species and μ_{ep} is the mean electrophoretic mobility. According to **Equation 1.15**, resolution is directly proportional to the square root of theoretical plate number[107].

Inspection of **Equation 1.11** demonstrates that the separation efficiency can be increased by reducing the plate height, which can be achieved by increasing the electric field strength as shown in **Equation 1.12**. However, increasing the applied potential to increase the separation efficiency is limited due to Joule heating caused by current flow through the solution. Joule heating results in a rise in the buffer temperature, which in turn causes band broadening and hence decreases the separation efficiency. To overcome

such a limitation, microfluidic devices can be used to dramatically increase surface area-to-volume ratios and thus enhance heat dissipation.

1.7.3 Chip-based capillary electrophoresis

Capillary electrophoresis has been performed in chip-based platforms since the early 1990s due to its ability to manipulate small sample volumes, excellent heat dissipation characteristics, high-throughput operation and ability to produce high-resolution separations[85]. Various CE modes can be performed efficiently in chip-based platforms. The principles and operation of chip-based capillary electrophoresis are similar to the conventional CE, but include significant and additional advantages.

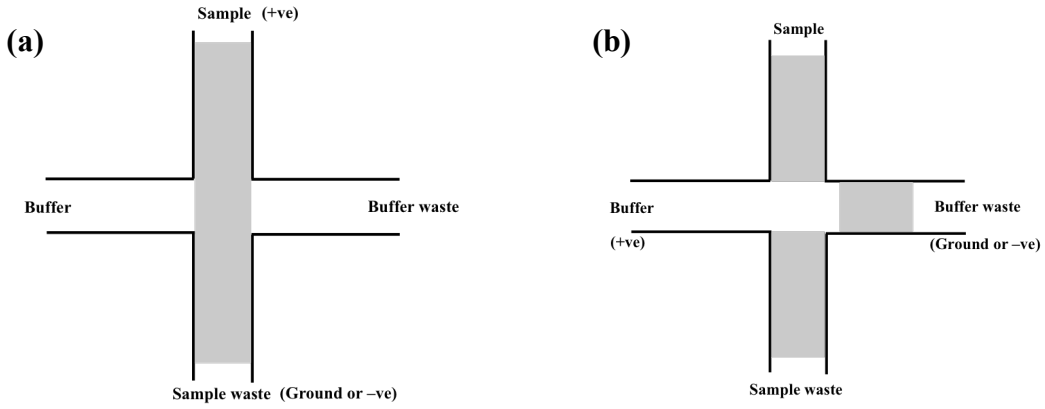

Figure 1.16: Schematics of a cross-piece microdevice with normal injection mode (a) During loading step; (b) During separation step

The simplest structure of a planar electrophoresis chip incorporates a cross-channel injection geometry as illustrated in **Figure 1.16**. The device consists of four reservoirs (a buffer, a buffer waste, a sample and a sample waste reservoir) located at each end of the channels. In the normal mode of injection, a voltage is applied between the sample and the sample waste reservoir to draw the sample towards the channel intersection in the loading step. The voltage is then switched and applied between the buffer and the buffer waste reservoir during the separation step. This mode of injection is simple but does not provide control over the injected sample volume due to two issues. The first is diffusion

of sample into the separation channel during sample loading and the second is sample leakage from the sample loading channel during separation. These issues can potentially cause peak broadening and increased background noise[108].

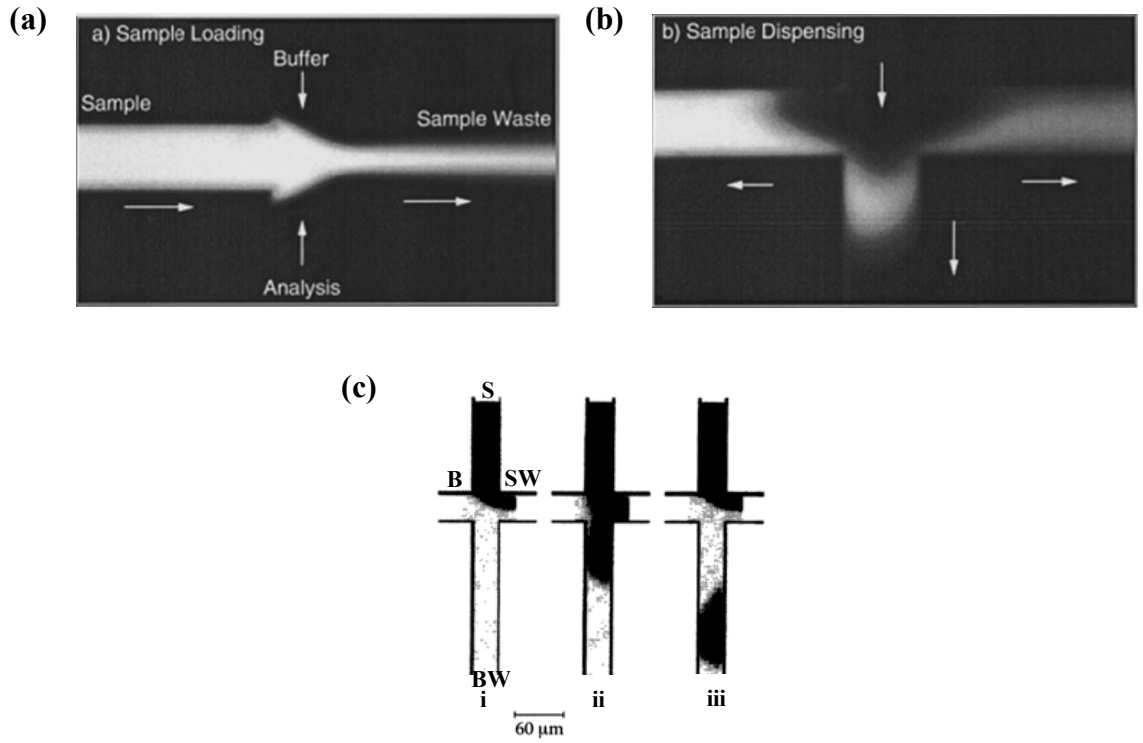

Figure 1.17: (a) Sample loading during pinched injection; (b) Sample dispensing during pinched injection; (c) Gated injection (i) Applied voltage for sample (S) = 700 V, buffer (B) = 1000 V, sample waste (SW) and buffer waste (BW) = 0 V, (ii) prior to injection: S = 700 V, B, BW and SW = 0 V, (iii) sample dispensing: voltages were shifted back to the same as those of (i). Image (a) and (b) reproduced from reference 108, while image (c) reproduced from reference 34.

To address these eventualities, "pinched" and "gated" injection schemes are commonly used to introduce samples. In pinched injection, a voltage (in addition to the voltage applied between the sample reservoir and sample waste reservoir) is also applied across a separation channel during the loading step to prevent sample from dispersing into a separation channel (**Figure 1.17a**). During separation, a small "push-back" voltage is also applied across the sample and the sample waste reservoirs to avoid sample leakage into the separation channel (**Figure 1.17b**). For gated injection, a sample migrates continually

along the flow of a buffer solution toward a sample waste reservoir. When the flow of the buffer stops (when the voltage is switched off), the sample is injected into a separation channel (**Figure 1.17c**)[34,85,108]. Use of either of these injection modes prevents dispersion of sample into a separation channel during the loading step and also leakage of the sample into a separation channel during the separation step. Furthermore, the amount of sample introduced can be controlled more precisely than when using normal injection modes.

Three types of materials are most commonly used to fabricate CE microdevices. These are glass or fused silica, polydimethylsiloxane (PDMS), and other plastics[108]. The adoption of glass (or silica-based materials), provides several advantages, including well-established microfabrication processes adapted from the semiconductor industry[33,85], excellent optical transparency over a wide range of wavelengths[85], well-understood surface chemistries, high EOF generation[109], low thermal expansion[33], good heat transfer (thermal conductivity ~1.4 W $m^{-1}K^{-1}$)[110] and low cost. However, the use of glass raises some problems including the need for time-consuming and complicated fabrication methods, high real costs of produced devices, device fragility and adsorption of biomolecules to the negatively charged channel surfaces[109]. To overcome these problems, alternative materials based on polymers have been investigated.

The major advantages associated with polymer-based microfluidic devices lie in the ability to mass produce devices at low unit cost using accessible fabrication methods such as hot embossing, injection molding, laser ablation, polymer casting[34,36] and 3D printing[111]. Moreover, polymer-based microfluidic devices are biocompatible and frequently more flexible than glass[112]. Commonly used polymers include polydimethylsiloxane (PDMS), poly methyl methacrylate (PMMA), polycarbonate (PC), poly ethylene terephthalate (PET), polystyrene (PS), cellulose acetate and polyvinylchloride (PVC).[36,51,108,109,47] Of these, PDMS has been the most popular substrate used to fabricate microfluidic devices[112].

PDMS is widely used in the fabrication of microfluidic devices because of the ease of device fabrication using soft photolithography that allows fast prototyping of complex designs[108,112]. PDMS is also optically transparent over a wide range of wavelengths[33], non-toxic, gas-permeable[33], elastomeric[51] and electrically insulating[51]. However, the

absorption of organic solvents, biopolymers, and small hydrophobic molecules can be a serious problem when using PDMS[108]. Native PDMS is hydrophobic, but still exhibits EOF[113]. EOF in PDMS microchannels is often found to be spatially inconsistent. Therefore, several methods have been employed for the modification of PDMS channels. These include dynamic and static wall coatings and oxygen plasma treatment[114,102]. For oxygen plasma treatment, oxygen radicals substitute the methyl group ($Si\text{-}CH_3$) with silanol groups (Si-OH). This renders the surface chemistry of the PDMS hydrophilic and broadly similar to glass. The surface can then be temporarily kept hydrophilic in a polar solvent. When a PDMS surface is in contact with an aqueous solution at pHs above 3, the silanol groups dissociate into SiO^- and H^+. Consequently, a negative surface charge is established. Since the hydrophilicity of a PDMS surface after oxygen plasma treatment is not permanent, hydrophilicity can be recovered by treating the channel with a strong base such as 1M NaOH[34].

1.8 Two-dimensional (2D) separation of proteins and problems with interfaces between two separation dimensions

In conventional protein and amino acid separations, two-dimensional gel electrophoresis is employed to achieve high peak capacities and high peak resolution[115]. The peak capacity defines the maximum number of peaks that can be resolved in separation space[116,117,118]. For two-dimensional separations, the total peak capacity is the product of peak capacities of the two orthogonal separation dimensions[115,119,120]. A two-dimensional separation is characterized as orthogonal if the separation mechanisms of the two dimensions are distinct. In other words, analytes are separated based on different physicochemical properties in each dimension[120]. For instance, 2D polyacrylamide gel electrophoresis (2D-PAGE) for protein analysis[121] employs IEF for the first dimension and SDS-PAGE for the second dimension (**Figure 1.18**). Although conventional 2D-PAGE provides peak capacities of 5000 or higher, it is slow, laborious and difficult to directly couple to mass spectrometry (MS) [86,122,123].

Two-dimensional capillary electrophoresis or column chromatography methods such as 2D-liquid chromatography (LC-LC), liquid chromatography-capillary electrophoresis

(LC-CE) and 2D-CE (CE-CE) are employed to provide higher speeds, easier automation and access to a broader range of biomolecules than conventional 2D-PAGE[115]. Several modes of CE (such as CZE, CGE, MEKC, cIEF and cITP) located either in the first or the second dimension are coupled to another LC or CE mode in an offline or online manner to provide 2D separations[123].

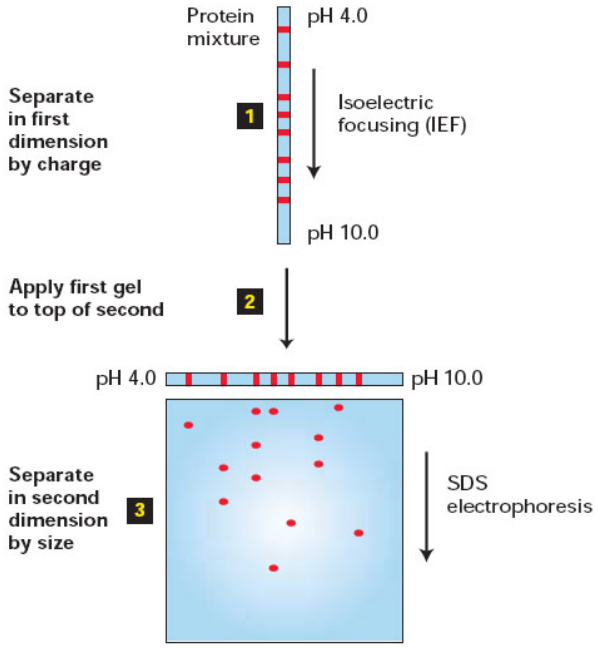

Figure 1.18: Two-dimensional gel electrophoresis. Proteins are separated by isoelectric focusing in the first dimension and by SDS gel electrophoresis in the second dimension. Image reproduced from reference 124.

In offline 2D systems, analytes are collected in several fractions after separation in a first dimension. The collected fractions are then treated prior to injection into the second dimension. Unfortunately, offline modes cannot provide for automated analysis, are time-consuming and plagued by sample dilution[123].

Online 2D separations can be categorized into three broad groupings: i) 2D separations in a single capillary, ii) coupling two separation techniques using an interface, and iii) coupling two separation techniques using mechanical valves[123]. 2D separations in a single capillary are achieved by performing one CE mode in the first dimension. Subsequently,

separated analytes remain in the capillary during the exchange of a buffer solution for a second CE separation. Chiral separations of amino acids, for example, can be performed using single-capillary 2D separations[125,126]. For hyphenated 2D separations, many interface systems have been employed. These include dialysis interfaces[127], porous junction interfaces[128,129], tee-union interfaces[130], flow gating interfaces[131], microreactor interfaces[132], nicked-sleeve interfaces[133] and hydrodynamic interfaces[134]. It is noted that six-port valves have usually been used as a mechanical valves for coupling two separation systems as reviewed in elsewhere[123].

Although the use of capillary electrophoresis or column chromatography for 2D separations is more convenient than that of 2D-PAGE, these techniques still exhibit some flaws. For instance, high analytical performance is difficult to achieve due to the inconvenient integration of different separation dimensions[135]. This also causes high dispersion at an interface between the two separation dimensions. Accordingly, much effort has been focused on the development of new techniques for protein separations based on two-dimensional microfluidic formats.

Table 1.3: Summary of two-dimensional protein separation within microfluidic platforms

First Dimension	Second Dimension	Chip Material	Interface	Detection	Peak Capacity	Analysis time (min)	Samples	Ref.
MEKC	CZE	Glass	Intersecting channels	Fluorescence	500-1000	< 10	Tryptic peptides from cytochrome c	136
MEKC	CZE	Glass	Intersecting channels	Fluorescence	4200	< 15	Tryptic digest of BSA	119
CGE	MEKC	PMMA	Intersecting channels	Fluorescence	1000	12	10-Protein mixture	137
CGE	MEKC	PMMA	Intersecting channels	Fluorescence	2600	< 30	Fetal calf serum (FCS) proteins	138
CGE	MEEKC	PMMA	Intersecting channels	Fluorescence	481	3.7	Cytosolic proteins of *E.coli*	139
IEF	CZE	PMMA	Intersecting channels	Fluorescence	1300	< 5	Standard proteins	140
IEF	CZE	Glass	Intersecting channels	Fluorescence	540	50	Digest of BSA and protein extracted from *E.coli*	141
IEF	CGE	PDMS	PDMS membrane	Fluorescence	-	-	Standard proteins	142
IEF	CGE	PC	Staggered configuration	Fluorescence	1700	< 10	Standard proteins	143
IEF	CGE/CZE	PDMS	Microvalve	Fluorescence	-	10	Standard proteins	144
IEF	CGE	Cyclic olefin	Gel pseudovalves	Fluorescence	-	10	Standard proteins	145

First Dimension	Second Dimension	Chip Material	Interface	Detection	Peak Capacity	Analysis time (min)	Samples	Ref.
IEF		Cyclic olefin	Gel pseudovalves	Fluorescence	-	-	GFP and R-phycoerythrin	146
IEF	CGE	PMMA	Gel pseudovalves	Fluorescence	2880	-	*E.coli* lysate	147
IEF	CGE	PMMA	Gel pseudovalves	Fluorescence	-	< 10	*E.coli* lysate	148
IEF	CGE	PMMA	Open channels	Fluorescence	-	-	Myoglobin	149
IEF	μ-RPLC	Cyclic olefin	Microvalves	Fluorescence	215	-	Angiotensin, BSA and cytochrome c	150
IEF	DIGE	Glass	Smaller channels	Fluorescence	-	-	E.coli lysate	151
OCEC	CZE	Glass	Intersecting channels	Fluorescence	150	13	Tryptic digest of β-casein	120
GEMBE	CZE	Glass	Intersecting channels	Fluorescence	35	210-240	Chiral amino acids	122

Recently, two-dimensional protein separations within microfluidic platforms based on MEKC-CZE, IEF-CGE and IEF-CZE have been reported in glass, PDMS and other polymer-based microfluidic devices[108] and are summarized in **Table 1.3**. *Ramsey et al*. used MEKC coupled with CZE to separate tryptic digests of BSA (**Figure 1.19a**)[119] and to separate tryptic peptides from cytochrome *c*[136] within a glass microchip using intersecting channels and gated injection of samples. The peak capacities and analysis times for the separation of a tryptic digest of BSA and for the separation of tryptic peptides from cytochrome *c* were 4200, < 15 minutes[119] and 500-1000, <10 minutes[136], respectively. Another report from this group[120] also used a glass microchip to separate tryptic digested proteins from β-casein (**Figure 1.19b**) within 13 minutes by coupling open channel electrochromatography (OCEC) with CZE, and yielding a total peak capacity of 150.

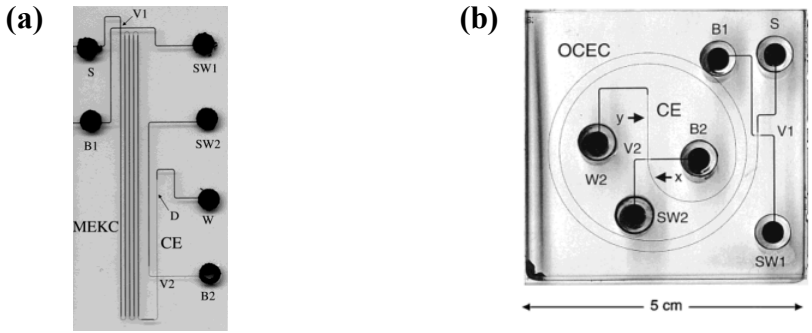

Figure 1.19: Images of microchips containing two intersecting channels as valves (V1 and V2) for the 2D separation of (a) a tryptic digest of BSA having MEKC as the first dimension and CZE as the second dimension, and (b) a tryptic digest of β-casein having OCEC coupled with CZE. Both microchips consist of a sample reservoir (S), two sample waste reservoirs (SW1 and SW2), two buffer reservoirs (B1 and B2) and one buffer waste reservoir (BW). The separated analytes are detected at the point D illustrated in Figure 1.18a and at the points x and y as shown in Figure 1.18b. Image (a) is reproduced from reference 119 and image (b) is reproduced from reference 120.

Soper and co-workers reported the coupling of CGE and MEKC within PMMA microchips to separate a 10-protein mixture with a peak capacity of 1000 in 12 minutes[137], and to separate fetal calf serum (FCS) proteins with a peak capacity of 2600 in less than 30 minutes[138]. The same group also reported the 2D separation of cytosolic

proteins of *E.coli* employing CGE as the first dimension and microemulsion electrokinetic chromatography (MEEKC) as the second dimension[139]. The separation was completed within 4 minutes with a peak capacity of 481 (**Figure 1.20**). All of these separations employed intersecting geometries as an interface between the two separation dimensions.

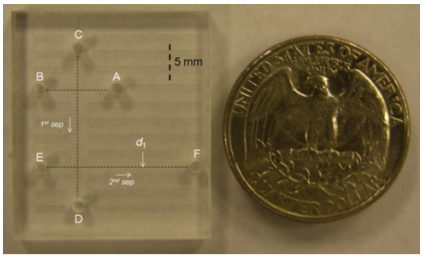

Figure 1.20: An image of a PMMA microchip with intersecting channel geometries as interfaces between CGE (1st dimension) and MEEKC (2nd dimension) for the separation of cytosolic proteins of *E. coli.* The reservoirs shown in the image are sample reservoir (A), sample waste reservoir (B), CGE buffer reservoir (C), CGE sample waste reservoir (D), MEEKC buffer reservoir (E) and MEEKC buffer waste reservoir (F). Detection is performed at the point d_1 as shown in the image. Image reproduced from reference 139.

2D protein separations achieved by coupling IEF and CZE using a simple cross-intersection PMMA microchip and glass microchip have been reported by *Herr et al.* (**Figure 1.21a**)[140] and *Cong et al*. (**Figure 1.21b**)[141] respectively.

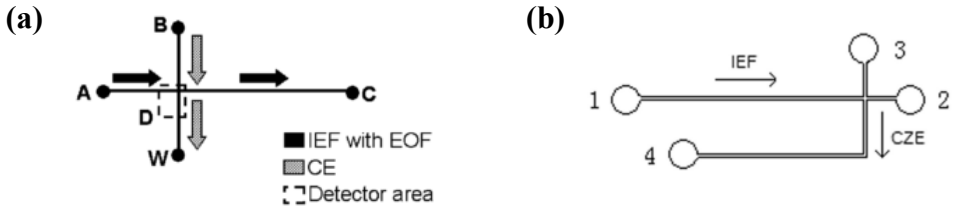

Figure 1.21: Schematics of simple cross-intersection geometries for protein separations by IEF coupled with CZE. A sample is first separated by IEF and when the analyte bands reach the intersection, they are then separated by CZE. The direction of IEF in the first dimension separation is from reservoir A to reservoir C in (a) and from reservoir 1 to reservoir 2 in (b). The direction of CZE is from reservoir B (buffer) to reservoir W (waste) in (a) and from reservoir 3 to reservoir 4 in (b). The dashed box D in part (a) shows the detection area. Schematics (a) and (b) reproduced from references 140 and 141, respectively.

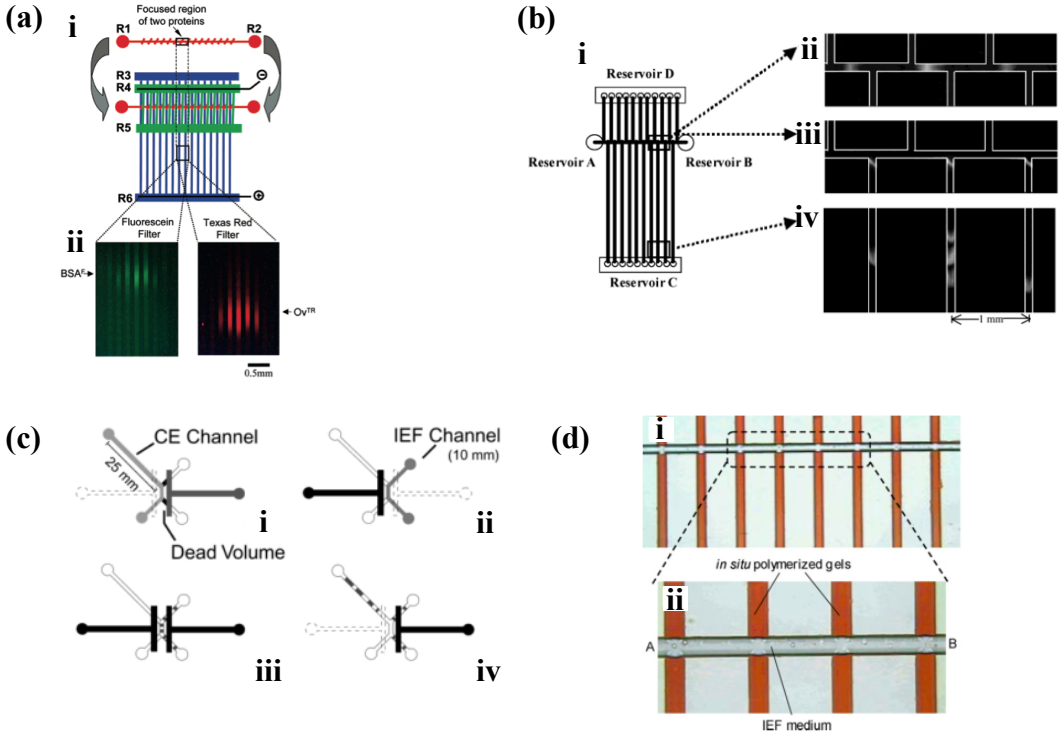

Figure 1.22: IEF coupled with CGE using a variety of interfaces between the two separation dimensions. (a) A 2D-separation microchip incorporating a PDMS membrane as an interface (i) A protein mixture is first separated in a composite PDMS membrane serving as an IEF channel (red line). The composite PDMS membrane is then assembled to the other two PDMS pieces: parallel green lines represent the channels in the top PDMS piece and parallel blue lines represent the channels in the bottom PDMS piece. Together they form a single PDMS device for CGE. The separated analytes from the IEF channel are transferred to parallel vertical channels to perform CGE in the second dimension, (ii) The separated fluorescein-conjugated bovine serum albumin (BSA^F) and Texas-red-conjugated ovalbumin (Ov^{TR}) bands are obtained using different filters for the detection of fluorescein and Texas Red. (b) A staggered-channel network within a planar PC microchip for 2D separations (i) A schematic of the microchip shows a horizontal channel for IEF separation traversing vertical channels for performing CGE, (ii) Shows IEF focusing of a protein mixture, (iii) The focused proteins are transferred electrokinetically to the second dimension, (iv) CGE is then performed in the vertical channels. (c) Schematics of 2D separation processes utilizing microvalves as interfaces between IEF and CGE separations (i) During CGE buffer loading, right valves connected to an IEF channel are closed, (ii) IEF buffer loading, left valves connected to a CGE channel are closed, (iii) All valves are closed after IEF focusing, (iv) Left valves are opened again for CGE separation. (d) An IEF-CGE microchip employing *in situ* polymerized gel as valves (i) A micrograph of the stained polymerized gel within vertical channels, (ii) The enlargement of (i) shows an IEF channel and an array of CGE channels containing polymerized gel. Image (a) reproduced from reference 142, image (b) reproduced from reference 143, image (c) reproduced from reference 144 and image (d) reproduced from reference 146.

Several groups have also reported the separation of proteins on microfluidic devices utilizing IEF as the first dimension and CGE as the second dimension[142-151]. For example, *Whitesides* and co-workers[142] fabricated a prototype 2D-CE device on a PDMS substrate in which the two dimensions were performed separately on different microfabricated devices, with separated proteins from the first dimension being transferred to the second via PDMS membranes, which could be assembled or disassembled (**Figure 1.22a**). Li *et al.*[143] reported the IEF-CGE separation of a five-protein sample in a polycarbonate microfluidic device in which the two dimensions were connected via a staggered configuration of channels as illustrated in **Figure 1.22b**. The analysis time was 10 minutes with a peak capacity of 1700. In addition, *Wang* and co-workers[144] introduced a PDMS microchip with microvalves to prevent mixing of separation buffers (**Figure 1.22c**). In this study, a four-protein mixture was separated by IEF and CGE within 10 minutes. *Das et al.*[145,146] and *Yang et al.*[147,148] also reported IEF coupled CGE separations of protein mixtures in plastic microchips incorporating photopolymerized gel plugs as pseudovalves to prevent cross-contamination between the two separation systems as demonstrated in **Figure 1.22d**. Finally, *Griebel et al.*[149] demonstrated a small open channel as an interface between IEF and CGE separation of myoglobin on a PMMA microchip.

Other modes of two-dimensional protein separations with various types of interfaces have also been proposed. For instance, IEF was coupled to micro reverse phase liquid chromatography (μ-RPLC) by a microvalve interface to separate Angiotensin, BSA and cytochrome c (**Figure 1.23a**)[150]. Proteins from *E.coli* lysate were separated by IEF-DIGE (differential gel electrophoresis) utilizing shallow and narrow channels as interfaces (**Figure 1.23b**)[151], and gradient elution moving boundary electrophoresis (GEMBE) coupled to CZE to separate chiral amino acids on a glass microchip (**Figure 1.23c**)[122].

In addition, MCE is also easily combined with mass spectrometry (MS) to perform protein and peptide analysis[152]. *Li et al.*[153] successfully sequenced 88.5% of a peptide mixture obtained from a proteolytic digest of cytochrome c using CE connected to low-sheath flow ESI via a connecting capillary. *Ramsey et al.*[154] proposed the coupling of CE-ESI-MS in which ESI was directly performed from a rectangular glass microchip and

coupled with MS without the use of an external pressure source. In this case, the separation of a peptide mixture was fully resolved in less than 30 seconds.

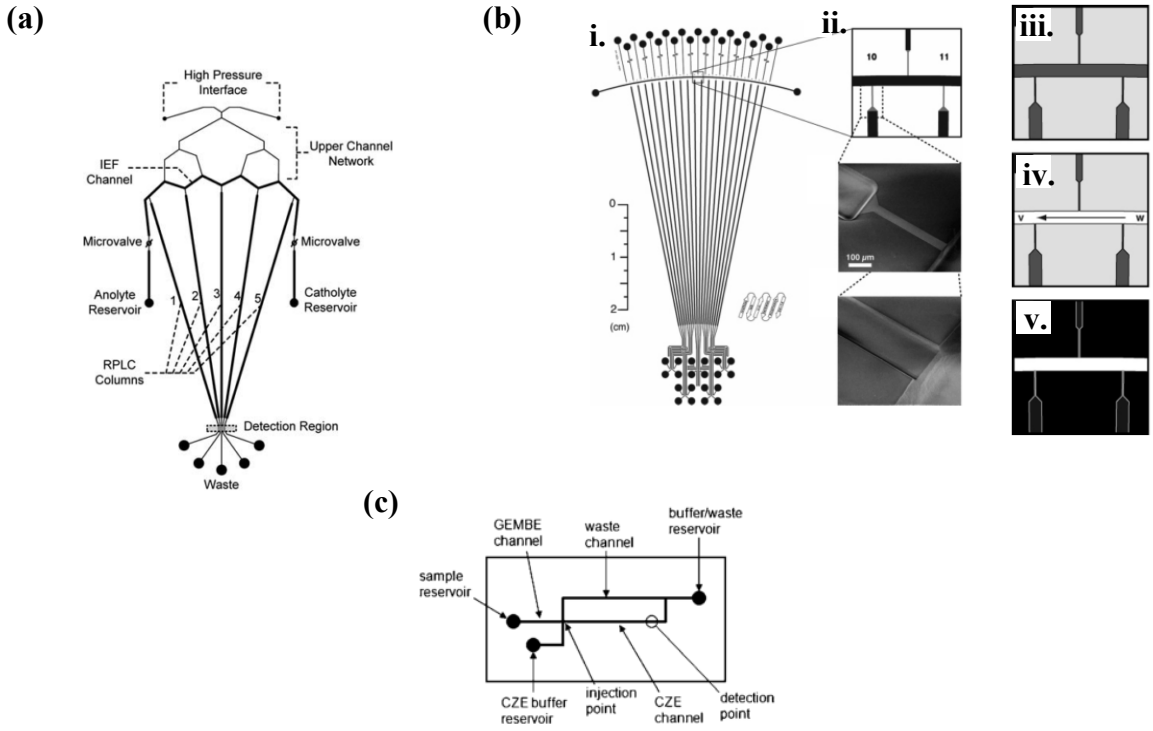

Figure 1.23: (a) A schematic of a microchip for IEF coupled with μ-RPLC using microvalves as interfaces. The microvalves are manually turned off after separation in an IEF channel. The analytes are then further separated using μ-RPLC. (b) 2D separation by IEF coupled with DIGE (i) An illustration of a microchip having an IEF channel laying across an array of DIGE channels, (ii) The connection between the IEF channel (horizontal channel) and DIGE channels (vertical channels) using very small channels that prevent gel buffer from dispersing into the IEF channel during the focusing operation, (iii) The gel buffer fills all channels, (iv) The IEF channel is cleared by applying a vacuum at one end and water at the other end, (v) IEF buffer is then introduced into the clean IEF channel. (c) Illustrations of GEMBE coupled with CZE separation. The microdevice consists of a sample reservoir, a CZE buffer reservoir, a buffer waste reservoir, a GEMBE channel connected to a CZE channel via an intersection geometry. By varying the bulk solution counterflow velocity in GEMBE, analytes are allowed to enter the channel at different times. The analyte bands from GEMBE are periodically injected into a CZE channel for further separation by turning on/off a computer-controlled relay. Image (a) reproduced from reference 150, image (b) reproduced from reference 151, image (c) reproduced from reference 122.

1.9 Project outline

Since the study of proteomics has received enormous attention in biological, medical and pharmaceutical science, the need for high-throughput, high-resolution and completely automated analysis of proteins is of undoubted importance. To achieve these goals, two-dimensional separation of proteins was first introduced in the form of 2D-PAGE. This was found to be slow, complex and laborious. 2D-PAGE was then transferred into 2D columns or capillary separations and later followed by 2D separations within microfluidic formats (to provide for higher resolution, improved automation, and faster analysis times). However, all multidimensional separations face one unavoidable problem; that is the difficulty in selecting an appropriate interface between each dimension to reduce dead volumes, minimize dispersion at the interface and limit resolution losses[122,135]. To this end, the compartmentalization of separated bands into droplets can be used as an interface between each dimension of the separation process[155,156].

In the current work, we present the development of a microfluidic interface that can be used to transfer analyte microdroplets into a second separation dimension or distinct analytical process. Herein we use a fluorescently labeled protein mixture as a representative of proteins separated from the first dimension. This protein mixture is segmented into droplets using a robotic droplet generator. These droplets can then be transferred through a novel microfluidic interface into the second separation dimension. For the second separation dimension, CGE is employed because of its suitability for protein separations and its ease of operation. For this reason, an appropriate buffer system that can provide not only for high-resolution and rapid separation but also compatibility with the materials used in this experiment was developed (**Chapter 3**). In addition, several fluorescent dyes for labeling proteins were assayed so as to achieve high fluorescence intensities appropriate for use with the developed droplet platform (**Chapter 4**). The interfacing of the droplet-based microfluidic device was then established in **Chapter 5**. Issues relating to previous designs are addressed and novel microfluidic interfaces were designed and evaluated. By integrating all the components developed in Chapters 3-5 (i.e. the appropriate interfacing chip design, the gel buffer solution, and the fluorescently labeled proteins), droplet-based separations of proteins are reported in **Chapter 6**. The developed interface device prevents dispersion of analyte bands and

sample loss at an interface between the two separation dimensions. The interface also provides for rapid separations, ease of operation and automation of complete oil depletion. All of these features are expected to enhance the separation performance of protein analysis in proteomic research.

1.10 References

1. Campbell, N. A. & Reece, J. B. *Biology*. (Pearson Benjamin Cummings, 2005).

2. Nelson, D. L. & Cox, M. M. *Lehninger Principles of Biochemistry*. (W.H. Freeman and Company, 2005).

3. Bianconi, E., Piovesan, A., Facchin, F., Beraudi, A., Casadei, R., Frabetti, F., Vitale, L., Pelleri, M.C., Tassani, S., Piva, F., Perez-Amodio, S., Strippoli, P. & Canaider, S. An estimation of the number of cells in the human body. *Ann. Hum. Biol.* **40,** 463–71 (2013).

4. Cancer information and support network. The Cell. at <http://cisncancer.org/research/what_we_know/biology/the_cell.html>

5. Freitas Jr., R. A. Human body chemical composition. *Foresight Inst.* (1998). at <https://www.foresight.org/Nanomedicine/Ch03_1.html>

6. Celis, J. E., Wolf, H. & Østergaard, M. Bladder squamous cell carcinoma biomarkers derived from proteomics. *Electrophoresis* **21,** 2115–2121 (2000).

7. Franzén, B., Linde, S., Alaiya, A. A., Eriksson, E., Fujioka, K., Bergman, A. C., Jörnvall, H. & Auer, G. Analysis of polypeptide expression in benign and malignant human breast lesions: down-regulation of cytokeratins. *Br. J. Cancer* **74,** 1632–1638 (1996).

8. Jain, K. K. Role of proteomics in diagnosis of cancer. *Technol. Cancer Res. Treat.* **1,** 281–286 (2002).

9. Soldes, O. S., Kuick, R. D., Thompson II, I. A., Hughes, S. J., Orringer, M. B., Iannettoni, M. D., Hanash, S. M. & Beer, D. G. Differential expression of Hsp27 in normal oesophagus, Barrett's metaplasia and oesophageal adenocarcinomas. *Br. J. Cancer* **79,** 595–603 (1999).

10. Seow, T. K., Liang, R. C., Leow, C. K. & Chung, M. C. Hepatocellular carcinoma: from bedside to proteomics. *Proteomics* **1,** 1249–1263 (2001).

11. Chen, G., Gharib, T. G., Huang, C. C., Thomas, D. G., Shedden, K. A., Taylor, J. M. G., Kardia, S. L. R., Misek, D. E., Giordano, T. J., Iannettoni, M. D., Orringer,

M. B., Hanash, S. M. & Beer, D. G. Proteomic analysis of lung adenocarcinoma: identification of a highly expressed set of proteins in tumors. *Clin. Cancer Res.* **8,** 2298–2305 (2002).

12. Sarto, C., Frutiger, S., Cappellano, F., Sanchez, J. C., Doro, G., Catanzaro, F., Hughes, G. J., Hochstrasser, D. F. & Mocarelli, P. Modified expression of plasma glutathione peroxidase and manganese superoxide dismutase in human renal cell carcinoma. *Electrophoresis* **20,** 3458–3466 (1999).

13. Guest, P. C., Gottschalk, M. G. & Bahn, S. Proteomics: improving biomarker translation to modern medicine? *Genome Med.* **5,** 17 (2013).

14. Meehan, K. L., Holland, J. W. & Dawkins, H. J. S. Proteomic analysis of normal and malignant prostate tissue to identify novel proteins lost in cancer. *Prostate* **50,** 54–63 (2002).

15. Sharma, P., Cosme, J. & Gramolini, A. O. Recent advances in cardiovascular proteomics. *J. Proteomics* **81,** 3–14 (2013).

16. Greenberg, S. G. & Davies, P. A preparation of Alzheimer paired helical filaments that displays distinct tau proteins by polyacrylamide gel electrophoresis. *Proc. Natl. Acad. Sci. U. S. A.* **87,** 5827–5831 (1990).

17. Kavallaris, M. & Marshall, G. M. Proteomics and disease: Opportunities and challenges. *Med. J. Aust.* **182,** 575–579 (2005).

18. Lesk, A. M. *Introduction to Protein Science: Architecture, Function and Genomics*. (Oxford University Press Inc., 2010).

19. Issaq, H. J. & Veenstra, T. D. The role of electrophoresis in disease biomarker discovery. *Electrophoresis* **28,** 1980–8 (2007).

20. Little, M. J., Paquette, D. M. & Roos, P. K. Electrophoresis of pharmaceutical proteins: status quo. *Electrophoresis* **27,** 2477–85 (2006).

21. Wilkins, M. R., Pasquali, C., Appel, R. D., Ou, K., Golaz, O., Sanchez, J. C., Yan, J. X., Gooley, A. A., Hughes, G., Humphery-Smith, I., Williams, K. L. & Hochstrasser, D. F. From proteins to proteomes: large scale protein identification by two-dimensional electrophoresis and amino acid analysis. *Biotechnology. (N. Y).* **14,** 61–65 (1996).

22. Zhang, C.-C. & Kast, J. Applications of current proteomics techniques in modern drug design. *Curr. Comput. Aided. Drug Des.* **6,** 147–64 (2010).

23. Liu, C. & Zhang, X. Multidimensional capillary array liquid chromatography and matrix-assisted laser desorption/ionization tandem mass spectrometry for high-throughput proteomic analysis. *J. Chromatogr. A* **1139,** 191–8 (2007).

24. Hanash, S. Disease proteomics. *Nature* **422,** 226–232 (2003).

25. Berg, J., Tymoczko, J. & Stryer, L. *Biochemistry*. (W.H. Freeman and Company, 2012).

26. Clark, J. Transcription-From DNA to RNA. (2007).

27. Clark, J. Protein Synthesis. at <http://www.chemguide.co.uk/organicprops/aminoacids/dna5.html#top>

28. Song, H., Chen, D. L. & Ismagilov, R. F. Reactions in droplets in microfluidic channels. *Angew. Chem. Int. Ed. Engl.* **45,** 7336–56 (2006).

29. Minor, L. K. *Handbook of assay development in drug discovery*. (CRC Press, Taylor&Francis Group, 2006).

30. Bellavance, L., Burbaum, J. & Dunn, D. Miniaturisation of HTS assays. *Innov. Pharm. Technol.* (2000).

31. Whitesides, G. M. The origins and the future of microfluidics. *Nature* **442,** 368–73 (2006).

32. Stone, H. & Kim, S. Microfluidics: basic issues, applications, and challenges. *AIChE J.* **47,** 1250–1254 (2001).

33. Zhang, X. & Haswell, S. J. Materials Matter in Microfluidic Devices. *MRS Bull.* **31,** 95–99 (2006).

34. Li, P. C. H. *Microfluidic Lab-on-a-Chip for Chemical and Biological Analysis and Discovery*. (CRC Press, Taylor&Francis Group, 2006).

35. Manz, A. & Eijkel, J. C. T. Miniaturization and chip technology. What can we expect? *Pure Appl. Chem.* **73,** 1555–1561 (2001).

36. Bilitewski, U., Genrich, M., Kadow, S. & Mersal, G. Biochemical analysis with microfluidic systems. *Anal. Bioanal. Chem.* **377,** 556–69 (2003).

37. Weibel, D. B. & Whitesides, G. M. Applications of microfluidics in chemical biology. *Curr. Opin. Chem. Biol.* **10,** 584–591 (2006).

38. Breslauer, D. N., Lee, P. J. & Lee, L. P. Microfluidics-based systems biology. *Macromolecules* 97–112 (2006). doi:10.1039/b515632g

39. Huebner, A., Sharma, S., Srisa-Art, M., Hollfelder, F., Edel, J. B. & deMello, A. J. Microdroplets: a sea of applications? *Lab Chip* **8,** 1244–54 (2008).

40. Elvira, K. S., Casadevall i Solvas, X., Wootton, R. C. R. & de Mello, A. J. The past, present and potential for microfluidic reactor technology in chemical synthesis. *Nat. Chem.* **5,** 905–15 (2013).

41. Ohno, K., Tachikawa, K. & Manz, A. Microfluidics: Applications for analytical purposes in chemistry and biochemistry. *Electrophoresis* **29,** 4443–4453 (2008).

42. Puccinelli, J. P. & Beebe, D. J. in *Microfluid. Biol. Appl.* (eds. Tien, W.-C. & Finehout, E.) 241–269 (Springer US, 2009).

43. Thorsen, T. a. Microfluidic Tools for High-Throughput Screening. *Biotechniques* **36,** 197–199 (2004).

44. Song, H., Tice, J. D. & Ismagilov, R. F. A Microfluidic System for Controlling Reaction Networks in Time. *Angew. Chemie Int. Ed.* **42,** 768–772 (2003).

45. Schulte, T. H., Bardell, R. L. & Weigl, B. H. Microfluidic technologies in clinical diagnostics. *Clin. Chim. Acta* **321,** 1–10 (2002).

46. Kricka, L. J. Miniaturization of analytical systems. *Clin. Chem.* **44,** 2008–2014 (1998).

47. Khandurina, J. & Guttman, A. Bioanalysis in microfluidic devices. *J. Chromatogr. A* **943,** 159–183 (2002).

48. Charon, L., Wheeler, A. R. & Lilge, L. Single cell analysis in microfluidic devices. *Encycl. Microfluid. Nanofluidics* 1851–1860 (2008). doi:10.1007/978-0-387-48998-8_1414

49. Amantonico, A., Urban, P. L. & Zenobi, R. Analytical techniques for single-cell metabolomics: State of the art and trends. *Anal. Bioanal. Chem.* **398,** 2493–2504 (2010).

50. Theberge, A. B., Courtois, F., Schaerli, Y., Fischlechner, M., Abell, C., Hollfelder, F. & Huck, W. T. S. Microdroplets in microfluidics: An evolving platform for discoveries in chemistry and biology. *Angew. Chemie - Int. Ed.* **49,** 5846–5868 (2010).

51. Casadevall i Solvas, X. & deMello, A. Droplet microfluidics: recent developments and future applications. *Chem. Commun. (Camb).* **47,** 1936–1942 (2011).

52. Teh, S.-Y., Lin, R., Hung, L.-H. & Lee, A. P. Droplet microfluidics. *Lab Chip* **8,** 198–220 (2008).

53. Gielen, F., Buryska, T., Vliet, L. V., Butz, M., Damborsky, J., Prokop, Z. & Hollfelder, F. Interfacing Microwells with Nanoliter Compartments: A Sampler Generating High-Resolution Concentration Gradients for Quantitative Biochemical Analyses in Droplets. *Anal. Chem.* **87,** 624-632 (2015).

54. Thorsen, T., Roberts, R. W., Arnold, F. H. & Quake, S. R. Dynamic Pattern Formation in a Vesicle-Generating Microfluidic Device. *Phys. Rev. Lett.* **86,** 4163–4166 (2001).

55. Anna, S. L., Bontoux, N. & Stone, H. a. Formation of dispersions using 'flow focusing' in microchannels. *Appl. Phys. Lett.* **82,** 364 (2003).

56. Trojanowicz, M. *Advances in Flow Analysis*. *Adv. Flow Anal.* (2008). doi:10.1002/9783527623259

57. Niu, X., Gielen, F., Edel, J. B. & deMello, A. J. A microdroplet dilutor for high-throughput screening. *Nat. Chem.* **3,** 437–442 (2011).

58. Gielen, F., Vliet, L. V., Koprowski, B. T., Devenish, S. R. A., Fischlechner, M., Edel, J. B., Niu, X., deMello, A. J. & Hollfelder, F. A fully unsupervised compartment-on-demand platform for precise nanoliter assays of time-dependent steady-state enzyme kinetics and inhibition. *Anal. Chem.* **85,** 4761–4769 (2013).

59. Wu, J., Zhang, M., Li, X. & Wen, W. Multiple and high-throughput droplet reactions via combination of microsampling technique and microfluidic chip. *Anal. Chem.* **84,** 9689–9693 (2012).

60. Niu, X., Gulati, S., Edel, J. B. & deMello, A. J. Pillar-induced droplet merging in microfluidic circuits. *Lab Chip* **8,** 1837–41 (2008).

61. Link, D. R., Anna, S. L., Weitz, D. A. & Stone, H. A. Geometrically Mediated Breakup of Drops in Microfluidic Devices. *Science (80-.).* 1–4 (2004). doi:10.1103/PhysRevLett.92.054503

62. Niu, X., Zhang, M., Peng, S., Wen, W. & Sheng, P. Real-time detection, control, and sorting of microfluidic droplets. *Biomicrofluidics* **1,** (2007).

63. Huebner, A., Bratton, D., Whyte, G., Yang, M., deMello, A. J., Abell, C. & Hollfelder, F. Static microdroplet arrays: a microfluidic device for droplet trapping, incubation and release for enzymatic and cell-based assays. *Lab Chip* **9,** 692–8 (2009).

64. Brown, R. B. & Audet, J. Current techniques for single-cell lysis. *J. R. Soc. Interface* **5 Suppl 2,** S131–S138 (2008).

65. *Cell Lysis Technical Handbook*. *Thermo Sci.* (2009).

66. Methods for working with proteins. at <http://www.siumed.edu/~bbartholomew/images/chapter6/F06-11.jpg>

67. Li, S. F. Y. *Capillary Electrophoresis: Principles, Practice and Applications*. (ELSEVIER SCIENCE PUBLISHERS B.V., 1992).

68. Altria, K. D. *Capillary Electrophoresis Guidebook: Principles, Operation and Applications*. (Humana Press Inc., 1996).

69. Munro, N. J., Snow, K., Kant, J. a. & Landers, J. P. Molecular diagnostics on microfabricated electrophoretic devices: From slab gel- to capillary- to microchip-

based assays for T- and B-cell lymphoproliferative disorders. *Clin. Chem.* **45,** 1906–1917 (1999).

70. Heidcamp, W. Cell Biology Laboratory Manual-Chapter 4: Electrophoresis-Introduction. at <http://homepages.gac.edu/~cellab/chpts/chpt4/intro4.html>

71. Guttman, A., Nolan, J. A. & Cooke, N. Capillary sodium dodecyl sulfate gel electrophoresis of proteins. **632,** 171–175 (1993).

72. Ganzler, K., Greve, K. S., Cohen, A. S., Karger, B. L., Guttman, A. & Cooke, N. C. High-Performance Capillary Electrophoresis of SDS-Protein Complexes Using UV-Transparent Polymer Networks. *Electrophoresis* (1992).

73. Whatley, H. *Basic principles and modes of capillary electrophoresis*. *Clin. Forensic Appl. Capill. Electrophor.* (2001). doi:10.1007/978-1-59259-120-6

74. Kristl, T., Stutz, H., Wenz, C. & Rozing, G. *Principles and applications of capillary isoelectric focusing*. (Agilent Technologies, Inc., 2014).

75. Dunn, M. J. *Gel electrophoresis of proteins*. (IOP Publishing Ltd., 1986).

76. Righetti, P. G. *Laboratory techniques in biochemistry and molecular biology: Immobilized pH gradients theory and methodology*. (ELSEVIER SCIENCE PUBLISHERS B.V., 1990).

77. Righetti, P. G., Simó, C., Sebastiano, R. & Citterio, A. Carrier ampholytes for IEF, on their fortieth anniversary (1967-2007), brought to trial in court: The verdict. *Electrophoresis* **28,** 3799–3810 (2007).

78. Twyman, R. M. *Principles of proteomics*. (Garland Science, Taylor & Francis Group, LLC., 2014).

79. Righetti, P. G. & Bossi, A. Isoelectric focusing of proteins and peptides in gel slabs and in capillaries. *Anal. Chim. Acta* **372,** 1–19 (1998).

80. Hjertén, S. Free zone electrophoresis. *Chromatogr. Rev.* **9,** 122–219 (1967).

81. Mikkers, F. E. P., Everaerts, F. M. & Verheggen, T. P. E. M. High-performance zone electrophoresis. *J. Chromatogr. A* **169,** 11–20 (1979).

82. Jorgenson, J. W. & Lukacs, K. D. Zone Electrophoresis in Open-Tubular Glass Capillaries. *Anal. Chem.* **53,** 1298–1302 (1981).

83. Dolník, V. Capillary electrophoresis of proteins 2005-2007. *Electrophoresis* **29,** 143–56 (2008).

84. Landers, J. P. *Handbook of capillary electrophoresis*. (CRC Press Inc., 1996).

85. Henry, C. S. *Microchip capillary electrophoresis: methods and protocols*. (Humana Press Inc., 2006).

86. Issaq, H. J. Thirty-Five Years of Capillary Electrophoresis: Advances and Perspectives. *J. Liq. Chromatogr. Relat. Technol.* **25,** 1153–1170 (2005).

87. Dovichi, N. J. DNA sequencing by capillary electrophoresis. *Electrophoresis* **18,** 2393–2399 (1997).

88. Cohen, A. S. & Karger, B. L. High-performance sodium dodecyl sulfate polyacrylamide gel capillary electrophoresis of peptides and proteins. *J. Chromatogr.* **397,** 409–417 (1987).

89. Hjerten, S. & Zhu, M. D. Adaptation of the equipment for high-performance electrophoresis to isoelectric focusing. *J. Chromatogr. A* **346,** 265–270 (1985).

90. Terabe, S., Otsuka, K., Ichikawa, K., Tsuchiya, a & Ando, T. Electrokinetic Separations with Micellar Solutions and Open-Tubular Capillaries. *Anal. Chem.* **56,** 111–113 (1984).

91. Terabe, S. Twenty-five years of micellar electrokinetic chromatography. *Procedia Chem.* **2,** 2–8 (2010).

92. Hancu, G., Simon, B., Rusu, A., Mircia, E. & Gyéresi, Á. Principles of micellar electrokinetic capillary chromatography applied in pharmaceutical analysis. *Adv. Pharm. Bull.* **3,** 1–8 (2013).

93. Hirokawa, T. Isotachophoresis. *Electrophoresis* **1,** 1272–1280 (2000).

94. Everaerts, F. M., Beckers, J. L. & Verheggen, T. P. E. M. *Isotachophoresis: Theory, Instrumentation and Applications*. (ELSEVIER SCIENCE PUBLISHERS B.V., 1976).

95. Westermeier, R. *Electrophoresis in Practice*. (WILEY-VCH Verlag, 2001).

96. Smith, N. *Capillary ElectroChromatography*. *Beckman Coulter* (Beckman Coulter, Inc., 1999). doi:10.2116/analsci.18.89

97. Bartle, K. D. & Myers, P. Theory of capillary electrochromatography. *J. Chromatogr. A* **916,** 3–23 (2001).

98. Harvanová, J. & Bloom, L. Capillary Electrophoresis Technique for Metal Species Determination: A Review. *J. Liq. Chromatogr. Relat. Technol.* **38,** 371–380 (2014).

99. Tagliaro, F. & Bortolotti, F. Recent advances in the applications of CE to forensic sciences (2005-2007). *Electrophoresis* **29,** 260–268 (2008).

100. Kvasnička, F. Capillary electrophoresis in food authenticity. *J. Sep. Sci.* **28,** 813–825 (2005).

101. Piñero, M. Y., Bauza, R. & Arce, L. Thirty years of capillary electrophoresis in food analysis laboratories: Potential applications. *Electrophoresis* **32,** 1379–1393 (2011).

102. Castañeda, G., Rodríguez-Flores, J. & Ríos, A. Analytical approaches to expanding the use of capillary electrophoresis in routine food analysis. *J. Sep. Sci.* **28,** 915–924 (2005).

103. Doln, V. Capillary zone electrophoresis of proteins. **18,** 2353–2361 (1997).

104. Natishan, T. K. Recent progress in the analysis of pharmaceuticals by capillary electrophoresis. *J. Liq. Chromatogr. Relat. Technol.* **28,** 1115–1160 (2005).

105. Atkins, P. & de Paula, J. *Atkins' physical chemistry*. (Oxford University Press Inc., 2002).

106. Faust, S. D. & Aly, O. M. *Chemistry of water treatment*. (CRC Press Inc., 1998).

107. Tran, N. T., Ayed, I., Pallandre, A. & Taverna, M. Recent innovations in protein separation on microchips by electrophoretic methods: an update. *Electrophoresis* **31,** 147–73 (2010).

108. Wu, D., Qin, J. & Lin, B. Electrophoretic separations on microfluidic chips. *J. Chromatogr. A* **1184,** 542–59 (2008).

109. Bruin, G. J. M. Recent developments in electrokinetically driven analysis on microfabricated devices. *Electrophoresis* **21,** 3931–3951 (2000).

110. Erickson, D., Sinton, D. & Li, D. Joule heating and heat transfer in poly(dimethylsiloxane) microfluidic systems. *Lab Chip* **3,** 141–149 (2003).

111. Gross, B. C., Erkal, J. L., Lockwood, S. Y., Chen, C. & Spence, D. M. Evaluation of 3D printing and its potential impact on biotechnology and the chemical sciences. *Anal. Chem.* **86,** 3240–53 (2014).

112. Liu, C.-Y., Xu, X., Gao, H.-J. & Chen, J.-R. Poly(dimethylsiloxane) Microchips with Two Sharpened Stretching Tips and Its Application to Protein Separation Using Dynamic Coating. *Chinese J. Chem.* **25,** 190–195 (2007).

113. Ocvirk, G., Munroe, M., Tang, T., Oleschuk, R., Westra, K. & Harrison, D. J. Electrokinetic control of fluid flow in native poly (dimethylsiloxane) capillary electrophoresis devices. *Electrophoresis* **21,** 107-115 (2000).

114. Muck, A. & Svatos, A. Chemical modification of polymeric microchip devices. *Talanta* **74,** 333–41 (2007).

115. Evans, C. R. & Jorgenson, J. W. Multidimensional LC-LC and LC-CE for high-resolution separations of biological molecules. *Anal. Bioanal. Chem.* **378,** 1952–61 (2004).

116. Giddings, J. C. Concepts and comparisons in multidimensional separation. *J. High Resolut. Chromatogr.* **10,** 319–323 (1987).

117. Giddings, J. C. Two-dimensional separations: concept and promise. *Anal. Chem.* **56,** 1258A–1260A, 1262A, 1264A passim (1984).

118. Giddings, J. Maximum number of components resolvable by gel filtration and other elution chromatographic methods. *Anal. Chem.* **39,** 1027–1028 (1967).

119. Ramsey, J. D., Jacobson, S. C., Culbertson, C. T. & Ramsey, J. M. High-Efficiency, Two-Dimensional Separations of Protein Digests on Microfluidic Devices. *Anal. Chem.* **75,** 3758–3764 (2003).

120. Gottschlich, N., Jacobson, S. C., Culbertson, C. T. & Ramsey, J. M. Two-dimensional electrochromatography/capillary electrophoresis on a microchip. *Anal. Chem.* **73,** 2669–74 (2001).

121. O'Farrell, P. H. High Resolution of Proteins * Electrophoresis. *J. Biol. Chem.* **250,** 4007–4021 (1975).

122. Ross, D., Shackman, J. G., Kralj, J. G. & Atencia, J. 2D separations on a 1D chip: gradient elution moving boundary electrophoresis-chiral capillary zone electrophoresis. *Lab Chip* **10,** 3139–48 (2010).

123. Kohl, F. J., Sánchez-Hernández, L. & Neusüß, C. Capillary electrophoresis in two-dimensional separation systems: Techniques and applications. *Electrophoresis* **36,** 144–158 (2015).

124. Sivakumar, S. Protein isolation with 2D gel electrophoresis. at <http://biosiva.50webs.org/proiso.htm>

125. Anouti, S., Vandenabeele-Trambouze, O., Koval, D. & Cottet, H. Heart-cutting 2-D CE using multiple detection points for chiral analysis of native amino acids. *Electrophoresis* **30,** 2–10 (2009).

126. Anouti, S., Vandenabeele-Trambouze, O. & Cottet, H. Heart-cutting 2D-CE with on-line preconcentration for the chiral analysis of native amino acids. *Electrophoresis* **31,** 1029–1035 (2010).

127. Yang, C., Liu, H., Yang, Q., Zhang, L., Zhang, W. & Zhang, Y. On-line hyphenation of capillary isoelectric focusing and capillary gel electrophoresis by a dialysis interface. *Anal. Chem.* **75,** 215–218 (2003).

128. Liu, H., Zhang, L., Zhu, G., Zhang, W. & Zhang, Y. An etched porous interface for on-line capillary electrophoresis-based two-dimensional separation system. *Anal. Chem.* **76,** 6506–6512 (2004).

129. Wang, T., Ma, J., Wu, S., Sun, L., Yuan, H., Zhang, L., Liang, Z. & Zhang Y. On-line combination of monolithic immobilized pH gradient-based capillary isoelectric focusing and capillary zone electrophoresis via a partially etched porous interface for protein analysis. *J. Chromatogr. B Anal. Technol. Biomed. Life Sci.* **879,** 804–810 (2011).

130. Zhang, Z. X., Zhang, M. Z. & Zhang, S. S. Online preconcentration and two-dimensional separation of cationic compounds via hyphenation of capillary zone electrophoresis with cyclodextrin-modified micellar electrokinetic capillary chromatography. *Electrophoresis* **30,** 1958–1966 (2009).

131. Lemmo, A. V & Jorgenson, J. Transverse flow gating interface for the coupling of microcolumn LC with CZE in a comprehensive two-dimensional system. *Anal. Chem.* **65,** 1576–1561 (1993).

132. Schoenherr, R. M., Ye, M., Vannatta, M. & Dovichi, N. J. CE-microreactor-CE-MS/MS for protein analysis. *Anal. Chem.* **79,** 2230–2238 (2007).

133. Flaherty, R. J., Huge, B. J., Bruce, S. M., Dada, O. O. & Dovichi, N. J. Nicked-sleeve interface for two-dimensional capillary electrophoresis. *Analyst* **138,** 3621–3625 (2013).

134. Zhang, J., Hu, H., Gao, M., Yang, P. & Zhang, X. Comprehensive two-dimensional chromatography and capillary electrophoresis coupled with tandem time-of-flight mass spectrometry for high-speed proteome analysis. *Electrophoresis* **25,** 2374–2383 (2004).

135. Niu, X. Z., Zhang, B., Marszalek, R. T., Ces, O., Edel, J. B., Klug, D. R. & deMello, A. J. Droplet-based compartmentalization of chemically separated components in two-dimensional separations. *Chem. Commun. (Camb).* 6159–61 (2009).

136. Rocklin, R. D., Ramsey, R. S. & Ramsey, J. M. A microfabricated fluidic device for performing two-dimensional liquid-phase separations. *Anal. Chem.* **72,** 5244–9 (2000).

137. Shadpour, H. & Soper, S. a. Two-dimensional electrophoretic separation of proteins using poly(methyl methacrylate) microchips. *Anal. Chem.* **78,** 3519–27 (2006).

138. Osiri, J. K., Shadpour, H., Park, S., Snowden, B. C., Chen, Z. Y. & Soper, S. A. Generating high peak capacity 2-D maps of complex proteomes using PMMA microchip electrophoresis. *Electrophoresis* **29,** 4984–4992 (2008).

139. Osiri, J. K., Shadpour, H. & Soper, S. a. Ultra-fast two-dimensional microchip electrophoresis using SDS μ-CGE and microemulsion electrokinetic chromatography for protein separations. *Anal. Bioanal. Chem.* **398,** 489–498 (2010).

140. Herr, A. E., Molho, J. I., Drouvalakis, K. A., Mikkelsen, J. C., Utz, P. J., Santiago, J. G. & Kenny, T. W. On-Chip Coupling of Isoelectric Focusing and Free Solution Electrophoresis for Multidimensional Separations. *Electrophoresis* **75,** 1180–1187 (2003).

141. Cong, Y., Zhang, L., Tao, D., Liang, Y., Zhang, W. & Zhang, Y. Miniaturized two-dimensional capillary electrophoresis on a microchip for analysis of the tryptic digest of proteins. *J. Sep. Sci.* **31,** 588–594 (2008).

142. Chen, X., Wu, H., Mao, C. & Whitesides, G. M. A prototype two-dimensional capillary electrophoresis system fabricated in poly(dimethylsiloxane). *Anal. Chem.* **74,** 1772–8 (2002).

143. Li, Y., Buch, J. S., Rosenberger, F., Devoe, D. L. & Lee, C. S. Integration of isoelectric focusing with parallel sodium dodecyl sulfate gel electrophoresis for multidimensional protein separations in a plastic microfluidic network. **76,** 742–748 (2004).

144. Wang, Y.-C., Choi, M. H. & Han, J. Two-dimensional protein separation with advanced sample and buffer isolation using microfluidic valves. *Anal. Chem.* **76,** 4426–31 (2004).

145. Das, C., Zhang, J., Denslow, N. D. & Fan, Z. H. Integration of isoelectric focusing with multi-channel gel electrophoresis by using microfluidic pseudo-valves. *Lab Chip* **7,** 1806–1812 (2007).

146. Das, C., Fredrickson, C. K., Xia, Z. & Fan, Z. H. Device fabrication and integration with photodefinable microvalves for protein separation. *Sensors Actuators, A Phys.* **134,** 271–277 (2007).

147. Yang, S., Liu, J., Lee, C. S. & Devoe, D. L. Microfluidic 2-D PAGE using multifunctional in situ polyacrylamide gels and discontinuous buffers. *Lab Chip* **9,** 592–599 (2009).

148. Liu, J., Yang, S., Lee, C. S. & DeVoe, D. L. Polyacrylamide gel plugs enabling 2-D microfluidic protein separations via isoelectric focusing and multiplexed sodium dodecyl sulfate gel electrophoresis. *Electrophoresis* **29,** 2241–2250 (2008).

149. Griebel, A., Rund, S., Schönfeld, F., Dörner, W., Konrad, R. & Hardt, S. Integrated polymer chip for two-dimensional capillary gel electrophoresis. *Lab Chip* **4,** 18–23 (2004).

150. Liu, J., Chen, C.-F., Yang, S., Chang, C.-C. & Devoe, D. L. Mixed-mode electrokinetic and chromatographic peptide separations in a microvalve-integrated polymer chip. *Lab Chip* **10,** 2122–2129 (2010).

151. Emrich, C., Medintz, I., Chu, W. & Mathies, R. Microfabricated two-dimensional electrophoresis device for differential protein expression profiling. *Anal. Chem.* **79,** 7360–7366 (2007).

152. Gawron, a J., Martin, R. S. & Lunte, S. M. Microchip electrophoretic separation systems for biomedical and pharmaceutical analysis. *Eur. J. Pharm. Sci.* **14,** 1–12 (2001).

153. Li, F. a., Huang, J. L. & Her, G. R. Chip-CE/MS using a flat low-sheath-flow interface. *Electrophoresis* **29,** 4938–4943 (2008).

154. Mellors, J. S., Gorbounov, V., Ramsey, R. S. & Ramsey, J. M. Fully integrated glass microfluidic device for performing high-efficiency capillary electrophoresis and electrospray ionization mass spectrometry. *Anal. Chem.* **80,** 6881–7 (2008).

155. Chiu, D. T. Interfacing droplet microfluidics with chemical separation for cellular analysis. *Anal. Bioanal. Chem.* **397,** 3179–83 (2010).

156. Edgar, J. S., Milne, G., Zhao, Y., Pabbati, C. P., Lim, D. S. W. & Chiu, D. T. Compartmentalization of chemically separated components into droplets. *Angew. Chemie* **121,** 2757–2760 (2009).

Chapter II

Instrumentation and fabrication

2.1 Microfluidic device fabrication

Among the materials that can be used to fabricate microfluidic devices (i.e. silicon, quartz, glass, polymers)[1], PDMS is one of the most widely used materials due to several inherent advantages. Using soft photolithography, PDMS can be rapidly and simply fabricated into complicated designs[2,3]. The transparency of PDMS allows optical detection at wide range of wavelengths. It is also biocompatible being both non-toxic and gas-permeable, which permits biomolecular or cellular analysis within PDMS microdevices[1]. In addition, the flexibility and robustness are the advantages of PDMS over glass. PDMS is thus used to fabricate most of the designs in this work.

Recently, the fabrication of microdevices using 3D printing technology has attracted much attention from researchers. This is due to some significant advantages in the fabrication process over the conventional soft photolithography. 3D printing is found to be much simpler in fabrication since there is no need to fabricate molds prior to achieving microdevices. The layout of microdevices can be directly transferred from the software (e.g. CAD) to material via a 3D printer to create the desired microdevices. By using 3D printing, it is foreseen that more rapid and automated fabrication processes between laboratories can be achieved with greater levels of standardisation[4]. Therefore, some microdevices used in this work were fabricated using the 3D printing technique.

2.1.1 PDMS microdevice fabrication

Typically, many processes are involved in the fabrication of PDMS microdevices. First, a design of a microdevice is transferred to a photomask that can be used to create an SU-8 master. However, in practice the pattern on the photomask is usually transferred onto a more durable material, often a chromium mask, to prolong the photomask usage. The patterned chromium mask is then used to create an SU-8 master using the photolithography technique. Finally, a PDMS replica is casted from the fabricated SU-8 master, This SU-8 master may be used to replicate microdevices several times.

2.1.1.1 Fabrication of chromium masks

Prior to the fabrication of a chromium mask, a microdevice design is created using AutoCAD (Autodesk, USA) and printed onto a polyester-based film mask (Micro Lithography Services Ltd, UK), which is a darkfield film mask (i.e. translucent channels printed on an opaque dark field).

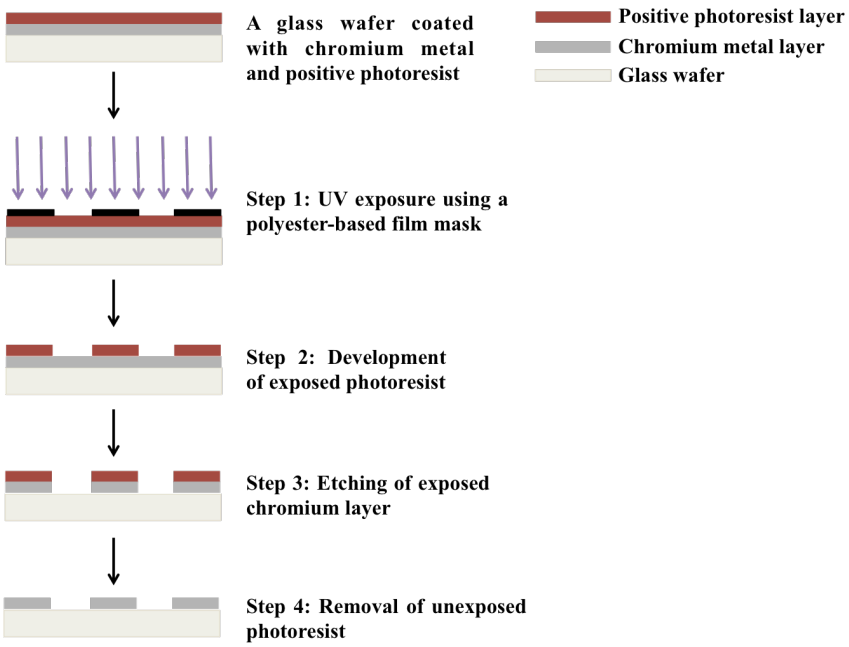

Figure 2.1: A schematic illustrating the process of chromium mask fabrication consisting of four steps. The pattern on a film mask is transferred to a chromium coated glass wafer by exposure to the UV light. The exposed photoresist and the chromium layer are then removed to reveal the pattern on the chromium mask.

The chromium mask is then fabricated as illustrated in **Figure 2.1**. The first step, the printed darkfield film mask serving as a primary mask is placed onto a glass wafer coated with chromium and positive photoresist (AZ1518, 5300 Å, Soda Lime, Nanofilm, USA). The pattern is transferred to the coated glass wafer by exposure to the UV light (Model 30, Optical Associates Inc., USA) through the film mask. The glass wafer is then immersed into a mixture of Microposit 351 Developer (Shipley Europe Limited, Coventry, UK) and deionized (DI) water (at 1:5 volume ratio) for 2 minutes to develop the positive photoresist and hence reveal the transferred pattern. After that the glass wafer

is rinsed with DI water and blown dry with nitrogen gas before it is immersed into a chromium etchant standard solution (Aldrich, UK) for 2 minutes to remove the exposed chromium layer. Subsequently, the glass wafer is rinsed with DI water, blown dry and sonicated in acetone (5-10 minutes) to remove the rest of the photoresist in the unexposed area.

2.1.1.2 Fabrication of SU-8 masters

SU-8 is a negative photoresist containing a Bisphenol A Novolak epoxy oligomer **(Figure 2.2)** and up to 10% triarylsulfonium hexafluroantimonate salt photoacid generator.

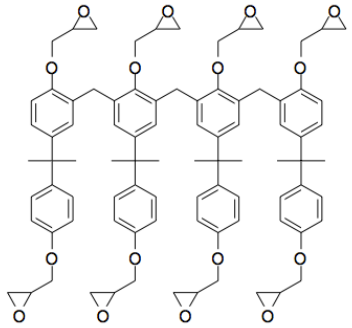

Figure 2.2: A chemical structure of Bisphenol A Novolak epoxy oligomer containing 8 epoxy groups provide for high degree of cross-linking after photoactivation. Image reproduced from reference 5.

The photoacid generator is firstly activated by irradiation. It transforms into an acid, which then protonates the epoxides on the oligomer. After heat application, the protonated epoxy groups react with neutral epoxides yielding the cross-linked SU-8 structure[5]. An SU-8 master is employed as a mold for casting PDMS microdevices. The fabrication process of a SU-8 master is illustrated in **Figure 2.3**. There are five main steps in the fabrication process: spin coat, soft bake, expose, post exposure bake and develop[6].

The first process is spin coating of SU-8 photoresist onto a silicon wafer. The appropriate SU-8 photoresist and spin conditions are selected to achieve the required thickness of the SU-8 layer. This in turn will determine the depth of the channels. In this work, channels

with 100 μm diameter are required. Approximately 4 ml of SU-8 100 (MicroChem, USA) is gently poured onto a 4-inch silicon wafer, 100 mm N <100> with a resistivity of 1-10 Ω•cm and a thickness of 525 μm (IDB Technologies Ltd, UK). The silicon wafer is then placed inside a spin coater (Laurell Technologies Corporation, USA). The first cycle is to cover the entire wafer with the resist by ramping the speed up to 500 rpm at 100 rpm/second acceleration and holding at this speed for 10 seconds. Next, the speed is ramped to 3000 rpm at an acceleration rate of 300 rpm/second and held for 30 seconds in order to achieve the photoresist thickness of 100 μm. The speed of the spin coater is then decreased to 0 rpm within 10 seconds at the acceleration rate of 408 rpm/second.

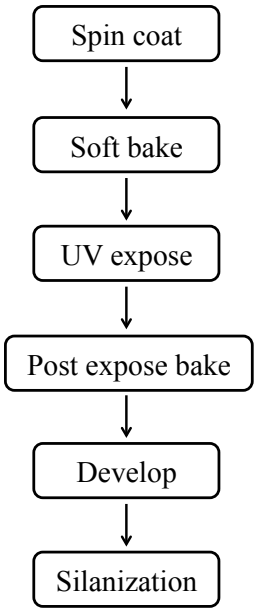

Figure 2.3: Flow chart showing the process of SU-8 master fabrication and surface treatment by silanization.

After spin coating of the silicon wafer is completed, it is soft baked to evaporate the solvent. It is pre-baked on a hot plate at the temperature of 65 °C for 10 minutes and then soft baked at 95 °C for 30 minutes. This condition is for spin coating the silicon wafer with SU-8 100 at 100 μm thickness. Subsequently, the silicon wafer is removed from the hot plate and left to gradually cool prior to the exposure step.

The patterned chromium mask (described in **Section 2.1.1.1**) is placed onto the coated silicon wafer after it is cool. Both silicon wafer and chromium mask are then irradiated with UV light (Model 30, Optical Associates Inc., USA) for 30 seconds. The irradiation initiates the polymerization of SU-8 100. The silicon wafer is then post exposure baked (PEB). This is achieved in two steps to minimize stress and photoresist cracking. The first PEB baked is at 65 °C for 1 minute and the second step is at 95 °C for 10 minutes.

A developer solvent consisting of 2-methoxy-1-methylethyl acetate (Microposit EC Solvent, Chestech Ltd, UK) is used to remove unexposed SU-8 on the silicon wafer. The PEB silicon wafer is then immersed into the developer solvent and strongly agitated for 10 minutes. It is then rinsed with isopropanol and blown dry with nitrogen gas.

Another important process after the fabrication of SU-8 master is the silanization of the master to prevent cured PDMS from adhering to the master. The master is exposed to vaporised silane (Trichloro (1H, 1H, 2H, 2H-perfluorooctyl) silane, Sigma Aldrich) under vacuum for 2 hours. The master is now ready for PDMS casting.

2.1.1.3 PDMS casting

After the fabrication of an SU-8 master, PDMS microdevices are cast by pouring a mixture of a base (tetra (trimethylsiloxy) silane) and a curing agent (tetramethyltetravinylcyclote-trasiloxane), in a SYLGARD 184 Silicone Elastomer Kit (Dow Corning Ltd, UK) at the weight ratio of 10:1 onto the SU-8 master[7]. This mixture is first thoroughly mixed and then applied to the mold. Following this the mold is degassed and heated in an oven at 65 °C for 2-4 hours prior to assembly.

2.1.1.4 Microdevice assembly

After PDMS casting, both top and bottom pieces of PDMS are cut and peeled off the mold. Holes are punched on the top piece of PDMS to create reservoirs using a biopsy punch (1, 2 or 4 mm I.D. biopsy punch, Kai Medical, Japan). Both top and bottom pieces of PDMS are sonicated in DI water for 5 minutes and blown dry with nitrogen gas. Following this cleaning stage, they are placed inside the oxygen plasma oven (Harrick

Plasma, USA) for 1 minute. The plasma-treated PDMS pieces are then aligned and placed under pressure to bond.

2.1.2 3D-printed microdevice

3D-printed microdevices used in this work were designed using AutoCAD 2013 (Autodesk, USA) and were printed using a ProJet® 3510 HD (3D systems GmbH, Germany)[8]. The material used to fabricate the 3D-printed microdevices was UV curable acrylonitrile butadiene styrene (ABS) resin. The ABS resin was jetted through a printhead to print layer by layer onto a platform; meanwhile, the wax support material was jetted through the other printhead to fill voids. The plastic part was then cured by UV light. The support wax was then melted away. Owing to the small dimension of channels in the microdevices (~ 200 μm), further treatment to completely wash out the wax was performed by sonicating the microdevice in 10% SDS at 70°C for 2 hours. The microdevices were then rinsed with water and placed in an oven at 70°C for 30 minutes.

2.2 Droplet-based microchip platform fabrication

A droplet-based microchip platform was designed using AutoCAD 2013 (Autodesk, USA) and was fabricated using a laser engraving and cutting machine (Laserscript LS3040 LSRCUT, HPC Laser Ltd.). Briefly, an acrylic plate was cut according to the design using a CO_2 laser, which emits infrared radiation (wavelength 10.6 μm). After the fabrication, the acrylic platform could be used immediately without other modification or treatment.

2.3 Robotic droplet generator

The droplets used in the experiments were predominantly generated using the robotic droplet generator (**Figure 2.4)** developed by *Gielen* and co-workers[9]. The entire system consists of three main parts that are a robotic droplet generator, a syringe pump and a computer.

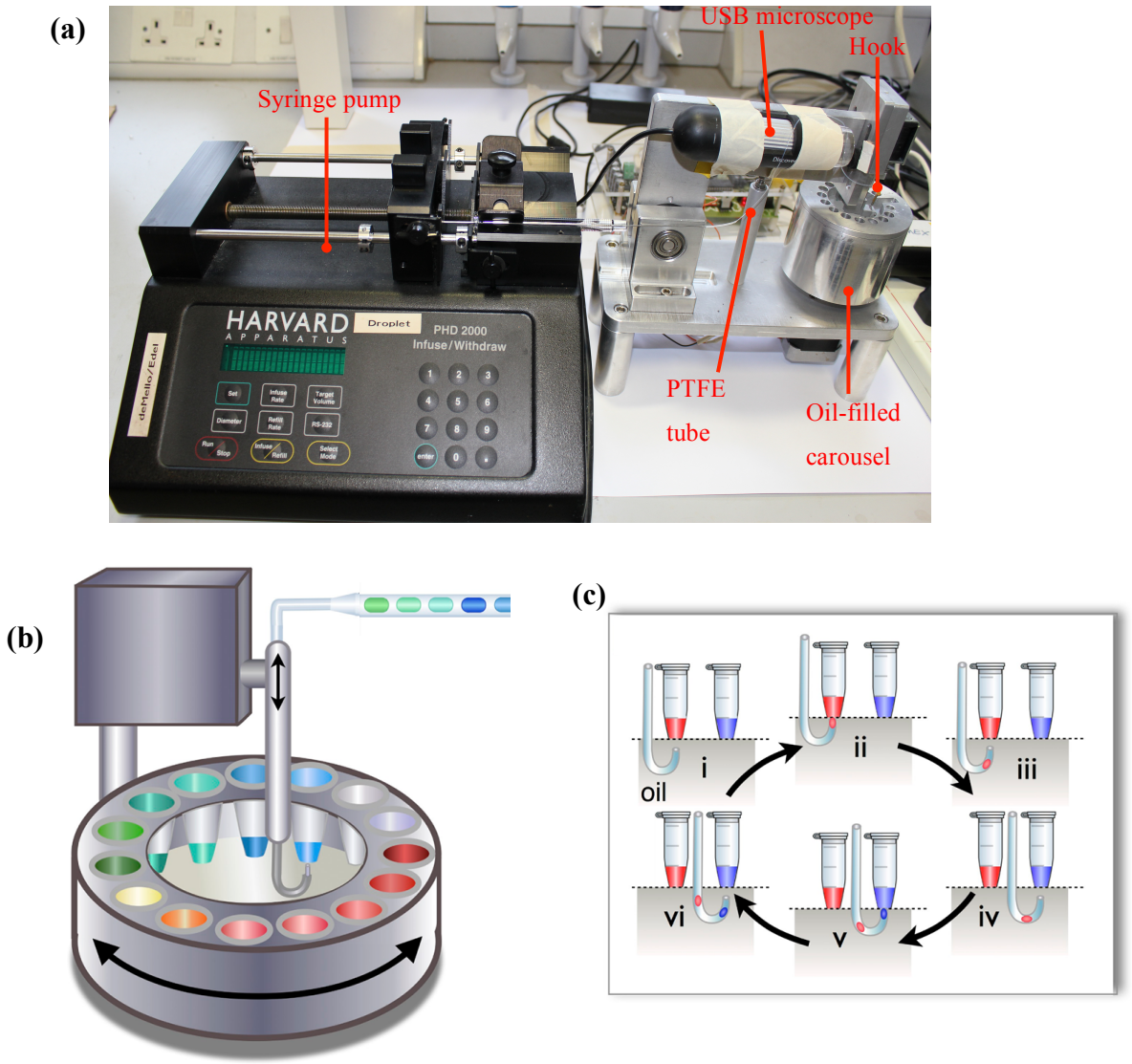

Figure 2.4: An image and schematics of a robotic droplet generator (a) An image showing the entire system of the robotic droplet generator consisting of a PTFE tube inserted into a metal hook, an oil-filled carousel, a camera, a glass syringe and a syringe pump; (b) An enlargement of the oil-filled carousel part showing the carousel that can move forward and backward as illustrated by the arrows and the hook that can be in the "up" and "down" position under the control of a solenoid. Fifteen samples can be held by holes on a metal ring for this model of the robotic droplet generator; (c) A schematic illustrating droplet generation from two samples using the robotic droplet generator (i) The carousel moves until the tip of the hook is in the oil phase beneath the first sample (red), (ii) The hook is in the "up" position and withdraws the sample (red), (iii) The hook is in the "down" position and withdraws the oil, (iv) The carousel moves again towards the second sample (blue) until the tip of the hook is underneath the sample, (v) The same process as that of (ii) occurs to achieve a droplet of the second sample (blue), (vi) The process in (iii) is repeated. Image (b) and (c) reproduced from reference 9.

To set up the experiment for droplet generation, around 60 ml of FC-40 oil (Fluorinert, Acota, UK) was poured into an oil-filled carousel. An aqueous sample was pipetted into a bottomless PCR tube (0.2 ml PCR tube with ~ 0.2 cm of bottom cut out, VWR, USA) placed into one of 15 holes on a metal ring depicted in **Figure 2.4b**. A 30 cm long PTFE tube (Ultramicrobore 100 μm I.D., 400 μm O.D., Cole Parmer, London, UK) was inserted into a stainless steel hook, and was allowed to protrude about 3-4 mm from the mouth of the hook to ensure that the entrance of the tube reached an aqueous sample when the tube was moved to the upward position. Upstream from the hook, nearer the central section of the tube, a USB microscope (VMS-001, Veho Discovery, UK) was fixed and focused to observe the generated droplets. The terminal end of the tube was connected to a glass syringe (Gastight 100 μL, Model 1710 N SYR, Hamilton), which was secured on a syringe pump (PHD 2000, Harvard Apparatus).

Prior to the droplet generation, the mouth of the tube was aligned to the middle of the bottomless PCR tube. A positive flow rate of 3.0 μl/min was applied for a while to eliminate any air bubbles remaining inside the tube. After that a negative flow rate set between 1.2 and 2.5 μl/min was exerted for 5-10 minutes to stabilize the pressure. Meanwhile, three parameters on a custom-written software (LabVIEW programme, National Instruments), used to control the robotic droplet generator were set. Normally, the frequency of droplet generation was set at 1 Hz. The retention times of the tube in the aqueous and the oil phase were 0.3 s and 0.7 s, respectively. The number of droplets to be generated was in the range of 100-150 droplets. These parameters could be varied to achieve the required droplet size and interdroplet spacing. When the pressure was stable, droplets were started generating at the set parameters.

The droplet robot functioned in the following way - firstly, the carousel moved from the zero position to the first position where the sample was located **(Figure 2.4ci)**. The hook controlled by a solenoid was then moved to the "up" position and the aqueous sample in the bottomless PCR tube was withdrawn into the tube for the determined period of time, i.e. the retention time of the tube in the aqueous phase **(Figure 2.4cii)**. After that the hook was in the "down" position **(Figure 2.4ciii)** for a while (i.e. the retention time of the tube in the oil phase) before the carousel moved to the next sample **(Figure 2.4civ)** or moved back to the zero position in case only one sample was used. The process was repeated

until the required number of droplets was achieved. The pump was then stopped. The droplet delivery tube was detached from the robot when the pressure inside the tube was stabilized – this is determined to be when the droplets stop moving. The droplets collected in the tube were then ready for further analysis or were stored in the dark (for fluorescent dye or fluorescently labeled protein droplets) until they were used.

2.4 Capillary electrophoresis operation

2.4.1 Commercial capillary electrophoresis machine (Peregrine)

The commercial capillary electrophoresis machine used in this work is called Peregrine (deltaDOT Ltd., UK). Peregrine is a High Performance Capillary Electrophoresis (HPCE) machine used to perform electrophoresis for label-free analytes using UV detection. The system instrumentation, operation and data analysis are described in detail in **Section 2.4.1.1- 2.4.1.3**.

2.4.1.1 Peregrine instrument

The overview of the Peregrine machine is depicted in **Figure 2.5a**. The main electrophoresis compartment and optical components are situated under the main cover **(Figure2.5b)**, whereas two carousels are located on the left and right side of Peregrine as shown in **Figure 2.5a**. The other components housed underneath the main cover are a deuterium lamp, a filter wheel (containing 214 nm, 254 nm and 280 nm filters), adjustable lens, a capillary block and a heat sink (for temperature control) and a photodiode array (PDA) detector as depicted in **Figure 2.6**. Each carousel contained 24 vial holders **(Figure 2.5b)** for glass sample and reagent vials (SMI-LabHut Ltd, Gloucestershire, UK). In operation, Peregrine is connected to a nitrogen gas tank used as a pressure source for hydrodynamic actions (i.e. flushing or filling of buffer/reagents and sample injection). During the experiment, the machine is controlled by P3Controler software, while the collected data are analysed and compared by the software named P3EVA provided by deltaDOT.

The principle of this machine is briefly described here. Both sample and reagent are delivered from glass vials through a capillary housed in the capillary block. When analytes pass a detection window, they absorb UV light from the lamp. Samples that absorb UV light like proteins and DNA create a drop in light intensity. The UV light is converted into an electrical signal at the detector and is transformed into a trace called an electropherogram.

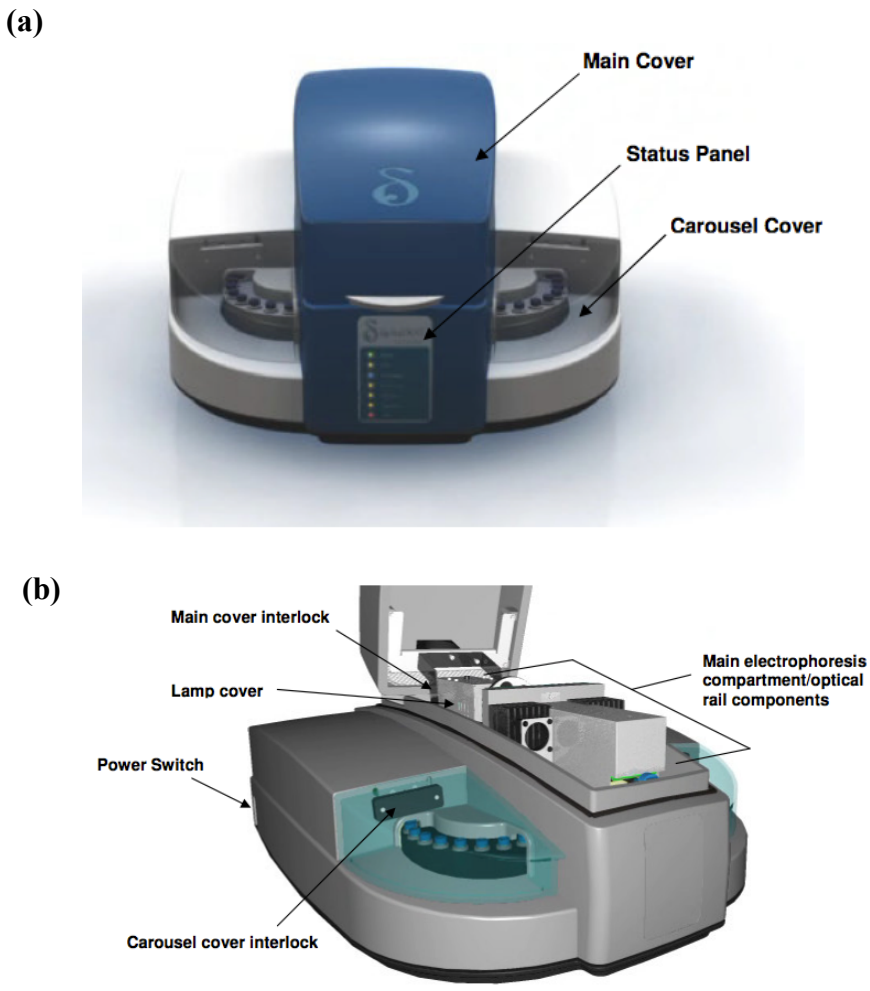

Figure 2.5: Schematics illustrating overall instrumentation of Peregrine (a) Outside of the machine showing main cover, status panel and carousel cover; (b) Inside the machine showing main cover interlock, lamp cover and main electrophoresis compartment/ optical rail components inside the main cover, carousel cover interlock inside the carousel cover and power switch at the side of the machine. Images reproduced from reference 10.

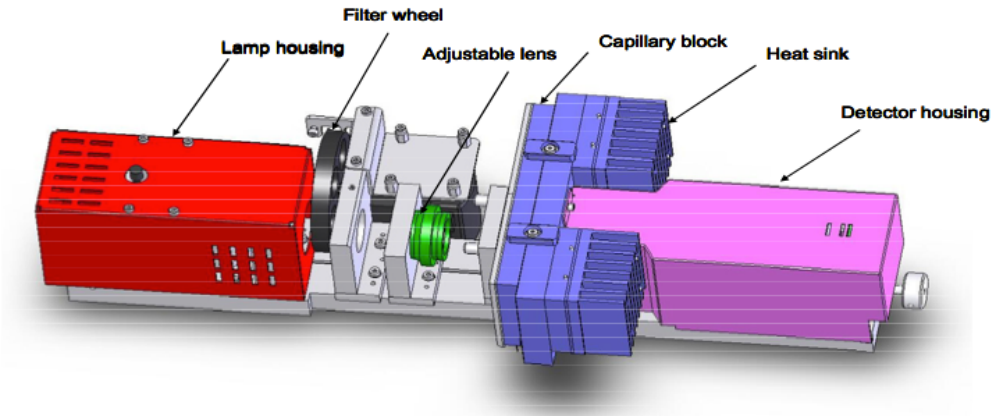

Figure 2.6: Schematic depicting the components inside the main cover of Peregrine. Image reproduced from reference 10.

One of the important components of the CE machine is the capillary within which the analysis takes place. For Peregrine, the capillary is located inside the aluminium capillary block **(Figure 2.7a)** that has capillary tracks (10-70 cm long) carved into its surface **(Figure 2.7b)**. The capillary can be placed into each pattern of the track according to its length; for example, a capillary with 20.2 cm separation length is situated in the capillary track as depicted in **Figure 2.7b**. The length of the capillary that can be fitted into the capillary track is determined as the separation length and the total length. The separation length of the capillary is defined as the length from the inlet end to the middle of the detection window **Figure 2.7c** and the total length is defined as the length from the inlet end to the outlet end. The separation length and the total length of the capillary fitted with the capillary track of Peregrine can be varied from 20 cm to 70 cm and from 34 cm to 82 cm, respectively.

For all experiments in this work performed using Peregrine, capillaries with a total length of 34 cm and a separation length of 20 cm (50 µm I.D., 375 µm O.D., Polymicro technologies, CM Scientific, UK) were employed. Capillaries were cut to the required length and were burned to remove polyimide coating to create 1.5 cm clear windows (the actual detection window is 1.25 cm) at the length of 20 cm. The burnt polyimide was wiped out using a fibre-free tissue soaked with ethanol. The capillaries were then placed into the track as illustrated in **Figure 2.7b** and were secured by the block cover and

several screws. After that the capillary block was placed into the block holder inside the main cover and was secured by two clamps.

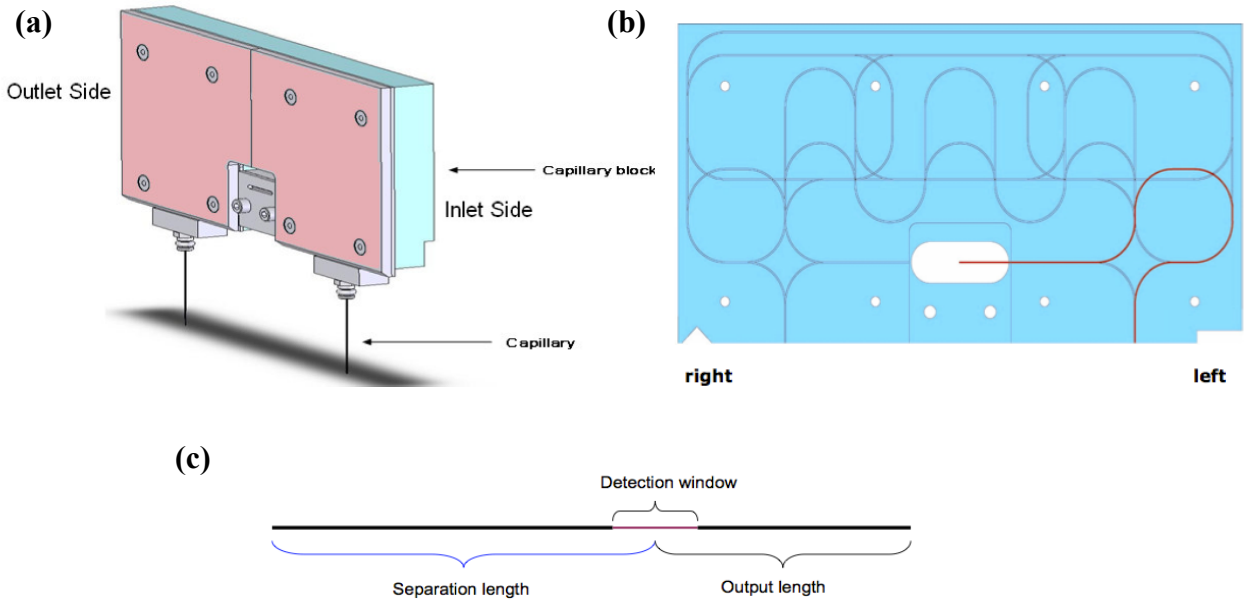

Figure 2.7: Schematics illustrating outside and inside of the capillary block used with Peregrine machine (a) Overview of the capillary block; (b) Capillary track (red line) of 20.2 cm input capillary length; (c) Illustrating a fused silica capillary with 1.25 cm detection window. Images reproduced from reference 10.

2.4.1.2 Peregrine standard operating protocol

In this work, the operating protocol of Peregrine was set for protein electrophoresis. The filter was set at 214 nm by adjusting the filter wheel. The temperature for electrophoresis was set at 25 °C. The reagent and sample vials were placed in their right carousel positions. Prior to the first protein electrophoresis, the capillary was conditioned according to **Table 2.1**. A sample was then electrokinetically injected at 5 kV for 20 seconds and separated at 6-15 kV for 35 minutes. Between each run, the capillary was conditioned according to step 2 to step 4 in **Table 2.1** prior to the next sample injection and separation.

Table 2.1: Conditioning steps for new capillaries

Step	Condition	Reagent	Pressure (psi)	Time (min)
1	Flush	1 M HCl	20	20
2	Flush	DI water	20	2
3	Flush	0.1 M HCl	30	3
4	Flush	Buffer solution	60	8

2.4.1.3 Data analysis

After the electrophoresis is completed, the collected data was processed and analysed using P3EVA software provided by deltaDOT. Two main analytical results obtained from P3EVA software and normally used in this work are GST processed electropherogram (**Figure 2.8b**) and Equiphase map (**Figure 2.9a**), which are discussed in detail in **Section 2.4.1.3.1 and 2.4.1.3.2**.

2.4.1.3.1 GST processed electropherogram

The detection format used in the Peregrine instrument is UV based, which typically suffers from low sensitivity (i.e. low signal-to-noise ratio (S/N)) and poor limit of detection (10^{-5}-10^{-6} M) for some analytes[11]. One of the methods to improve sensitivity and detection limits is to use multi-point detection (e.g. the use of photodiode array (PDA)) on a single run measurement.

Peregrine employs a PDA as a detector. Herein, 512 diodes are placed in a linear array having 25 μm width and a total length of 1.28 cm. Each diode produces an electropherogram; hence, 512 diodes provide for 512 individual electropherograms. General separation transform (GST) is used to combine 512 individual electropherograms **(Figure 2.8a)** resulting in a single electropherogram **(Figure 2.8b)** retaining the same peak shape as the original electropherograms with significantly higher signal-to-noise ratio. Consequently, by using multi-point detection, there is no need to modify the

capillary shape to achieve a longer path-length and several measurements are not required to achieve signal averaging in order to enhance the sensitivity and detection limits.

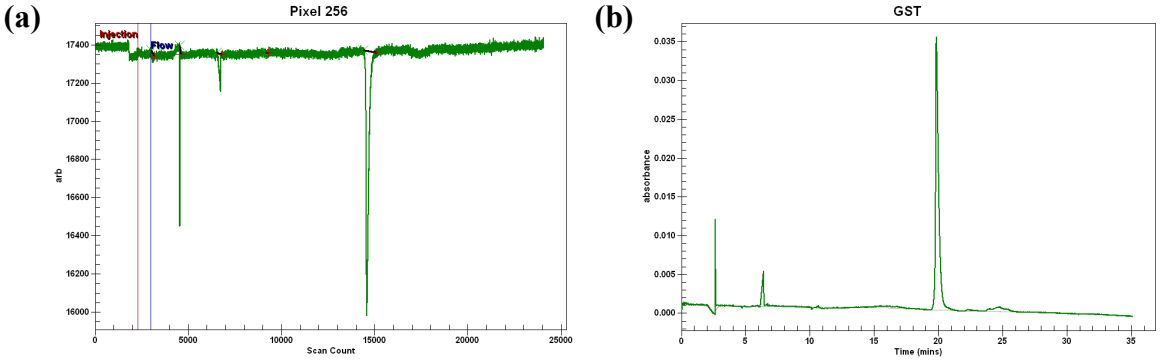

Figure 2.8: An example of (a) raw data obtained from 1-pixel detector showing transmittance vs. time (scan count) and (b) GST processed electropherogram in which the axes are absorbance vs. time (min).

2.4.1.3.2 Equiphase map

An equiphase map is a 3D map showing the tracks of analytes passing through the detector (**Figure 2.9a**). The map consists of absorption, distance and time axes. **Figure 2.9b** illustrates the generated tracks of analytes obtained from one of the 512 pixels of the detector. By dividing the distance (between pixel 1 and pixel 512) by the time the analyte passes the PDA, the velocity of the analyte, which depends on its intrinsic properties (e.g. overall charge and molecular mass) and an applied electric field, is obtained. The velocity is therefore equal to the slope of the track and the inclination of the slope indicates the magnitude of the velocity of the analyte (i.e. the steeper slope represents the higher velocity.)

In addition, the track may be extrapolated back to the injection point so that any peaks being not related to the analytes and moving in the opposite direction will not be present in the processed signal. On the other hand, analytes moving from the outlet towards the detector can be observed by reversing the order of the pixels. This is useful for the determination of EOF during the performance of electrophoresis. The track may also be

extrapolated forward to predict the elution time of each analyte so that it can be selectively collected after separation.

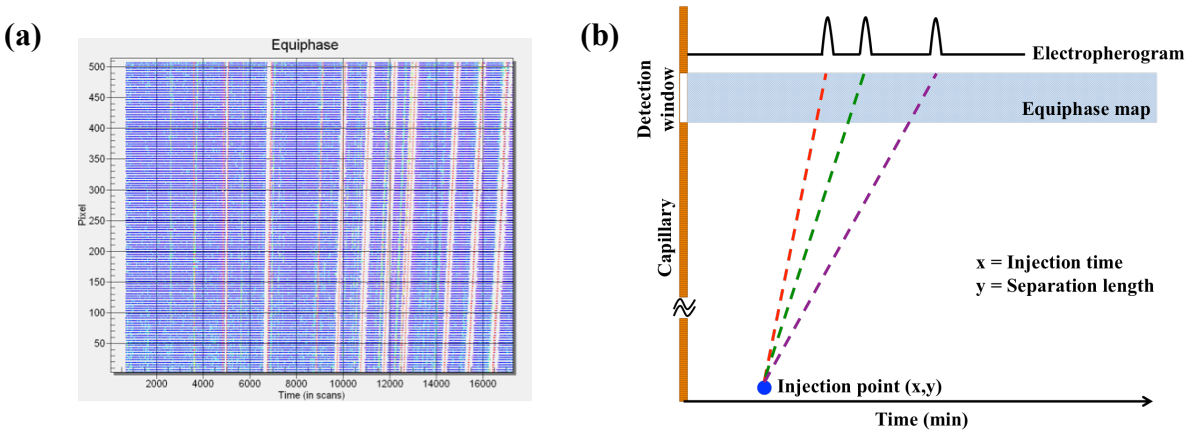

Figure 2.9: Equiphase map (a) An example of equiphase map; (b) Schematic illustrating how the equiphase map is generated. Image (a) reproduced from reference 10 and (b) adapted from reference 12.

2.4.2 Microchip-based electrophoresis

The setup for microchip-based electrophoresis consisted of a microdevice (i.e. cross-piece PDMS microdevice, cross-piece PDMS microdevice coupled to a fused-silica (glass) capillary and interfacing droplet-based microdevice), a platform for holding the microdevice, a high voltage power supply and a fluorescence detector. The cross-piece PDMS microdevice and the cross-piece PDMS microdevice coupled to the capillary are illustrated in **Figure 3.2a** and **Figure 3.2b** and described in detail in **Chapter 3**, while the interfacing droplet-based microdevices are depicted in **Chapter 5**. An aluminium platform was used to hold the cross-piece PDMS microdevice and the cross-piece PDMS microdevice coupled to the capillary (**Figure 3.2c** in **Chapter 3**), while either old (**Figure 5.25** in **Chapter 5** and **Figure 6.2** in **Chapter 6**) or new (**Figure 6.8** in **Chapter 6**) acrylic platform was employed to hold the interfacing droplet-based microdevices. Illustrations of different types of microdevices and platforms are depicted with fully descriptive detail in different chapters where they are mentioned in the specific experimental setup.

2.4.2.1 Fluorescence detection

Fluorescence detection in this work was performed using a Nikon Eclipse E400 (Nikon Ltd., Surrey, UK). The light from a 100 W mercury lamp (Nikon UK Ltd.) passed through a FITC filter cube (an excitation filter at 470-490 nm, a long pass emission filter at 510 nm cut-on, Nikon Instruments UK) and focused on the detection area on the microdevice through x4 or x10 objective lens. Fluorescence emission was detected by a CCD camera (C4742-96, Hamamatsu Photonic Systems, Bridgewater, NJ), which was controlled using Wasabi program version 2.0. The collected images were analysed with Image J software (NIH). The extracted data from images were used to create electropherograms.

2.4.2.2 Microdevice-based instrument setup

After the microdevice used to perform electrophoresis was filled with a buffer solution, the microdevice was then placed on a platform that was screwed to a motorized microscope stage (Optiscan, Prior Scientific Instruments Ltd., UK). A conductivity check was carried out by applying voltages through Pt electrodes across the separation channel prior to electrophoresis. After that, the electric field was applied in the injection and separation mode using a high voltage power supply (HVS448 3000V, Labsmith, CA, USA).

2.5 References

1. Zhang, X. & Haswell, S. J. Materials Matter in Microfluidic Devices. *MRS Bull.* **31,** 95–99 (2006).

2. Wu, D., Qin, J. & Lin, B. Electrophoretic separations on microfluidic chips. *J. Chromatogr. A* **1184,** 542–59 (2008).

3. Liu, C.-Y., Xu, X., Gao, H.-J. & Chen, J.-R. Poly(dimethylsiloxane) Microchips with Two Sharpened Stretching Tips and Its Application to Protein Separation Using Dynamic Coating. *Chinese J. Chem.* **25,** 190–195 (2007).

4. Gross, B. C., Erkal, J. L., Lockwood, S. Y., Chen, C. & Spence, D. M. Evaluation of 3D printing and its potential impact on biotechnology and the chemical sciences. *Anal. Chem.* **86,** 3240–53 (2014).

5. Campo, a Del & Greiner, C. SU-8: a photoresist for high-aspect-ratio and 3D submicron lithography. *J. Micromechanics Microengineering* **17,** R81–R95 (2007).

6. MicroChem. NANO^{TM} SU-8 Negative Tone Photoresist Formulations 50-100.

7. Friend, J. & Yeo, L. Fabrication of microfluidic devices using polydimethylsiloxane. *Biomicrofluidics* **4,** 1–5 (2010).

8. Martino, C., Berger, S., Wootton, R. C. R. & deMello, A. J. A 3D-printed microcapillary assembly for facile double emulsion generation. *Lab Chip* **14,** 4178–82 (2014).

9. Gielen, F., Vliet, L. V., Koprowski, B. T., Devenish, S. R. A., Fischlechner, M., Edel, J. B., Niu, X., deMello, A. J. & Hollfelder, F. A fully unsupervised compartment-on-demand platform for precise nanoliter assays of time-dependent steady-state enzyme kinetics and inhibition. *Anal. Chem.* **85,** 4761–4769 (2013).

10. deltaDOT. *PEREGRINE I HPCE Instrument Manual Version 1.3*. (deltaDOT Ltd, 2008).

11. Swinney, K. & Bornhop, D. J. Detection in capillary electrophoresis. *Electrophoresis* **21,** 1239–1250 (2000).

12. Pereira, F. Continuous and Segmented-Flow Microfluidics for Biomolecular Analysis. (2011).

Chapter III

Development of novel buffers for protein separations

3.1 Introduction

For many years, protein electrophoresis was performed in slab gel formats, employing polyacrylamide as a sieving matrix. Due to the long analysis times and laborious process of slab gel preparation, proteins separations were subsequently transferred to capillary-based formats. However, gel shrinkage and the generation of bubbles inside capillaries often occur during *in situ* polymerization of polyacrylamide[1,2]. In addition, column stability is typically poor when cross-linked polyacrylamide is used[3]. Consequently, non-crosslinked polymers, which are replaceable, have been proposed and used for a variety of protein separations using capillary electrophoresis. Significantly, due to their low viscosities, such polymer-based buffers may also be used in conjunction with microfluidic channels[4].

Examples of non-crosslinked polymers that have been used as sieving matrices for separations of SDS-protein complexes include linear polyacrylamide (LPA)[1,2,3,5], polyethylene oxide (PEO)[1,3,6,7], dextran[1,3,7,8], pullulan[1,4,9,10], polydimethylacrylamide (PDMA)[4,11,12], and pluronic[4,13]. Many commercial buffers for SDS-protein capillary electrophoresis (including SDS-MW gel buffer from *Beckman Coulter*, ProSort SDS-protein buffer from *Applied Biosystems*, SDS-protein calibration kit for CE from *Sigma Aldrich* and CE-SDS run buffer from *Bio-Rad*) also employ non-crosslinked polymers due to the ability to be easily replaced after each run. Unfortunately, some of these commercial buffers are no longer available, so they were not tested in this work.

Of the non-crosslinked polymers described, PEO, dextran and PDMA have been widely used in the preparation of laboratory-made buffers and are assessed in the current work. PEO is a linear polymer that has been extensively studied as the functional component in sieving matrices. It provides several advantages, including low viscosity, minimal absorption in the UV region of the electromagnetic spectrum, utility as a dynamic surface coating, limited reactivity with fluorogenic labeling reagents and proteins and most importantly access to high resolution separations[14]. Owing to these properties, PEO has been used as a sieving matrix in commercial buffers[14]. Dextran is a hydrophilic-branched polymer, which has low viscosity and good transparency in the UV region of the electromagnetic spectrum. It also provides for high resolution separations of a wide range

of proteins and peptides[14]. For the background electrolytes, Tris (hydroxymethyl) aminomethane and N-Cyclohexyl-2-aminoethanesulfonic acid (TRIS-CHES) are compatible with PEO and 2-Amino-2-methyl-1,3-propanediol and cacodylic acid (AMPD-CACO) are compatible with dextran in terms of conductivity and UV absorption characteristics[3]. TRIS-CHES buffer also suppresses SDS adsorption to PEO[15]. PDMA is a low viscosity polymer with excellent sieving capabilities and a high surface coating capacity. It is employed as a sieving matrix in the *Agilent Bioanalyzer* 2100 running buffer[14]. Moreover, *Tabuchi* and co-workers[11] have reported the use of PDMA in borate buffer as a sieving matrix for protein separations in microfluidic devices.

Since the studies described in this thesis are focused on the rapid and high-resolution separation of proteins, an appropriate buffer system that is compatible with the droplet-based microfluidic format is required. In addition, the developed buffer should be compatible with both PDMS and glass capillary systems that are used in this work. Both commercial and laboratory-made buffers were tested and optimized for protein separations using a commercial capillary electrophoresis system, a cross-piece PDMS microdevice and a cross-piece PDMS microdevice coupled to a glass capillary as illustrated in the diagram (**Figure 3.1**). The most appropriate buffer from the testing was then used for the droplet-based separation of proteins discussed in **Chapter 6**.

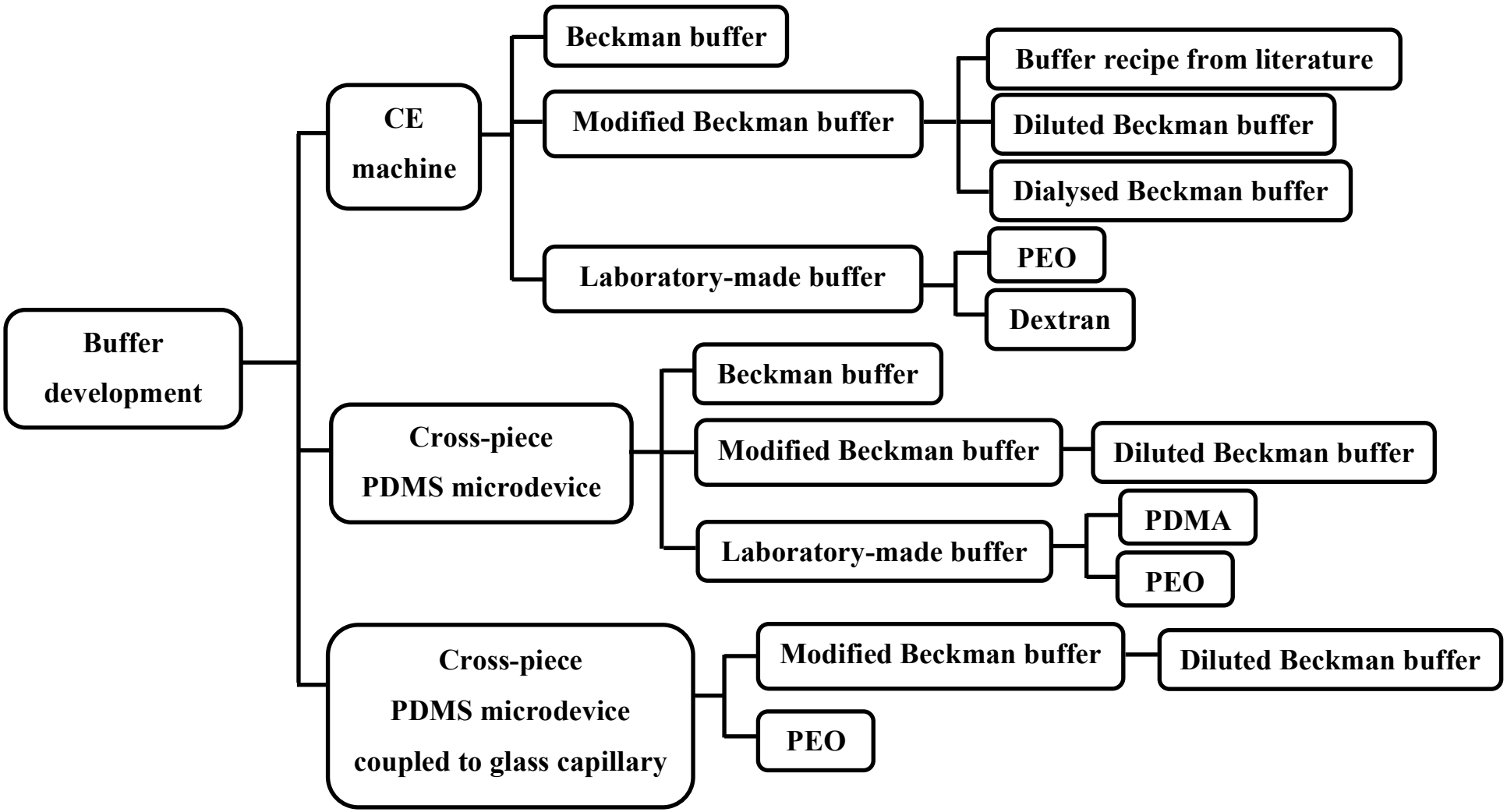

Figure 3.1: Diagram showing the process of buffer development for protein separations.

3.2 Experimental

3.2.1 Chemicals

All chemicals used in the experiments discussed in this chapter are listed in **Table 3.1**.

Table 3.1: Samples and chemicals used to perform protein electrophoresis in **Chapter 3.**

No.	Chemical	Supplier
1.	2-Amino-2-methyl-1,3-propanediol (AMPD)	Sigma Aldrich, UK
2.	2-(Cyclohexylamino)ethanesulfonic acid (CHES)	Sigma Aldrich, UK
3.	β-Mercaptoethanol (BME)	Sigma Aldrich, UK
4.	Albumin from bovine serum (BSA)	Sigma Aldrich, UK
5.	Albumin, Fluorescein isothiocyanate conjugate bovine (BSA-FITC)	Sigma Aldrich, UK
6.	Ammonium peroxydisulfate (APS)	Sigma Aldrich, UK
7.	Benchmark™ Fluorescent protein standard (11-155 kDa) in 0.45 M TRIS-HCl pH 8.5, 2% SDS, 12% glycerol, 0.0025% Coomassie G-250	Thermo Fisher Scientific, UK
8.	Cacodylic acid (CACO)	Sigma Aldrich, UK
9.	Carbonic anhydrase from bovine erythrocytes (CA)	Sigma Aldrich, UK
10.	Dextran from *Leuconostoc* spp. 70 kDa and 2 MDa	Sigma Aldrich, UK
11.	EOTrol™ polymer solution LN	Target Discovery, USA
12.	Fluorescein ACROS Organic™	Fisher Scientific, UK
13.	Fluorescent molecular weight marker (20-200 kDa) containing 62 mM Tris-HCl, pH 8.0, 1 mM EDTA, 3% sucrose, 0.5% dithiothreitol, 2% SDS, and 0.005% bromophenol blue	Sigma Aldrich, UK
14.	Glycerol	Sigma Aldrich, UK
15.	Hydrochloric acid	Sigma Aldrich, UK
16.	Isopropanol	Sigma Aldrich, UK
17.	Lysozyme from chicken egg white	Sigma Aldrich, UK
18.	N, N-dimethylacrylamide	Sigma Aldrich, UK
19.	N, N, N', N'-tetramethylenediamine (TEMED)	Sigma Aldrich, UK
20.	PA 800 plus SDS-MW gel buffer, proprietary formulation, 0.2% SDS, pH 8 (Beckman buffer)	Beckman Coulter, UK

No.	Chemical	Supplier
21.	PA 800 plus sample buffer, 0.1 M TRIS-HCl, 1% SDS, pH 9 (Beckman sample buffer)	Beckman Coulter, UK
22.	Polyethylene oxide (PEO) 100 kDa, 200 kDa and 1 MDa	Sigma Aldrich, UK
23.	Sodium dihydrogen phosphate	Sigma Aldrich, UK
24.	Sodium dodecyl sulfate (SDS)	Sigma Aldrich, UK
25.	Sodium sulfide	Sigma Aldrich, UK
26.	Sodium tetraborate	Sigma Aldrich, UK
27.	Sulfuric acid	Sigma Aldrich, UK
28.	Thiourea	Sigma Aldrich, UK
29.	TRIS-Borate-EDTA buffer (10x TBE)	Sigma Aldrich, UK
30.	Tris(hydroxymethyl)aminomethane (Trizma® base or TRIS)	Sigma Aldrich, UK
31.	Tris(hydroxymethyl)aminomethane hydrochloride (Trizma® hydrochloride or TRIS-HCl)	Sigma Aldrich, UK

Note: Benchmark fluorescent protein standard (Thermo Fisher Scientific, UK) consists of seven proteins with molecular weight of 12, 23, 33, 41, 65, 100 and 155 kDa[16]. Fluorescent molecular weight marker (Sigma Aldrich, UK) consists of six proteins i.e. trypsin inhibitor (20 kDa), carbonic anhydrase (29 kDa), alcohol dehydrogenase (39.8 kDa), bovine serum albumin (66 kDa), β-galactosidase (116 kDa) and myosin (200 kDa) [17].

3.2.2 Preparation of samples

Table 3.2: Sample buffers for protein separation using the commercial CE machine.

No.	Sample buffer
1.	Beckman sample buffer added 5% v/v BME
2.	5 mM SDS, 5 mM sodium tetraborate buffer, pH 8.5
3.	5 mM SDS, 5 mM sodium tetraborate buffer, pH 8.8
4.	5 mM SDS, 5 mM sodium tetraborate buffer, pH 9.0
5.	0.01 M TRIS-HCl, 0.1% SDS, pH 6.6
6.	1x TBE, 0.1% SDS, pH 7.56 added 5% (v/v) BME

For capillary gel electrophoretic separations of proteins using the commercial CE system, a 6-mg/ml stock solution of each protein standard (lysozyme, CA and BSA) was prepared in deionized water (DI water, Direct-Q, Merck Millipore, UK). Each protein standard and a mixture of these three proteins were then prepared by diluting the stock solution using an appropriate buffer (**Table 3.2)**. All protein samples were heated at 95°C for 5 minutes. The final concentration of protein standards and each protein in the mixture was 0.5 mg/ml. For all experiments, 0.5 mg/ml of thiourea dissolved in DI water was used as an EOF marker.

Fluorescein, BSA-FITC, benchmark fluorescent protein standard (11-155 kDa) and fluorescent molecular weight marker (20-200 kDa) were used to investigate protein separations using the cross-piece PDMS microdevice and the cross-piece PDMS microdevice coupled to a glass capillary. Fluorescein (4.5 mM) was prepared in 960 µl of DI water and added 40 µl of 1 M NaOH. BSA-FITC was dissolved in 0.2% SDS to achieve a concentration of 1 mg/ml and then heated at 95 °C for 5 minutes. The benchmark fluorescent protein standard (11-155 kDa) was used as received and without heating, while the fluorescent molecular weight marker (20-200 kDa) was heated at 65 °C for 5 minutes prior to being used. Fluorescein and protein samples were pipetted and mixed in a sample reservoir of a cross-piece PDMS microdevice prior to injection.

3.2.3 Preparation of running buffers

3.2.3.1 Diluted Beckman buffers

Beckman buffer was diluted in DI water to concentrations of 0.2x, 0.25x, 0.33x and 0.5x. The diluted Beckman buffers were then stirred at 25 °C overnight. For the diluted Beckman buffer mixed with EOTrol, 0.5 ml of EOTrol was added to 9.5 ml of 0.2x Beckman buffer and the mixture was stirred thoroughly. All buffers were degassed prior to use.

3.2.3.2 Dialysed Beckman buffers

Beckman buffer was dialysed against DI water or 0.1x TBE buffer, pH 7 using a cellulose dialysis tube, benzoylated (Sigma Aldrich, UK), which separates compounds with a molecular weight of ≤ 1200 Da from compounds with molecular weights above 2000 Da. The dialysis tube was prepared by excessive washing with water to remove glycerin. Sulfur compounds were also removed from the tube by treating with a 0.3% (w/v) sodium sulfide solution at 70 °C for 1 minute. The tube was then washed with 60°C water for 2 minutes, followed by 0.2% sulfuric acid and rinsed with hot water to remove the acid. Subsequently, Beckman buffer was poured into the dialysis tube, which was then immersed into DI water or 0.1x TBE buffer. Dialysis was performed for two days at 25 °C, with the DI water or 0.1x TBE buffer being stirred throughout. After the dialysis process, 0.5% SDS was added to the dialysed Beckman buffer against 0.1x TBE buffer. All dialysed Beckman buffers were degassed before they were used.

3.2.3.3 80/20 Beckman: 5 mM SDS, 5 mM sodium tetraborate buffer, pH 9

8 ml of Beckman buffer was mixed with 2 ml of 5 mM SDS, 5 mM sodium tetraborate buffer, pH 9 to achieve a 8:2 volumetric ratio. The mixture was stirred thoroughly and degassed before use.

3.2.3.4 PEO and dextran based buffers

PEO having molecular weights of 100 kDa, 200 kDa and 1 MDa and dextran having molecular weight of 70 kDa and 2 MDa were investigated in this work. Both polymers were used to prepare buffers with different compositions (e.g. background electrolytes, polymer molecular weight and concentration, pH and additives) as shown in **Table 3.4**. For PEO, butylated hydroxytoluene (BHT) is added as a stabilizer to slow PEO degradation. However, the properties of BHT, most notably its poor solubility in water and significant absorption in the UV region of the electromagnetic spectrum, mean that it interferes with protein electrophoresis. By extensively rinsing PEO with acetone, BHT could be removed and washed out to a large extent. PEO was then left to dry in the air prior to use.

Samples with the chosen molecular weights of PEO and dextran were weighed to achieve the required concentration (%w/v). For PEO-based buffers, PEO was dissolved in 0.1 M (or 0.05 M) TRIS-CHES, 0.1% SDS buffer in which the pH of this buffer was adjusted with CHES to achieve a pH between 8.2 and 8.7. Most samples of dextran and dextran mixed with PEO were prepared in 0.05 M AMPD-CACO, 0.1% SDS buffer. Other dextran-based buffers were prepared in 0.1 M TRIS-HCl, 0.1% SDS buffer; 0.1 M TRIS-borate, 0.1% SDS buffer or 0.1 M TRIS- NaH_2PO_4, 0.1% buffer. Other additives (i.e. 2% to 10% (v/v) glycerol and EOTrol) could be added to these buffers. All buffers were stirred at 25°C overnight, filtered through a 5 μm polyethersulfone (PES) membrane filter and degassed before use.

3.2.3.5 PDMA based buffer

PDMA was synthesized in water according to the protocol reported by *Ren* and co-workers[18]. Briefly, 13.75 ml water and 0.475 ml isopropanol were added to the reaction flask containing 1.25 ml N, N-dimethylacrylamide. The mixture was degassed for 30 minutes and heated in a water bath at 50°C for 20 minutes. After that, 0.08 ml of 10%(v/v) N, N, N', N'-tetramethylenediamine (TEMED) and 0.08 ml of 10% (w/v) ammonium peroxydisulfate (APS) were added. The polymerization was carried out at 50°C for 1.5 hours. The reaction product was then dialysed against DI water for 2 days using a 1200 molecular weight cut-off dialysis sac and lyophilized. The yield of the final product was found to be 70.23%.

The synthesized PDMA was dissolved in DI water at the concentration of 0.6 mg/ml and was characterized by gel permeation chromatography (PL-GPC 50, Agilent Technologies, UK). The average molecular weight of the synthesized PDMA obtained from the calibration curve of PEO standards (10-1000 kDa) was found to be ~388 kDa with the polydispersity index (PDI) of 3.21.

3.2.4 Capillary gel electrophoresis using commercial CE instrument (Peregrine)

The protocol for capillary gel electrophoresis of proteins is described in detail in **Section 2.4.1.2**. Three protein standards (lysozyme, CA and BSA) and a mixture of these proteins

were injected from a cathode, while thiourea (the EOF marker) was injected from an anode. Each sample was repeated three times for each investigated buffer. The data were analysed as described in **Section 2.4.1.3.1 and Section 2.4.1.3.2**. Electropherograms and equiphase maps obtained from each buffer were compared.

3.2.5 Capillary gel electrophoresis on microfluidic devices

Two microdevices were used to perform protein separations for buffer assessment. One consists of a cross-piece injector and a separation channel made of PDMS (**Figure 3.2a**), while the other consists of a cross-piece PDMS injector and a glass capillary as a separation channel (**Figure 3.2b**).

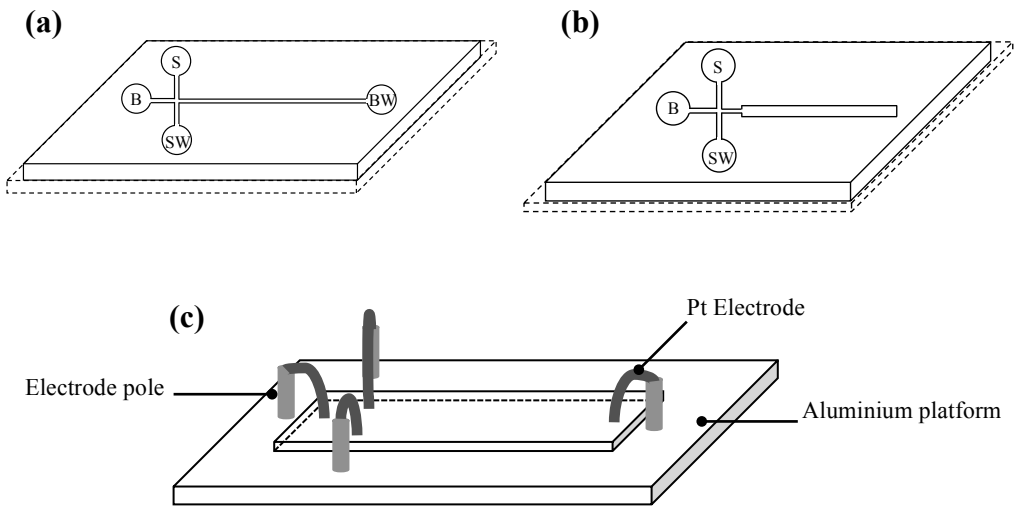

Figure 3.2: Microfluidic devices used to perform protein gel electrophoresis (a) A cross-piece PDMS microdevice; (b) A cross-piece PDMS microdevice with an enlarged channel for the insertion of a glass capillary; (c) Aluminium platform for holding either a cross-piece PDMS microdevice or a cross-piece PDMS microdevice coupled to a glass capillary. S = sample reservoir, SW = sample waste reservoir, B = buffer reservoir and BW = buffer waste reservoir.

Both microdevices were filled with DI water after oxygen plasma bonding until they were used. For the wholly PDMS microdevice (**Figure 3.2a**), a tested polymer-based buffer was replaced DI water by filling the buffer via the buffer waste reservoir using a plastic

syringe. For the cross-piece PDMS microdevice coupled to a glass capillary (**Figure 3.2b**), DI water was removed and a non-polymer buffer (i.e. 0.1x TBE buffer) was filled into the PDMS part. A 5-cm long detection window on a 7-cm long glass capillary was created by burning the polyimide coating off and cleaning with ethanol. The glass capillary was then treated with 1 M HCl for 5 minutes and filled with a polymer-based buffer using pressure for 20 minutes prior to being inserted into the enlarged end of the microdevice. The other end of the glass capillary was immersed in a buffer waste reservoir (a microcentrifuge tube), not shown in **Figure 3.2b**. The experimental setup for both microdevices is described in detail in **Section 2.4.2**.

CE separations involved both an injection and separation phase. In the injection step, negative voltages were applied to the sample, the buffer and the buffer waste reservoir, while a positive voltage was applied to the sample waste reservoir for a given period of time. After injection, positive voltages were applied to the sample, the sample waste and the buffer waste reservoir, while negative voltage was applied to the buffer reservoir for a given period of time to allow separation. The magnitudes of the applied voltages were varied for each experiment.

3.3 Results and discussion

3.3.1 Separations of proteins in commercial Beckman buffer and its modified buffers using a commercial CE machine (Peregrine)

3.3.1.1 Beckman running buffer and Beckman sample buffer

One of the commercially available SDS-based buffers for capillary electrophoresis of proteins that were extensively used in many reports is SDS-MW gel buffer from Beckman Coulter[19–40]. This buffer referred to in this work as "Beckman buffer" was investigated to ascertain if it had the potential to be employed for droplet-based protein separation. Initially and as a control, Beckman buffer was employed as it typically is, as a sieving matrix in protein gel electrophoresis. Here a three-protein mixture was separated using a commercial capillary electrophoresis machine (Peregrine, deltaDOT Ltd., UK). All protein samples were prepared in the Beckman sample buffer. The capillary gel

electrophoresis was performed according to the protocol described in detail in **Section 2.4.1.2**.

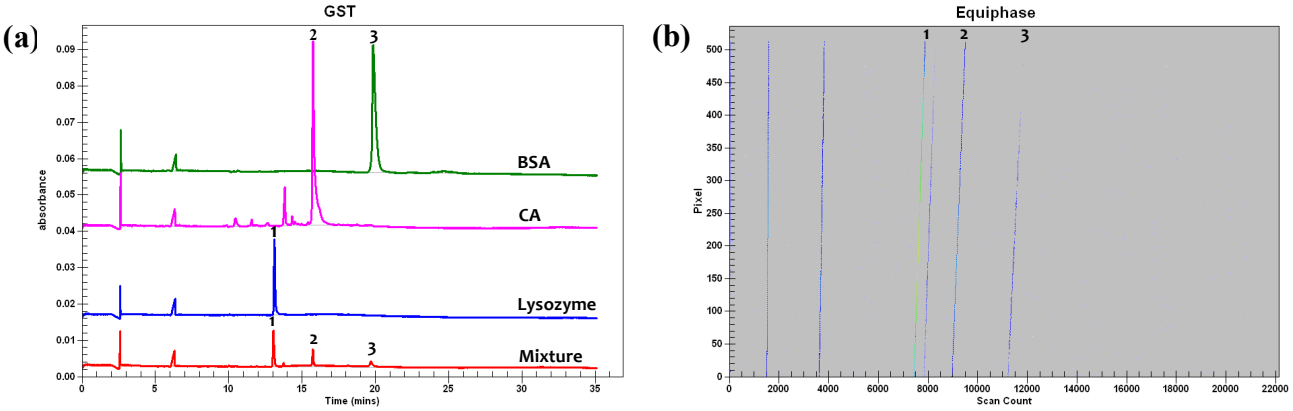

Figure 3.3: The separation of a 3-protein mixture in Beckman buffer using the CE machine (a) GST processed electropherograms of lysozyme (1), CA (2), BSA (3) and a mixture of these proteins performed in Beckman buffer using a 34 cm long capillary having an effective length of 20 cm, at 25°C and using electric field strength of 441.18 V/cm (Note: Y-axes are offset due to overlaying). All samples were prepared in Beckman sample buffer with the addition of 2-mercaptoethanol (BME); (b) An equiphase map obtained from the separation of the mixture.

Electropherograms of the three-protein mixture (red line) and the individual protein standards (lysozyme – blue line, carbonic anhydrase (CA) – pink line and bovine serum albumin (BSA) – green line) electrophoresed in Beckman buffer are overlaid as shown in **Figure 3.3a**. Of these three proteins, lysozyme (14.3 kDa) elutes first followed by CA (30 kDa) and BSA (66 kDa), respectively. The elution order of proteins in gel electrophoresis is according to their size (or molecular weight); that is smaller proteins elute first followed by larger proteins[41]. To enable comparison to other buffer systems evaluated in this work, the overall analysis time and the resolution between the peaks was determined and logged. The overall analysis time (OAT) can be defined as the length of time between sample injection and when the last analyte elutes. The OAT is influenced not only by the separation matrix but also by the length of the capillary, the applied voltage, the largest protein analyte (in a size separation) and the presence of EOF. Under the conditions described above, in Beckman buffer it is ~ 20 minutes. The resolution of separation

between lysozyme (1) and CA (2) and between CA (2) and BSA (3) according to **Equation 1.14** are 5.42 and 7.71, respectively (**Table 3.3**).

The investigation of EOF can be performed by injecting thiourea, a neutral marker, from the capillary outlet at the same time the sample is injected at the capillary inlet. Typically, SDS-protein complexes in gel electrophoresis will migrate under an electric field from a cathode (inlet) towards an anode (outlet). Meanwhile, thiourea injected from the outlet will migrate from the anode towards the cathode if the cathodic EOF (the flow of EOF towards a cathode) is present. The migrations of proteins and thiourea are therefore in the opposite direction and this can be observed in an equiphase map (see **Section 2.4.1.3.2** for the generation of equiphase map). In this case, the equiphase map (**Figure 3.3b**) shows only the lines with positive slope, which represent the migration of proteins injected from the inlet, whereas the lines with negative slope representing the migration of thiourea from the outlet are not observed. This indicates the absence or small magnitude of EOF when using Beckman buffer. Most protein size separation buffers contain reagents to suppress or eliminate EOF, as its presence leads to run-to-run variability in separation, leading to inaccuracy in size assessment of unknown proteins. Therefore testing for the presence of EOF in buffers created here is essential.

3.3.1.2 Beckman running buffer and modified sample buffers

Other reported modified Beckman buffer[42] or modified sample buffers[21,22, 29,23] for protein separation were also tested. **Figure 3.4** shows electropherograms and equiphase maps of proteins in different sample buffers separated in Beckman buffer. Protein standards (lysozyme, CA and BSA) and a protein mixture of these protein standards were prepared in 10 mM TRIS-HCl buffer with 0.1% SDS, pH 6.6 (**Figure 3.4a**), 5 mM SDS, 5 mM sodium tetraborate buffer, pH 8.5 (**Figure 3.4b**) and 5 mM SDS, 5 mM sodium tetraborate buffer, pH 8.8 (**Figure 3.4c**).

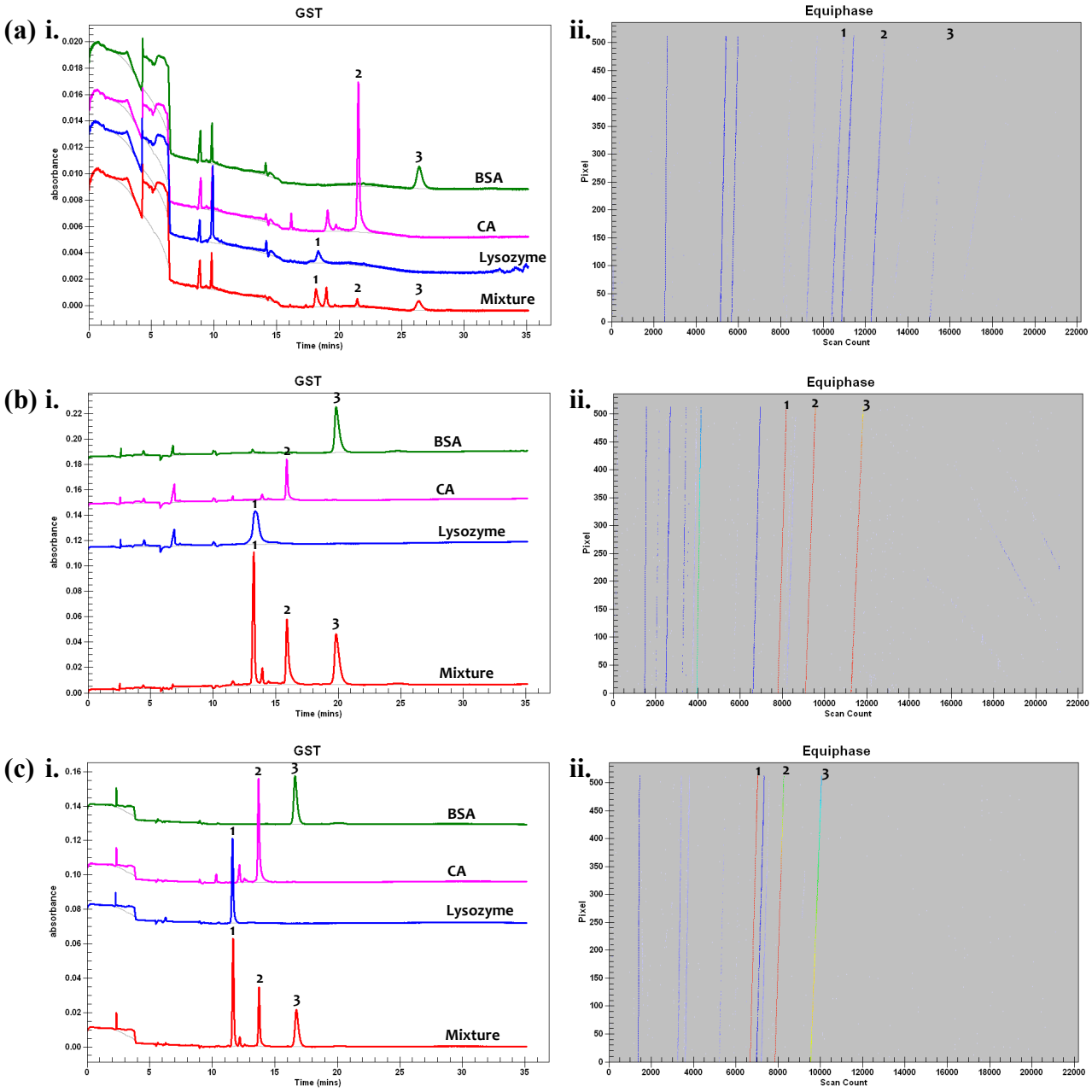

Figure 3.4: The separation of a 3-protein mixture in Beckman buffer in which samples were prepared in (a) 10 mM TRIS-HCl, 0.1% SDS, pH 6.6; (b) 5 mM SDS, 5 mM sodium tetraborate buffer, pH 8.5; (c) 5 mM SDS, 5 mM sodium tetraborate buffer, pH 8.8. For (a), (b) and (c), (i) Showing GST processed electropherograms of lysozyme (1), CA (2), BSA (3) and a mixture of these proteins performed in Beckman buffer using the CE machine that employed a 34 cm long capillary having an effective length of 20 cm, at 25°C (Note: Y-axes are offset due to overlaying), (ii) Showing the equiphase map from the separation of the mixture. The electric field strength used in (a) was 300 V/cm and used in (b) and (c) was 450 V/cm.

Obvious peaks of salts (in the background electrolyte) are observed in the front of the electropherogram in **Figure 3.4a** (TRIS-HCl sample buffer) and the total analysis time is found to be 26.3 minutes for the separation field strength of 300 V/cm. Since the modified buffers were obtained from various published articles, different electric fields were used according to the published protocols. The electric fields were then extrapolated for the comparison of analysis times using **Equation 1.8**. Therefore, the analysis time for TRIS-HCl sample buffer is estimated to be 17.5 minutes at 450 V/cm by extrapolation to compare with sodium tetraborate sample buffers at pH 8.5 and pH 8.8 at 450 V/cm in which their analysis times are found from the electropherograms (**Figure 3.4b and Figure 3.4c**) to be 19.8 and 16.7 minutes, respectively. The total analysis times obtained from using different sample buffers are not significantly different from that of commercial Beckman sample buffer (~19 minutes at 450 V/cm by extrapolation). Also, no EOF is observed in the equiphase maps of these three sample buffers.

Table 3.3: Analytical results of proteins prepared in Beckman sample buffer or modified sample buffers separated in original or modified Beckman buffer.

Buffer solution			Glass capillary (Peregrine)			Cross-piece PDMS microdevice			Cross-piece PDMS coupled to a glass capillary			Ref.
No.	**Running buffer**	**Sample buffer**	**Field strength (V/cm)**	**Analysis time (min)**	**R**	**Field strength (V/cm)**	**Analysis time (min)**	**R**	**Field strength (V/cm)**	**Analysis time (min)**	**R**	
1.	Beckman buffer	Beckman sample buffer added 5% BME/ Sample buffer containing in protein ladder (Sigma Aldrich)	441.18	20	5.42 7.71	135	3.2	NS	NT	NT	NT	-
2.	0.2x Beckman buffer	Beckman sample buffer added 5% BME	441.18	NS	NS	NT	NT	NT	NT	NT	NT	-
3.	0.25x Beckman buffer	Beckman sample buffer added 5% BME	441.18	NS	NS	NT	NT	NT	NT	NT	NT	-
4.	0.33x Beckman buffer	Beckman sample buffer added 5% BME	441.18	NS	NS	NT	NT	NT	NT	NT	NT	-
5.	0.5x Beckman buffer	Beckman sample buffer added 5% BME	441.18	NS	NS	NT	NT	NT	NT	NT	NT	-
6.	0.2x Beckman buffer added EOTrol	Sample buffer containing in protein ladder (Sigma Aldrich)	NT	NT	NT	121.67	NS	NS	NT	NT	NT	-
7.	Dialysed Beckman against DI water	Sample buffer containing in protein ladder (Sigma Aldrich)	NT	NT	NT	NT	NT	NT	88.75	NS	NS	-
8.	Dialysed Beckman against 0.1x TBE	Sample buffer containing in protein ladder (Sigma Aldrich)	NT	NT	NT	NT	NT	NT	88.75	NS	NS	-
9.	Dialysed Beckman against 0.1x TBE added 0.5% SDS	Sample buffer containing in protein ladder (Sigma Aldrich)	NT	NT	NT	NT	NT	NT	88.75	NS	NS	-
10.	80:20 Beckman: 5 mM SDS, 5 mM sodium tetraborate buffer, pH 9	5 mM SDS, 5 mM sodium tetraborate buffer, pH 9	462.4	16.5	4.30 3.69	NT	NT	NT	NT	NT	NT	42
11.	Beckman buffer	0.01 M TRIS-HCl, 0.1% SDS, pH 6.6	300	26.3	5.67 6.28	NT	NT	NT	NT	NT	NT	29
12.	Beckman buffer	5 mM SDS, 5 mM sodium tetraborate buffer, pH 8.5	450	19.8	4.47 4.31	NT	NT	NT	NT	NT	NT	21,22
13.	Beckman buffer	5 mM SDS, 5 mM sodium tetraborate buffer, pH 8.8	450	16.7	4.57 4.47	NT	NT	NT	NT	NT	NT	23

*** Note:** Two numbers of resolutions are the resolutions of lysozyme and CA peaks and CA and BSA peaks, respectively. NS = No Separation and NT = Not Tested.

The effect of pH of samples on protein separation was also investigated from these experiments. It was found that proteins prepared in sodium tetraborate buffer at pH 8.8 migrated faster (**Figure 3.5a**) and the resolutions (**Figure 3.5b**) were higher than those prepared in pH 8.5 ($R_{lyso\text{-}CA}$ = 4.47 (pH 8.5) and 4.57 (pH 8.8); $R_{CA\text{-}BSA}$ = 4.31 (pH 8.5) and 4.47 (pH 8.8)). This might be because SDS-protein complexes in sample buffer pH 8.8 expose in more negatively charged environment than that of pH 8.5 and then tend to migrate towards the anode faster providing for less band broadening. Consequently, the resolution of separation of SDS-protein complexes in higher pH environment is higher than that of the lower pH.

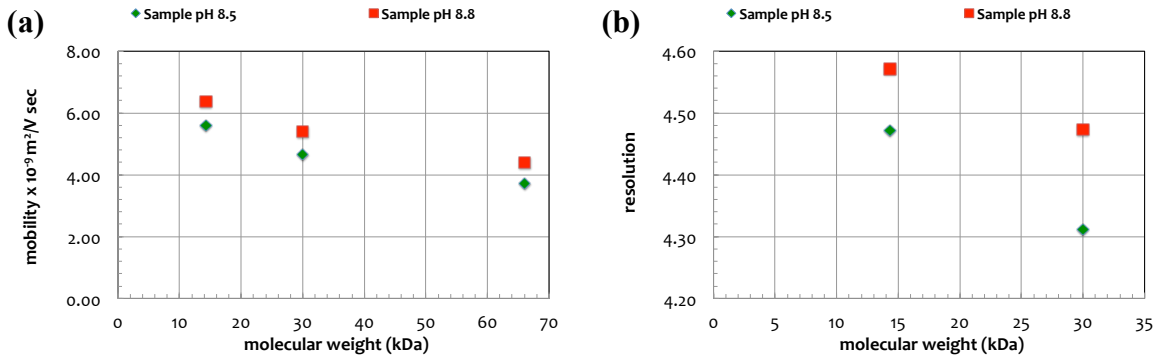

Figure 3.5: Effect of pH of samples on protein separation. (a) A plot of mobility versus molecular weight of proteins; (b) A plot of resolution versus molecular weight. Two sets of a 3-protein mixture (lysozyme, CA and BSA) prepared in 5 mM borate buffer, 5 mM SDS at pH 8.5 and pH 8.8 were separated in Beckman buffer using the CE machine that employed a 34 cm long capillary having an effective length of 20 cm, at 25°C and using separation field strength of 450 V/cm.

3.3.1.3 Modified Beckman running buffer and modified sample buffer

The modified Beckman buffer according to *Fruetel*'s work[42] was also tested. Beckman buffer was mixed with 5 mM SDS, 5 mM tetraborate buffer, pH 9.0 at the ratio of 80:20 and was used to separate a protein mixture at 462.4 V/cm within 16.5 minutes. The resolutions between lysozyme and CA peaks and between CA and BSA peaks are 4.30 and 3.69, respectively. By extrapolating the electric field strength to 450 V/cm, the total analysis time is found to be ~17 minutes, which is not significantly different comparing to the original Beckman buffer. However, thiourea peaks are observed both in the

electropherograms (**Figure 3.6a**) and in the equiphase map (**Figure 3.6b**) indicating the presence of EOF.

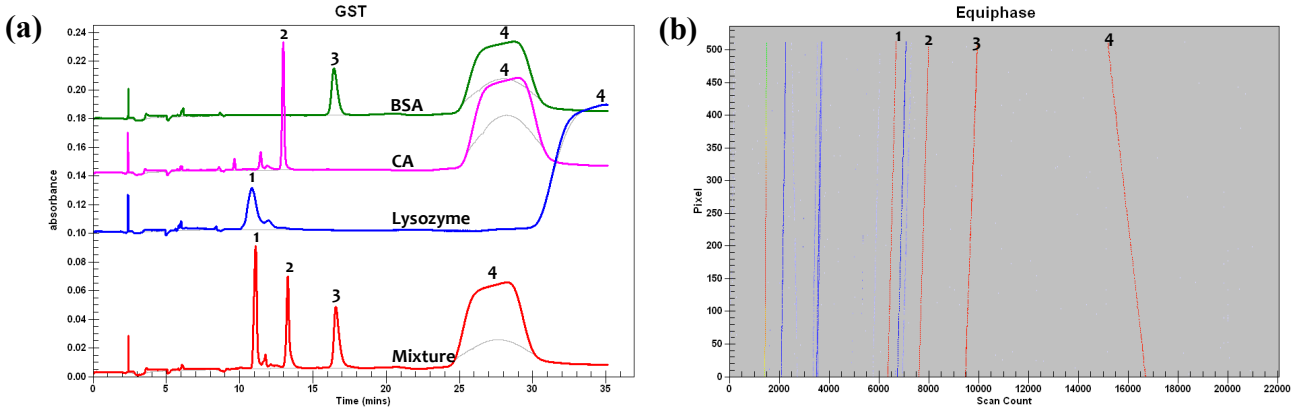

Figure 3.6: The separation of a 3-protein mixture in an 80/20 mixture of Beckman buffer and 5 mM SDS in 5 mM sodium tetraborate buffer, pH 9.0 using the CE machine (a) GST processed electropherograms of lysozyme (1), CA (2), BSA (3) and a mixture of these proteins performed using a 34 cm long capillary having an effective length of 20 cm, at 25°C and using electric field strength of 462.4 V/cm. Thiourea peaks (4) are also observed in these electropherograms (Note: Y-axes are offset due to overlaying); (b) The equiphase map from the separation of the mixture.

3.3.2 Separations of proteins in commercial Beckman buffer using a cross-piece PDMS microdevice

The original Beckman running buffer was also tested in a PDMS microdevice for two reasons. First, the original Beckman running buffer serving as a baseline for other buffers in this work due to its reputation as an industrial gold standard shows good performance for protein separations as demonstrated in **Section 3.3.1**. Second, if this buffer works for protein separations in a PDMS microdevice, the development of buffers for droplet-based separations will be easier and less time-consuming.

The electrophoresis of fluorescently labeled protein ladder (20-200 kDa from Sigma Aldrich, UK) was performed using the original Beckman buffer in a cross-piece PDMS microdevice. The sample was injected at t = 120 s according to the time in the electropherogram (**Figure 3.7**) and was detected at 0.5 cm from the injection point with

the analysis time of ~ 4 minutes. It was found that seven proteins in the ladder were not separated properly at this separation length using the separation field strength of 135 V/cm. If the separation length is increased, the total analysis time will also increase. Too long of an analysis time will make this buffer not suitable for droplet-based protein separation in which rapid separation for each droplet is required. The other way to achieve higher resolution is to increase separation field strength. However, when higher voltages were applied to this buffer system, the current increased, leading to the buffer boiling and the formation of bubbles that interfered with the separation.

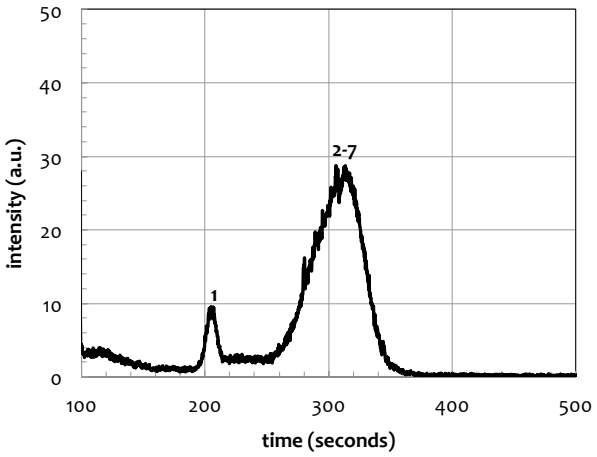

Figure 3.7: Electropherogram of a fluorescently labeled protein ladder (20-200 kDa fluorescent molecular weight marker, Sigma Aldrich, UK) performed in Beckman buffer solution in a cross-piece PDMS microdevice using electric field strength of 135 V/cm. Detection was done at 0.5 cm from the intersection. Note: The injection time was at 120 seconds according to the electropherogram.

Although the original Beckman running buffer was not suitable to be used in PDMS microdevices due to the poor heat dissipation of the PDMS[43], it was still useful as a control for buffer development in the commercial CE machine. Since the buffer development was performed parallel to the development of interfacing droplet-based microdevices (**Chapter 5**), it was found that some parts of the interfacing microdevices needed to be hydrophilic and some needed to be hydrophobic to achieve successful droplet injection. As a result, the change of the microdevice material to allow better heat dissipation was not easy.

Another way to address the buffer boiling was to deal with the background electrolyte of the Beckman buffer. The concentration of the background electrolyte in Beckman buffer can be modified to reduce the salt level, so it might be used with increased electric field strength and without buffer boiling[44]. The decrease in concentration of background electrolyte was performed by dilution and dialysis of Beckman buffer as discussed in detail in **Section 3.3.3**.

3.3.3 Separations of proteins in diluted and dialysed Beckman buffer

3.3.3.1 Diluted Beckman buffer in DI water

Beckman buffer was diluted in DI water to achieve concentrations of 0.2x, 0.25x, 0.33x and 0.5x Beckman buffer. The diluted Beckman buffers were tested on the Peregrine instrument to investigate the separation efficiency of buffers. A protein standard (BSA) was injected in tandem with thiourea prepared in various concentrations of diluted Beckman buffer at either end of the capillary as described earlier and was electrophoresed at 441.18 V/cm.

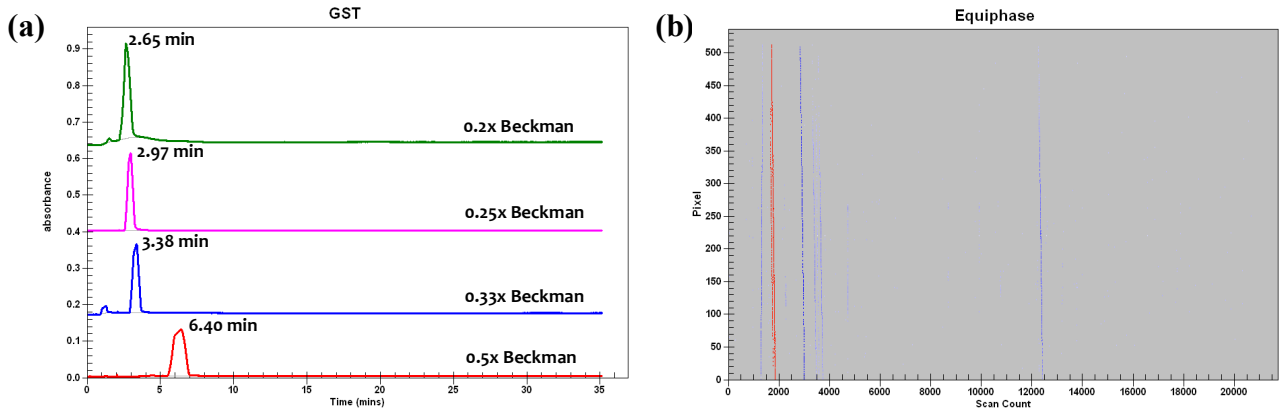

Figure 3.8: Electrophoresis of BSA and thiourea in various concentrations of diluted Beckman buffer using the CE machine. (a) GST processed electropherograms of BSA and thiourea performed in Beckman diluted in DI water at concentrations of 0.2x (green line), 0.25x (pink line), 0.33x (blue line) and 0.5x (red line) using a 34 cm long capillary having an effective length of 20 cm, at 25°C and using electric field strength of 441.18 V/cm. The peaks shown in these electropherograms are thiourea injected from the opposite end of the capillary to BSA, which is not observed (Note: Y-axes are offset due to overlaying); (b) An equiphase map shows the opposite direction of migration of thiourea due to high EOF.

Only thiourea peaks were observed, confirmed by the negative slopes of the lines in the equiphase map (**Figure 3.8b**), in the electropherograms (**Figure 3.8a**). It was found that thiourea migrated faster in lower concentration of Beckman buffer indicating the presence of higher EOF.

To compensate for the reduction in concentration of the EOF suppressant in the diluted buffers, the 0.2x Beckman buffer was mixed with EOTrol (Target Discovery Inc., CA, USA). This is a dynamic coating solution for controlling EOF[45] and was tested in a cross-piece PDMS microdevice. Although the EOF was decreased, which allowed the successful injection of fluorescently labeled protein ladder into the separation channel, protein ladder was not separated either at 0.5 cm or at 1.0 cm from the injection point (**Figure 3.9**). The loss of resolution might be due to the dilution of the sieving matrix in Beckman buffer.

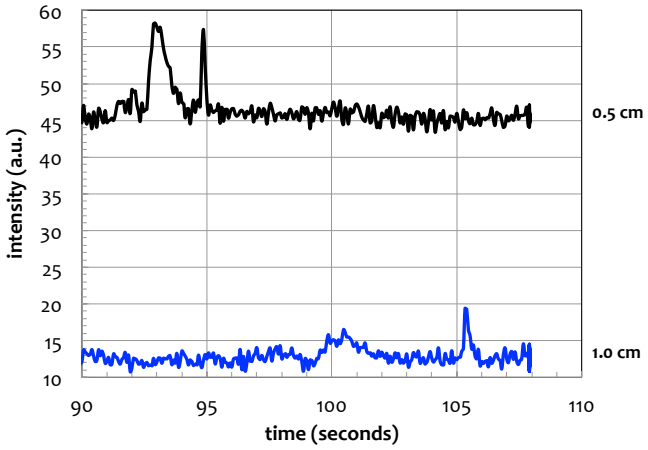

Figure 3.9: Electropherograms of protein ladder (20-200 kDa fluorescent molecular weight marker, Sigma Aldrich, UK) performed in 0.2x Beckman mixed with EOTrol buffer on a cross-piece PDMS microdevice using electric field strength of 121.67 V/cm. The separations were observed at two detection points: 0.5 cm (black line) and 1.0 cm (blue line) measured from the intersection. Note: The actual injection time was not recorded and y-axes are offset due to overlaying.

3.3.3.2 Dialysed Beckman buffer against DI water or 0.1x TBE

In order to reduce the concentration of background electrolyte without the dilution of the sieving matrix, Beckman buffer was dialysed against either DI water or 0.1x TBE buffer and both of them were tested for protein separations using a cross-piece PDMS microdevice filled with 0.1x TBE buffer coupled to a glass capillary filled with the dialysed Beckman buffer (against DI water or against 0.1x TBE buffer). The testing was performed using the PDMS microdevice coupled to the glass capillary due to two reasons. First, the coupling between PDMS and glass devices was also employed in the development of interfacing droplet-based microdevices from "Design 3" to "Design 6", which is further described in **Chapter 5**. Second, using the glass capillary as a separation channel might improve the heat dissipation and hence allowed the use of a higher electric field to achieve greater resolution. It was found that there was sample leakage into the separation channel after the injection as shown in the electropherogram (**Figure 3.10**) as two long bright bands although high pull-back voltages were applied.

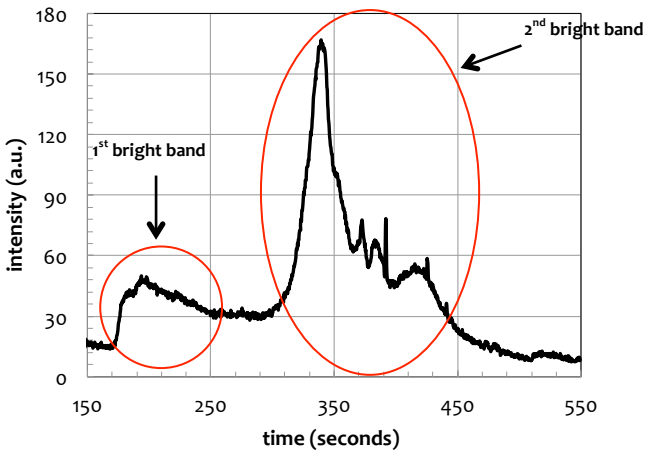

Figure 3.10: An electropherogram of protein ladder (20-200 kDa fluorescent molecular weight marker, Sigma Aldrich, UK) electrophoresed in dialysed Beckman against DI water on a cross-piece PDMS microdevice coupled to a glass capillary using electric field strength of 88.75 V/cm. The cross-piece PDMS microdevice contained 0.1x TBE solution, while the 7-cm glass capillary contained dialysed Beckman buffer. Note: The actual injection time was not recorded.

EOTrol was then applied to 0.1x TBE buffer in the PDMS part to control EOF. However, proteins were not separated in both dialysed Beckman buffers even if the EOF in the

PDMS part was successfully controlled and there was no sample leakage after the injection (**Figure 3.11a**). It was also found that by employing the dialysed Beckman buffer, the speed of protein migration in the glass capillary during separation within a run extremely fluctuated (moving too fast or too slow) due to the unstable current and proteins sometimes migrated in the wrong direction i.e. moving towards the cathode. These might be a result of the depletion of some background electrolyte molecules (such as SDS, salts and small molecules used to suppress EOF) during dialysis. The depletion of SDS might result in a change in the charge distribution within the SDS-protein complexes, which in turn will affect the separation of proteins. SDS at concentration of 0.5% w/v was added to the Beckman buffer following dialysis; however, proteins were still not separated as depicted in **Figure 3.11b**. The dialysed Beckman buffers were not further used since the dialysis conditions were not reproducible and resulted in extreme effects on the buffer compositions, which in turn affected protein separations.

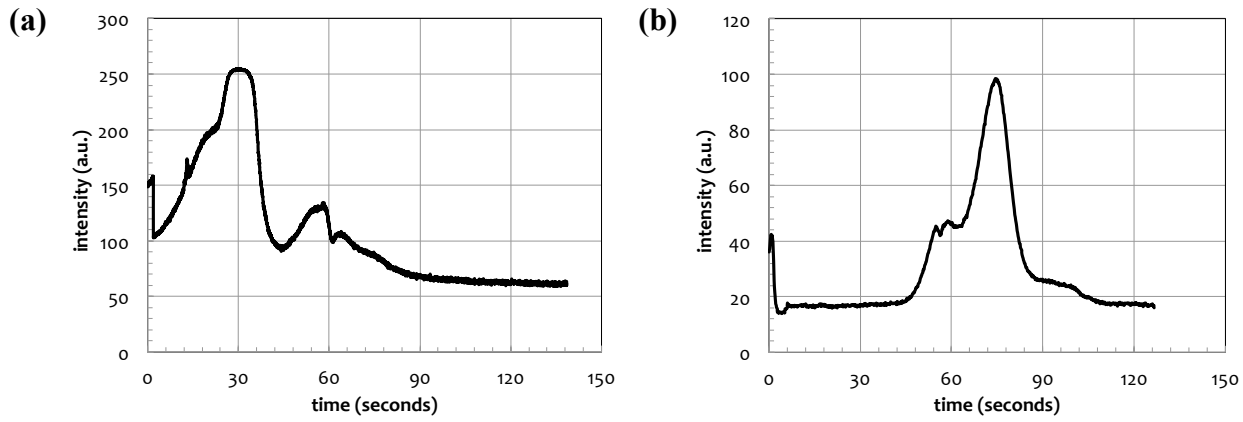

Figure 3.11: Electropherograms of protein ladder (20-200 kDa fluorescent molecular weight marker, Sigma Aldrich, UK) performed in (a) dialysed Beckman against 0.1x TBE and (b) dialysed Beckman against 0.1x TBE added 0.5% SDS on a cross-piece PDMS microdevice coupled to a glass capillary using electric field strength of 88.75 V/cm. The cross-piece PDMS microdevice contained 0.1x TBE mixed with EOTrol solution, while the 7-cm glass capillary contained dialysed Beckman buffer. Note: Time shown in the electropherograms was not the actual time from the injection.

3.3.4 Separations of proteins in laboratory-made buffer solutions

Three types of polymer (i.e. PDMA, PEO and dextran) were chosen based on published reports[3,46,47,48] to prepare laboratory-made running buffers for gel electrophoresis of proteins. Several parameters (i.e. polymer concentration, molecular weight of polymer, background electrolyte buffer and pH) were varied and tested using either the commercial CE machine or cross-piece microdevices. The aim was to achieve a buffer that provided for rapid and high-resolution separation of proteins with compatibility for both PDMS and glass separation channels.

3.3.4.1 Separations of proteins in PDMA-based buffer using a cross-piece PDMS microdevice

The first polymer to be investigated was polydimethylacrylamide (PDMA), which was used to separate proteins in a microdevice within 15 seconds[46]. PDMA was synthesized as described in **Section 3.2.3.5** and was characterized using gel permeation chromatography (PL-GPC 50, Agilent Technologies, UK). The average molecular weight and polydispersity were found to be ~ 388 kDa and 3.21, respectively. Since PDMA itself absorbs UV light, buffer testing was not carried out using the CE machine (Peregrine) as the detection system is based on UV absorption. Instead, protein separations were conducted in cross-piece PDMS microdevices and detection was performed using fluorescence detection.

The electropherograms (**Figure 3.12**) show two peaks of fluorescein (1 and 2) separated from BSA-FITC (3) in both 1.5% and 3% PDMA buffers with the resolution of 0.82 and 1.08, respectively. The presence of overlapping fluorescein peaks may be due to the fact that fluorescein can exhibit in various forms[49] (**Figure 3.13**) and might exhibit as monoanion and dianion forms in strongly basic solution. The low resolution of separation between small fluorescein molecule (MW = 332.31 g/mol) and the large BSA conjugate (MW ~ 66 kDa) indicates that the pore sizes afforded by 1.5% and 3% PDMA buffers were insufficient to provide for resolution and consequently the separation of proteins having molecular weight less than 66 kDa in the protein ladder (20-200 kDa fluorescent

molecular weight marker, Sigma Aldrich). However, the proteins having molecular weight more than 66 kDa were not tested.

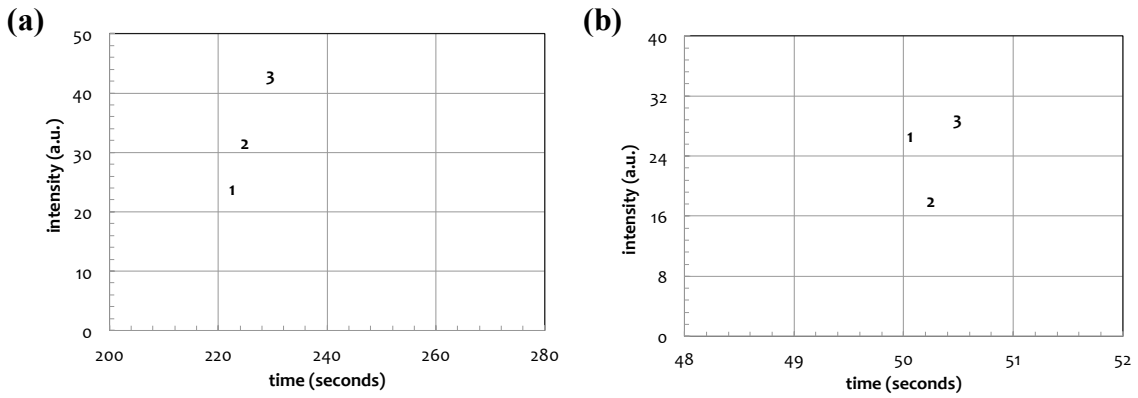

Figure 3.12: Electropherograms of fluorescein (1 and 2) and BSA-FITC (3) separated in (a) 1.5% PDMA in 0.085 M, 0.1% SDS, pH 9.3 using separation field strength of 133 V/cm (detection at 0.5 cm) and (b) 3% PDMA in 0.085 M, 0.1% SDS, pH 9.3 using separation field strength of 200 V/cm (detection at 2 cm). The sample was prepared in 0.2% SDS.

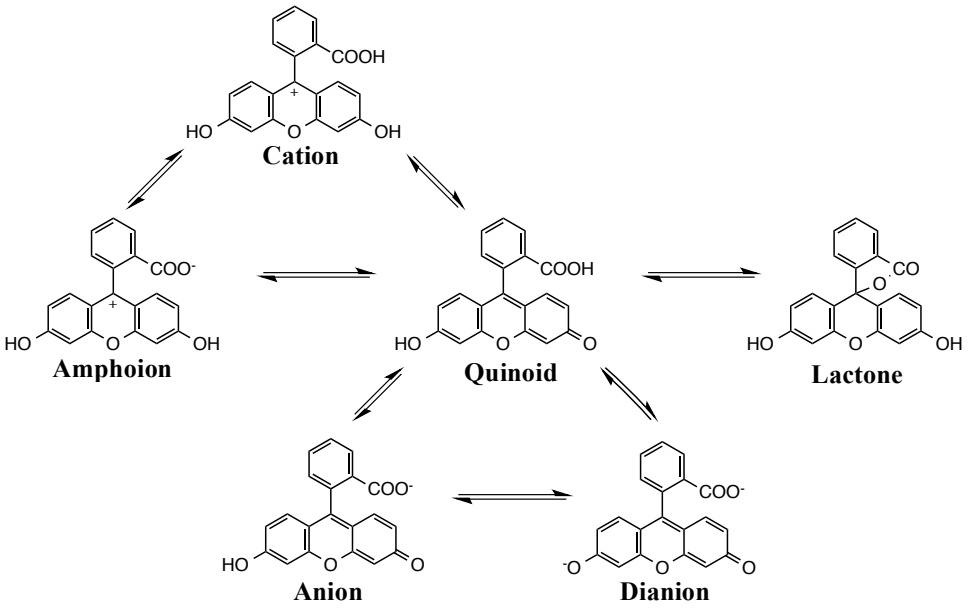

Figure 3.13: Possible existing structures of fluorescein. Image reproduced from reference 49.

3.3.4.2 Separations of proteins in PEO and/or dextran-based buffer using the CE machine

The second and the third tested polymers were poly (ethylene oxide) or PEO and dextran, which are linear and branched polymer, respectively. Various molecular weights and concentrations of PEO and dextran were initially tested using the CE machine (Peregrine). The analytical results of the tested buffers are shown in **Table 3.4**. Since the protein separations in dextran-based buffers did not yield good results (i.e. some protein peaks were difficult to be distinguished and that no resolution results are available as shown in **Table 3.4**), only results obtained from PEO-based buffers are discussed in detail.

The effect of polymer concentration on protein separations was studied. There is a threshold concentration of a polymer in a solution. Below this threshold concentration, the polymer chains in the solution will be isolated from one another and is called dilute polymer solution[50]. Above the threshold concentration, the polymer chains begin to overlap and interact via the van der Waals force and hydrogen bonding to form a polymer network, which is called an entangled polymer solution[50,51]. The average pore size for the network in entangled polymer solution is expressed as

$$\xi_b = 1.43 R_g \left(\frac{c}{c^*}\right)^{-3/4} \tag{3.1}$$

where ξ_b is an average pore size, c is the polymer concentration, c^* is the threshold concentration obtained from

$$c^* \cong \frac{2.5}{[\eta]} \tag{3.2}$$

and R_g is the radius of gyration of the polymer, which is defined as

$$R_g^3 \cong [\eta] M_w / 6.2 N_A \tag{3.3}$$

where η is viscosity, M_w is molecular weight of polymer and N_A is Avogadro number[12]. According to **Equation 3.1**, the average pore size is inversely proportional to the concentration of polymer. Therefore the greater the concentration of the polymer smaller the resulting pore size.

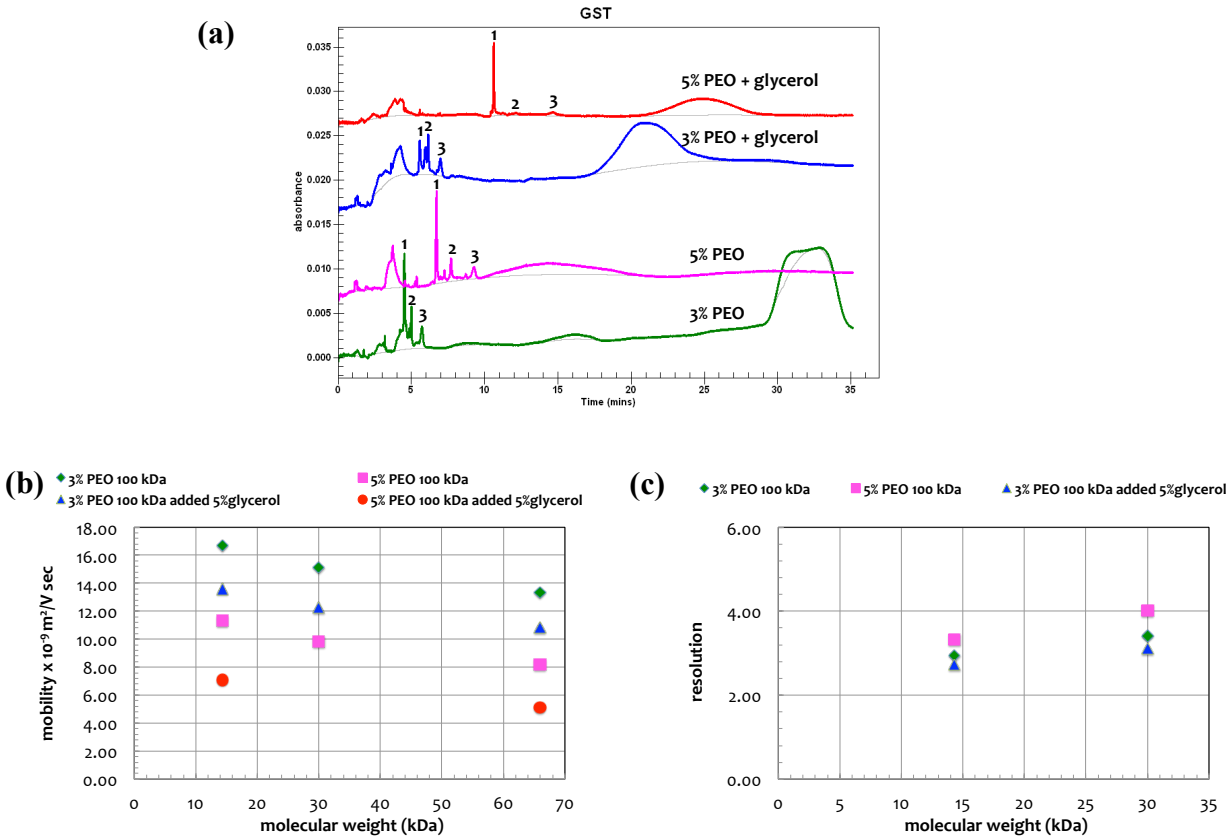

Figure 3.14: Effect of polymer concentration and effect of adding glycerol in running buffer. (a) Electropherograms of a protein mixture separated in 3% PEO 100 kDa (green line) and 5% PEO 100 kDa (pink line) in 0.1 M TRIS-CHES, 0.1% SDS, pH 8.7 and 3% PEO 100 kDa (blue line) and 5% PEO 100 kDa (red line) in 0.1 M TRIS-CHES, 0.1% SDS, 5% glycerol, pH 8.7 (Note: Y-axes are offset due to overlaying); (b) Plot of mobility vs. molecular weight; (c) Plot of resolution vs. molecular weight. The separations of a protein mixture (lysozyme (1), CA (2) and BSA (3)) were performed using a 34 cm long capillary having an effective length of 20 cm, at 25°C and using electric field strength of 441.18 V/cm. All samples were prepared in 1x TBE buffer, 0.1% SDS, pH 7.56. Note: CA peak (2) in 5% PEO 100 kDa buffer containing 5% glycerol (red line) is indistinguishable. Therefore, mobility for CA and resolution results for this buffer are not available.

It was found from the electropherograms (**Figure 3.14a**) and the plot between mobility and the molecular weight of proteins (**Figure 3.14b**) comparing between 3% and 5% PEO 100 kDa that proteins migrated slower in higher concentration of PEO. The lower mobility of proteins in higher polymer concentration indicates that proteins have to migrate through a smaller pore size that makes the migration more difficult. This matches the relationship between the concentration of polymer and the pore size described in **Equation 3.1**. The slower migration of proteins in 5% PEO buffer was found to improve the resolution of protein separations (**Figure 3.14c**). Another way to improve resolution of protein separation was to add glycerol into buffer solutions. The adding of glycerol made buffers more viscous and hence made protein migration slower than that in the buffer without glycerol adding (**Figure 3.14a and Figure 3.14b**). However, the resolution of protein separation in the buffer with glycerol was actually found to be lower than that without glycerol (compare between 3% PEO buffer with and without glycerol as shown in **Figure 3.14c**). This might be because the slow migration of proteins in viscous buffers resulted in band broadening and consequently affected the resolution. Here, further work to establish the appropriate concentration of glycerol to increase resolution was not further investigated.

Table 3.4: Analytical results of protein separated in various buffer solutions using a commercial CE machine (Peregrine).

Buffer Solution				Glass capillary (Peregrine)			Ref.
No.	**Polymer (%w/v)**	**Polymer**	**Base buffer**	**Field strength (V/cm)**	**Analysis time (min)**	**Resolution**	
1.	3%	PEO 100 kDa	0.1 M TRIS-CHES, 0.1% SDS, pH 8.21	441.18	6.4	IDP	-
2.	3%	PEO 100 kDa	0.1 M TRIS-CHES, 0.1% SDS, pH 8.7	441.18	5.7	2.94, 3.41	3
3.	3%	PEO 100 kDa	0.1 M TRIS-CHES, 0.1% SDS, 5% glycerol, pH 8.7	441.18	7.0	2.73, 3.09	-
4.	5%	PEO 100 kDa	0.1 M TRIS-CHES, 0.1% SDS, pH 8.7	441.18	9.3	3.32, 4.03	-
5.	5%	PEO 100 kDa	0.1 M TRIS-CHES, 0.1% SDS, 5% glycerol, pH 8.21	441.18	11.9	NS	-
6.	5%	PEO 100 kDa	0.1 M TRIS-CHES, 0.1% SDS, 5% glycerol, pH 8.7	441.18	14.6	IDP	-
7.	5%	PEO 100 kDa	0.1 M TRIS-CHES, 0.1% SDS, 2% glycerol, pH 8.53	441.18	10.9	1.96, 0.77	-
8.	7%	PEO 100 kDa	0.1 M TRIS-CHES, 0.1% SDS, 2% glycerol, pH 8.53	441.18	14.2	5.31, 5.72	-
9.	3%	PEO 200 kDa	0.1 M TRIS-CHES, 0.1% SDS, 2.5% glycerol, pH 8.4	441.18	8.2	IDP	-
10.	1%	PEO 1 MDa	0.1 M TRIS-CHES, 0.1% SDS, 10% glycerol, pH 8.24	441.18	5.6	0.94, 2.00	-
11.	3%	PEO 1 MDa	0.1 M TRIS-CHES, 0.1% SDS, pH 8.22	441.18	NS	NS	-
12.	3%	PEO 1 MDa	0.1 M TRIS-CHES, 0.1% SDS, 2.5% glycerol, pH 8.4	441.18	NS	NS	-
13.	3% 2%	PEO 100 kDa PEO 200 kDa	0.1 M TRIS-CHES, 0.1% SDS, 2% glycerol, pH 8.3	441.18	10.4	2.46, 5.13	-
14.	3% 2%	PEO 100 kDa PEO 200 kDa	0.1 M TRIS-CHES, 0.1% SDS, 2% glycerol, pH 8.53	441.18	11.3	IDP, 0.3	-
15.	4% 0.5%	PEO 100 kDa PEO 200 kDa	0.1 M TRIS-CHES, 0.1% SDS, 2% glycerol, pH 8.51	441.18	11.1	1.34, 1.66	-
16.	4% 1%	PEO 100 kDa PEO 200 kDa	0.1 M TRIS-CHES, 0.1% SDS, 2% glycerol, pH 8.51	441.18	NS	NS	-
17.	5% 1.5%	PEO 100 kDa PEO 200 kDa	0.1 M TRIS-CHES, 0.1% SDS, 2% glycerol, pH 8.53	441.18	12.7	1.57, 1.87	-
18.	6% 0.5%	PEO 100 kDa PEO 200 kDa	0.1 M TRIS-CHES, 0.1% SDS, 2% glycerol, pH 8.53	441.18	13.4	2.70, 2.59	-
19.	2.5%	Dextran 2 MDa	0.05 M AMPD-CACO, 0.1% SDS, pH 7.72	441.18	5.2	IDP	-
20.	5%	Dextran 2 MDa	0.05 M AMPD-CACO, 0.1% SDS, pH 7.72	441.18	NS	NS	-
21.	6%	Dextran 2 MDa	0.1 M TRIS-HCl, 0.1% SDS, pH 8	441.18	NS	NS	47
22.	10%	Dextran 2 MDa	0.05 M AMPD-CACO, 0.1% SDS, pH 8.82	441.18	NS	NS	3
23.	10%	Dextran 2 MDa	0.1 M TRIS-Borate, 0.1%SDS, 10% glycerol, pH 8.3	441.18	23.5	IDP	-
24.	10%	Dextran 2 MDa	0.1 M TRIS-NaH_2PO_4, 0.1%SDS, 10% glycerol, pH 8.3	320	13.2	2.78, 2.47	48
25.	15%	Dextran 70 kDa	0.1 M TRIS-CHES, 0.1%SDS, pH 8.7	441.18	NS	NS	-

Buffer Solution				Glass capillary (Peregrine)			Ref.
No.	**Polymer (%w/v)**	**Polymer**	**Base buffer**	**Field strength (V/cm)**	**Analysis time (min)**	**Resolution**	
26.	2.5% 1%	Dextran 2 MDa PEO 100 kDa	0.05 M AMPD-CACO, 0.1% SDS, pH 7.72	441.18	8	IDP	-
27.	5% 0.5%	Dextran 2 MDa PEO 100 kDa	0.05 M AMPD-CACO, 0.1% SDS, 2% glycerol, pH 7.72	441.18	12.6	IDP	-
28.	7% 0.5%	Dextran 2 MDa PEO 100 kDa	0.05 M AMPD-CACO, 0.1% SDS, 2% glycerol, pH 7.72	441.18	8.3	1.94, 3.72	-
29.	2.5% 0.5%	Dextran 2 MDa PEO 1 MDa	0.05 M AMPD-CACO, 0.1% SDS, pH 7.72	441.18	6.2	IDP	-
30.	5% 0.25%	Dextran 2 MDa PEO 1 MDa	0.05 M AMPD-CACO, 0.1% SDS, pH 7.72	441.18	7.3	IDP, 2.52	-
31.	5% 0.5%	Dextran 2 MDa PEO 1 MDa	0.05 M AMPD-CACO, 0.1% SDS, pH 7.72	441.18	9.2	2.66, 3.69	-
32.	5%. 0.5%	Dextran 2 MDa PEO 1 MDa	0.05 M AMPD-CACO, 0.1% SDS, 2% glycerol, pH 7.72	441.18	9.5	IDP	-
33.	5% 0.5%	Dextran 2 MDa PEO 1 MDa	0.05 M AMPD-CACO, 0.1% SDS, EOTrol, pH 7.72	441.18	9.4	IDP	-

*** Note:** Two numbers of resolutions are the resolutions of lysozyme and CA peaks and CA and BSA peaks, respectively. NS = No Separation and IDP = Indistinguishable Peaks.

Table 3.5: Analytical results of protein separated in various buffer solutions using a cross-piece PDMS microdevice or a PDMS microdevice coupled to a glass capillary.

Buffer solution				Cross-piece PDMS microdevice			Cross-piece coupled to a glass capillary		
No.	**Polymer (%w/v)**	**Polymer**	**Base buffer**	**Field strength (V/cm)**	**Analysis time (min)**	**Resolution**	**Field strength (V/cm)**	**Analysis time (min)**	**Resolution**
1.	1.5%	PDMA	0.085 M sodium tetraborate buffer, pH 9.3	75	NS	NS	NT	NT	NT
2.	3.0%	PDMA	0.085 M sodium tetraborate buffer, pH 9.3	100	NS	NS	NT	NT	NT
3.	5%	PEO 100 kDa	0.05 M TRIS-CHES, 0.1% SDS, pH 8.5	208.33	1.58 (at 1.3 cm)	1.0^{1-2}, 1.3^{2-3}, 1.2^{3-4}, 1.3^{4-5}, 1.5^{5-6}, 1.6^{6-7}	NT	NT	NT
4.	6%	PEO 100 kDa	0.05 M TRIS-CHES, 0.1% SDS, pH 8.5	167.5	1.46 (at 1.0 cm)	1.0^{1-2}, 1.5^{2-3}, 1.1^{3-4}, 1.2^{4-5}, 1.9^{5-6}, 1.6^{6-7}	188	3.15 (at 2.0 cm)	0.8^{1-2}, 1.0^{2-3}, 0.8^{3-4}, 1.1^{4-5}, 1.1^{5-6}, 1.3^{6-7}

*** Note:** The superscript numbers on the resolution value designate the number of the peak (e.g. 1.0^{1-2} is the resolution value between peak 1 and peak 2). NS = No Separation and NT = Not Tested.

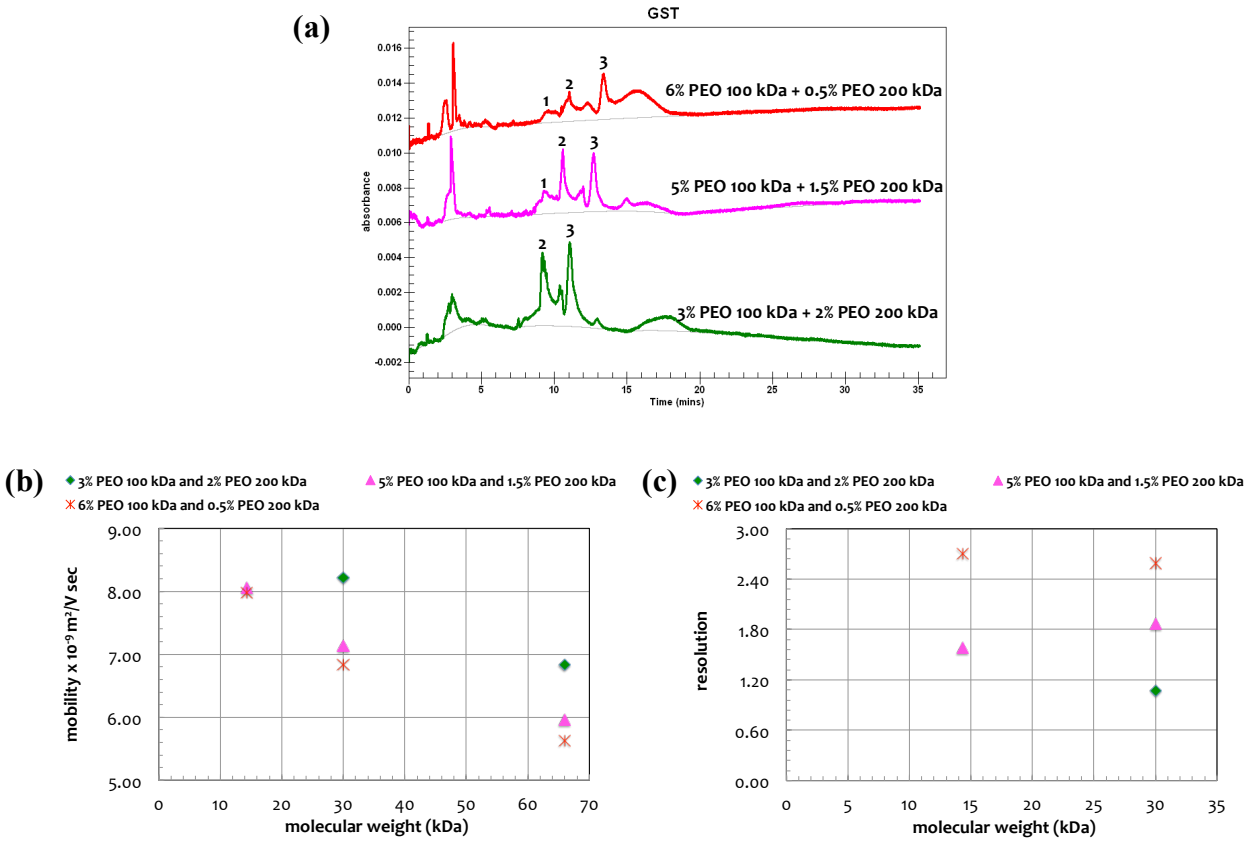

Figure 3.15: Effect of polymer concentration of mixed polymer molecular weight. (a) Electropherograms of a protein mixture separated in 3% PEO 100 kDa mixed with 2% PEO 200 kDa (green line), 5% PEO 100 kDa mixed with 1.5% PEO 200 kDa (pink line), and 6% PEO 100 kDa mixed with 0.5% PEO 200 kDa (red line) in 0.1 M TRIS-CHES, 0.1% SDS, 2% glycerol, pH 8.5 (Note: Y-axes are offset due to overlaying); (b) Plot of mobility vs. molecular weight; (c) Plot of resolution vs. molecular weight. The separations of a protein mixture (lysozyme (1), CA (2) and BSA (3)) were performed using a 34 cm long capillary having an effective length of 20 cm, at 25°C and using electric field strength of 441.18 V/cm. All samples were prepared in 1x TBE buffer, 0.1% SDS, pH 7.56. Note: Lysozyme peak (1) is not shown in 3% PEO 100 kDa mixed with 2% PEO 200 kDa buffer. Therefore, mobility for lysozyme and resolution between lysozyme and CA are not available.

Mixtures of polymers with different molecular weights were also investigated. Protein migration in the mixed polymers from the highest to the lowest mobility was in the order of (**Figure 3.15a and Figure 3.15b**).

- 3% PEO 100 kDa mixed with 2% PEO 200 kDa,
- 5% PEO 100 kDa mixed with 1.5% PEO 200 kDa and
- 6% PEO 100 kDa mixed with 0.5% PEO 200 kDa

Since higher concentrations of PEO 100 kDa than that of PEO 200 kDa were used in this case and the fact that the polymer with shorter chain length forms denser polymer networks than the polymers with longer chain length[52], the pore size seemed to depend more on the concentration of PEO 100 kDa than that of PEO 200 kDa. The highest resolution was obtained from 6% PEO 100 kDa mixed with 0.5% PEO 200 kDa having the slowest mobility, as expected.

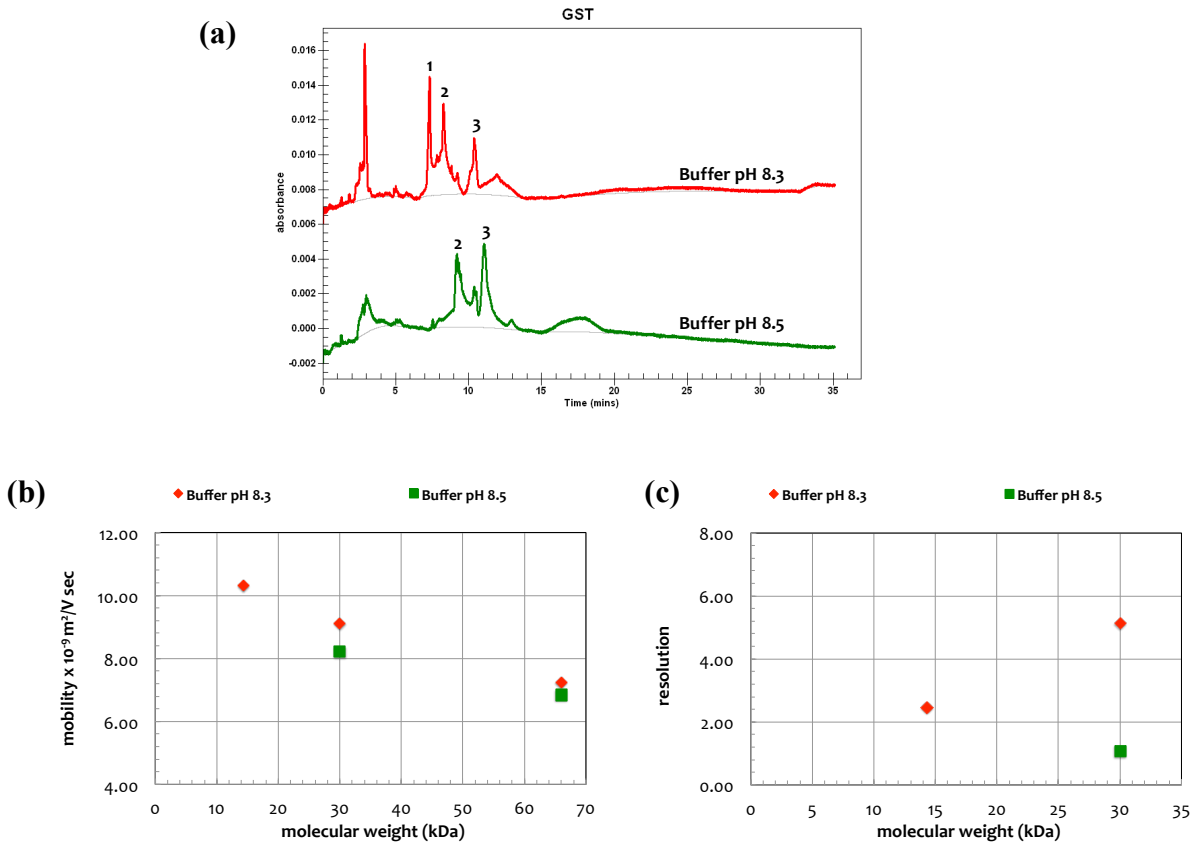

Figure 3.16: Effect of buffer pH. (a) Electropherograms of a protein mixture separated in 3% PEO 100 kDa mixed with 2% PEO 200 kDa in 0.1 M TRIS-CHES, 0.1% SDS, 2% glycerol, pH 8.3 (red line) and pH 8.5 (green line) (Note: Y-axes are offset due to overlaying); (b) Plot of mobility vs. molecular weight; (c) Plot of resolution vs. molecular weight. The separations of a protein mixture (lysozyme (1), CA (2) and BSA (3)) were performed using a 34 cm long capillary having an effective length of 20 cm, at 25°C and using electric field strength of 441.18 V/cm. All samples were prepared in 1x TBE buffer, 0.1% SDS, pH 7.56. Note: Lysozyme peak (1) is not shown in buffer pH 8.5. Therefore, mobility for lysozyme and resolution between lysozyme and CA are not available.

The other effect that was investigated was the pH of the buffer (**Figure 3.16a**). In this experiment, a mixture of proteins prepared in 1x TBE buffer at pH 7.56 containing 0.1% SDS was injected from the inlet of the capillary and separated in two similar buffers having the same components (3% PEO 100 kDa mixed with 2% PEO 200 kDa in 0.1 M TRIS-CHES, 0.1% SDS, 2% glycerol) but different pH (pH 8.3 and pH 8.5). It was found that proteins migrated faster in pH 8.3 than that of pH 8.5 as shown in **Figure 3.16b**. The resolution was improved when proteins migrated faster (**Figure 3.16c**) resulting in less band broadening[53, 54].

According to the literature, at high pH, cathodic EOF (EOF direction towards a cathode) is normally present as a result of the deprotonation of the silanol groups on the capillary wall[55]. The cathodic EOF causes the migration of proteins in gel electrophoresis to slow down. Herein, the peak of thiourea injected from the outlet of the capillary as EOF marker (moving in the opposite direction to the samples) was observed in the electropherograms of both buffers at 17.12 s and 34.79 s and corresponded to the electrophoretic mobilities (μ_{eo}) of 3.09×10^{-9} $cm^2/V \cdot s$ and 1.52×10^{-9} $cm^2/V \cdot s$ for buffer pH 8.5 and buffer pH 8.3, respectively. Accordingly, EOF occurred in buffer pH 8.5 was higher than that of pH 8.3 and this might cause the slow migration of protein in pH 8.5.

Another possible reason, during the stability check prior to the separation (**Figure 3.17a**), the current was recorded at every 1 V, while the voltage was varied from 0 V to 16 V. The current was also recorded at the separation voltage (15 kV) over the period of separation (**Figure 3.17b** and **Figure 3.17c**). It was found that the recorded current obtained from buffer pH 8.3 was always higher than that of buffer pH 8.5 either before or during separation. The higher current observed in buffer pH 8.3 might be as a result of the increase in ionization of the organic base (TRIS) leading to faster migration of proteins.

Consequently, the results of the mobility calculations for proteins and EOF, along with the differences in current observed during the experiments indicate that the reduced migration of proteins in higher pH of buffer may be a result of either the presence of cathodic EOF or the low separation current or both of them.

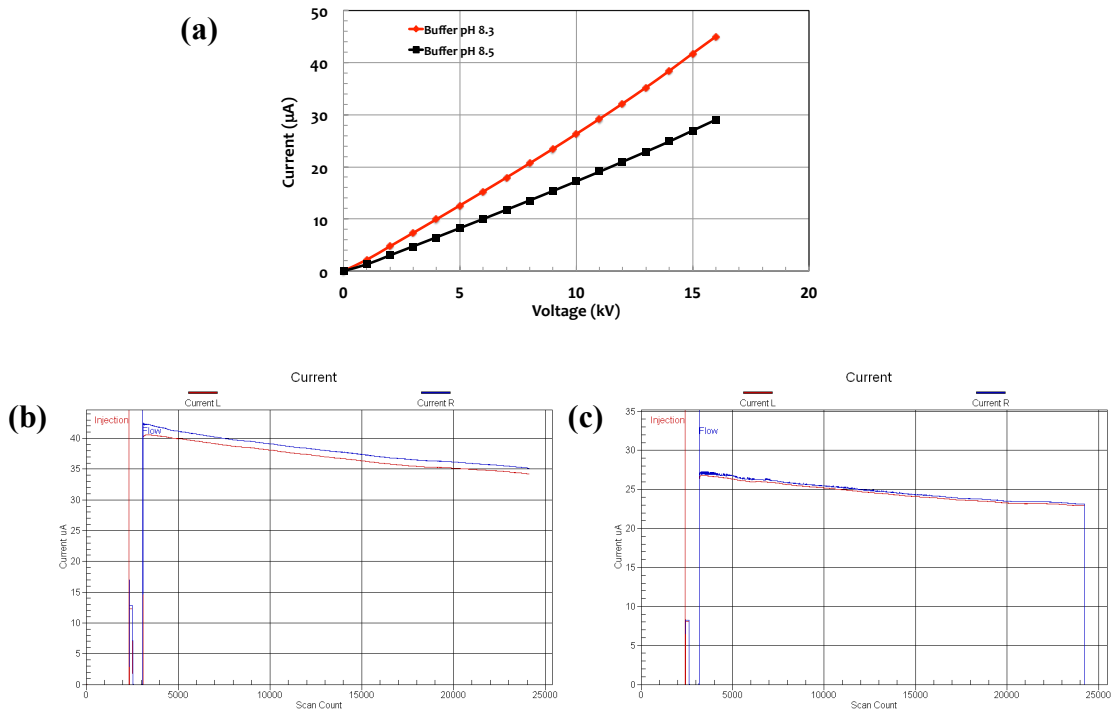

Figure 3.17: Comparison of the current during electrophoresis in 3% PEO 100 kDa mixed with 2% PEO 200 kDa in 0.1 M TRIS-CHES, 0.1% SDS, 2% glycerol, pH 8.3 and pH 8.5. (a) Plots between current and voltage of buffer pH 8.3 (red line) and buffer pH 8.5 (black line). Plots of current and time during separation in (b) buffer pH 8.3 and (c) buffer pH 8.5.

According to the results, protein separations in some tested buffers provided such low resolution that some protein peaks could not be distinguished from the others (no resolution, as shown in **Table 3.4**). It was found that the buffer that provided for the highest resolution was 7% PEO 100 kDa in 0.1 M TRIS-CHES, 0.1% SDS, 2% glycerol, pH 8.53. The resolution of separation between lysozyme and CA peaks and between CA and BSA peaks are 5.31 and 5.72, respectively. However, the analysis time was quite long (~14 minutes) compared to most of the tested buffers in **Table 3.4**, which might not be suitable for protein separations using a droplet-based format in which rapid separation is necessary.

The next buffer providing highest resolution was 5% PEO 100 kDa in 0.1 M TRIS-CHES, 0.1% SDS, pH 8.7. The resolution of separation between lysozyme and CA peaks and between CA and BSA peaks are 3.32 and 4.03, respectively. The analysis time for

using this buffer is only 9.3 minutes. Due to the high resolution and shorter analysis time this buffer provided, it was chosen to be tested further in the cross-piece PDMS microdevice.

3.3.4.3 Separations of proteins in PEO-based buffer using microdevices

The mixture of fluorescein and a fluorescently labeled protein ladder (11-155 kDa Benchmark fluorescent protein standard) was separated in 5% PEO 100 kDa in 0.05 M TRIS-CHES, 0.1% SDS, pH 8.5 in a cross-piece PDMS microdevice (**Figure 3.18**).

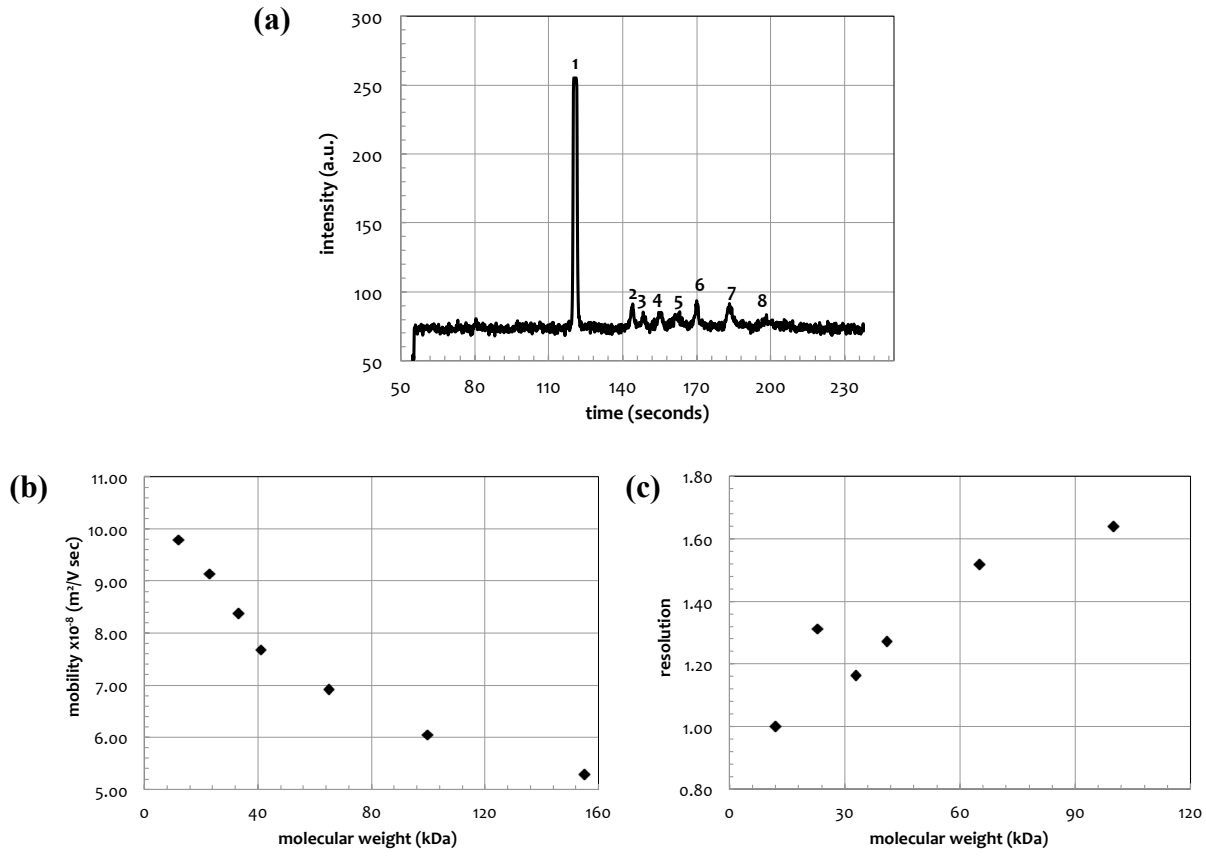

Figure 3.18: Electrophoretic separation of a fluorescently labeled protein ladder (11-155 kDa Benchmark fluorescent protein standard) performed in a cross-piece PDMS microdevice. (a) An electropherogram showing the fluorescein peak in the front followed by 7 protein bands of protein ladder separated in 5% PEO (100 kDa) in 0.05 M TRIS-CHES 0.1% SDS, pH 8.5 using electric field strength of 208.33 V/cm. Detection was done at 1.3 cm from the intersection; (b) A plot of mobility versus molecular weight of 11-155 kDa protein ladder; (c) A plot of resolution versus molecular weight. Note: The injection time was at 80 seconds according to the electropherogram.

Fluorescein was added as a marker for ease of observation due to its high fluorescence intensity. Although the concentration of the buffer used in the CE instrument was 0.1 M, the buffer concentration used in the PDMS microdevice was 0.05 M to address the buffer boiling. The pH of the buffer was also decreased from 8.7 to 8.5 to reduce EOF. According to the electropherogram (**Figure 3.18a**), seven peaks of proteins were successfully separated in 5% PEO 100 kDa buffer (using the field strength of ~208 V/cm and detected at 1.3 cm).

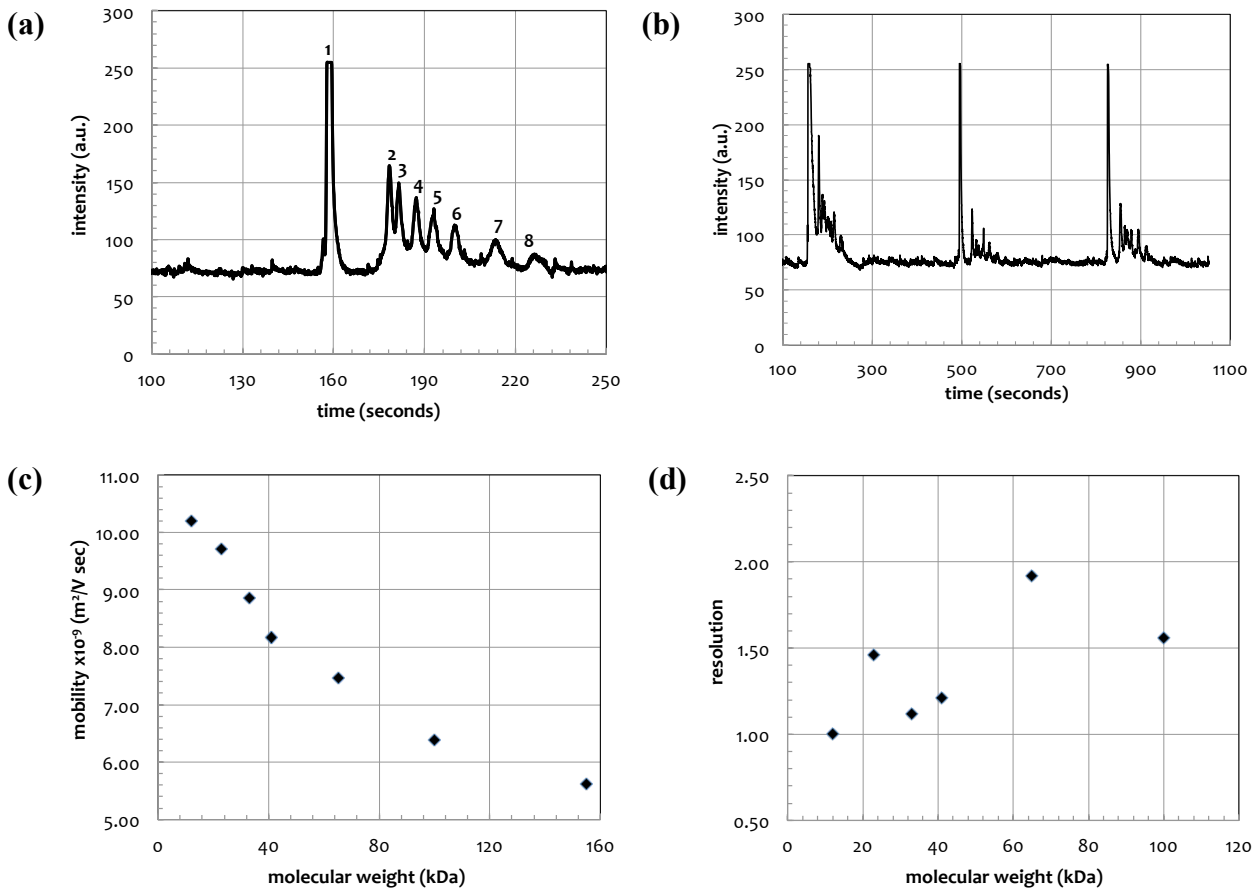

Figure 3.19: Electrophoretic separation of a fluorescently labeled protein ladder (11-155 kDa Benchmark fluorescent protein standard) performed in a cross-piece PDMS microdevice. (a) An electropherogram showing the fluorescein peak in the front followed by 7 protein bands of protein ladder separated in 6% PEO (100 kDa) in 0.05 M TRIS-CHES 0.1% SDS, pH 8.5 using electric field strength of 167.5 V/cm. Detection was done at 1.0 cm from the intersection; (b) Showing three repetitions of protein separations; (c) A plot of mobility versus molecular weight; (d) A plot of resolution versus molecular weight. Note: The injection time was at 120 seconds according to the electropherogram.

The higher resolution could be improved by increasing the concentration of PEO 100 kDa. The separation of the protein ladder was therefore performed in 6% PEO 100 kDa in 0.05 M TRIS-CHES, 0.1% SDS, pH 8.5 (using the field strength of ~168 V/cm and detected at 1.0 cm) and the results were shown in **Figure 3.19**. By comparing the resolutions of protein ladder separated in 5% PEO and 6% PEO buffers (**Table 3.3**), it was found that they were not significantly different for most of the peaks. 6% PEO 100 kDa buffer was therefore chosen and tested in another format of the separation device, which was a PDMS microdevice coupled to a glass capillary (**Figure 3.2b**), because similar resolutions were achieved when using this buffer with shorter length of detection and lower separation field strength.

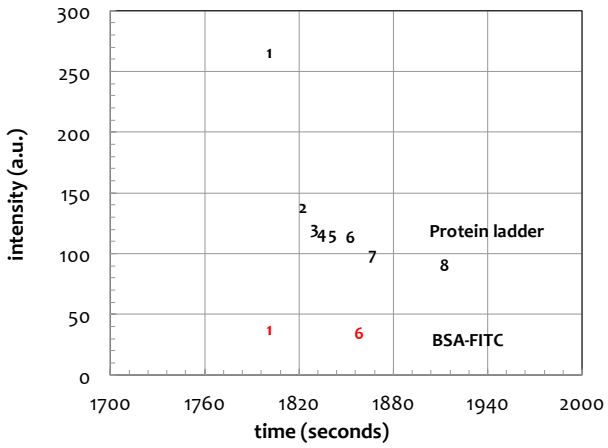

Figure 3.20: Electropherograms comparing between BSA peak in fluorescently labeled protein ladder (11-155 kDa Benchmark fluorescent protein standard) and the injected BSA-FITC. The separations were performed in a cross-piece PDMS microdevice using 6% PEO (100 kDa) in 0.05 M TRIS-CHES, 0.1% SDS, pH 8.5 at separation field strength of 167.5 V/cm and were detected at 1.0 cm from the injection point (Note: Y-axes are offset due to overlaying).

The mixture of BSA-FITC and fluorescein was also separated in 6% PEO 100 kDa in 0.05 M TRIS-CHES, 0.1% SDS, pH 8.5 in the cross-piece PDMS microdevice using the same conditions as that of protein ladder separation. The electropherogram of fluorescein mixed with BSA-FITC (red line in **Figure 3.20**) shows three peaks in which the first peak labeled as 1 is fluorescein and the other two peaks are BSA-

FITC. The two peaks of BSA-FITC belong to monomer (66 kDa) and dimer (132 kDa) since BSA can typically form covalent dimer and oligomers[53]. The formation of BSA aggregation is due to the thiol-disulfide interchange reaction. BSA contains 35 cysteine residues of which 34 residues are covalently bonded via intramolecular disulfide bonds. This leaves one cysteine residue with a free thiol group ($R\text{-}S^-$) that then reacts with a disulfide group on another BSA and forms an intermolecular disulfide bond and generates a new free thiol group, which may further react with another BSA[54].

The electropherograms of BSA-FITC and the protein ladder are overlaid and fluorescein peaks are aligned as depicted in **Figure 3.20** to confirm the order of protein elution in the protein ladder. The electrophoretic mobilities of the BSA peak in the protein ladder and in BSA-FITC (with respect to fluorescein peak) are found to be 1.04×10^{-8} m^2/Vs and 1.08×10^{-8} m^2/Vs, respectively. The similar electrophoretic mobilities confirm that the sixth peak in the electropherogram of the protein ladder was BSA (66 kDa) and that the first four peaks of the protein ladder (excluding fluorescein peak) are proteins having lower molecular weights than BSA and the last two peaks are proteins having higher molecular weights than BSA.

The separation of the protein ladder was then performed in 6% PEO 100 kDa buffer using a cross-piece PDMS microdevice coupled to a glass capillary. Although different buffers were employed in the PDMS part (0.1x TBE buffer) and the capillary part (6% PEO buffer), seven separated protein bands were successfully obtained within ~3 minutes at the detection point of 2.0 cm. It was found that the mobilities of proteins separated in this format (**Figure 3.21b**) were lower than that of the entire PDMS format (**Figure 3.19c**) despite the separation field using in the cross-piece PDMS coupled to the glass capillary was higher. EOF in the glass capillary might be higher than that of the PDMS microdevice; therefore, this retarded the migration of the proteins in the capillary. In addition, the slow migration of proteins in the glass capillary caused the broadening of the peaks, which in turn resulted in a decreasing in the resolution (**Table 3.5**). According to this result, it indicated that 6% PEO 100 kDa buffer could be used for droplet-based protein separation. The analysis time could be decreased by increasing the separation field and decreasing the distance

of detection. The glass capillary could also be treated with 1 M HCl for a longer period of time prior to filling up with the running buffer to suppress EOF.

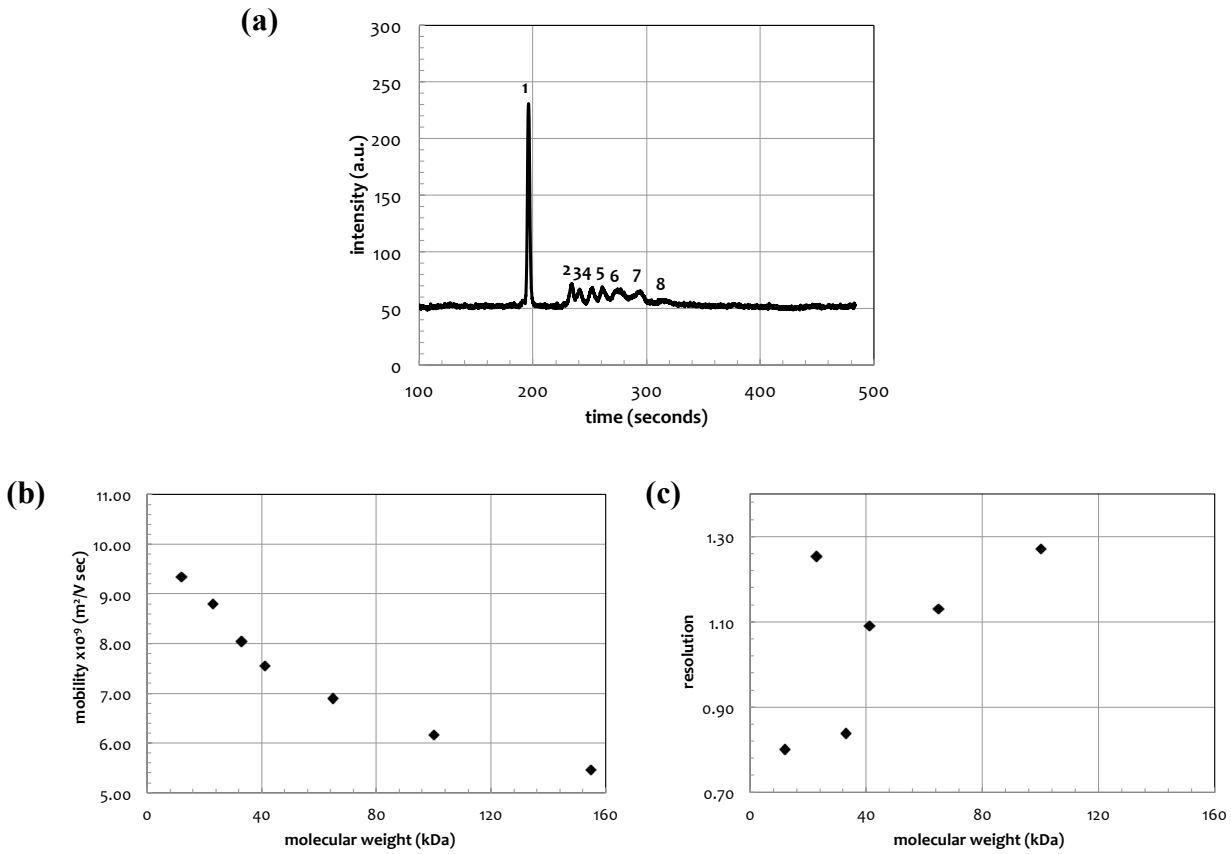

Figure 3.21: Electrophoretic separation of a fluorescently labeled protein ladder (11-155 kDa Benchmark fluorescent protein standard) performed in a cross-piece PDMS microdevice coupled to a glass capillary. (a) An electropherogram showing the fluorescein peak in the front followed by 7 protein bands of protein ladder separated in 6% PEO (100 kDa) in 0.05 M TRIS-CHES 0.1% SDS, pH 8.5 using electric field strength of 188 V/cm. Detection was done at 2.0 cm from the intersection; (b) A plot of mobility versus molecular weight; (d) A plot of resolution versus molecular weight. Note: The injection time was at 120 seconds according to the electropherogram.

3.4 Conclusion

Protein gel electrophoresis using droplet-based microfluidic devices require high-speed and high-resolution separation; therefore, a buffer solution that can provide for these aspects was developed in this work. The developed buffer also needs to be

compatible with the materials from which the microchannels are fabricated (i.e. PDMS and a glass capillary). Both commercial and laboratory-made buffers were investigated in terms of analysis time, resolution and compatibility with PDMS and glass channels.

One of the commercial buffers for SDS-protein complex separation (Beckman buffer) was studied. The original and the modified Beckman buffers were tested using both a commercial CE machine and PDMS microdevices. It was found that when the original Beckman running buffer together with either original or modified Beckman sample buffers was employed for protein separation using the CE machine, high-resolution separation of proteins was achieved but with a long analysis time (~ 20 minutes). However, Beckman running buffer could not be used to separate proteins in PDMS microdevices since high Joule heating occurred due to the inefficient heat dissipation the PDMS provided when a high separation field was applied. Consequently, the dilution and dialysis of Beckman running buffer was performed to reduce the concentration of the background electrolyte, which should in turn reduce Joule heating and permit a higher field to be applied. It was found that the loss of resolution and high EOF were problems when diluted Beckman buffer was employed. The dialysed Beckman buffer; on the other hand, resulted in changes in buffer composition, which affected the migration dynamics of proteins. Overall, the Beckman buffer, though an excellent matrix for size separation on capillary systems, proved challenging to adapt to a chip format. The buffer recipe is maintained as company know-how and could not be ascertained prior to this work, making its modification tedious and irreproducible. Consequently, buffers developed within the scope of this work allowed greater control over their recipe and preparation, and proved more successful.

Different compositions of laboratory-made buffers based on PEO and dextran were prepared and initially tested using the CE machine. Although, many buffer recipes provided for shorter analysis time than that of Beckman buffer, the resolution afforded at times was so low that a significant number of the protein peaks could not be distinguished. However, from the range of polymers and polymer lengths, one recipe provided for high-resolution and short analysis time. This was 5% PEO 100

kDa in 0.1 M TRIS-CHES, 0.1% SDS, pH 8.7 and it was chosen to test the separations on-chip.

5% PEO 100 kDa in 0.05 M TRIS-CHES, 0.1% SDS, pH 8.5 was then tested for protein separation in a cross-piece PDMS microdevice. The lower concentration of the background electrolyte and the lower pH were employed to minimize Joule heating and EOF. This buffer was further optimized by increasing the concentration of PEO from 5% (w/v) to 6% (w/v). The results show that proteins separated in 6% PEO buffer with shorter separation length and lower field strength and had similar resolution to that of 5% PEO buffer. Moreover, proteins were also successfully separated in 6% PEO buffer using a cross-piece PDMS microdevice coupled to a glass capillary. Consequently, 6% PEO 100 kDa in 0.05 M TRIS-CHES, 0.1% SDS, pH 8.5 was chosen as the buffer for droplet-based protein separation, which will be described in detail in **Chapter 6**.

3.5 References

1. Zhu, Z., Lu, J. J. & Liu, S. Protein separation by capillary gel electrophoresis: A review. *Anal. Chim. Acta* **709,** 21–31 (2012).

2. Wu, D. & Regnier, F. E. gel electrophoresis Sodium dodecyl sulfate-capillary proteins using non-cross-linked polyacrylamide. **608,** 349–356 (1992).

3. Ganzler, K., Greve, K. S., Cohen, A. S., Karger, B. L., Guttman, A. & Cooke, N. C. High-Performance Capillary Electrophoresis of SDS-Protein Complexes Using UV-Transparent Polymer Networks. *Electrophoresis* (1992).

4. Miksík, I., Sedláková, P., Mikulíková, K., Eckhardt, A., Cserhati, T. & Horváth, T. Matrices for capillary gel electrophoresis--a brief overview of uncommon gels. *Biomed. Chromatogr.* **20,** 458–65 (2006).

5. Nagata, H., Tabuchi, M., Hirano, K. & Baba, Y. Microchip electrophoretic protein separation using electroosmotic flow induced by dynamic sodium dodecyl sulfate-coating of uncoated plastic chips. *Electrophoresis* **26,** 2247–53 (2005).

6. Guttman, a. On the separation mechanism of capillary sodium dodecyl sulfate-gel electrophoresis of proteins. *Electrophoresis* **16,** 611–6 (1995).

7. Cooke, N. Influence of Temperature on the Sieving Effect of Different Polymer Matrices in Capillary SDS Gel Electrophoresis of Proteins. 199–203 (1993).

8. Lausch, R., Scheper, T., Reif, O. W., SchlGsser, J., Fleischer, J. & Freitag, R. Rapid capillary gel electrophoresis of proteins. *J. Chromatogr. A* **654,** 190–195 (1993).

9. Hu, S., Zhang, L., Krylov, S. & Dovichi, N. J. Cell cycle-dependent protein fingerprint from a single cancer cell: Image cytometry coupled with single-cell capillary sieving electrophoresis. *Anal. Chem.* **75,** 3495–3501 (2003).

10. Griebel, A., Rund, S., Schönfeld, F., Dörner, W., Konrad, R. & Hardt, S. Integrated polymer chip for two-dimensional capillary gel electrophoresis. *Lab Chip* **4,** 18–23 (2004).

11. Tabuchi, M., Kuramitsu, Y., Nakamura, K. & Baba, Y. A 15-s protein separation employing hydrodynamic force on a microchip. *Anal. Chem.* **75,** 3799–805 (2003).

12. Oliver, G., Simpson, C., Kerby, M. B., Tripathi, A. & Chauhan, A. Electrophoretic migration of proteins in semidilute polymer solutions. *Electrophoresis* **29,** 1152–1163 (2008).

13. Mikšík, I., Eckhardt, A., Forgács, E., Cserháti, T. & Deyl, Z. The effect of sodium dodecyl sulfate and Pluronic F127 on the electrophoretic separation of protein and polypeptide test mixtures at acid pH. *Electrophoresis* **23,** 1882–1886 (2002).

14. Chung, M., Kim, D. & Herr, A. E. Polymer sieving matrices in microanalytical electrophoresis. *Analyst* **139,** 5635–5654 (2014).

15. Sumitomo, K., Mayumi, K., Minamikawa, H., Masuda, M., Asahi, T., Shimizu, T., Ito, K. & Yamaguchi, Y. Buffers to suppress sodium dodecyl sulfate adsorption to polyethylene oxide for protein separation on capillary polymer electrophoresis. *Electrophoresis* **32,** 448–454 (2011).

16. Life Technology. Benchmark fluorescent protein standard. (2012).

17. Sigma Aldrich. Fluorescent molecular weight marker (M.W. 20,000-200,000). *Prod. Inf.*

18. Ren, J., Ulvik, a, Refsum, H. & Ueland, P. M. Applications of short-chain polydimethylacrylamide as sieving medium for the electrophoretic separation of DNA fragments and mutation analysis in uncoated capillaries. *Anal. Biochem.* **276,** 188–94 (1999).

19. Guttman, A., Nolan, J. A. & Cooke, N. Capillary sodium dodecyl sulfate gel electrophoresis of proteins. **632,** 171–175 (1993).

20. Ou, J. P., Chan, S. T. H. & Yeung, W. S. B. Separation of bovine serum albumin and its monoclonal antibody from their immunocomplexes by sodium dodecyl sulfate-capillary gel electrophoresis and its application in capillary electrophoresis-based immunoassay. *J. Chromatogr. B Biomed. Sci. Appl.* **731,** 389–394 (1999).

21. Pizarro, S. A., Lane, P., Lane, T. W., Cruz, E., Haroldsen, B. & VanderNoot, V. A. Bacterial characterization using protein profiling in a microchip separations platform. *Electrophoresis* **28,** 4697–4704 (2007).

22. Fruetel, J. A., West, J. A. A., Debusschere, B. J., Hukari, K., Lane, T. W., Najm, H. N., Ortega, J., Renzi, R. F., Shokair, I. & VanderNoot, V. A. Identification of viruses using microfluidic protein profiling and bayesian classification. *Anal. Chem.* **80,** 9005–9012 (2008).

23. Renzi, R. F., Stamps, J., Horn, B. A., Ferko, S., VanderNoot, V. A., West, J. A. A., Crocker, R., Wiedenman, B., Yee, D. & Fruetel, J. A. Hand-held microanalytical instrument for chip-based electrophoretic separations of proteins. *Anal. Chem.* **77,** 435–441 (2005).

24. Shadpour, H. & Soper, S. a. Two-Dimensional Electrophoretic Separation of Proteins Using Poly (methyl methacrylate) Microchips. *Anal. Chem.* **78,** 3519–3527 (2006).

25. Yao, S., Anex, D. S., Caldwell, W. B., Arnold, D. W., Smith, K. B. & Schultz, P. G. SDS capillary gel electrophoresis of proteins in microfabricated channels. *Proc. Natl. Acad. Sci. U. S. A.* **96,** 5372–7 (1999).

26. Chen, X., Wu, H., Mao, C. & Whitesides, G. M. A prototype two-dimensional capillary electrophoresis system fabricated in poly(dimethylsiloxane). *Anal. Chem.* **74,** 1772–8 (2002).

27. Salas-Solano, O., Tomlinson, B., Du, S., Parker, M., Strahan, A. & Ma, S. Optimization and validation of a quantitative capillary electrophoresis sodium dodecyl sulfate method for quality control and stability monitoring of monoclonal antibodies. *Anal. Chem.* **78,** 6583–6594 (2006).

28. Zhang, J., Burman, S., Gunturi, S. & Foley, J. P. Method development and validation of capillary sodium dodecyl sulfate gel electrophoresis for the characterization of a monoclonal antibody. *J. Pharm. Biomed. Anal.* **53,** 1236–43 (2010).

29. Vieillard, J., Mazurczyk, R., Morin, C., Hannes, B., Chevolot, Y., Desbe`ne, P. L. & Krawczyk, S. Application of microfluidic chip with integrated optics for electrophoretic separations of proteins. *J. Chromatogr. B Anal. Technol. Biomed. Life Sci.* **845,** 218–225 (2007).

30. Blazek, V. & Caldwell, R. a. Comparison of SDS gel capillary electrophoresis with microfluidic lab-on-a-chip technology to quantify relative amounts of 7S

and 11S proteins from 20 soybean cultivars. *Int. J. Food Sci. Technol.* **44,** 2127–2134 (2009).

31. Osiri, J. K., Shadpour, H. & Soper, S. a. Ultra-fast two-dimensional microchip electrophoresis using SDS μ-CGE and microemulsion electrokinetic chromatography for protein separations. *Anal. Bioanal. Chem.* **398,** 489–498 (2010).

32. Goux, A., Athias, A., Persegol, L., Lagrost, L., Gambert, P. & Lallemant, C. Capillary gel electrophoresis analysis of apolipoproteins A-I and A-II in human high-density lipoproteins. *Anal. Biochem.* **218,** 320–324 (1994).

33. Michels, D. a., Brady, L. J., Guo, A. & Balland, A. Fluorescent derivatization method of proteins for characterization by capillary electrophoresis-sodium dodecyl sulfate with laser-induced fluorescence detection. *Anal. Chem.* **79,** 5963–5971 (2007).

34. Sotelo, C. G., Piñeiro, C., Pérez-Martín, R. I. & Gallardo, J. M. Analysis of fish and squid myofibrillar proteins by capillary sodium dodecyl sulfate gel electrophoresis: actin and myosin quantification. *Eur. Food Res. Technol.* **211,** 443–448 (2000).

35. Gerber, S. & Planchon, C. Genetics of seed quality in soybean analysed by capillary gel electrophoresis. **152,** 181–189 (2000).

36. Lacher, N. A., Wang, Q., Roberts, R. K., Holovics, H. J., Aykent, S., Schlittler, M. R., Thompson, M. R. & Demarest, C. W. Development of a capillary gel electrophoresis method for monitoring disulfide isomer heterogeneity in IgG2 antibodies. *Electrophoresis* **31,** 448–458 (2010).

37. Cherkaoui, S., Bettinger, T., Hauwel, M., Navetat, S., Allémann, E. & Schneider, M. Tracking of antibody reduction fragments by capillary gel electrophoresis during the coupling to microparticles surface. *J. Pharm. Biomed. Anal.* **53,** 172–178 (2010).

38. Rustandi, R. R., Washabaugh, M. W. & Wang, Y. Applications of CE SDS gel in development of biopharmaceutical antibody-based products. *Electrophoresis* **29,** 3612–3620 (2008).

39. Kaneta, T., Inoue, J., Koizumi, M. & Imasaka, T. On-column capture of a specific protein in capillary electrophoresis using magnetic beads. *Electrophoresis* **27,** 3218–3223 (2006).

40. Techanukul, T., Pereira, F., Lipka, A., Suckling, J., Wood, S. L., Lewis, P., Hassard, S., Cass, A. E. G. & Nagy, J. M. CE-based sample quality assessment prior to 2-D gel electrophoresis: Towards the standardization of gel-based proteomics. *J. Sep. Sci.* **33,** 2536–2546 (2010).

41. Schwartz, H. & Pritchett, T. Separation of proteins and peptides by Capillary Electrophoresis: Application to Analytical Biotechnology. *Development*

(1994). at <http://www.ibt.unam.mx/computo/pdfs/met/Electroforesis/Electroforesis/CE/General/Aplicaciones/Proteins.pdf>

42. Fruetel, J. A., Renzi, R. F., VanderNoot, V. A., Stamps, J., Horn, B. A., West, J. A. A., Ferko, S., Crocker, R., Bailey, C. G., Arnold, D., Wiedenman, B., Choi, W. Y., Yee, D., Shokair, I., Hasselbrink, E., Paul, P., Rakestraw, D. & Padgen, D. Microchip separations of protein biotoxins using an integrated hand-held device. *Electrophoresis* **26,** 1144–1154 (2005).

43. Erickson, D., Sinton, D. & Li, D. Joule heating and heat transfer in poly(dimethylsiloxane) microfluidic systems. *Lab Chip* **3,** 141–149 (2003).

44. Frazier, R. A., Ames, J. M. & Nursten, H. E. *Capillary Electrophoresis for Food Analysis: Method Development*. (The Royal Society of Chemistry, 2000).

45. Discovery, T. & Alto, P. EOTrol Product Technical Guide With EOTrol. *Control* (2004).

46. Tabuchi, M., Kuramitsu, Y., Nakamura, K. & Baba, Y. A 1 5 -s Prot e in Se pa ra t ion Em ploying H ydrodyna m ic Forc e on a M ic roc hip. **75,** 5165–5171 (2003).

47. Okada, H., Kaji, N., Tokeshi, M. & Baba, Y. Rinse and evaporation coating of poly(methyl methacrylate) microchip for separation of sodium dodecyl sulfate-protein complex. *J. Chromatogr. A* **1192,** 289–293 (2008).

48. Huang, H., Xu, F., Dai, Z. & Lin, B. On-line isotachophoretic preconcentration and gel electrophoretic separation of sodium dodecyl sulfate-proteins on a microchip. *Electrophoresis* **26,** 2254–2260 (2005).

49. Song, A., Zhang, J., Zhang, M., Shen, T. & Tang, J. Spectral properties and structure of fluorescein and its alkyl derivatives in micelles. *Colloids Surfaces A Physicochem. Eng. Asp.* **167,** 253–262 (2000).

50. Grossman, P. D. & Soane, D. S. Capillary electrophoresis of DNA in entangled polymer solutions. *J. Chromatogr.* **559,** 257–266 (1991).

51. Corradini, D. Buffer additives other than the surfactant sodium dodecyl sulfate for protein separations by capillary electrophoresis. *J. Chromatogr. B Biomed. Sci. Appl.* **699,** 221–256 (1997).

52. Bergman, M., Claessens, H. & Cramers, C. Properties of Entangled Polymer Solutions in High-Performance Capillary Electrophoresis. 19–26 (1998).

53. Arakawa, T. & Kita, Y. Protection of Bovine Serum Albumin from Aggregation by TWEEN 80. *J. Pharm. Sci.* **89,** 646–651 (2000).

54. Maruyama, T., Katoh, S., Nakajima, M. & Nabetani, H. Mechanism of bovine serum albumin aggregation during ultrafiltration. *Biotechnol. Bioeng.* **75,** 233–238 (2001).

55. Hayes, M. a, Kheterpal, I. & Ewing, a G. Effects of buffer pH on electroosmotic flow control by an applied radial voltage for capillary zone electrophoresis. *Anal. Chem.* **65,** 27–31 (1993).

Chapter IV

Protein labeling with fluorescent dyes

4.1 Introduction

Many detection methods are employed for capillary electrophoresis such as absorbance detection, fluorescence detection, electrochemical detection and refractive index detection[1,2]. Of these detection methods, the UV-Vis detector and fluorescence detector are primarily utilized in commercial CE instruments. However, fluorescence detection is 1000-fold more sensitive than absorbance detection[3]. Consequently, the high sensitivity of fluorescence detection is more suited to the detection of low volume samples as typically handled in the microdroplets employed in this work.

In order to use fluorescence detection, samples need to have a fluorophore or be labeled with fluorophore that matches the excitation and emission wavelength of the detection system. Due to the high cost of commercial fluorescently labeled proteins, laboratory-labeled proteins were used in this work. The in-house development and use of these protocols had the additional benefit of enabling a variety of proteins including proteins released from cultured cells to be labeled. Some of the fluorescent dyes cited in the literature for labeling proteins and used to perform capillary electrophoresis in microdevices are listed in **Table 4.1**.

Table 4.1: Fluorescent dyes used to label proteins for electrophoresis in microdevices.

Fluorescent dye	λ_{ex} (nm)	λ_{em} (nm)	Samples	Ref.
Agilent dye	650	680	- BioRad protein ladder	4
Alexa Fluor 488	490	525	- myoglobin	5
			- OV, trypsin inhibitor and lipoprotein	6
Alexa Fluor 633	633	652	- actin, BSA, CO, HPA, PNA, OV, protein A, streptavidin, transferrin and WG	7
			- fetal calf serum proteins	8
FC	390	465	- SEA, SEB, ricin, OV, IgG and α-lactalbumin	9
			- proteins from *E.coli* lysate	10
			- viral proteins	11
			- CCK, α-lactalbumin, CA, BSA, OVA and IgG	12
Fluorescein-MAL	494	518	- Calmodulin	13
FITC	495	525	- β-lactoglobulin A, thyroglobin and myoglobin, HSA	14,15
			- CA, OV, BSA and conalbumin	16
			- fluorescent high molecular weight standard (Sigma)	17
			- OV	18
			- Digestion of BSA and proteins extracted from *E.coli*	19
			- BSA tryptic digest	20
			- proteins extracted from *E.coli*	21
Cy3	550	570	- CA II, β-lactoglobulin A and streptavidin	22

Fluorescent dye	**λ_{ex} (nm)**	**λ_{em} (nm)**	**Samples**	**Ref.**
Cy5	650	670	- lysozyme, CA, trypsin inhibitor	23
NanoOrange	470	570	- α-lactalbumin, β-lactoglobulin A and β-lactoglobulin B	24, 25
NHS-Fluorescein	491	518	- α-lactalbumin, pepsinogen, egg albumin, BSA, β-galactosidase and lysozyme	13
OPA	340	455	- amino acids	26
Sypro Orange	450	590	- bovine insulin, lysozyme, myoglobin, trypsin inhibitor, trypsin, CA, OV, serum albumin, BSA, phosphorylase B, β-galactosidase , myosin, proteins extracted from human Jurkat cells	27
			- BSA	4
Sypro Red	547	631	- α-lactalbumin, β-lactoglobulin A and β-lactoglobulin B	24
			- actin, parvalbumin, BSA and trypsin inhibitor	28
5/6-TAMRA, SE	546	579	- tryptic digest of BSA	29
			- tryptic digest from cytochrome c	30
TRITC	557	576	- tryptic peptides of β-casein	31
TNS	325	450	- IgG, transferrin, l-antitrypsin and albumin	32

Note: bovine serum albumin (BSA), carbonic anhydrase (CA), Cholecystikinin flanking peptide (CCK), concanavalin A (CO), *helix pomatia* lectin (HPA), human serum albumin (HSA), immunoglobulin G (IgG), lectin peanut agglutinin (PNA), ovalbumin (OV), staphylococcal enterotoxin A (SEA), staphylococcal enterotoxin B (SEB), wheat germ agglutinin (WG), Fluorescamine (FC), Fluorescein-5-maleimide (Fluorescein-MAL), Fluorescein isothiocyanate (FITC), Indocarbocyanine (Cy3), Indodicarbocyanine (Cy5), 5/6-carboxyfluorescein succinimidyl ester (NHS-Fluorescein), *ortho*-Phthalaldehyde (OPA), 5/6-carboxytet- ramethylrhodamine, succinimidyl ester (5/6-TAMRA, SE), Tetramethylrhodamine isothiocyanate (TRITC), 2-Toluidinonaphthalene-6-sulfonate (TNS)

Among the dyes having the excitation and emission wavelengths to match our detection system (i.e. λ_{ex} = 470-490 nm and λ_{em} = 510 nm cut-on), fluorescein isothiocyanate (FITC), 5/6-carboxyfluorescein succinimidyl ester (NHS-fluorescein) and NanoOrange were employed for labeling proteins in this work. FITC was employed since it has been studied for a long time and widely used as a fluorescent label for proteins[33,34,35,36]. FITC combines with a protein through a reaction between the isothiocyanate group of FITC and free amino groups (amino terminal and primary amines) of the protein to form a stable thiourea bond as shown in **Figure 4.1**.

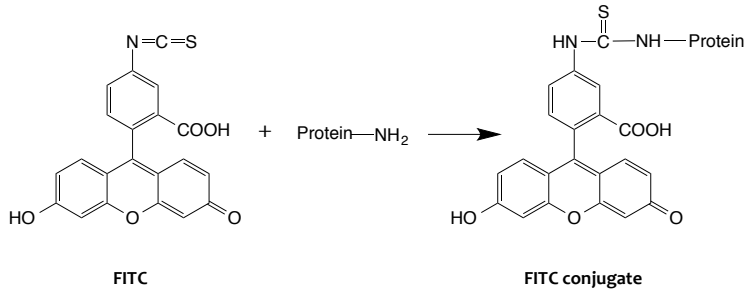

Figure 4.1: The reaction of protein conjugated with FITC.

NHS-Fluorescein is the second fluorescent dye chosen for labeling proteins due to its high reactivity toward primary amines leading to the formation of a stable linkage. NHS-Fluorescein reacts with primary amines on proteins to form amide bonds and release NHS as a by-product as illustrated in **Figure4.2**.

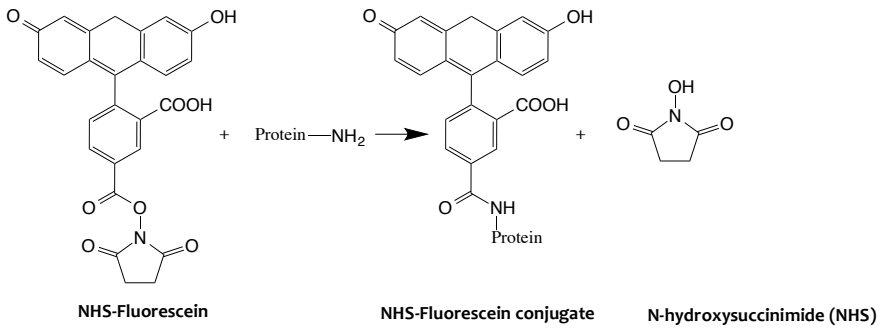

Figure 4.2: The reaction of protein conjugated with NHS-Fluorescein.

The third fluorescent dye chosen to label proteins in this work was NanoOrange, due to the many benefits it provides. For example, the labeling process is simple, fast and sensitive[37]. Moreover, NanoOrange is non-fluorescent when it is not bound to proteins. This allows the direct use of the protein-dye conjugate after labeling without a complicated excess dye removal process. Although, the information on the structure of NanoOrange has not been made public, it has been reported to interact with proteins via non-covalent bonds (i.e. electrostatic and/or hydrophobic interactions), which was performed with detergent-coated proteins[38,39].

4.2 Experimental

4.2.1 Chemicals

Samples and chemicals used in this chapter, which have not been mentioned in **Chapter 3**, are shown in **Table 4.2**.

Table 4.2: Samples and chemicals used in **Chapter 4**.

No.	Chemical	Supplier
1.	5-(and 6-)carboxyfluorescein, succinimidyl ester (NHS-Fluorescein)	Thermo Fisher Scientific, UK
2.	Ammonium chloride	Sigma Aldrich, UK
3.	Dimethyl sulfoxide (DMSO)	Sigma Aldrich, UK
4.	Fluorescein-5, 6-isothiocyanate (FITC)	Sigma Aldrich, UK
5.	NanoOrange® Protein Quantitation Kit	Thermo Fisher Scientific, UK
6.	Sodium azide	Sigma Aldrich, UK
7.	Sodium carbonate	Sigma Aldrich, UK
8.	Sodium bicarbonate	Sigma Aldrich, UK
9.	Trypsin inhibitor from chicken egg white	Sigma Aldrich, UK
10.	Xylene cyanol FF	Sigma Aldrich, UK

4.2.2 Labeling protocol

4.2.2.1 FITC labeling

Lysozyme and BSA were labeled with fluorescein isothiocyanate (FITC) according to the Sigma Aldrich protocol[40]. 2 mg/ml of each protein was dissolved in 0.1 M sodium carbonate buffer pH 9.0, while FITC was dissolved in anhydrous dimethyl sulfoxide (DMSO) at 1 mg/ml. 50 µl of FITC solution was added to a 1 ml of protein in 5 µl aliquots, while continuously stirring the protein solution. The protein-FITC solution was then incubated in the dark at 4°C for 8 hours. After that ammonium chloride (NH_4Cl) was added to the solution to a final concentration of 50 mM and the solution was further incubated for 2 hours at 4°C. Then xylene cyanol and glycerol were added at 0.1% (v/v) and 0.5% (v/v), respectively. The unbound FITC was separated from the conjugate using 5 kDa MWCO polyethersulfone (PES) membrane (Vivaspin 500 MWCO 5000, GE Healthcare Life Sciences, UK). Finally, sodium azide at a concentration of 15 mM was added as a preservative before the conjugate solution was stored in the dark at 4°C. Following the conjugation, the conjugate (diluted in DI water) was then measured for absorption at 495 and 280 nm using a LAMBDA 25 UV/Vis spectrophotometer (Perkin Elmer, UK). Then, the molar F/P ratio was calculated according to **Equation 4.1** to determine the efficiency of the FITC-protein conjugation.

$$\frac{\mathrm{MW}}{389} \times \frac{\mathrm{A}_{495}/195}{\mathrm{A}_{280}-[(0.35\times\mathrm{A}_{495})]/\mathrm{E}_{280}^{0.1\%}} = \frac{\mathrm{A}_{495}\times\mathrm{C}}{\mathrm{A}_{280}-(0.35\times\mathrm{A}_{495})} \qquad (4.1)$$

MW is the molecular weight of the protein, 389 is the molecular weight of FITC, 195 is the absorption $E_{280}^{0.1\%}$ of bound FITC at 490 nm at pH 13.0, (0.35×A495) is the correction factor due to the absorbance of FITC at 280 nm, $E_{280}^{0.1\%}$ is the absorption at 280 nm of a protein at 1.0 mg/ml and C is a constant value given for a protein defined as

$$\mathrm{C} = \frac{\mathrm{MW}\times\mathrm{E}_{280}^{0.1\%}}{389\times195} \qquad (4.2)$$

4.2.2.2 NHS-Fluorescein labeling

The first step in this process[41] involved the dissolution of 1.3 mg (2.75 μmol) NHS-Fluorescein in 50 μl DMSO. A 15-fold molar excess of NHS-Fluorescein (an optimal ratio) was used to label protein with this dye. Accordingly, 1.05 μmol (19.1 μl) and 0.23 μmol (4.15 μl) of NHS-Fluorescein were added to 2 mg/ml lysozyme and 2 mg/ml BSA, respectively. The mixtures were incubated at room temperature for 1 hour. After that the excess dye was removed using a Pierce dye removal column (Thermo Fisher Scientific, UK). The removal process was performed twice for more complete dye removal. 0.1% (w/v) sodium azide was then added to the labeled protein solutions. After the conjugation, the conjugate (diluted in DI water) was measured absorption at 494 and 280 nm. The molar F/P ratio was calculated as **Equation 4.3** to determine the efficiency of the NHS-Fluorescein-protein conjugation.

$$\text{Moles fluor/mole protein} = \frac{A_{max} \text{ of the labeled protein}}{\varepsilon_{fluor} \times \text{protein concentration (M)}} \times \text{dilution factor} \quad (4.3)$$

Where ε_{fluor} = NHS-Fluorescein molar extinction coefficient = 70,000 $M^{-1}cm^{-1}$

$$\text{Protein concentration (M)} = \frac{A_{280} - (A_{max} \times CF)}{\varepsilon_{protein}} \times \text{dilution factor} \quad (4.4)$$

Where $\varepsilon_{protein}$ is protein molar extinction coefficient, A_{max} is A_{494} and CF is correction factor (A_{280}/ A_{max} = 0.3).

4.2.2.3 NanoOrange labeling

NanoOrange reagent (500x in DMSO) and NanoOrange diluent (10x contains 2 mM sodium azide) were obtained as part of the NanoOrange protein quantitation kit (Thermo Fisher Scientific, UK). 1x NanoOrange diluent was prepared by diluting the NanoOrange protein quantitation diluent 10-fold in DI water. NanoOrange protein reagent was then diluted 500-fold into the 1x protein quantitation diluent. The protein with the desired concentration was diluted 1:200 into the 1x NanoOrange reagent. The sample was

incubated in the dark at 95°C for 10 min and cooled to room temperature in the dark for 20 min prior to being used.

4.2.3 Electrophoresis of fluorescently labeled proteins

Free FITC, lysozyme conjugated FITC, NHS-Fluorescein and lysozyme conjugated NHS-Fluorescein, were used to investigate protein separations using cross-piece PDMS microdevices. Lysozyme conjugated FITC and lysozyme conjugated NHS-Fluorescein were prepared in 0.1% SDS buffer and heated at 95 °C for 5 min. The stock solution of FITC (3.85 mM) was prepared in 960 µl of DI water and added 40 µl of 1 M NaOH to completely dissolve FITC. 38.5 µM FITC was then prepared from the stock solution in DI water. The stock solution of NHS-Fluorescein (59.1 mM) was prepared in DMSO and was diluted to 0.59 mM in 0.1x TBE buffer. The electrophoresis of FITC, NHS-Fluorescein, lysozyme conjugated with FITC and lysozyme conjugated NHS-Fluorescein were performed in 6% PEO 100 kDa in 0.05 M TRIS-CHES, 0.1% SDS, pH 8.5 using cross-piece PDMS microdevices as described in detail in **Section 3.2.5**.

For BSA conjugated NanoOrange, it was generated as droplets using the robotic droplet generator as described in **Section 2.3**. The electrophoresis was performed in 6% PEO buffer using the interfacing droplet-based microdevice "Design 6" as described in detail in **Section 5.3.6**.

4.2.4 Study the influence of SDS on the fluorescence intensity of the protein conjugated NanoOrange

This study was performed to investigate the effect of 0.1% SDS contained in the separation buffer, which was higher than the recommended value (0.01% SDS), on the fluorescence intensity of protein conjugated NanoOrange. The fluorescence intensities of the buffers only i.e. 0.05 M TRIS-CHES with 0%, 0.01% and 0.1% SDS were measured as the control using the fluorescence detection described in **Section 2.4.2.1**. Then 10 µl of 0.01 mg/ml lysozyme conjugated 1x NanoOrange was added to each buffer and the fluorescence intensity was measured again.

4.3 Results and Discussion

4.3.1 FITC labeling proteins

Lysozyme and BSA were labeled with FITC according to the protocol described in **Section 4.2.2.1**. The absorption of the conjugates was measured at the wavelengths of 280 nm (maximum absorbance of protein) and 495 nm (maximum absorbance of FITC) to permit calculation of the efficiency of labeling. **Figure 4.3a** and **Figure 4.3b** show the absorption spectra of lysozyme-FITC and BSA-FITC, respectively. The degree of labeling is expressed as a ratio between fluorophore and protein molar concentrations (F/P ratio) of the conjugate, which represents the number of dye molecules conjugated to the protein molecule[42].

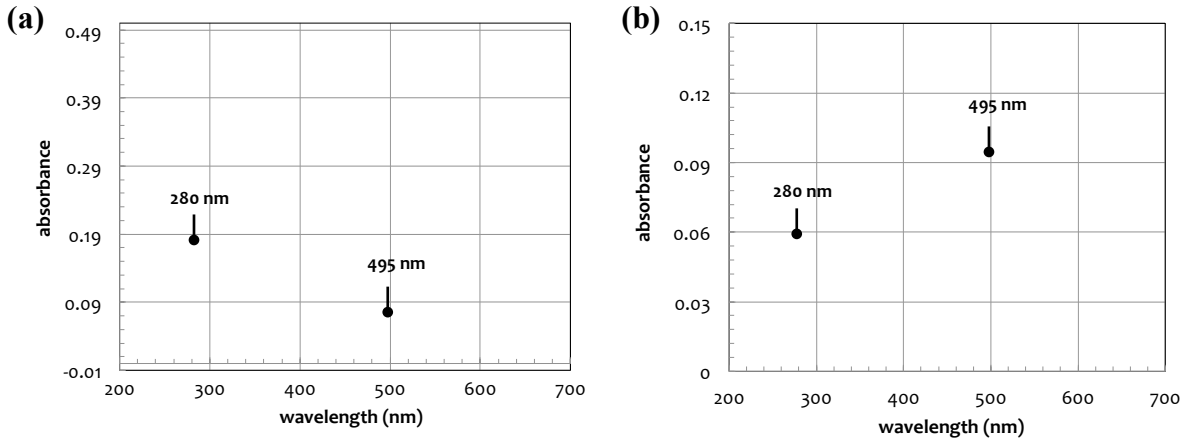

Figure 4.3: Absorption spectra of (a) lysozyme conjugated FITC and (b) BSA conjugated FITC. Both protein conjugates were prepared in DI water.

The molar F/P ratio calculated according to the **Equation 4.1** (**Section 4.2.2.1**) for lysozyme-FITC is 0.045 and for BSA-FITC is 0.218; however, the acceptable value for molar F/P ratio should be between 0.3-1.0. The low molar F/P ratio might be due to the exposure of the conjugates to the light during the unbound FITC removal process. This can cause the degradation of the conjugate products since FITC is light-sensitive[43,44]. Another possibility is the use of mixed-isomer FITC to label proteins since it is less reactive than the use of N-Hydroxysuccinimide (NHS)-fluorescein[41].

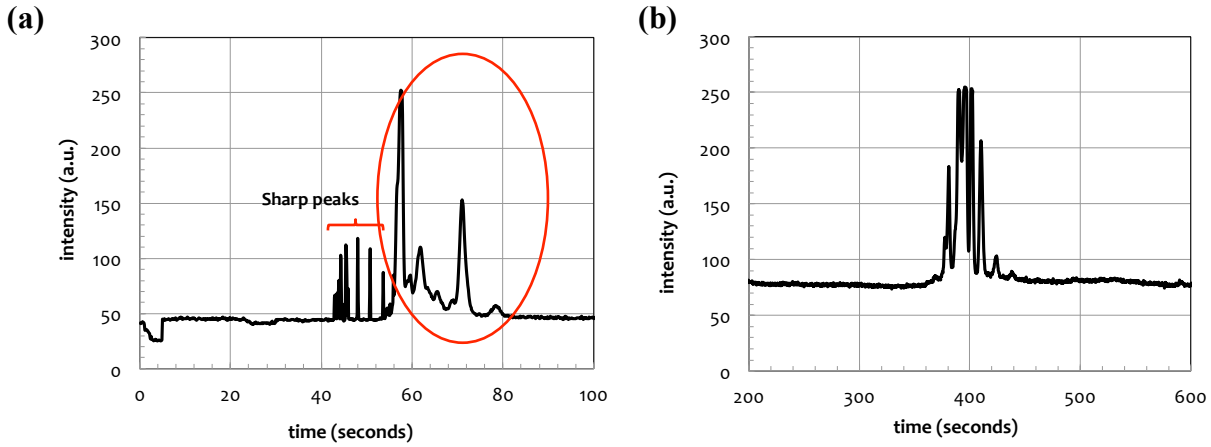

Figure 4.4: Electrophoresis performed in 6% PEO 100 kDa in 0.05 M TRIS-CHES, 0.1% SDS, pH 8.5 using a cross-piece PDMS microdevice. The electric field was applied at ~168 V/cm and the detection was made at 1 cm. The electropherograms of (a) lysozyme-FITC prepared in 0.1% SDS buffer and heated at 95 °C for 5 min and (b) 38.5 µM FITC dissolved in DI water.

The lysozyme conjugated FITC was also electrophoresed in 6% PEO 100 kDa in 0.05 M TRIS-CHES, 0.1% SDS, pH 8.5 buffer using a cross-piece PDMS microdevice. Lysozyme conjugated FITC is expected to provide a single peak; however, several sharp peaks and several broader peaks are observed in the electropherogram (**Figure 4.4a**). The sharp peaks are air bubbles migrating into the glass capillary, whereas several broader peaks (in red circle of **Figure 4.4a**) are from the single injection of lysozyme conjugated FITC. These broad peaks might belong to lysozyme-FITC and unbound FITC that was not completely removed from the sample. Free FITC was also electrophoresed in 6% PEO buffer and it was found that seven obvious peaks were observed in the electropherogram (**Figure 4.4b**). The peaks obtained from free FITC might be from various forms of FITC in aqueous solution (**Figure 4.5**) and the product of the unbound FITC that reacted with primary amine of TRIS in 6% PEO buffer (**Figure 4.6**). Among the possible forms of free FITC (**Figure 4.5**) of those analysed in 6% PEO buffer (pH 8.5), the anionic and dianionic forms should be most abundant in the basic solution, while the cationic form should not exist[45].

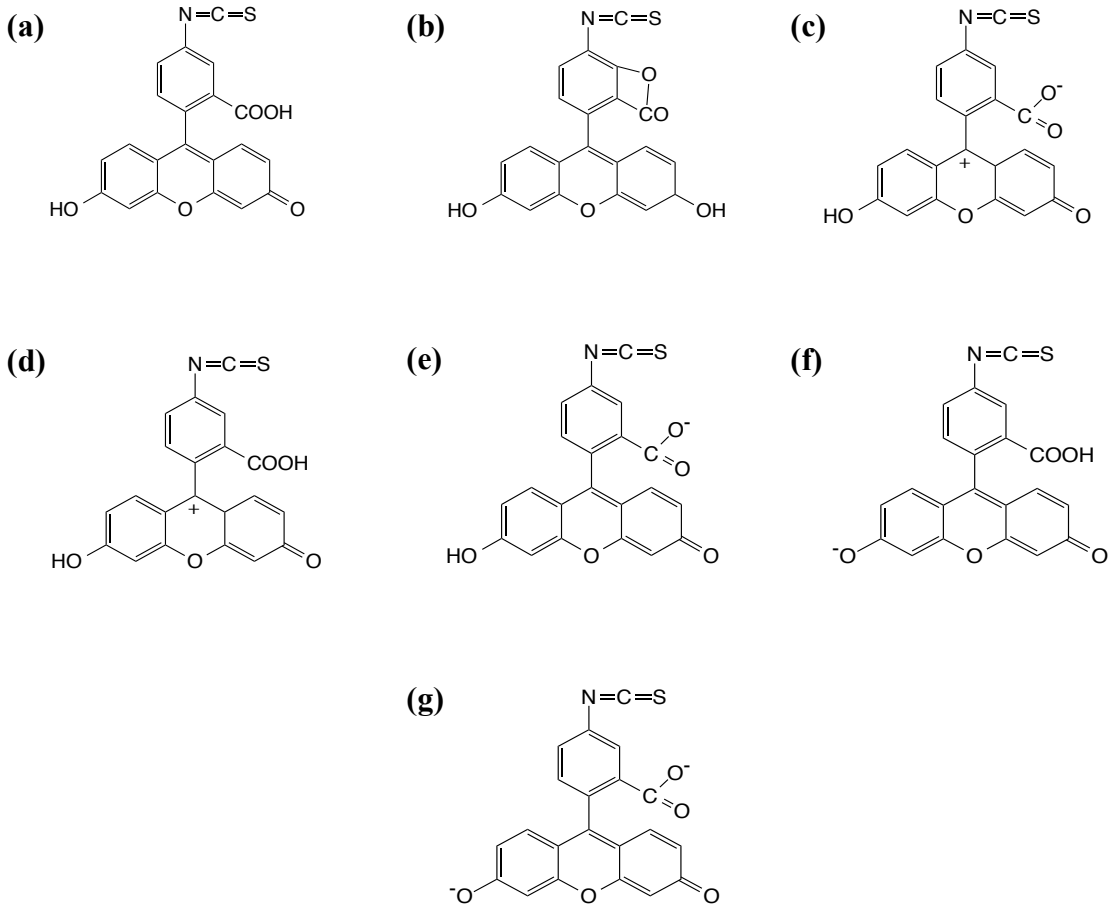

Figure 4.5: Possible forms of FITC in an aqueous solution (a) neutral species (p-quinoid); (b) neutral species (lactone); (c) neutral species (zwitterion); (d) cation; (e) anion (carboxylate); (f) anion (phenolate) and (g) dianion

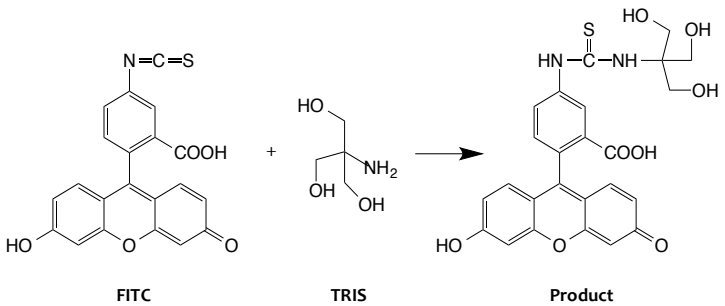

Figure 4.6: The reaction of free FITC with TRIS containing in 6% PEO buffer.

According to the results, protein labeling with FITC provided for a lower degree of labeling (F/P ratio) than the recommended value from literature. The fluorescence intensity might therefore be too low to be detected, especially when the protein–FITC complex is employed in the droplet format. In addition, the unbound FITC remaining in the conjugate samples due to the incomplete removal provided for several peaks in the electropherogram. This made it very difficult to distinguish the protein conjugates from the other irrelevant peaks. The protocol for protein labeling with FITC was also complicated and time-consuming. Consequently, a more reactive fluorescent dye with simpler labeling and dye removing protocols that could provide for higher F/P ratios was employed and discussed in **Section 4.3.2**.

4.3.2 NHS-Fluorescein labeling proteins

According to the results, the labeling protocol of NHS-Fluorescein was simpler than that of FITC. Proteins (lysozyme and BSA) were labeled with NHS-Fluorescein according to the protocol described in **Section 4.2.2.2** and the conjugates were measured for the absorbance at 280 nm (maximum absorbance of protein) and 494 nm (maximum absorbance of NHS-Fluorescein) (**Figure 4.7**) for the calculation of the F/P ratio.

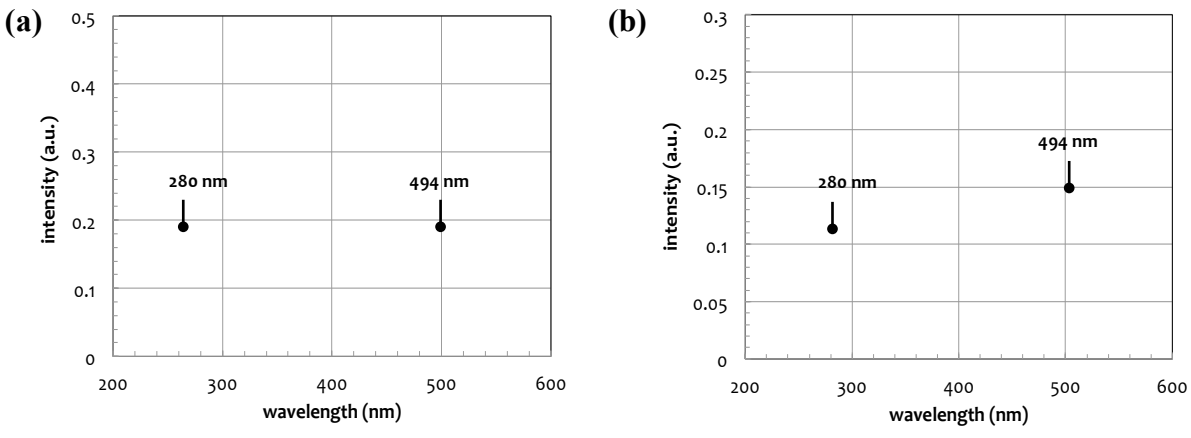

Figure 4.7: Absorption spectra of (a) lysozyme conjugated NHS-Fluorescein and (b) BSA conjugated NHS-Fluorescein. Both protein conjugates were prepared in DI water.

The F/P ratio for lysozyme conjugated NHS-Fluorescein is 0.23, which is higher than that of FITC and for BSA conjugated NHS-Fluorescein is 0.13, which is lower than that of FITC. However, the degrees of labeling of both proteins are still lower than the recommended values (F/P ratio ~ 0.3-1.0).

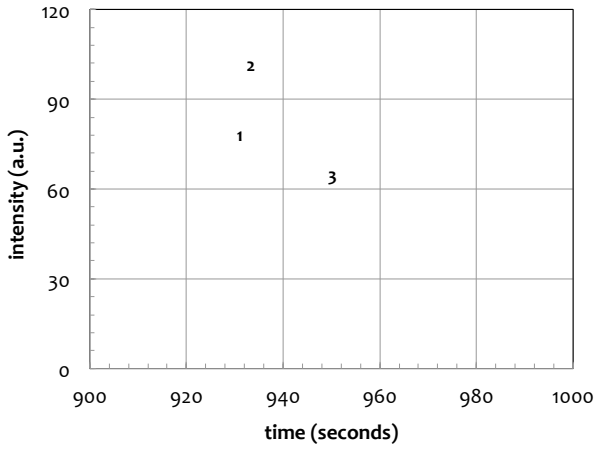

Figure 4.8: The electropherogram of NHS-Fluorescein performed in 6% PEO 100 kDa in 0.05 M TRIS-CHES, 0.1% SDS, pH 8.5 using a cross-piece PDMS microdevice. The electric field was applied at ~168 V/cm and the detection was made at 1 cm. 0.5 mM NHS-Fluorescein was prepared in 0.1x TBE buffer.

Free NHS-Fluorescein was electrophoresed in 6% PEO buffer as a control. At least three peaks are obviously observed in the electropherogram (**Figure 4.8**). These peaks might be NHS-Fluorescein, hydrolysed NHS-Fluorescein and the product from the reaction between NHS-Fluorescein and TRIS in 6% PEO buffer (**Figure 4.9**). The electrophoretic mobilities for peak 1, 2 and 3 are 1.60×10^{-8}, 1.53×10^{-8} and 7.65×10^{-9} $m^2/V\cdot s$, respectively.

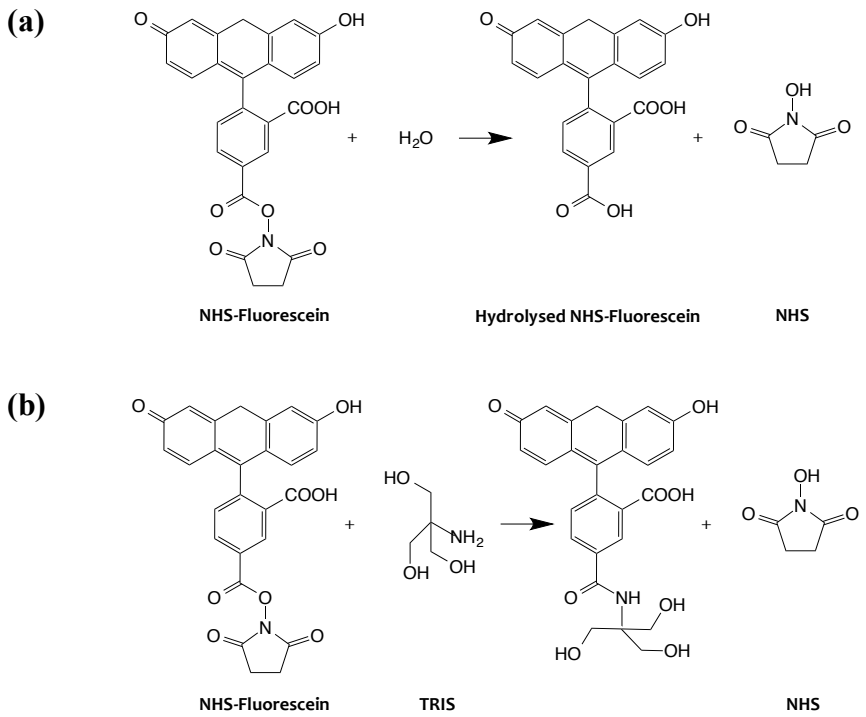

Figure 4.9: The reaction of NHS-Fluorescein in 6% PEO buffer (a) The hydrolysis of NHS-Fluorescein and (b) The reaction between NHS-Fluorescein and TRIS.

When lysozyme conjugated NHS-Fluorescein was electrophoresed in 6% PEO buffer, three peaks are observed in the electropherogram (**Figure 4.10a**) with the mobilities of 1.31×10^{-8} (peak 1), 1.27×10^{-8} (peak 2) and 1.02×10^{-8} $m^2/V\bullet s$ (peak 3). Since it was difficult to distinguish the lysozyme conjugate peak from the products of free NHS-Fluorescein peaks, the free NHS-Fluorescein was then added to the lysozyme conjugate sample, which was depleted from the sample reservoir after several runs, to help distinguish the lysozyme conjugate peak. **Figure 4.10a** shows the first electrophoresis of lysozyme conjugated NHS-Fluorescein, which was initially added at the volume of 16 µl in the sample reservoir. The second electrophoresis was performed right after the first run as shown in **Figure 4.10b**. It was found that the intensity of all three peaks of the second run slightly decreased from the first run (**Table 4.2**). The free NHS-Fluorescein (0.1 mM) was added at 4-µl increments to the sample reservoir containing the rest of the lysozyme conjugate sample. The intensities of peak 1 and peak 2 significantly increased in the third run (**Table 4.3**) in which the NHS-Fluorescein was first added to the sample reservoir (**Figure 4.10c**). However, after NHS-Fluorescein was further added to the sample

reservoir in the fourth run, the intensities of all three peaks were higher (**Table 4.3**). It was also found that the fourth peak having the lowest mobility appeared in this run (**Figure 4.10d**). Since the first three peaks observed in the electropherograms of the lysozyme conjugate shows a significant change in the intensities after NHS-Fluorescein was added, it could be inferred that all the observed peaks belong to NHS-Fluorescein rather than the lysozyme conjugate. The fourth peak appeared in the electropherogram (**Figure 4.10d**) might be another form of NHS-Fluorescein; however, it might be only readily observed when the concentration of NHS-Fluorescein is high enough.

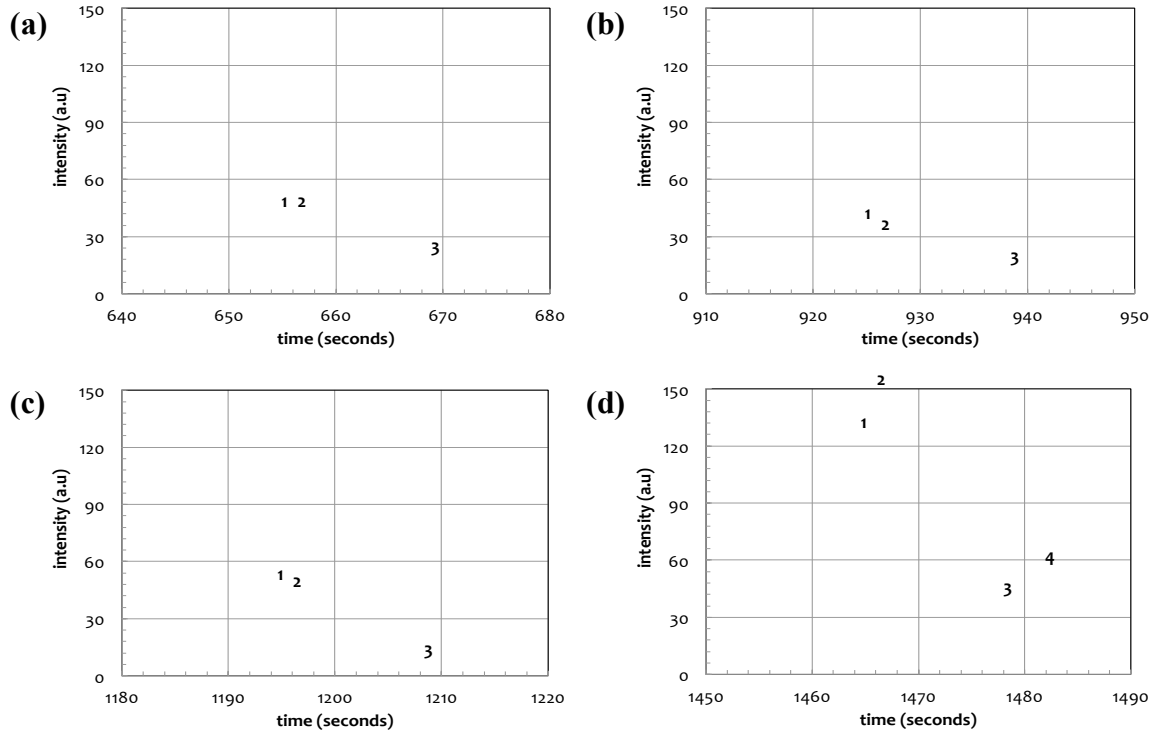

Figure 4.10: The electropherograms of lysozyme-NHS-Fluorescein electrophoresed in 6% PEO 100 kDa in 0.05 M TRIS-CHES, 0.1% SDS, pH 8.5 using a cross-piece PDMS microdevice (a) First injection of lysozyme-NHS-Fluorescein; (b) Second injection of lysozyme-NHS-Fluorescein; (c) First addition of 4 µl 0.1 mM NHS-Fluorescein to the depleted lysozyme-NHS-Fluorescein and (d) Second addition of 4 µl 0.1 mM NHS-Fluorescein to the depleted lysozyme-NHS-Fluorescein. The electric field was applied at ~168 V/cm and the detection was made at 1 cm. Lysozyme-NHS-Fluorescein was prepared in 0.1% SDS buffer and heated at 95 °C for 5 min, while 0.1 mM NHS-Fluorescein was prepared in 0.1x TBE buffer.

Table 4.3: Showing the mobility and intensity of the peaks obtained from the electrophoresis of lysozyme conjugated NHS-Fluorescein with the addition of NHS-Fluorescein.

Experiment	Mobility ($\times 10^{-8}$ $m^2/V \bullet s$)				Intensity (a.u.)			
	Peak 1	Peak 2	Peak 3	Peak 4	Peak 1	Peak 2	Peak 3	Peak 4
1st run: injection of lysozyme conjugate	1.32	1.27	0.99	-	37	35	13	-
2nd run: injection of lysozyme conjugate	1.32	1.28	1.02	-	34	30	10	-
3rd run: 1st addition of 4 µl NHS-Fluorescein	1.32	1.27	1.02	-	46	43	5	-
4th run: 2nd addition of 4 µl NHS-Fluorescein	1.32	1.27	1.02	0.95	126	150	34	54

According to the results, proteins conjugated with NHS-Fluorescein had low F/P ratios indicating the low fluorescence intensity of the conjugates. This was confirmed by the electrophoresis of the lysozyme conjugate since the lysozyme conjugate peak was not observed. The low degree of protein labeling with NHS-Fluorescein might be due to the less reactive NHS-Fluorescein, which was possibly caused by the hydrolysis of NHS-Fluorescein when it encountered the moisture after the thawing process. Another possible reason might be the incomplete removal of the unbound dye, which in turn interfered with the absorption measurement and therefore the calculation of F/P ratio. The intensities of the free NHS-Fluorescein and its products in the protein conjugate samples might overcome the intensity of the protein conjugate. As a result, a fluorescent dye that could be used to label proteins without the dye removal process after the labeling was required.

4.3.3 NanoOrange labeling proteins

In addition to the advantages of using NanoOrange described in **Section 4.1**, NanoOrange does not react with primary amines or undergo hydrolysis in the presence of water. Consequently, it does not react with TRIS in the aqueous buffer as FITC and NHS-Fluorescein do, resulting in fewer free-dye related peaks in the electropherogram.

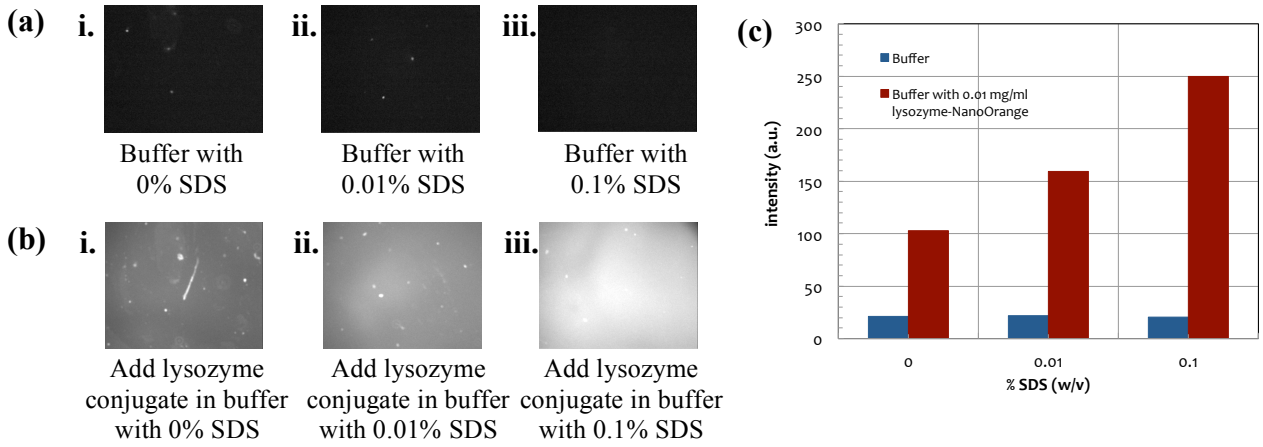

Figure 4.11: Effect of SDS concentration on the fluorescence intensity of protein conjugated NanoOrange. (a) The background intensity of 0.05 M TRIS-CHES, pH 8.5 buffer containing various concentrations of SDS (i) 0% SDS, (ii) 0.01% SDS and (iii) 0.1% SDS; (b) 10 µl of 0.01 mg/ml lysozyme conjugated 1x NanoOrange was added to 0.05 M TRIS-CHES, pH 8.5 buffer containing (i) 0% SDS, (ii) 0.01% SDS and (iii) 0.1% SDS; (c) A graph translating the fluorescence intensity from the images in **Figure 4.11a** and **Figure 4.11b** into the values in which the blue columns show the intensity of the background buffer containing 0-0.1% SDS and the red columns show the intensity of the buffer added 10 µl of 0.01 mg/ml lysozyme conjugated NanoOrange.

Prior to performing the electrophoresis, lysozyme conjugated NanoOrange was employed to demonstrate the effect of the concentration of SDS on the fluorescence intensity of the protein conjugated NanoOrange since a higher concentration of SDS (i.e. > 0.1% SDS) than the recommended concentration in the protocol (i.e. 0.01% SDS) was used in the separation system (i.e. both sample buffer and separation buffer contained SDS). The fluorescence intensity of the background buffers with various concentrations of SDS (i.e. 0 - 0.1% SDS) was recorded as a control (**Figure 4.11a** and **Figure 4.11c**). 10 µl of 0.01 mg/ml lysozyme conjugated NanoOrange was then added to each buffer prior to measuring the fluorescence intensity again. It was found that the fluorescence intensity increased with rising SDS concentration in the buffer (**Figure 4.11b** and **Figure 4.11c**). According to the literature, NanoOrange diluent already contains detergents including SDS; as a result, the addition of SDS in the buffer could lead to the formation of micelles (if the total concentration of SDS reaches the CMC) that can bind to the dye leading to the high background fluorescence[39]. The CMC of SDS in the similar buffer system (0.1 M TRIS-CHES buffer, pH 8.6 containing 1% PEO) to the one in the experiment was

reported to be ~ 3 mM[46]; therefore, it was possible that SDS micelles might be present in our buffer system leading to the increase in the fluorescence intensity due to the binding of the dye to SDS micelles.

It was also found that when NanoOrange was added to lysozyme solution, precipitation occurred (**Figure 4.11b** and **Figure 4.12a**) even at the concentration recommended in the protocol (0.01 mg/ml). The precipitation was also observed with the other proteins (i.e. BSA (**Figure 4.12b**) and trypsin inhibitor (data not shown)) that conjugated with NanoOrange. These precipitates interfered with the separation of proteins in that they flowed into the separation channel and generated erroneous peaks in the electropherograms. This could lead to misinterpretation and difficulty in distinguishing protein peaks, especially when several proteins were separated. The precipitation might also be one cause of the low fluorescence intensity of protein conjugates as observed in **Figure 4.12**. Owing to the low fluorescence intensity of proteins conjugated NanoOrange and the high fluorescence intensity of the background electrolyte containing SDS, the signal to noise ratio could be low and made the protein conjugates difficult to detect.

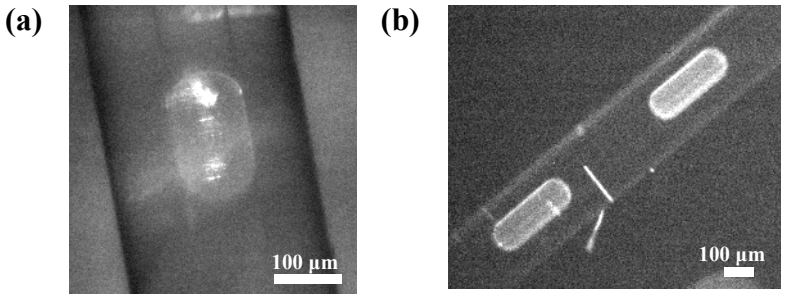

Figure 4.12: Fluorescence intensity of protein conjugated NanoOrange. (a) Lysozyme conjugated NanoOrange droplet and (b) BSA conjugated NanoOrange droplet. The concentration of the proteins conjugated dye used to generate droplets were 0.5 mg/ml.

The electrophoresis of BSA conjugated NanoOrange released from droplets was performed to investigate the fluorescence intensity and determine whether it was strong enough to be observed using our detection system. The electrophoresis of five BSA-NanoOrange droplets in 6% PEO buffer using the interfacing microdevice "Design 6"

(discussed in **Chapter 5**) was successfully detected as illustrated in the electropherogram (**Figure 4.13**). In this experiment, each droplet performed double injections resulting in two peaks.

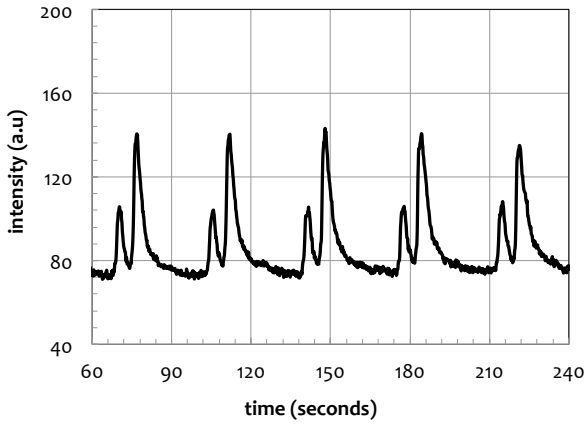

Figure 4.13: An electropherogram of BSA conjugated NanoOrange obtained from the injections of five droplets into 6% PEO 100 kDa in 0.05 M TRIS-CHES, 0.1% SDS, pH 8.5 using the interfacing droplet-based microdevice "Design 6". The electrophoresis was performed at the electric field strength of ~ 333 V/cm and detected at 1.0 cm.

Although the fluorescence intensity of BSA-NanoOrange droplets was acceptable, other proteins conjugated with NanoOrange (i.e. lysozyme and trypsin inhibitor) did not provide sufficiently high enough intensity. Their peaks could not be distinguished from the baseline due to the high background fluorescence intensity (data not shown). Additionally, the presence of precipitates in protein conjugates was also a problem when using NanoOrange dye as discussed in detail earlier. Consequently, NanoOrange was not further used for protein labeling for droplet-based separations in this work.

4.4 Conclusion

Three fluorescent dyes were investigated in this work for protein labeling. The initial criterion for the chosen fluorescent dyes was the compatibility of the excitation and emission wavelengths with the detection system used in this work (λ_{ex} = 470-490 nm and λ_{em} = a long pass 510 nm cut-on filter). FITC was the first dye used to label proteins as it

has already been extensively studied and widely applied. It was found that the labeling protocol of FITC was a multi-step, complicated and time-consuming procedure. The degree of labeling (F/P ratio) was also low therefore resulting in the low fluorescence intensity of the conjugate. In addition, it was difficult to entirely remove the unbound FITC from the conjugate. The unbound FITC remaining in the conjugate sample could react with water and TRIS in the running buffer yielding additional fluorescent products, which interfered with protein separations.

NHS-Fluorescein was the second dye that was studied since it was more reactive than FITC and the labeling protocol was simpler than that of FITC. However, similar problems were encountered with NHS-Fluorescein to those observed with FITC. These included low F/P ratios and interference of the fluorescent products from the reaction of the unbound dye with water and primary amines. Therefore, the fluorescent labeling of proteins, which does not involve the unbound dye removal, was employed instead.

NanoOrange was the third dye to be tested since it provided for more convenient and more rapid labeling than that of two aforementioned dyes. Moreover, dye removal was not required because the unbound NanoOrange does not fluoresce and does not react with water or TRIS in the running buffer. It was nonetheless found that proteins conjugated to NanoOrange easily precipitated and provided for low fluorescence intensity. Although the total fluorescence intensity increased in the presence of SDS in the running buffer, the increase in the intensity might be due to the binding between NanoOrange and SDS micelles instead of the protein conjugate.

Owing to the problems caused by these fluorescent dyes, commercial fluorescently labeled proteins were finally employed in this work despite the fact that they were expensive. The criteria for choosing the commercially fluorescent protein conjugates were that they had to be compatible with our detection system, provided for high fluorescence intensity and did not react with the components of the separation buffer. It was found that some purchased protein conjugates failed to fluoresce and could not be used. Therefore, only three commercially available fluorescently labeled proteins were used in this work. These were BSA-FITC (Sigma Aldrich), fluorescent molecular weight marker (20-200 kDa, Sigma Aldrich) and benchmark fluorescent protein standard (11-155

kDa, Thermo Fisher Scientific). Of these three purchased protein conjugates, the protein ladder from Sigma Aldrich was no longer available during this work despite the fact that it provided for higher intensity than the protein ladder from Thermo Fisher Scientific. Consequently, only BSA-FITC from Sigma Aldrich and the protein ladder from Thermo Fisher Scientific were used as benchmarks for the majority of microchip separations performed in this work.

4.5 References

1. Swinney, K. & Bornhop, D. J. Detection in capillary electrophoresis. *Electrophoresis* **21,** 1239–1250 (2000).

2. Swinney, K. & Bornhop, D. A Review of CE Detection Methodologies. *Crit. Rev. Anal. Chem.* **30,** 1–30 (2000).

3. Turner Designs. An introduction to fluorescence measurements. *Tech. Note* 1–15 at <http://www.turnerdesigns.com/t2/doc/appnotes/998-0050.pdf>

4. Bousse, L., Mouradian, S., Minalla, A., Yee, H., Williams, K. & Dubrow, R. Protein sizing on a microchip. *Anal. Chem.* **73,** 1207–12 (2001).

5. Griebel, A., Rund, S., Schönfeld, F., Dörner, W., Konrad, R. & Hardt, S. Integrated polymer chip for two-dimensional capillary gel electrophoresis. *Lab Chip* **4,** 18–23 (2004).

6. Wang, Y., Choi, M. H. & Han, J. Two-dimensional protein separation with advanced sample and buffer isolation using microfluidic valves. *Anal. Chem.* **76,** 4426–4431 (2004).

7. Shadpour, H. & Soper, S. a. Two-Dimensional Electrophoretic Separation of Proteins Using Poly (methyl methacrylate) Microchips. *Anal. Chem.* **78,** 3519–3527 (2006).

8. Osiri, J. K., Shadpour, H., Park, S., Snowden, B. C., Chen, Z. Y. & Soper, S. A. Generating high peak capacity 2-D maps of complex proteomes using PMMA microchip electrophoresis. *Electrophoresis* **29,** 4984–4992 (2008).

9. Fruetel, J. A., Renzi, R. F., VanderNoot, V. A., Stamps, J., Horn, B. A., West, J. A. A., Ferko, S., Crocker, R., Bailey, C. G., Arnold, D., Wiedenman, B., Choi, W. Y., Yee, D., Shokair, I., Hasselbrink, E., Paul, P., Rakestraw, D. & Padgen, D. Microchip separations of protein biotoxins using an integrated hand-held device. *Electrophoresis* **26,** 1144–1154 (2005).

10. Pizarro, S. A., Lane, P., Lane, T. W., Cruz, E., Haroldsen, B. & VanderNoot, V. A. Bacterial characterization using protein profiling in a microchip separations platform. *Electrophoresis* **28,** 4697–4704 (2007).

11. Fruetel, J. A., West, J. A. A., Debusschere, B. J., Hukari, K., Lane, T. W., Najm, H. N., Ortega, J., Renzi, R. F., Shokair, I. & VanderNoot, V. A. Identification of viruses using microfluidic protein profiling and bayesian classification. *Anal. Chem.* **80,** 9005–9012 (2008).

12. Renzi, R. F., Stamps, J., Horn, B. A., Ferko, S., VanderNoot, V. A., West, J. A. A., Crocker, R., Wiedenman, B., Yee, D. & Fruetel, J. A. Hand-held microanalytical instrument for chip-based electrophoretic separations of proteins. *Anal. Chem.* **77,** 435–41 (2005).

13. Yao, S., Anex, D. S., Caldwell, W. B., Arnold, D. W., Smith, K. B. & Schultz, P. G. SDS capillary gel electrophoresis of proteins in microfabricated channels. *Proc. Natl. Acad. Sci. U. S. A.* **96,** 5372–7 (1999).

14. Liu, J., Sun, X. & Lee, M. L. Adsorption-resistant acrylic copolymer for prototyping of microfluidic devices for proteins and peptides. *Anal. Chem.* **79,** 1926–1931 (2007).

15. Sun, X., Liu, J. & Lee, M. L. Surface modification of glycidyl-containing poly(methyl methacrylate) microchips using surface-initiated atom-transfer radical polymerization. *Anal. Chem.* **80,** 856–863 (2008).

16. Huang, H., Xu, F., Dai, Z. & Lin, B. On-line isotachophoretic preconcentration and gel electrophoretic separation of sodium dodecyl sulfate-proteins on a microchip. *Electrophoresis* **26,** 2254–2260 (2005).

17. Foote, R. S., Khandurina, J., Jacobson, S. C. & Ramsey, J. M. Preconcentration of proteins on microfluidic devices using porous silica membranes. *Anal. Chem.* **77,** 57–63 (2005).

18. Herr, A. E., Molho, J. I., Drouvalakis, K. A., Mikkelsen, J. C., Utz, P. J., Santiago, J. G. & Kenny, T. W. On-Chip Coupling of Isoelectric Focusing and Free Solution Electrophoresis for Multidimensional Separations. *Electrophoresis* **75,** 1180–1187 (2003).

19. Cong, Y., Zhang, L., Tao, D., Liang, Y., Zhang, W. & Zhang, Y. Miniaturized two-dimensional capillary electrophoresis on a microchip for analysis of the tryptic digest of proteins. *J. Sep. Sci.* **31,** 588–594 (2008).

20. Liu, J., Chen, C.-F., Yang, S., Chang, C.-C. & Devoe, D. L. Mixed-mode electrokinetic and chromatographic peptide separations in a microvalve-integrated polymer chip. *Lab Chip* **10,** 2122–2129 (2010).

21. Yang, S., Liu, J., Lee, C. S. & Devoe, D. L. Microfluidic 2-D PAGE using multifunctional in situ polyacrylamide gels and discontinuous buffers. *Lab Chip* **9,** 592–599 (2009).

22. Vieillard, J., Mazurczyk, R., Morin, C., Hannes, B., Chevolot, Y., Desbe`ne, P. L. & Krawczyk, S. Application of microfluidic chip with integrated optics for electrophoretic separations of proteins. *J. Chromatogr. B Anal. Technol. Biomed. Life Sci.* **845,** 218–225 (2007).

23. Okada, H., Kaji, N., Tokeshi, M. & Baba, Y. Rinse and evaporation coating of poly(methyl methacrylate) microchip for separation of sodium dodecyl sulfate-protein complex. *J. Chromatogr. A* **1192,** 289–293 (2008).

24. Liu, Y., Foote, R. S., Jacobson, S. C., Ramsey, R. S. & Ramsey, J. M. Electrophoretic separation of proteins on a microchip with noncovalent, postcolumn labeling. *Anal. Chem.* **72,** 4608–13 (2000).

25. Jin, L. J., Giordano, B. C. & Landers, J. P. Dynamic labeling during capillary or microchip electrophoresis for laser-induced fluorescence detection of protein-SDS complexes without pre- or postcolumn labeling. *Anal. Chem.* **73,** 4994–4999 (2001).

26. Jacobson, S. C., Koutny, L. B., Hergenroder, R., Moore, A. W. & Ramsey, J. M. Microchip Capillary Electrophoresis with an Integrated Postcolumn Reactor. *Anal. Chem.* **66,** 3472–3476 (1994).

27. Tabuchi, M., Kuramitsu, Y., Nakamura, K. & Baba, Y. A 1 5 -s Prot e in Se pa ra t ion Em ploying H ydrodyna m ic Forc e on a M ic roc hip. **75,** 5165–5171 (2003).

28. Li, Y., Buch, J. S., Rosenberger, F., Devoe, D. L. & Lee, C. S. Integration of isoelectric focusing with parallel sodium dodecyl sulfate gel electrophoresis for multidimensional protein separations in a plastic microfluidic network. **76,** 742–748 (2004).

29. Ramsey, J. D., Jacobson, S. C., Culbertson, C. T. & Ramsey, J. M. High-Efficiency, Two-Dimensional Separations of Protein Digests on Microfluidic Devices. *Anal. Chem.* **75,** 3758–3764 (2003).

30. Rocklin, R. D., Ramsey, R. S. & Ramsey, J. M. A microfabricated fluidic device for performing two-dimensional liquid-phase separations. *Anal. Chem.* **72,** 5244–9 (2000).

31. Gottschlich, N., Jacobson, S. C., Culbertson, C. T. & Ramsey, J. M. Two-dimensional electrochromatography/capillary electrophoresis on a microchip. *Anal. Chem.* **73,** 2669–74 (2001).

32. Colyer, C. L., Mangru, S. D. & Harrison, D. J. Microchip-based capillary electrophoresis of human serum proteins. *J. Chromatogr. A* **781,** 271–276 (1997).

33. Hemmiliä, I. Fluoroimmunoassays and Immunofluoreometric Assays. *Clin. Chem.* **31,** 359–370 (1985).

34. Goding, J. W. Conjugation of Antibodys with Fluorochromes: Modification of the standard methods. *J. Immunol. Methods* **13,** 215–226 (1976).

35. The, T. H. & Feltkamp, T. E. W. Conjugation of fluorescein isothiocyanate to antibodies I. Experiments on the conditions of conjugation. *Immunology* **18,** 865–873 (1970).

36. The, T. H. & Feltkamp, T. E. W. Conjugation of fluorescein isothiocyanate to antibodies II. A reproducitble method. *Immunology* **18,** 875–881 (1970).

37. Silberblatt, S., Felder, R. A. & Mifflin, T. E. Optimizing reaction conditions of the NanoOrange protein quantitation method for use with microplate-based automation. *J. Lab. Autom.* **6,** 83 (2001).

38. Harvey, M. D., Bablekis, V., Banks, P. R. & Skinner, C. D. Utilization of the non-covalent fluorescent dye, NanoOrange, as a potential clinical diagnostic tool. Nanomolar human serum albumin quantitation. *J. Chromatogr. B. Biomed. Sci. Appl.* **754,** 345–56 (2001).

39. Jones, L. J., Haugland, R. P., Singer, V. L. & Probes, M. Development and Characterization of the NanoOrange ® Protein Quantitation Assay : A Fluorescence-Based Assay of Proteins in Solution. *Biotechniques* **34,** 850–861 (2003).

40. Sigma. Fluorescein isothiocyanate product information. 2–4

41. Thermo Scientific. NHS-Fluorescein. *Instructions*

42. Thermo Scientific. Calculate dye:protein (F/P) molar ratios. *Tech Tip #31* (2011).

43. Banks, P. R. & Paquette, D. M. Comparison of three common amine reactive fluorescent probes used for conjugation to biomolecules by capillary zone electrophoresis. *Bioconjug. Chem.* **6,** 447–58 (1995).

44. Imhof, A., Megens, M., Engelberts, J. J., De Lang, D. T. N., Sprik, R. & Vos, W. L. Spectroscopy of Fluorescein (FITC) Dyed Colloidal Silica Spheres. *J. Phys. Chem. B* **103,** 1408–1415 (1999).

45. Ma, L. Y., Wang, H. Y., Xie, H. & Xu, L. X. A long lifetime chemical sensor: study on fluorescence property of fluorescein isothiocyanate and preparation of pH chemical sensor. *Spectrochim. Acta. A. Mol. Biomol. Spectrosc.* **60,** 1865–72 (2004).

46. Sumitomo, K., Mayumi, K., Minamikawa, H., Masuda, M., Asahi, T., Shimizu, T., Ito, K. & Yamaguchi, Y. Buffer to suppress sodium dodecyl sulfate adsorption to

polyethylene oxide for protein separation on capillary polymer electrophoresis. *Electrophoresis* **32,** 448-454 (2011).

Chapter V

Evaluation of interfacing droplet-based microdevices for protein separation

5.1 Introduction

The importance of multidimensional protein separations in modern day biology has been discussed in detail in **Section 1.8**, but at a basic level multidimensional separations provide for high peak capacity and high resolution separations of complex mixtures of proteins and other biomolecules[1]. Critical to the success of any multidimensional separation methodology, is the efficient interfacing (or joining) of two or more distinct separation techniques so that separated analytes from one dimension can be transferred to the next.

The coupling between capillary electrophoresis and/or column chromatography (e.g. CE-CE, LC-LC and LC-CE) can be achieved by employing several types of interfaces (such as dialysis interfaces[2], porous junction interfaces[3,4], tee-union interfaces[5], flow gating interfaces[6], microreactor interfaces[7], nicked-sleeve interfaces[8], hydrodynamic interfaces[9] and six-port valves[10]) to connect the separation dimensions. Another format that has been increasingly used for 2D separations involves the use of planar chip-based microfluidic devices for performing multidimensional electrophoretic separations. In previous reports, dimensions were most usually connected through the use of intersecting channels[11–19], PDMS membranes[20], staggered configurations of two-dimensional separation channels[21], microvalves[22,23], gel-based pseudo-valves[24,25,26,27], narrow channels[28] and small open channels[29] connecting between two-dimensional separation channels as an interface (described in detail in **Section 1.8**). Although these formats provide for improved automated and rapid separations, significant dispersion of analytes at such interfaces has proved to be highly problematic. In addition, when CE is performed in either a capillary or chip-based format injection, bias is commonly encountered. This describes the situation when analytes are injected electrokinetically, with higher mobility analytes moving faster and being injected in higher amounts than lower mobility analytes within the same sample. This phenomenon significantly hampers the ability to perform reliable and quantitative analyses[30]. On the other hand, hydrodynamic injection provides for bias-free introduction of analyte molecules, but is less well-suited to the delivery of precise and sub-nL sample volumes to the separation column. Accordingly, we proposed a novel approach for transferring separated analytes from a first to a second dimension by

compartmentalizing the separated analyte bands into droplets contained within a continuous carrier phase[31–33]. Droplet contents can subsequently be released and injected into a separation channel for further analysis. By adopting this method, band dispersion at the interface is minimized and the injected amount of analyte is better controlled.

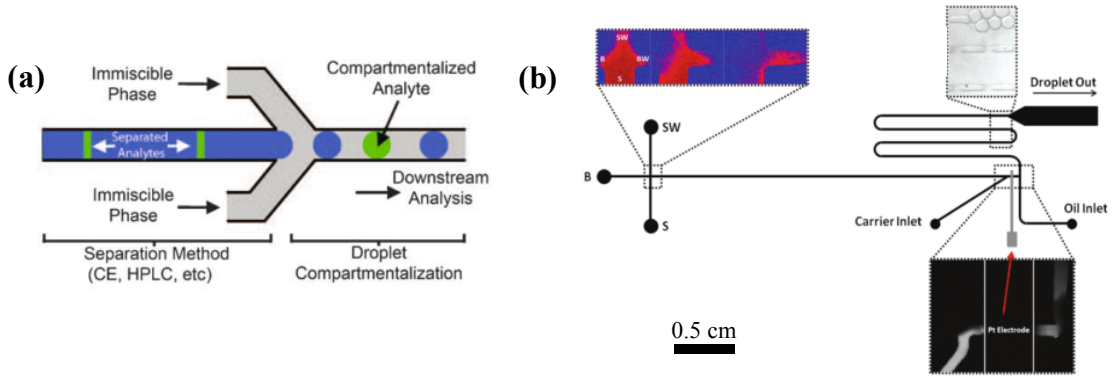

Figure 5.1: Compartmentalization of analyte bands into droplets (a) A schematic showing separated analyte bands from a first dimension being compartmentalized into droplets that are transferred downstream for further analysis; (b) A mixture of fluorescent dyes was injected at the cross-channel part of a microdevice shown in the inset (color images). The mixture was separated using CGE and the separated bands moved along the straight channel to a T-junction where droplets could be generated. Schematics are reproduced from reference 34 and 35.

Previously, *Edgar* and co-workers[34] reported the compartmentalization of separated amino acids containing D/L glutamate into droplets for further separation in a second dimension. In his work, the amino acid mixture was first separated by CZE, with the separated bands being encapsulated into droplets at a modified flow-focusing geometry where droplet generation was induced by EOF (**Figure 5.1a**). The generated droplets were collected at an exit reservoir placed downstream and the droplet contents were then injected into a glass capillary for separation by MEKC. Recently, the compartmentalization of separated analytes into droplet format was reported by *Draper* and co-workers[35], who separated a mixture of two fluorescent dyes (5-Carboxyfluorescein and Fluorescein) by CGE. Such an approach is potentially advantageous, since the gel buffer minimizes EOF and longitudinal diffusion of analytes. The authors demonstrated

that separated analyte bands could be maneuvered towards a T-junction where droplets of eluted bands were formed (**Figure 5.1b**). Both studies show successful compartmentalization of separated analyte bands from a first separation dimension into droplets, and that the generated droplets can be transferred to another separation dimension or another analytical component.

Many research groups have investigated the transfer of droplets to a second separation dimension. Typically, droplets containing eluted analyte bands from a first separation dimension are aqueous and dispersed within an immiscible oil phase. In order to transfer droplet contents to a buffer solution in a second dimension, the oil surrounding each droplet must be depleted and removed so that it will not interfere with the separation. To this end, *Edgar* and co-workers[36] presented the fusion of aqueous droplets containing a mixture of amino acids with an immiscible boundary to release droplet contents into a separation channel. A PDMS microdevice consisting of a droplet generation part and a separation part was fabricated for this purpose (**Figure 5.2a**). The surface of the separation channel was then selectively patterned to achieve a hydrophilic surface, while the surface of the droplet generation region remained hydrophobic. Droplets of labeled amino acids could be generated at a T-junction geometry, with droplets then moving towards the separation channel where they fused with the immiscible boundary to release droplet contents into the hydrophilic CZE separation channel. Significantly, the hydrophilic surface of the separation channel prevented oil from entering and wetting the surface and enhanced EOF, which allowed the efficient separation of amino acids. However, the selective patterning of the microdevice surface is complex, inconvenient and time-consuming.

Kennedy and co-workers[37] reported on the use of a K-shaped channel for sampling analyte plugs segmented within an immiscible oil stream into an electrophoresis channel. In this study, a T-junction (where sample plugs were generated) and a serpentine channel were rendered hydrophobic, whereas, a K-shaped interface and an electrophoresis channel were hydrophilic. At the junction between the K-shaped interface and the segmented flow channel (**Figure 5.2b**) where an aqueous buffer met an oil stream, a virtual wall (water/oil interface) is created. Briefly, a generated sample plug (a mixture of amino acids) flows along the serpentine channel until it reaches the K-shaped interface.

The sample plug then makes contact with the virtual wall and the aqueous sample in the plug merges with the aqueous buffer solution in the interface. A small amount of sample is then electrokinetically injected into the electrophoresis channel for further separation. In this case, the virtual wall prevents the oil stream in the segmented flow channel from entering the electrophoresis channel. In addition, it also prevents the aqueous buffer from flowing into the segmented flow channel.

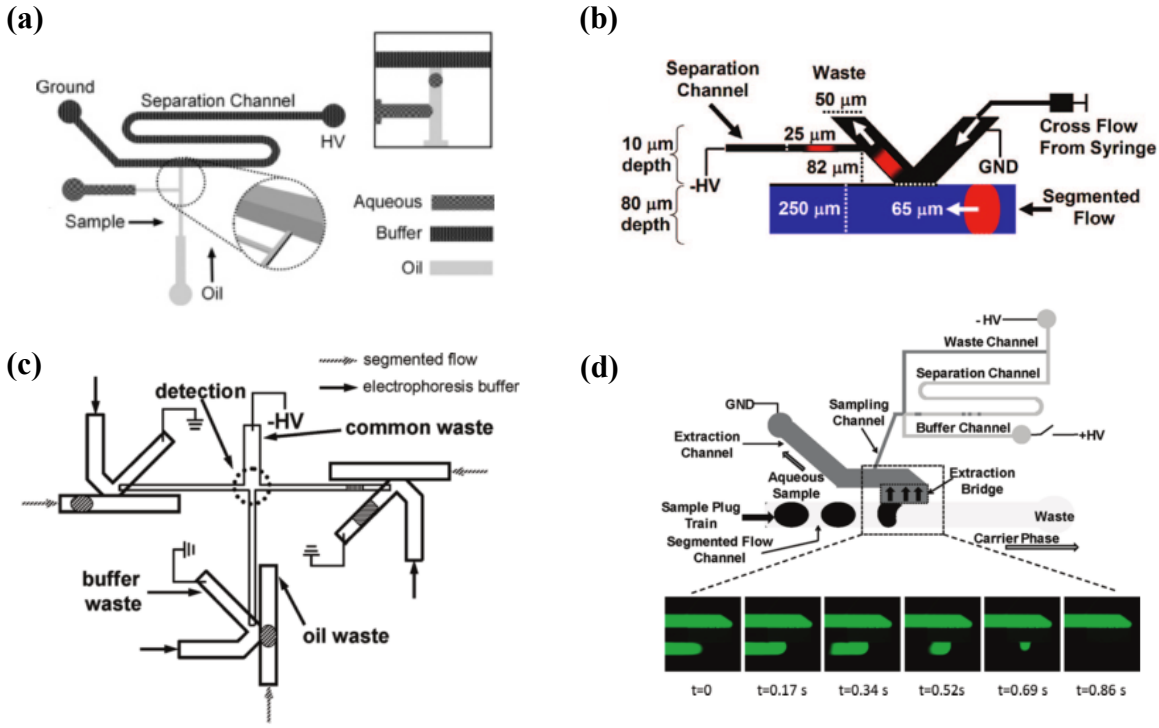

Figure 5.2: Droplet-based interfacing microdevices employing surface modification. (a) A droplet generated at a hydrophobic T-junction channel moves towards a hydrophilic separation channel where it fuses with an immiscible boundary allowing the droplet contents to be injected into the separation channel; (b) A schematic showing a sample plug moving along a segmented flow channel prior to merging with a virtual wall at a K-shaped interface. Here, only small amount of the sample is injected into the separation channel; (c) A parallel electrophoretic analysis on a microdevice employing K-shaped interfaces for the transfer of sample plugs; (d) A schematic and images showing the transfer of sample plugs obtained from a microdialysis probe (not shown) into a separation channel using a hydrophilic extraction bridge. Schematics and images reproduced from reference 36, 37, 38 and 39, respectively.

Another study by *Kennedy* and co-workers[38] employs K-shaped interfaces for parallel electrophoretic separations. A glass microdevice consisting of three sets of a K-shaped interface and an electrophoretic separation system is depicted in **Figure 5.2c**. Each set was composed of a segmented flow channel that was selectively made hydrophobic, a K-shaped interface and an electrophoresis channel containing an aqueous buffer solution. The operation of the system was similar to that described in the previous study[37], with the added advantage that it provided for high-throughput analysis of segmented samples in a parallel manner.

A final study by *Kennedy* and co-workers[39] involved the use of a hydrophilic extraction bridge as an interface to extract microdialysis samples from segmented plugs into a separation channel. A dual-chip system consisting of a PDMS microdevice integrated with a microdialysis probe for the generation of sample plugs and a glass microdevice with selectively modified surfaces to perform electrophoresis was used in this work. Sample plugs containing dialysate and other reagents were generated in the PDMS microdevice and were transferred to the glass microdevice via a high purity perfluoroalkoxy plus (HPFA+) tube. When the sample plug contacted the hydrophilic extraction bridge, the aqueous sample was transferred into the extraction channel with some delivered into the electrophoresis channel for further separation as depicted in **Figure 5.2d**.

Although all interfacing microdevices developed by *Kennedy* and co-workers were successful in their aims, they suffered from two disadvantages. First, they all required selective modification of channel walls, and second they wasted a large proportion of the analytical sample since only small amount is sampled into the electrophoresis channel, whilst the rest flows to waste.

Kelly and co-workers[40] proposed a droplet-based interfacing microdevice coupled to ESI-MS for the separation and analysis of peptides (**Figure 5.3a**). Briefly, analyte droplets were generated and moved downstream to an interface where an array of 3 μm wide apertures formed by cylindrical posts were located. Several apertures at the interface provided for an imbalance of pressure that prevented appreciable mixing of oil and aqueous streams. Therefore, aqueous droplet contents could merge with the aqueous

stream and pass through an ESI emitter placed downstream. The major difficulty associated with this technique was the requirement for precise pressure control to release droplet contents into the aqueous stream.

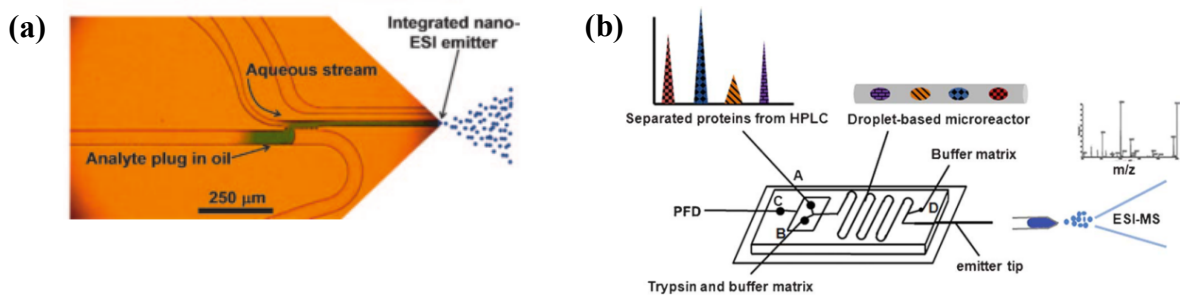

Figure 5.3: Droplet-based interfacing microdevices coupled to mass spectrometry analysis (a) A micrograph showing an analyte plug being transferred into an aqueous stream employing an array of apertures as an interface for pressure control; (b) An integrated platform for protein analysis consisting of a droplet generation part, which compartmentalizes eluted bands from HPLC, and an electrospray ionization emitter for mass spectrometry analysis of proteins in droplets. Schematics and image reproduced from reference 40 and 41, respectively.

Ji and co-workers[41] demonstrated another droplet-based microdevice coupled to ESI-MS. In this work, separated proteins from HPLC were encapsulated in droplets along with trypsin to allow for on-line digestion prior to delivery to the ESI emitter (**Figure 5.3b**). When ESI occurs (ionization voltage = 2.0 kV), the oil phase forming droplets at the emitter tip moved along the outer surface of the emitter away from the tip, possibly by the effects of gravity and interfacial tension[41,42]. However, the drawback of this technique is that oil interferes with MS analysis when ionization voltages above 2.0 kV are used.

Niu and co-workers[31] presented an extremely interesting approach for interfacing microdevices. In this work, separated bands of a peptide mixture from an LC separation were collected in the form of droplets prior to transferal to a second CE separation. The droplet contents were injected into a separation channel by employing a pillar-structured microdevice with a pressure source to eliminate the oil surrounding droplets, as shown in **Figure 5.4a.** This technique provided for several advantages over the immiscible

boundary technique[36], the use of K-shaped interfaces[37, 38] and the use of an extraction bridge[39] in that there is no need to selectively modify channel walls. However, oil depletion occurs in an active manner (since a pressure source is used) making it difficult to reduce the size of the entire system.

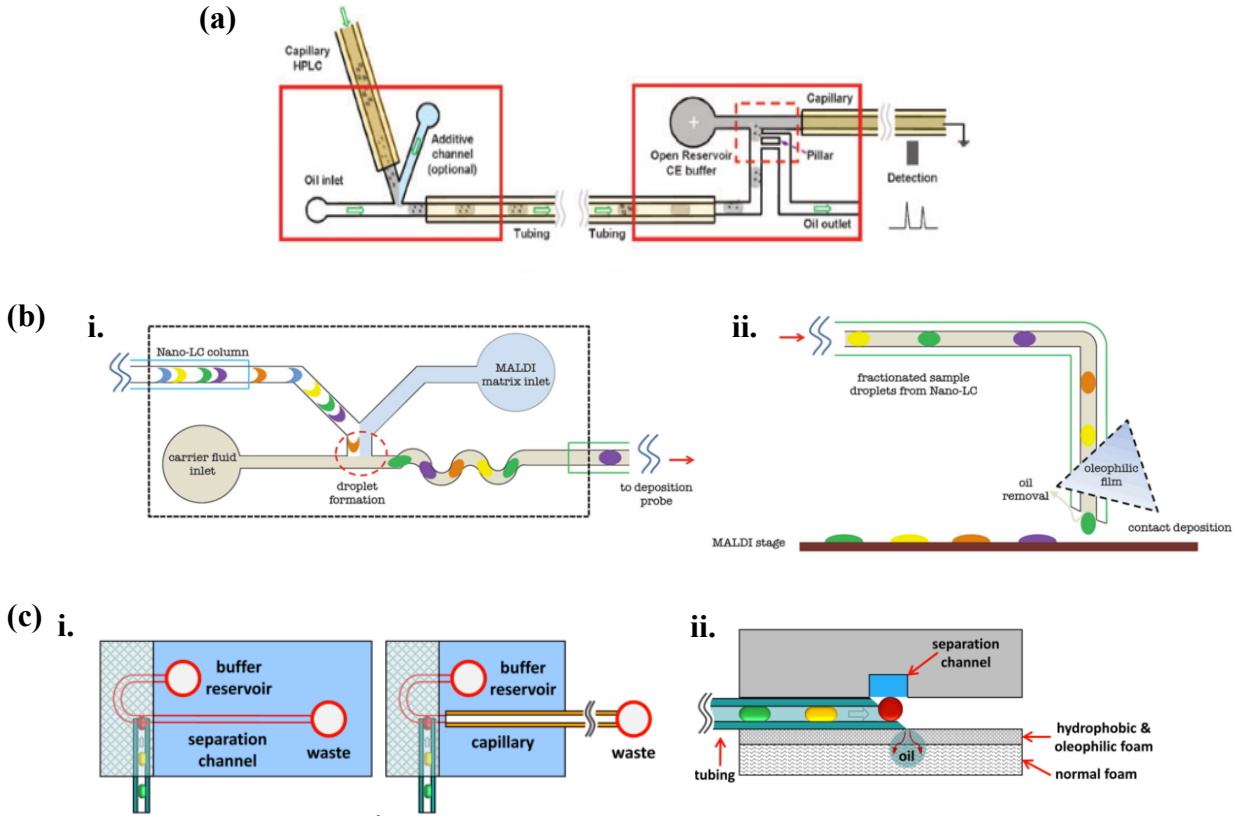

Figure 5.4: Droplet-based interfacing microdevices developed by *Niu* and co-workers (a) A schematic showing the compartmentalization of eluted bands from the first separation dimension into droplets (left) and droplet injection into the second dimension employing a pillar-structured microdevice to eliminate oil surrounding droplets (right); (b) Schematics of the Nano LC-MALDI-MS droplet-based interfacing microdevice (i) Separated analyte bands from Nano-LC are compartmentalized into droplets, (ii) Droplet contents are collected at the tip of the probe prior to the deposition onto the MALDI stage, whilst oil is absorbed into an oleophilic film; (c) Schematics illustrating the interfacing microdevices utilizing an oleophilic membrane as an oil depletion unit (i) An entire microdevice made of PDMS (left) and a PDMS microdevice coupled to a glass capillary (right), (ii) A schematic depicting the injection of a droplet through an open channel, while oil is depleted via the oleophilic membrane. Schematics reproduced from reference 31, 32 and 33, respectively.

The same group later introduced the use of an oleophilic foam to eliminate the oil phase during droplet injection[32,33]. **Figure 5.4bi** shows the encapsulation of Nano LC-separated proteins into droplets that were then delivered for further analysis by matrix-assisted laser desorption/ionization (MALDI) mass spectrometry. The oil phase was eliminated by absorption into an oleophilic foam, while droplet contents were collected at the tip of the tube prior to deposition onto a MALDI plate as depicted in **Figure 5.4bii**[32]. The oleophilic foam was also employed for droplet-based separation of proteins[33]. Herein, two designs of the interfacing microdevices were proposed for the separation of proteins using CZE and CGE. **Figure 5.4ci** shows an entire PDMS microdevice (left) used for CZE separations and a PDMS microdevice coupled to a glass capillary (right) used for CGE separations. Droplet injection in both designs occurs at the open channel of the PDMS part where oil is absorbed into an oleophilic foam, while droplet contents are injected into a separation channel as shown in **Figure 5.4cii**. Although this technique provided for passive oil depletion, the difficulty in the setup of the experiment was still a problem that needed to be addressed.

Although much effort has focused on the development of interfacing microdevices for droplet-based separation of amino acids, peptides and proteins; microdevices reported in the literature still suffer from many disadvantages such as the need for selective surface modification, unacceptable sample wastage, the need for precise pressure control, active oil depletion and difficulty in experimental setup. The development of an interfacing microdevice for droplet-based analysis that provides for ease of fabrication, automation of oil depletion in a passive manner and high-throughput separation of proteins is therefore required. The evaluation of six novel interfacing microdevices are discussed and contrasted in detail in this chapter, with a view to their application in droplet-based separation of proteins.

5.2 Droplet generation

5.2.1 Techniques for droplet generation

5.2.1.1 Droplet generation using a T-junction microdevice

A T-junction PDMS microdevice (100 μm wide and 100 μm deep) was fabricated as described in **Section 2.1.1**. FC-40 oil filled up a 3-ml plastic syringe connected to a polyethylene tube (I.D. 1.09 mm and O.D. 2.98 mm purchased from Smiths Medical, Kent, UK), while an aqueous sample filled up a 1-ml plastic syringe connected to the other polyethylene tube. Both tubes were placed into reservoirs on the microdevice and the infused flow rates were set at 12 and 1.8 μl/min for the oil and the sample, respectively. The generated droplets were collected in a 100 μm I.D. PTFE tube that was inserted into an open enlarged channel of the microdevice until they were used.

5.2.1.2 Droplet generation using a robotic droplet generator

The experimental setup and the operation of droplet generation using a robotic droplet generator were described in detail in **Section 2.3**.

5.2.2 Results and Discussion

T-junction microdevices were employed to generate droplets used to evaluate developed interfacing microdevices, Design 1 and Design 2, while the robotic droplet generator was employed to generate droplets used in Design 3-Design 6. It was found from these experiments that appropriate droplet sizes were required to achieve successful single droplet injection and frequency of droplet generation (which in turn defines the distance between each droplet) needed to be optimized to ensure successful separation without cross contamination between adjacent droplets.

In the case of T-junction microdevices, it was difficult to achieve the required droplet size and the required frequency of droplet generation simultaneously by synchronous adjustment of both oil and aqueous liquid flow rates. The other problem with T-junction

microdevices was the difficulty in handling or manipulating the entire system when low sample volume (tens microliters) was used.

By utilizing the robotic droplet generator to generate droplets, those two problems found in T-junction microdevices were solved. By adjusting a refilled flow rate, the frequency of droplet generation and the residence times of the tube in the oil and in the sample phase, droplet size and distance between each droplet were varied to achieve the requirement. Normally, the droplet size increases with the increase of the refilled flow rate and/or the residence time of the tube in each phase. Meanwhile, the distance between each droplet increases with the increasing of the refilled flow rate and/or with the decreasing of the droplet generation frequency and the residence time of the tube in each phase. In addition, the sample volume used with the robotic droplet generator could be very low (i.e. down to ~20 μl)[43]. Due to the limitation of sample volume (protein ladder) used in this work and the need to control the size and the distance between each droplet, the robotic droplet generator was therefore used in most of our experiments.

5.3 Evaluation of interfacing droplet-based microfluidic designs

5.3.1 Design 1

5.3.1.1 Schematics of designs and fabrication

The initial interface design is illustrated in **Figure 5.5a**, with the top and the bottom layers being shown in **Figure 5.6ai** and **Figure 5.6aii**, respectively. This embodiment of the interfacing microdevice was designed for use with single-channel or parallel-channel separations, containing two identical separation systems (located on the upper half and the lower half of the blue dashed box in **Figure 5.5b** and also shown in **Figure 5.6b**). Each droplet-based separation system consists of a separation channel (100 μm wide and 100 μm deep) connected to a buffer reservoir at one end and a buffer waste reservoir at the other end, an orthogonal side channel (droplet delivery channel) with an enlarged end for the insertion of a droplet delivery tube and two oil depletion units containing a pillar in each unit. It should be noted that open spaces are structured in the bottom layer

(**Figure 5.6aii**) below at the oil depletion units to allow oil to absorb into a PTFE membrane underneath the microdevice.

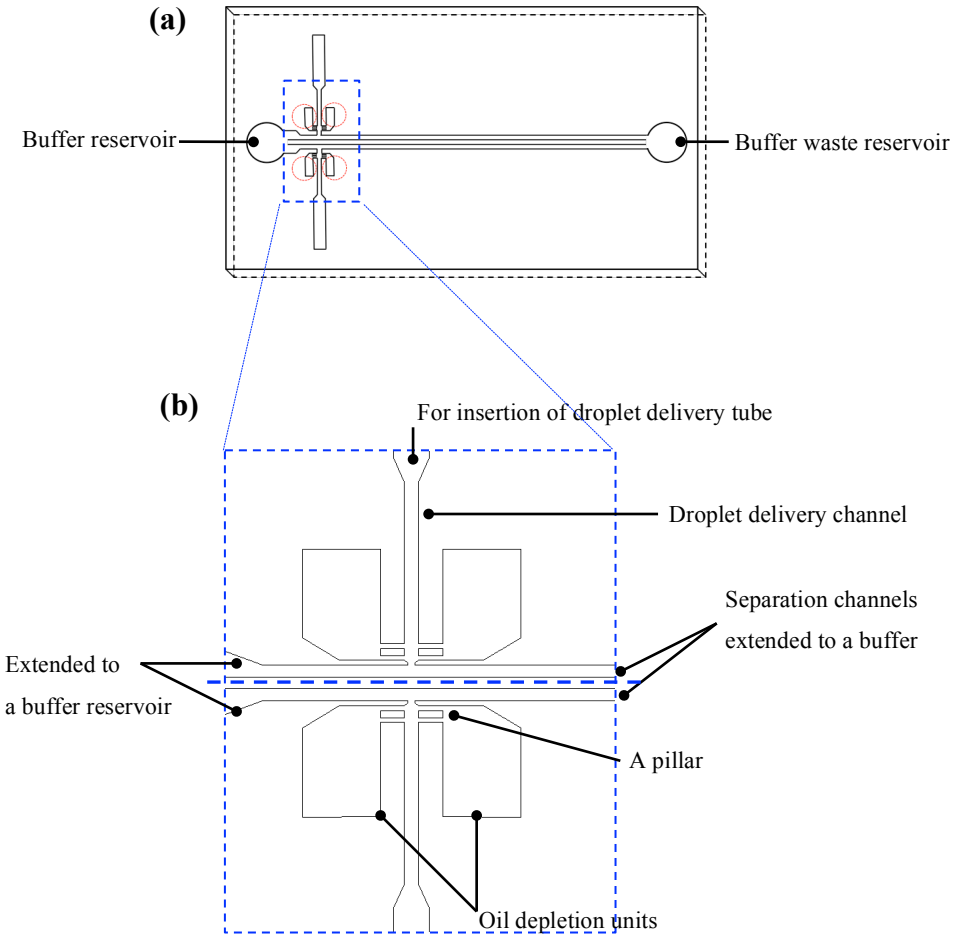

Figure 5.5: Schematics and an image illustrating the structure of the initial interface design used to perform single or multiple separations (a) A schematic of the entire microdevice consisting of a top layer (black solid lines) and a bottom layer (black and red dashed lines) of PDMS. The top PDMS layer contains two parallel separation channels with reservoirs at each end (the left reservoir is the "buffer reservoir" and the right reservoir is the "buffer waste reservoir"), two channels with enlarged ends to allow insertion of the droplet delivery tubes and four oil depletion units (with a pillar in each unit). The bottom PDMS layer consists of four open circles at the same positions as the oil depletion units in the top layer; (b) An enlargement of the oil depletion units.

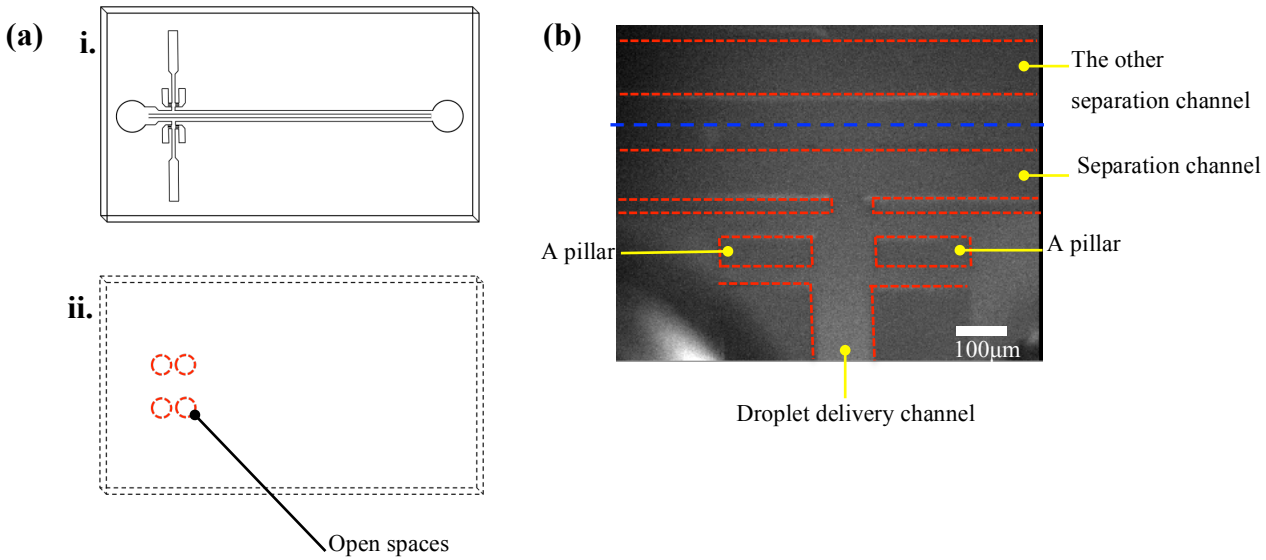

Figure 5.6: (a) A schematic showing the separated top and bottom PDMS layers: (i) Top layer, (ii) Bottom layer; (b) An image showing a separation channel connected to two sides of pillar-structured oil depletion units and a channel for delivering droplets.

The entire microdevice was made of PDMS and fabricated as described in detail in **Section 2.1.1**. The top and the bottom PDMS layers were 3 mm and 300-500 mm deep, respectively. The reduced thickness of the bottom layer ensured that the oil depletion units were as close to the PTFE membrane as possible, thus allowing efficient oil removal. Prior to assembly of the PDMS layers, biopsy punches (1 and 4 mm in diameter) were used to create four open spaces in the bottom layer and to create two reservoirs in the top layer. The two PDMS layers were then bonded under a microscope after oxygen plasma treatment to ensure that all open spaces were precisely aligned underneath the oil depletion units.

5.3.1.2 Droplet injection

The microdevice was filled with 3% PDMA in 8.5 mM borate buffer through the buffer reservoir. Any buffer remaining in the oil depletion units was removed using a non-fibrous tissue. For single-channel separations, a small part of one side channel was cut open for the insertion of a droplet delivery tube (100 μm I.D. PTFE tube, Cole Parmer) as

shown in **Figure 5.7**. The microdevice along with the inserted tube was then placed onto the PTFE membrane. While an electric field was applied across the separation channel (with the cathode being placed in the buffer reservoir and the anode in the buffer waste reservoir), droplets were delivered from the droplet delivery tube to the microdevice using a precision syringe pump (PHD 2000, Harvard Apparatus). Droplets were then injected and separations performed inside the separation channel.

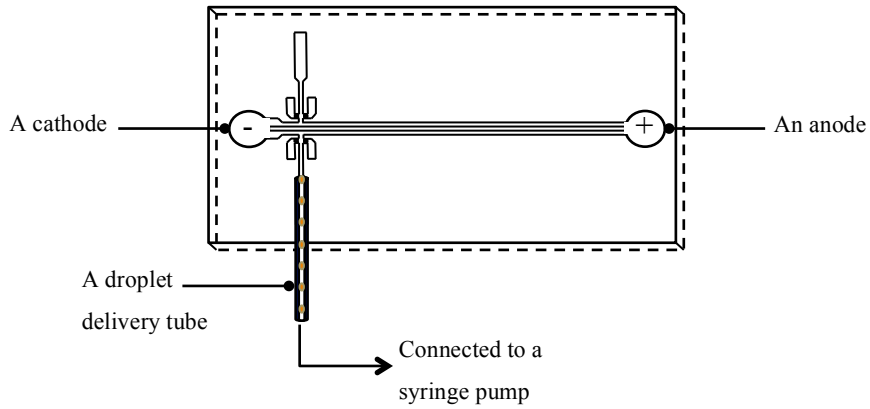

Figure 5.7: A top view schematic of the microdevice during droplet injection experiment. One end of the droplet delivery tube is inserted into a side channel of the microdevice, while the other end is connected to the syringe pump to drive droplets towards a separation channel. An electric field is applied across the separation channel by placing a cathode in the buffer reservoir and an anode in the buffer waste reservoir.

5.3.1.3 Results and Discussion

The first microfluidic interface was inspired by the previous work of *Niu et al*[31] as discussed in **Section 5.1**. Briefly, a pillar-structured channel together with an oil aspiration system was employed to eliminate oil that surrounds droplets prior to their injection into a separation channel. This structure should provide for a number of key advantages. For example, oil depletion could be achieved without surface modification of the channel walls and oil contamination in the separation channel could be drastically reduced. However, the need for two pumps to deliver droplets and to aspirate the oil makes the size of the entire system unacceptably large for many applications. Ideally, complete oil depletion should be achieved in an entirely passive manner (i.e. without the

need for a pump to aspirate the continuous oil phase). Accordingly, the droplet interface described by *Niu*[31] was redesigned as depicted in **Figure 5.5a** and is described in detail in **Section 5.3.1.1**.

There are three key features of this new design. First, although the pillar-structures are similar to those in *Niu*'s original design[31], instead of using a one-sided oil removal channel, two oil-removal channels containing pillars are used to accelerate the oil removal process. Second, passive oil depletion is achieved by placing a thin PTFE hydrophobic/oleophilic membrane underneath the microdevice, so that oil is absorbed into the foam. Third, the new design allows either single-channel or parallel-channel separations to be performed.

The basic principle behind droplet injection using this new design makes use of a pre-formed droplet being delivered by a pressure source towards a separation channel. Prior to entering the separation channel, the droplet is trapped between the pillars on two sides and the oil surrounding the droplet is filtered out through small channels between the pillars and absorbed into the PTFE membrane. In principle, this construct should allow droplet contents to be injected into the separation channel without appreciable oil contamination.

Unfortunately, it was found that this interfacing droplet-based design was plagued by a number of operational issues. First, the bottom PDMS layer needed to be cut to the same size and located at the same position as the oil depletion units on the top PDMS layer. Owing to the fact that the size of each oil depletion unit was small (790 × 650 μm) and the bottom layer thin (~ 500 μm), it was difficult to ensure precise alignment. A biopsy puncher (with an inner diameter of 1 mm) was used to create the open spaces instead of using a blade. Although the size of the open spaces was larger than that of the oil depletion units, the use of the biopsy puncher provided for better localization of the open spaces. The design also required precise alignment between the two PDMS slabs so that the open spaces on the bottom layer were placed exactly underneath the oil depletion units. Although this process was performed under a microscope, it was still difficult to align all the oil depletion units at the same time.

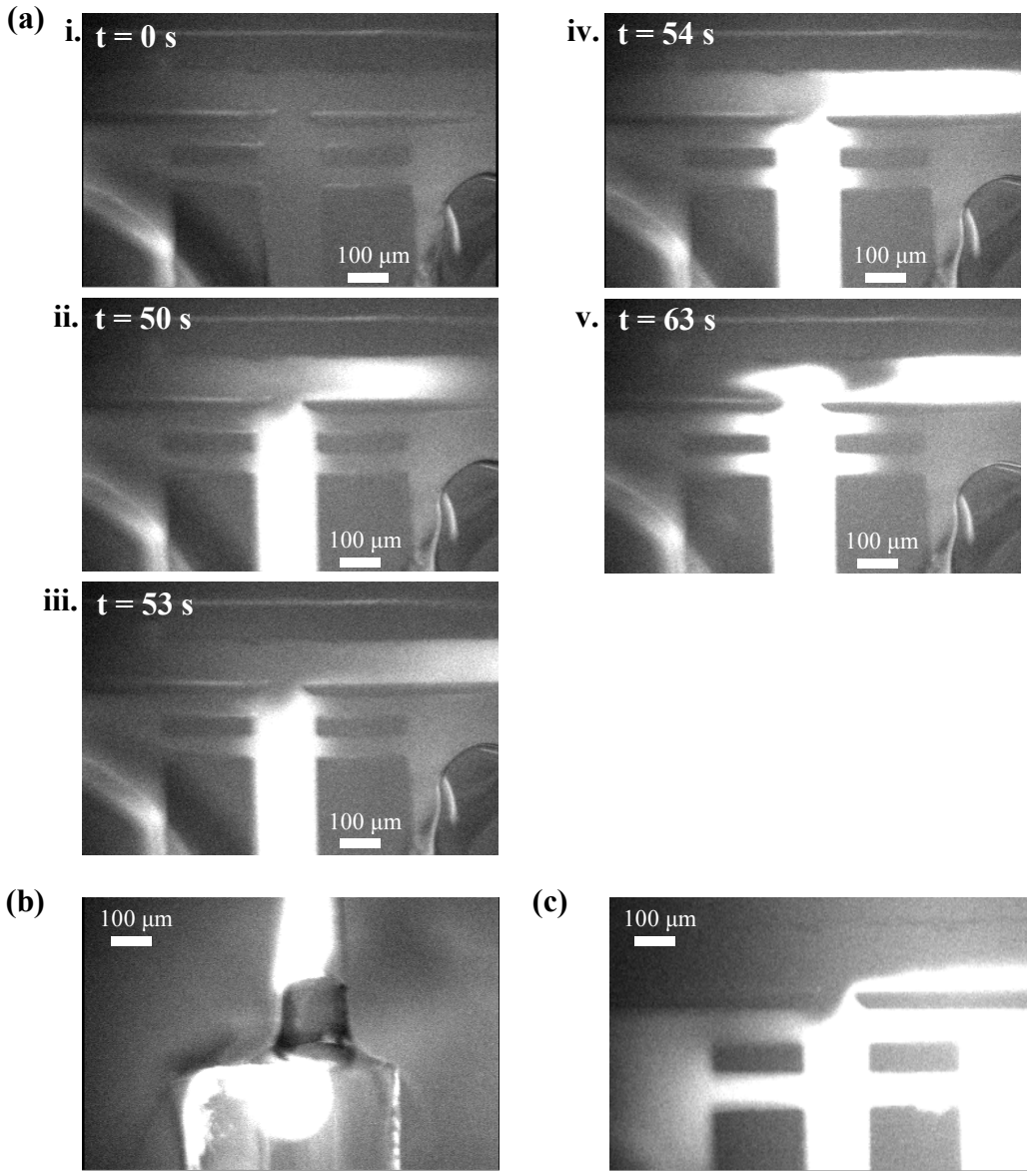

Figure 5.8: Illustration of the droplet injection process. (a) The injection of a mixture of a fluorescent dye and a food dye. (i) The microdevice prior to injection at t = 0 s, (ii) The first sample plug is injected into the separation channel (t = 50 s) and moves towards the anode, (iii) The first sample plug stops being injected at t = 53 s, (iv) The next sample plug is injected at t = 54 s (v) A sample plug is injected at t = 63 s, whilst the previous one is still being injected. Buffer solution leakage can be observed at the right oil depletion unit in each image; (b) A dead volume exists at the connection between the droplet delivery tube and the droplet delivery channel. Oil surrounding the droplets is thus accumulated and causes droplets merge prior to injection; (c) Diffusion of the sample into the oil depletion units. Experiments were performed at an infusing flow rate of 0.12 µl/min and an electric field strength of 85.7 V/cm.

Prior to droplet injection, the microdevice was filled with 3% PDMA buffer solution, which was one of the tested laboratory-made buffers described in **Section 3.3.4.1**, through the buffer reservoir. Two problems can potentially occur at this stage. First, the microdevice is easily broken since the thin bottom layer cannot withstand the high pressures that often occur when filling the microdevice with highly viscous fluids. Conversely, low viscosity buffer may leak out through the open spaces of the oil depletion units as exemplified in **Figure 5.8a**. This occurs since the surface at the edge of the open spaces is hydrophilic due to the plasma treatment prior to device bonding. After filling up the microdevice with buffer solution, the system was set up for droplet injection as described in **Section 5.3.1.2**.

An electric field strength of 85.7 V/cm was applied across the separation channel. Importantly, the associated current was found to be stable over the timescale of the experiment. Droplets were delivered to the separation channel at the flow rate of 0.12 µl/min, with the first injection in **Figure 5.8aii** commencing at t = 50 s. Although injections are successful with the contained analytes migrating along the separation channel toward an anode, each injection was not entirely associated with a single droplet. Indeed, it was found that the dead volume at the connection between the droplet delivery tube and the droplet delivery channel (shown in **Figure 5.8b**) caused droplets moving from the tube into the channel to merge either before or immediately after passing this dead volume, thus forming an extended sample plug.

It was also observed (**Figure 5.8aii**, **5.8aiv** and **5.8av**) that the injection frequency and the injection volume of the sample plug were not perfectly reproducible. The volume of the injected plug depends on the period of the injection time, which in turn is controlled by the flow of the oil in the tube (data not shown). It was observed that each time the oil flow pushed a droplet to merge with the long sample plug, the sample plug was injected into the separation channel and the injection temporarily terminated (**Figure 5.8aiii**) when droplets stopped merging. Accordingly, the frequency and the volume of the merging droplet had a direct influence on the injection behaviour. Moreover, it was observed that analytes gradually diffused into the small channels between pillars and eventually filled the oil depletion unit (**Figure 5.8c**). This suggested that the oil

surrounding droplets was depleted (to some extent) into the dead volume instead of being depleted by the pillars and the oil depletion units. Once this dead volume was full of the oil and the oil depletion units were full of analytes, droplets stopped merging and injection was completely terminated.

Although the use of pillars along with the PTFE membrane for passive oil depletion was not investigated due to the dead volume issue, the initial interface design was discarded due to the problems associated with difficulties in fabrication, the fragility of the device, compatibility with buffer solutions and the unacceptably large dead volume between the connection. Accordingly, a new design of interfacing droplet-based microdevices was investigated and is described in **Section 5.3.2**.

5.3.2 Design 2

5.3.2.1 Schematics of designs and fabrication

The entire "Design 2" microdevice is depicted in **Figure 5.9a** and consists of a top layer (**Figure 5.9bi**) and bottom layer (**Figure 5.9biii**). This microdevice was designed to perform both single-channel and parallel-channel separations. The upper PDMS layer contains two separation channels (100 μm wide and 100 μm deep) sharing a common buffer reservoir and a common buffer waste reservoir (4 mm I.D.) at each end (**Figure 5.9bi**). The bottom PDMS layer is 150-300 μm thick (**Figure 5.9bii**) and is used to seal the device. Both top and bottom layers were treated with oxygen plasma to activate the surface. The bottom layer was then cut into two pieces, placed 2-3 mm apart (**Figure 5.9biii**) and bonded to the top layer. The separation in the bottom layer allows droplets to be transferred into the separation channels via open channels.

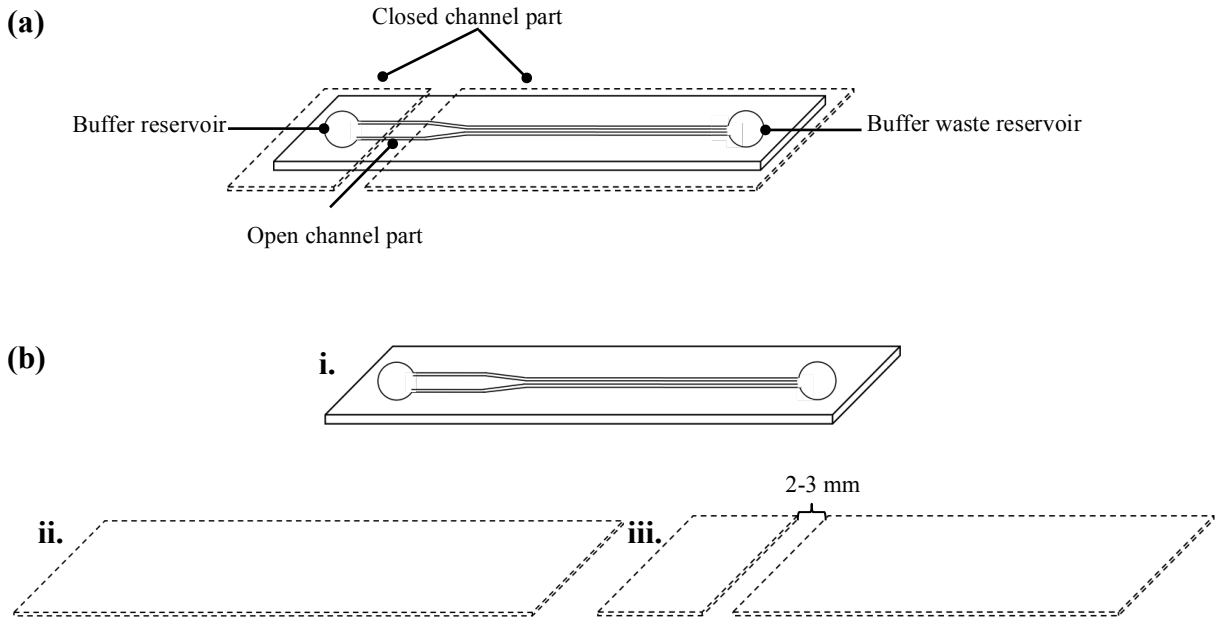

Figure 5.9: Schematics illustrating the structure of "Design 2" for single or multiple separations (a) A schematic of the entire microdevice consisting of a top layer (solid lines) and a bottom layer (dashed lines) in PDMS. The top PDMS layer consists of two parallel separation channels with reservoirs at each end (the left reservoir is the "buffer reservoir" and the right reservoir is the "buffer waste reservoir"). The bottom PDMS layer is cut into two pieces and placed 2-3 mm apart beneath the top layer; (b) Schematics showing the separated top and bottom PDMS layers: (i) Top layer, (ii) Bottom layer before being cut and (iii) Bottom layer cut after oxygen plasma treatment.

5.3.2.2 Droplet injection

Two droplet delivery tubes (containing droplets of fluorescein mixed with food dye) were cut at a 30° angle at one end and placed onto a PTFE membrane as shown in **Figure 5.10**. The microdevice was filled with 0.1x TBE buffer through the buffer reservoir. It was then aligned with the delivery tubes such that the open channels were placed onto the 30° cut of the tubes. Both the microdevice and the tubes were secured in place by an acrylic plate. Droplets in the delivery tubes were pumped towards the microdevice, while an electric field was applied across the separation channels. At the junction (as with the previous devices) the oil surrounding the droplets was absorbed into the PTFE membrane, whilst the droplet contents were released and injected into the separation channels, where they moved towards the detector.

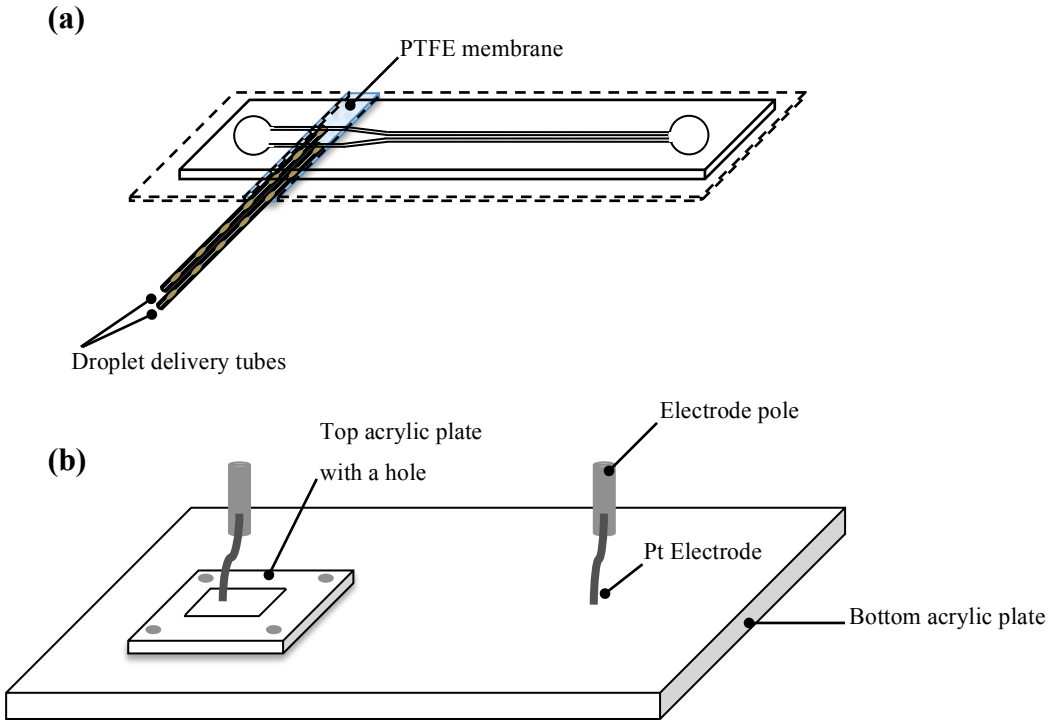

Figure 5.10: Schematics showing the experimental setup used for droplet injection using the interfacing microdevice "Design 2". (a) The interfacing microdevice placed on droplet delivery tubes. Both tubes are on a PTFE membrane. The open channels are aligned to the mouths of the two droplet delivery tubes cut at 30° to the edge. The other ends of the tubes are connected to precision syringe pumps; (b) A platform to hold the microdevice during the experiments consists of two acrylic plates: a top plate and a bottom plate. The microdevice along with the tubes and the PTFE membrane is placed on the bottom plate of the platform, whilst the top plate is put on the microdevice to secure everything in place. There is a square cavity on the top plate at the position of the buffer reservoir so that a Pt electrode can be immersed into the buffer reservoir through the cavity.

5.3.2.3 Results and Discussion

"Design 2" was developed based on previous work by *Niu* and co-workers[33], as described in **Section 5.1**. The interfacing microdevice in this study allowed the oil surrounding droplets to be absorbed passively into a hydrophobic and oleophilic PTFE membrane via an open channel prior to droplet injections. The design of this microdevice (**Figure 5.4ci**) was simpler than that of his previous work (**Figure 5.4a**)[31]. Accordingly, it was used as a model to create "Design 2" as illustrated in **Figure 5.9a**.

The outstanding feature of "Design 2" is that the design is not complicated and thus should be easy to fabricate and multiplex. Furthermore, the carrier phase is passively depleted using a thin PTFE membrane. Finally, droplets can be transferred to the separation channel directly, which should alleviate the problems in "Design 1" associated with dead volumes.

The process of droplet injection using "Design 2" involves a pre-generated droplet in the droplet delivery tube being delivered towards a separation channel using a syringe pump. When the droplet reaches the mouth of the tube, the oil surrounding the droplet is passively absorbed into the PTFE membrane, while the contents of the aqueous droplet merge with a buffer solution in a separation channel above.

The fabrication of microdevices based on "Design 2" was easier than those based on "Design 1" since the alignment of the top and the bottom layers could be achieved without a microscope. After plasma treatment, the bottom layer was cut and separated with 2-3 mm gap (**Figure 5.9biii**) and bonded to the top layer. The separation channels therefore contain two parts; a closed-channel part formed by three hydrophilic walls and an open-channel part (2-3 mm long) confined by two hydrophobic edges of the bottom layer. The width of the open-channel part needs to be 2-3 mm so that two droplet delivery tubes could be placed in between the open channels. Current fluctuations within the closed-channel were found to be similar to those observed in open-channels with a 2-3 mm gap and typically between 1 and 3 μ A. However, when the gap of the open channel was over 6 mm, significantly larger current fluctuations were observed.

The entire PDMS microdevice was filled with 0.1x TBE buffer solution through the buffer reservoir. The buffer solution flowed by capillary action from the buffer reservoir along the separation channel to the buffer waste reservoir, but did not leak at the edges of the intersection since the edges of the bottom layer are hydrophobic. A droplet delivery tubes placed between the open channel and the PTFE membrane created a junction where droplets could be transferred into the separation channel.

Figure 5.11 shows the successful injection of the mixture of fluorescein and food dye in parallel separation channels: upper channel (**Figure 5.11a**) and lower channel (**Figure**

5.11b). Droplets were injected continuously using this design without the accumulation of buffer solution at the junction (which causes dilution of droplet contents) as a result of Laplace's law (**Equation 5.1**)

$$\Delta P \; \alpha \; \frac{\gamma}{r} \tag{5.1}$$

According to **Equation 5.1**, the differential pressure across the liquid surface (ΔP) is directly proportional to the surface tension (γ) and inversely proportional to the axial radius of the curvature along the channel direction (r)[33].

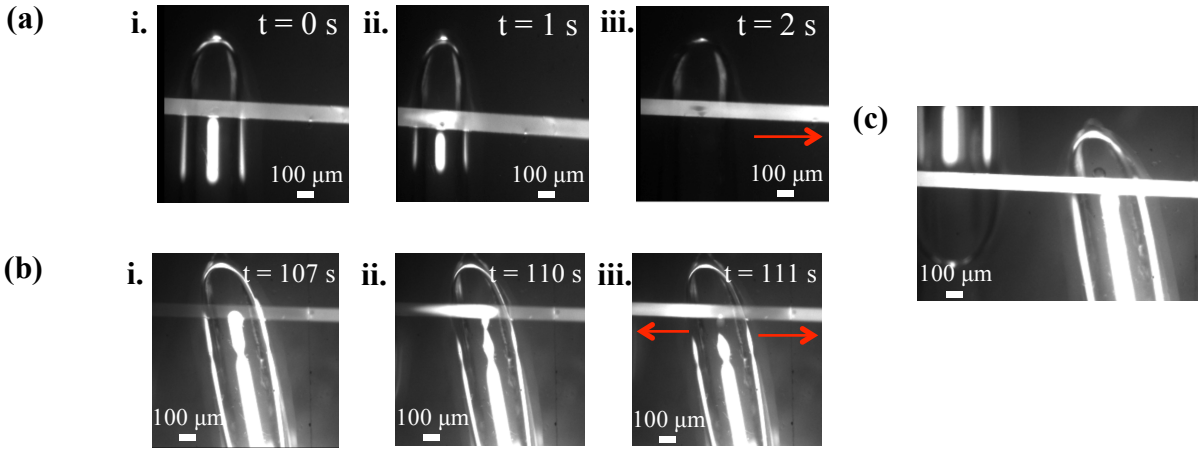

Figure 5.11: Droplet injections in parallel channels. (a) The injection of an analyte mixture droplet into the upper separation channel. (i) The droplet prior to injection at t = 0 s, (ii) The droplet is injected at t = 1 s, (iii) The whole droplet is successfully injected and moves along the separation channel towards the anode at t = 2 s; (b) The injection of the analyte mixture droplet into the lower separation channel. (i) The droplet prior to injection at t = 107 s, (ii) The droplet is injected at t = 110 s, (iii) The whole droplet is successfully injected into the separation channel at t = 111 s. Some of the analyte mixture moves towards the anode (right arrow) but some moves in the opposite direction towards the cathode (left arrow). The arrows indicate the direction of the analyte mixture movement; (c) Droplet injection in the lower channel (right), while a droplet in the other tubing (left) moves towards the upper channel.

At the junction, droplet curvature could be either convex or concave with respect to the channel walls. Specifically, it will be convex if the liquid surface is above the channel walls and concave if the liquid surface is below the channel walls. According to Laplace's law, the radius of the mouth of the droplet delivery tube (r_1 > 50 μm) is larger than that of the channel (r_2 = 50 μm); hence, the pressure in the channel (P_2) is greater than that of the tube (P_1). The liquid in the channel where it meets the mouth of the tube should therefore be pushed due to the higher pressure in the channel such that the curvature of the liquid is over the channel walls. Moreover, the oil will be absorbed into the PTFE membrane when it reaches the mouth of the tube. Consequently, the pressure due to the oil flow at the mouth of the tube decreases. Accordingly, the curvature of the buffer solution at the junction could be convex when there is no injection. However, when the buffer solution at the junction evaporates, the liquid curvature could be concave and the liquid from the buffer reservoir will be pulled to fill up the junction.

During droplet injections, the aqueous droplet contents (released from a droplet after oil depletion) accumulate at the junction and the oil flow pushes it into the channel. Since the radius of the buffer or buffer waste reservoir (r_3 = 2 mm) is much larger than that of the separation channel (r_2 = 50 μm), the differential pressure at the reservoir is almost negligible. Accordingly, the same volume of buffer (as the volume of the injected droplet) flows towards the buffer reservoir. This prevents buffer solution from accumulating at the junction and dilution of the released droplet contents therefore does not occur.

Two factors affecting droplet injections are the injected droplet volume and the distance between the separation channel and the mouth of the tube. It was found that each droplet was injected into both separation channels as multiple injections instead of single injection (**Figure 5.11a and Figure 5.11b**). The average volume of the droplets generated by the T-junction geometry and stored in tubing (100 μm I.D.) was 3.4 nL corresponding to the average droplet length of 435 μm. This droplet volume provided for double injections for each droplet in which the volume of each injection was between 1.4 and 1.9 nL (corresponding to injection lengths between 185 and 232 μm). Unsurprisingly, multiple injections made it difficult to distinguish separated bands originating from each droplet. However, if the volume of the droplet is less than 1.4 nL, the droplet might not be

immediately injected into the separation channel but might remain at the mouth of the tube until it merges with the next droplet(s) to reach the threshold volume required for injection. In order to achieve a single injection, the minimum volume required is that which enables a droplet to contact the buffer solution in the separation channel, thus allowing droplet contents to merge (with the facilitation of pressure from oil flow in the tube) with the buffer solution. Based on our experiments (for this design) the minimum and maximum volume for droplets to be injected as a single injection was approximately 1.4 nL and 1.9 nL, respectively. The volume of injected droplets actually depends on the distance between the separation channel and the mouth of the tube in which the distance is determined by the thickness of the bottom layer and the pressure obtained from the top piece of the platform used to secure the microdevice in place (**Figure 5.10b**).

Figure 5.11bi shows a long droplet forming via the merging of several small droplets since the distance between each droplet is small and no surfactant has been added to the oil. Increasing the oil flow rate could increase the distance between each droplet, but this would change the size of droplets produced. To achieve both the required droplet size and the required distance between each droplet, both oil and sample flow rates needed to be adjusted in the concerted manner. Although possible, this was difficult to achieve using a T-junction geometry.

Another problem encountered using the current design was the increase in EOF while performing droplet injection (as shown in **Figure 5.11biii**). Once the droplet was injected into the separation channel, some of the fluorescein mixture moved towards the anode (right handed-side arrow) as expected, but some analyte moved towards the cathode (left handed-side arrow). This indicated the presence of EOF. It should also be noted that another possible reason for movement towards the cathode is evaporation of the buffer solution.

Although this design was successful in allowing injection of droplets into parallel separation channels, it could not be used in conjunction with high viscosity buffer solutions commonly developed for protein separations. The high viscosity buffer solutions caused not only the damage to the microdevice, but also leakage of the buffer in

the open channel. Moreover, the surface chemistry of the entire PDMS microdevice was difficult to control since the hydrophilic properties of oxidized PDMS surfaces degrade over time reverting to their native hydrophobic state[44,45,46]. The resulting change of EOF due to the change in surface chemistry over the experimental timescale was difficult to eliminate. Additionally, the experimental setup was not convenient since it needed precise alignment between the mouth of droplet delivery tube and the open channel. Accordingly, a third generation interfacing microdevice was designed.

5.3.3 Design 3

5.3.3.1 Design schematics and fabrication procedures

The third generation interfacing microdevices illustrated in **Figure 5.12** consist of identical top layers (**Figure 5.12ai**) with two different designs for the bottom layers (**Figure 5.12aii** and **Figure 5.12aiii**). The top layer (**Figure 5.12ai**) is composed of a T-junction droplet delivery channel (100 μm wide and 100 μm deep) in which the left and the right ends are enlarged to allow insertion of a droplet delivery tube and a glass capillary (that serves as a separation channel). The side channel is connected to a 4 mm I.D. buffer reservoir, while a buffer waste reservoir (a microcentrifuge tube) is placed at the end of the glass capillary. Two different structures for the bottom layer were designed and are depicted in **Figure 5.12aii** and **Figure 5.12aiii**. Both bottom layers were cut into different shapes after plasma treatment. The first design ("Design 3.1") is identical to "Design 2" shown in **Figure 5.9biii**. This was cut and placed 2-3 mm separately prior to being bonded with the top layer, in which an open channel (for oil depletion) was confined between the droplet delivery tube and the buffer reservoir (**Figure 5.12bi**). A rectangular PDMS piece was removed from the second design of the bottom layer after plasma treatment. This bottom layer was bonded to the top layer by placing the open rectangular space of the bottom layer at the T-junction geometry of the top layer and was designated as "Design 3.2" (**Figure 5.12bii**).

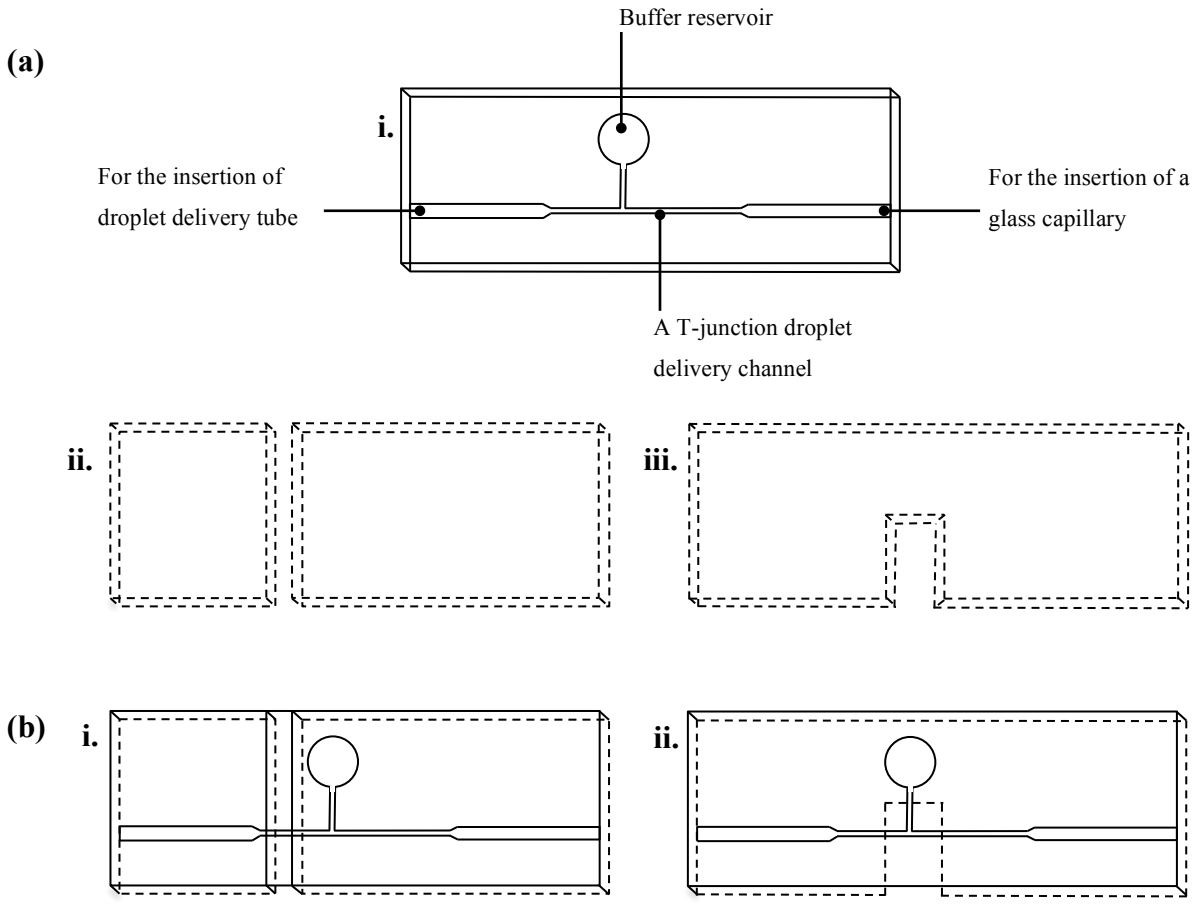

Figure 5.12: Schematics illustrating the third generation interfacing microdevice with two open-channel structures. (a) Separated top layer and bottom PDMS layers (i) Top layer consisting of a T-junction droplet delivery channel with an expansion at the left and right sides to allow insertion of droplet delivery tube and a glass capillary, respectively. A buffer reservoir is placed at one end of the channel, whilst a buffer waste reservoir (not shown) is placed at the end of the capillary, (ii) Initial design of the bottom layer. A flat PDMS layer is cut and placed 2-3 mm separately after oxygen plasma treatment, (iii) Second design of the bottom layer. A rectangular, thin PDMS layer is removed after oxygen plasma treatment; (b) Entire microdevices after bonding the top and bottom layers (i) The top layer of microdevice bonded with the first design of the bottom layer "Design 3.1", (ii) The top layer of microdevice bonded with the second design of the bottom layer "Design 3.2".

5.3.3.2 Droplet injection

Both microdevices depicted in **Figure 5.13** were configured and operated in the same manner for droplet injection experiments. Each setup comprised a PDMS microdevice, a droplet delivery tube, a glass capillary, a syringe pump, two electrodes, a high-voltage

power supply and a fluorescence detector. The PDMS part of the microdevice was filled with 0.1% (w/v) SDS. A 5-cm long detection window on a 7-cm long glass capillary was created by burning the polyimide coating off and cleaning with ethanol. The glass capillary was then treated with 1 M HCl for 5 minutes and filled with 6% PEO in 0.05 M TRIS-CHES, 0.1% SDS, pH 8.5 prior to being inserted into the right end of the microdevice. One end of the droplet delivery tube containing only FC-40 oil (for oil leakage testing) or fluorescein droplets was inserted into the left end of the microdevice, while the other end of the tube was connected to a syringe pump. The entire microdevice was then placed onto a PTFE membrane, ensuring that the open channel was precisely above the membrane. Oil surrounding droplets was absorbed into the PTFE membrane via the open channel, while the droplet contents migrated further under an electric field into the glass capillary to be separated.

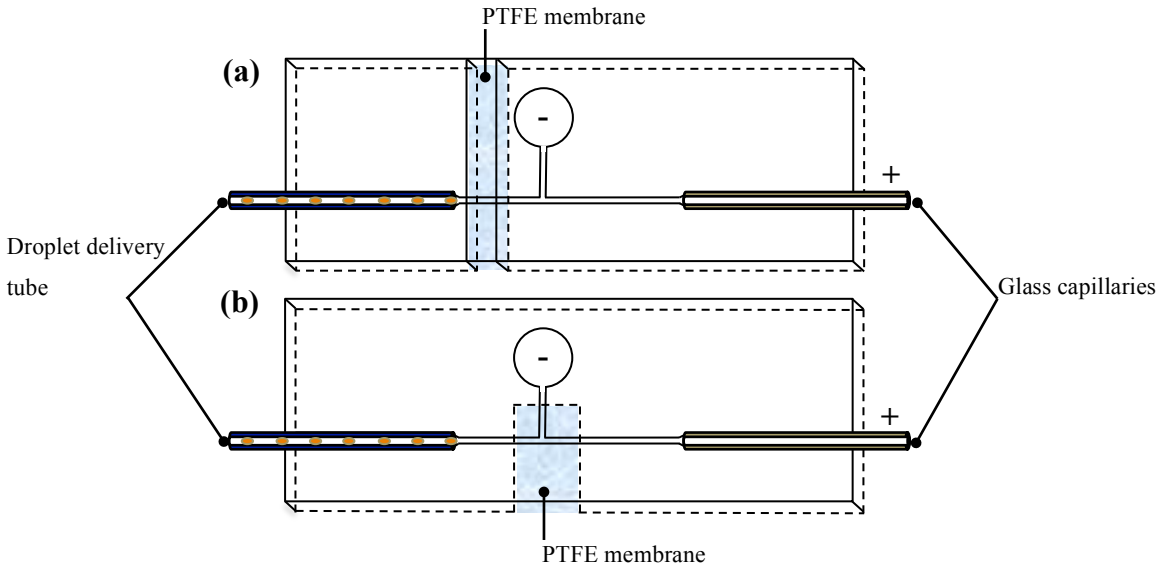

Figure 5.13: Schematics illustrating the experimental set up used for droplet injection using the third generation interfacing microdevices. (a) "Design 3.1" with the separated bottom layer; (b) "Design 3.2" with the open, rectangular bottom layer. Both microdevices are configured in the same manner, i.e. droplet delivery tube and a glass capillary are inserted into the left and the right enlarged channels, respectively, and the open channel is placed on a PTFE membrane for oil depletion. A cathode is placed at a buffer reservoir, while an anode is placed at a buffer waste reservoir for application of an electric field.

5.3.3.3 Results and Discussion

The basic idea behind "Design 3" was to simplify the experimental setup and operation when compared to "Design 2" (**Section 5.3.2.2**) and to ensure that viscous buffer solutions could be used without any problems. Briefly, "Design 2" needed precise alignment between the open channel and the mouth of the delivery tube so that droplet contents could be successfully injected into the separation channel, while the oil surrounding the droplets could be absorbed into the PTFE membrane. Moreover, the entire microdevice (for "Design 2") was made of PDMS, making it difficult to fill the microdevice with viscous buffer solution without structural deformation and/or leakage of the buffer solution in the open channel. Accordingly, the third generation interfacing microdevices were designed to solve these problems. Three key features of "Design 3" are desired. First, the design should be simple and the devices are easy to fabricate. Second, the device should be buffer-friendly, allowing operation with both non-viscous and viscous buffer solutions without leakage. Finally, the microdevice should be easy to handle and configure during experiment.

To solve the problems described above, two T-junction interfacing microdevices ("Design 3.1" and "Design 3.2") were fabricated as illustrated in **Figure 5.12b**. The fabrication of both deisgns was facile and the insertion of either droplet delivery tube or a glass capillary into enlarged ends of both microdevices was easy and rapid.

The difference between the two microdevices lies in the bottom layers. **Figure 5.12bi** shows the microdevice with two separated sections of the bottom layer ("Design 3.1") to provide for an open channel. It should be noted that the position of the open channel in "Design 3.1" differed from that of "Design 2", in that the open channel of "Design 3.1" was on the left-hand side of the buffer reservoir, while the open channel in "Design 2" was on the right-hand side of the buffer reservoir. **Figure 5.12bii** shows the microdevice with a rectangular open space on the bottom layer ("Design 3.2") creating a T-geometry open channel in which the buffer reservoir is close to the open channel. The purpose of assessing both "Design 3.1" and "Design 3.2" was to investigate whether the different position of the buffer reservoir with respect to the open channel would affect droplet injection.

First, the effect of the presence of oil in the PDMS part of the microdevice containing 0.1% SDS was studied by pressurizing only the FC-40 oil through the tube into the PDMS channel and observing any variation in current. It was found from the experiments that current varied between 10 and 13 μA and 5 and 8 μA for "Design 3.1" and for "Design 3.2", respectively, as the oil flow rate increased from 0.1 to 1.5 μl/min. At a flow rate of 0.15 μl/min (which was the same used to deliver droplets), the current was stable over the period that the electric field was applied (cathode = -500 V, anode = 800 V for 30 minutes) for both designs. This indicated that the presence of the FC-40 oil in the PDMS channel containing the aqueous buffer did not affect current variation since the oil must already have absorbed into the PTFE membrane at the open channels in both microdevices.

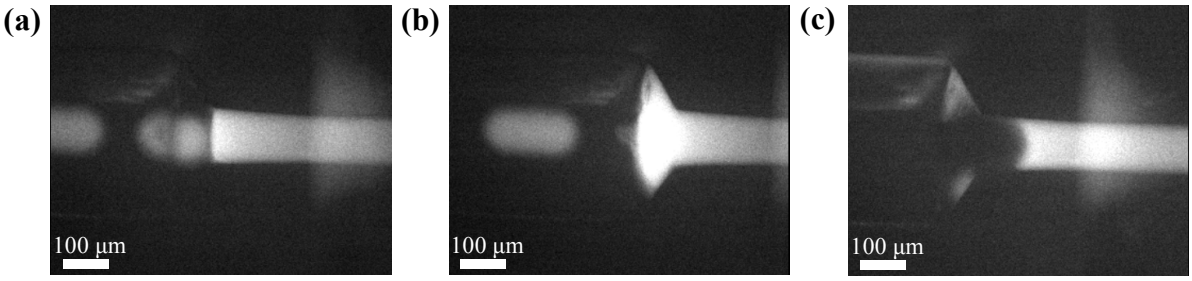

Figure 5.14: Images showing the injection of droplets and the migration of droplet content towards the separation channel performed in microdevice "Design 3.1". (a) A droplet leaves the mouth of the droplet delivery tube and moves into the droplet delivery channel; (b) The droplet content is accumulated at the mouth of the tube and its movement ceases; (c) After a period of time, the droplet contents start moving again.

Figure 5.14a is obtained using Design 3.1 and shows a fluorescein droplet reaching the mouth of the tube and entering the PDMS channel, where the oil surrounding the droplet is depleted and the droplet contents are released from the droplet. Instead of moving along the PDMS channel into the glass capillary under an applied electric field, the droplet contents move slowly and finally stopped (**Figure 5.14b**). After a given period of time (50 s) droplet movement begins again, as shown in **Figure 5.14c**. Unfortunately, the subsequent movement of the droplet content is parabolic in nature and likely to be caused

by hydrodynamic pressure from the oil flow rather than the electric field. This suggests that the electric field distribution along the entire microdevice is non-uniform due to the poor positioning of the buffer reservoir. The electric field in the left branch of the T-junction was far weaker than that in the right branch; hence, droplet contents could move under the pressure until reaching a location (at the T-junction) with a stronger electric field, thus allowing further movement under an electric field into the glass capillary. Since the position of the buffer reservoir in "Design 3.1" and "Design 3.2" were at the same place, it could be assumed that the electric field distribution was approximately constant. Accordingly, both designs were deemed unsuitable for droplet injection.

5.3.4 Design 4

5.3.4.1 Schematics of designs and fabrication

The fourth generation of interfacing microdevices depicted in **Figure 5.15** consists of two different designs of the top PDMS layers (**Figure 5.15ai** and **Figure 5.15aii**) and a common bottom PDMS layer containing a rectangular open space for oil depletion (**Figure 5.15aiii**). The top layer designs are similar in that each design consists of a U-shaped droplet delivery channel (100 μm wide and 100 μm deep) with an enlarged channel for the insertion of a droplet delivery tube at the middle of the U-shaped channel, a buffer reservoir (4 mm I.D.) and the other enlarged channel for insertion of a glass capillary, which are placed at each end of the U-shaped channel. The key difference between these two designs relates to the geometry of the U-shaped channel. The U-shaped channel designated as "Design 4.1" is round, whereas the U-shaped channel designated as "Design 4.2" is square in shape. However, the bottom layer for both designs is identical. A small rectangular open space in the middle of the bottom layer was cut after plasma treatment. A small amount of methanol was then deposited on the plasma-treated surface of the bottom layer to protect the oxidized surface during the bonding process[47,48]. Subsequently, the plasma-treated top and bottom layers were aligned and bonded under a microscope to ensure that the edge of the open space on the bottom layer was in alignment with the edge between the enlarged channel (for droplet delivery tubing) and the curve ("Design 4.1") or the straight line ("Design 4.2") of the U-shaped channel.

Finally, the bonded microdevice was placed on a hot plate at 65°C for 3 minutes to remove the methanol prior to being filled with water to maintain device hydrophilicity.

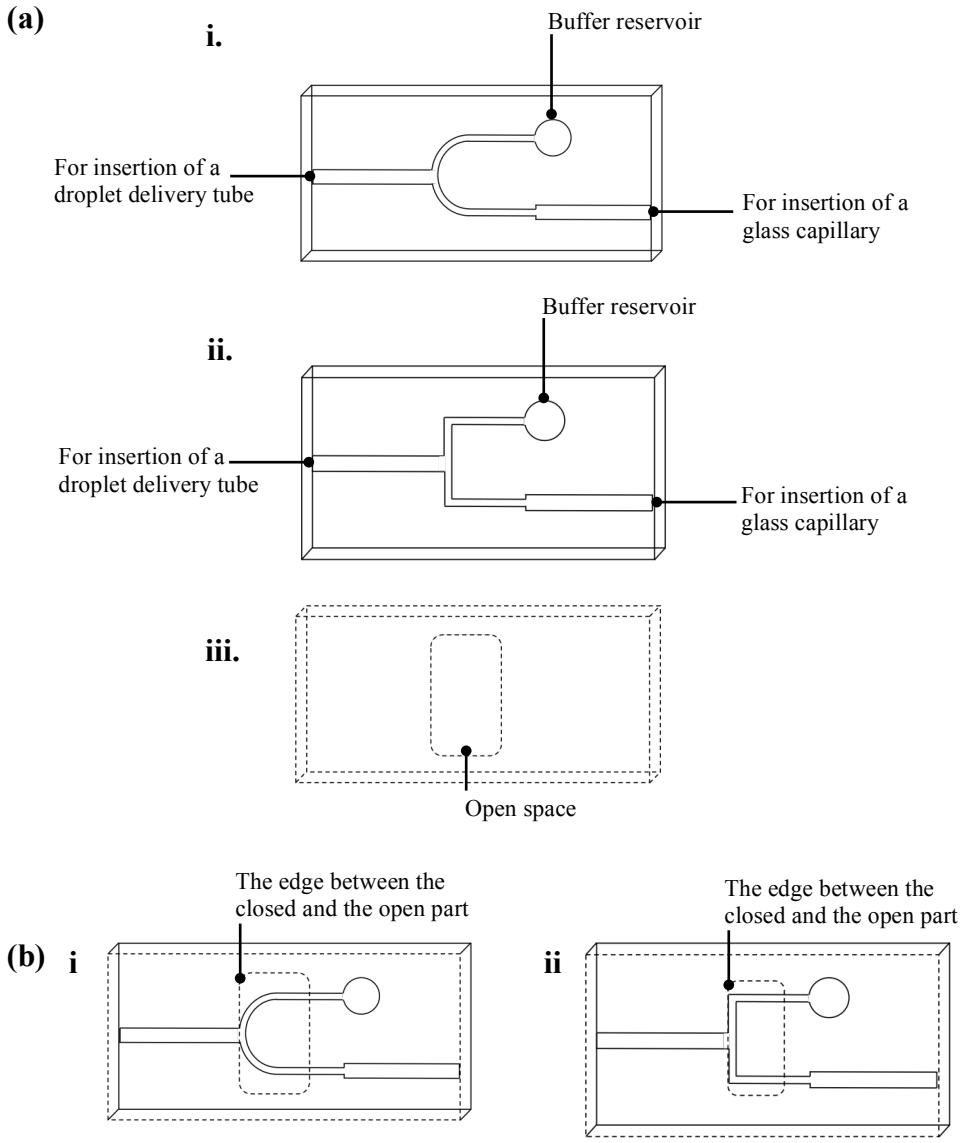

Figure 5.15: Schematics illustrating the fourth interfacing microdevices containing two similar open-channel designs. (a) Separated top and bottom PDMS layers: (i) Top layer of "Design 4.1" consisting of a round U-shaped droplet delivery channel, (ii) Top layer of "Design 4.2" consisting of a square U-shaped droplet delivery channel. Both designs consist of an enlarged channel in the middle of the U-shaped channel for insertion of droplet delivery tube, a buffer reservoir and the other enlarged channel for the insertion of a glass capillary at each end of the U-shaped channel, (iii) Bottom layer of both "Design 4.1" and "Design 4.2" consisting of a rectangular open space on a PDMS sheet, which is cut after oxygen plasma treatment; (b) The entire microdevices after bonding: (i) "Design 4.1", (ii) "Design 4.2".

5.3.4.2 Droplet injection

Both (completed) microdevices are depicted in **Figure 5.16** and operated in the same manner for droplet injection experiments. The PDMS part of the microdevice was filled with 0.1% (w/v) SDS. A 5-cm long detection window of a 7-cm long glass capillary was prepared as described in **Section 5.3.3.2**. The glass capillary was then treated with 1 M HCl for 5 minutes, filled with 6% PEO in 0.05 M TRIS-CHES, 0.1% SDS (pH 8.5) and inserted into the right enlarged channel of the microdevice. The droplet delivery tube connected to a syringe pump at one end was inserted into the left enlarged channel of the microdevice. The entire microdevice was then placed on a PTFE membrane. During droplet injection, the oil surrounding droplets was absorbed into the PTFE membrane at the open channel, while droplet contents migrated further under an applied electric field into the glass capillary for separation.

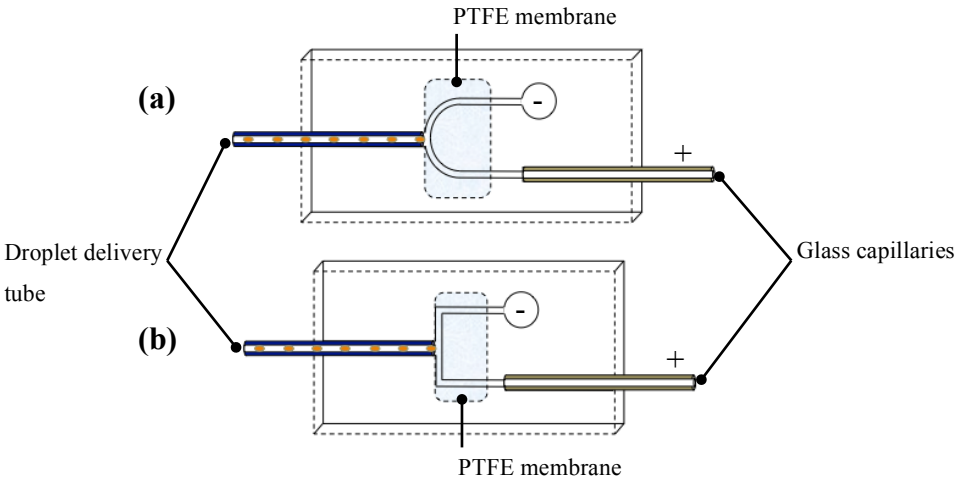

Figure 5.16: Schematics illustrating the process of droplet injection using the fourth generation of interfacing microdevices. (a) "Design 4.1" with a round U-shaped PDMS channel; (b) "Design 4.2" with a square U-shaped PDMS channel. Both microdevices are operated in the same manner. A droplet delivery tube is inserted into the enlarged channel at the middle of the U-shaped channel, while a glass capillary is inserted into the other enlarged channel. The entire microdevice is placed on a PTFE membrane, which serves as an oil depletion unit. A cathode is placed at a buffer reservoir, while an anode is placed at a buffer waste reservoir.

5.3.4.3 Results and Discussion

The fourth generation interfacing microdevices were developed to address the issue of unequal electric field distribution that occurred in the third design structures. The fourth generation devices possess three key features. First, the electric field can be equally distributed all over the entire microdevice due to the appropriate positioning of buffer reservoirs. Second, both designs can be used with either viscous or non-viscous buffer solutions since the running buffer (either viscous or non-viscous) is only filled up in the capillary part, which prevents the leakage of the buffer at the open channel in the PDMS part. Finally, the experimental setup and device operation are simple and convenient.

Fabrication of microdevices based on "Design 4.1" and "Design 4.2" was more complicated than that of the third generation microdevices described previously. Extremely precise alignment of the top and the bottom layer was required for both "Design 4.1" and "Design 4.2" to ensure successful droplet injection. The key factors affecting droplet injection in both designs were the volume of incoming droplets and the position of the mouth of the delivery tube. Droplets used in these experiments were generated by a robotic droplet generator as described in **Section 5.2.1.2**; therefore, the volume of the generated droplets could be controlled by adjusting the parameters of the robotic droplet generator during droplet generation. In addition, the position of the mouth of the droplet delivery tube was ideally placed exactly at the edge between the closed and the open part of the microdevice (shown in **Figure 5.15bi**), allowing a droplet with an optimized volume to be injected as a whole droplet (a single injection). However, lower droplet volumes were required to achieve droplet injection when the mouth of the tubing extended into the U-shaped PDMS channel. This could result in multiple injections of droplet contents. Conversely, higher droplet volumes were required when the mouth of the tubing was placed behind the edge. Several droplets therefore merged together to achieve the required volume prior to injection, causing sample contamination if each droplet possesses a different chemical payload.

Initially, "Design 4.1" was fabricated and tested. The results indicated that a single injection of each droplet could be achieved when the mouth of the tube was placed in the correct position as shown in **Figure 5.17**. The droplet content (fluorescein) formed a

spherical plug in the U-shaped PDMS channel, while the oil was completely absorbed into a PTFE membrane placed underneath the open part of the microdevice (**Figure 5.17b**). Subsequently, fluorescein migrated under an applied electric field along the PDMS channel (red dashed lines) towards the anode and finally entered a glass capillary for detection.

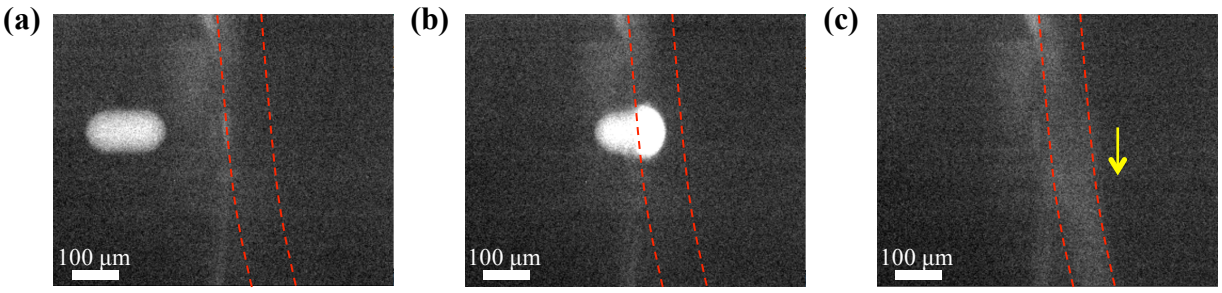

Figure 5.17: Images showing the injection of a droplet in "Design 4.1". The red dashed lines indicate the open PDMS channel of the microdevice. (a) A droplet moves towards the mouth of the droplet delivery tube; (b) The droplet contents form a spherical plug when the droplet reaches the open PDMS channel, while the oil is absorbed into the PTFE membrane underneath; (c) The droplet content migrates towards a glass capillary placed downstream (the movement direction indicated by a yellow arrow).

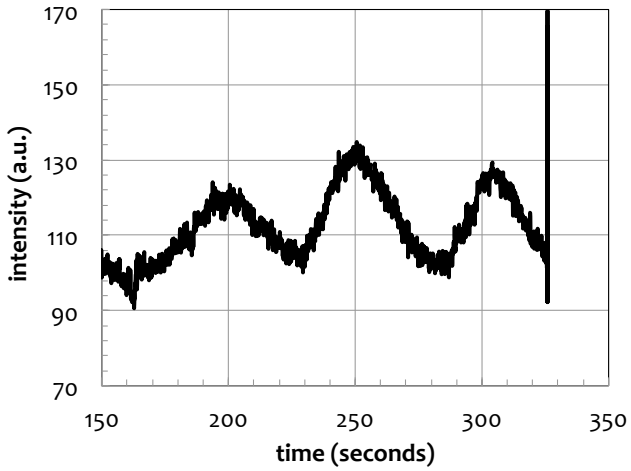

Figure 5.18: An electropherogram of fluorescein obtained from droplet injections performed in the microdevice "Design 4.1". Three fluorescein droplets were injected and detected inside a glass capillary. Each droplet was injected as single injection. The electric field used in this experiment was ~ 253 V/cm.

Unfortunately, a number of experimental issues were encountered using the fourth generation microdevices. First, misalignment between the top and the bottom layer, especially at the edge between the closed and the open part of the microdevice, caused leakage of droplet content outside the U-shaped PDMS channel during droplet injection. Second, insertion of the droplet delivery tube was difficult to perfectly reproduce, resulting in a change in the required volume for a successful single injection. Third, the sealing of the top and the bottom layer at the edge illustrated in **Figure 5.15bi** was easily compromised during the insertion of the tube, which could cause leakage of droplet content during droplet injection. The final issues related to the fact that the distance that droplet content travelled in the U-shaped PDMS channel after injection was too long and resulted in significant dilution as shown in the electropherogram of fluorescein in **Figure 5.18**. Each broad peak in the electropherogram was obtained from a single injection of a fluorescein droplet, reflecting the dilution of fluorescein after injection.

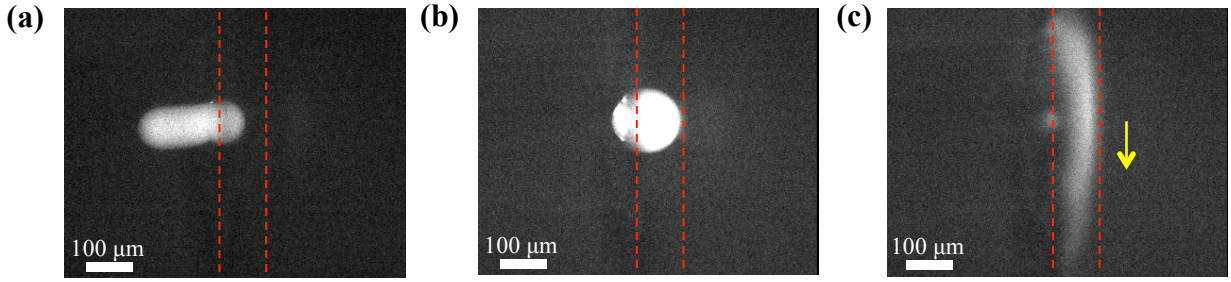

Figure 5.19: Images showing the injection of a droplet performed using "Design 4.2". The red dashed lines indicate the open PDMS channel of the microdevice. (a) A droplet enters the PDMS channel of the microdevice; (b) The droplet contents form a spherical plug; (c) The droplet content migrates along the PDMS channel and then into a glass capillary (with movement direction indicated by a yellow arrow).

To this end, "Design 4.2" was then developed by replacing the round U-shaped channel with a square U-shaped channel as depicted in **Figure 5.15bii**. The alignment of the square U-shaped channel on the top layer with the open space on the bottom layer was far simpler than that of the round U-shaped channel in "Design 4.1". Precise alignment facilitated insertion of a droplet delivery tube at the right position and therefore allowed successful single injection of fluorescein droplets as shown in **Figure 5.19**. However, if

the microdevice was misaligned, leakage of droplet contents as in "Design 4.1" occurred as shown in **Figure 5.20c**.

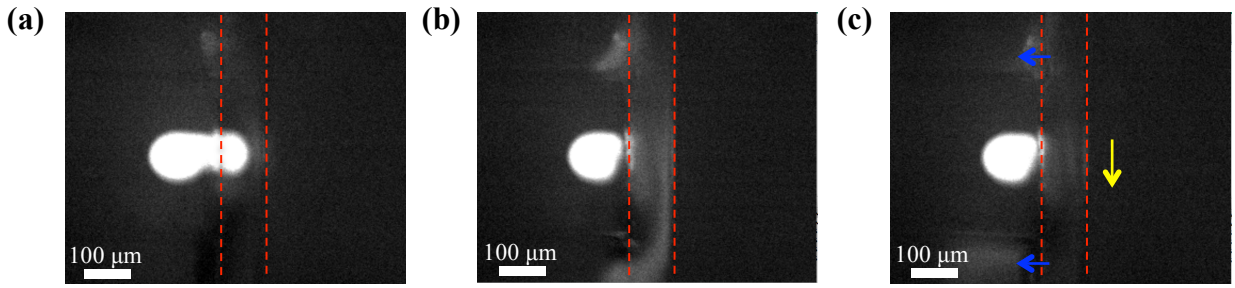

Figure 5.20: Images showing multiple injection of a droplet performed using Design 4.2. The red dashed lines indicate the open PDMS channel of the microdevice. (a) A part of a droplet is injected into the PDMS channel; (b) The injected droplet content migrates along the PDMS channel, with material being left at the mouth of the tube; (c) Most of the droplet content migrates towards a glass capillary (the movement direction indicated by a yellow arrow), while a small portion of the droplet diffuses at the top and the bottom edges of the tube (blue arrows).

According to the observation in the experiment, each fluorescein droplet was not injected as a whole droplet due to the imperfect position of the inserted droplet delivery tube. The required volume to be injected was less than the volume of the generated droplet; therefore, the major part of the droplet was injected into the square U-shaped channel with the minor portion being left at the mouth of the tube until it merges with the next droplet, thus achieving the required volume. It could be inferred from the size of the fluorescein peaks in the electropherogram (**Figure 5.21**) that the volume of each injection was essentially identical. The reproducible injected volume could be useful for quantitative analysis. However, if each droplet contains different analytes, merging of droplets prior to injection will cause unacceptable cross contamination. Another observation was the existence of "narrower" fluorescein peaks due to the decrease in the length of the U-shaped channel.

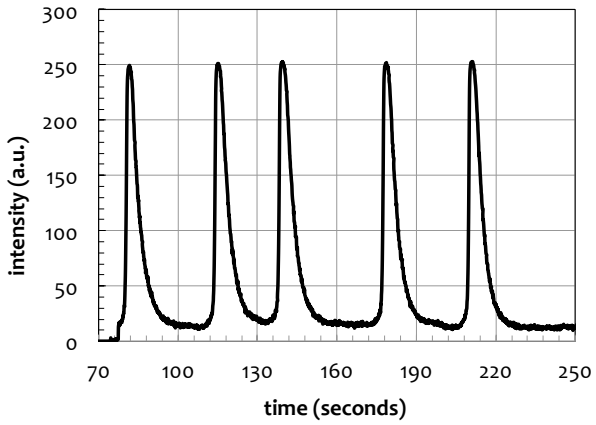

Figure 5.21: An electropherogram of fluorescein obtained from droplet injections performed in a "Design 4.2" microdevice. Five fluorescein droplets were injected and detected inside a glass capillary. Each droplet was injected as multiple injections.

Although "Design 4.2" provided for a more convenient way of alignment between the top and the bottom layer of the microdevice (leading to better performance of droplet injection), the easy breakage of the sealing at the edge (**Figure 5.15bii**) was still problematic. The fourth generation of the interfacing microdevices was therefore improved and is discussed in **Section 5.3.5**.

5.3.5 Design 5

5.3.5.1 Schematics of designs and fabrication

The design of the fifth generation interfacing microdevice is illustrated in **Figure 5.22** and is similar to that of "Design 4.2". The 3D-printed microdevice consists of a top and a bottom layer made of acrylonitrile butadiene styrene (ABS). The top layer consists of a square U-shaped channel (200 μm × 200 μm cross-section) with an enlarged channel for the insertion of a droplet delivery tube at the middle of the U-shaped channel, a buffer reservoir (4 mm I.D.), the other enlarged channel for the insertion of a glass capillary placed at each end of the U-shaped channel and four small round holes at four edges of the top layer as depicted in **Figure 5.22ai** and **Figure 5.22aiii**.

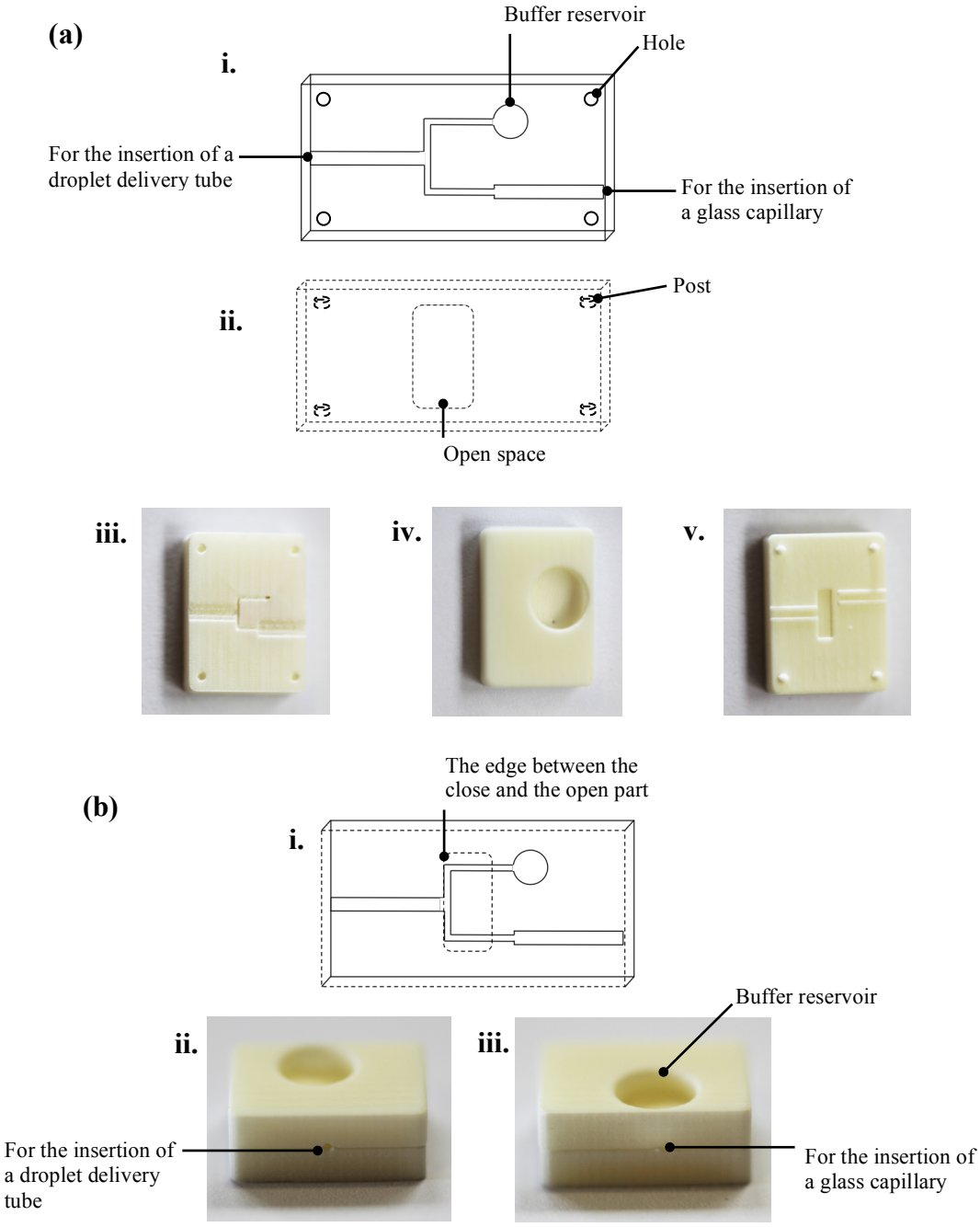

Figure 5.22: Schematics and images depicting the structure of the fifth generation interfacing microdevices made of acrylonitrile butadiene styrene or ABS (a) Separated top and bottom layer: (i) Modified top layer from "Design 4.2" with four holes, (ii) Bottom layer with four post, (iii) A photograph showing the back of the top layer of the 3D-printed microdevice, (iv) A photograph of the front of the top layer showing a 4 mm I.D. buffer reservoir, (v) A photograph of the bottom layer; (b) The entire microdevice after assembling: (i) A schematic showing inside the microdevice, (ii) A photograph of the assembled microdevice showing the buffer reservoir and the side channel for the insertion of a droplet delivery tube, (iii) A photograph of the assembled microdevice showing the buffer reservoir and the side channel for the insertion of glass capillary.

The bottom layer consists of a rectangular hole in which a PTFE membrane will be placed (**Figure 5.22av**) and four posts at four edges of the bottom layer. The fabrication of the microdevice by 3D printing is described in detail in **Section 2.1.2**. By employing posts and holes, the top and the bottom layers were easily assembled or disassembled. **Figure 5.22bi** shows the inside structure of the microdevice after assembling the top and the bottom pieces. The edge of the rectangular hole in the bottom layer is placed underneath the top layer between the U-shaped channel and the enlarged channel for the insertion of the droplet delivery tube. After the 3D-printed microdevice had been fabricated, the wax filling (used as a support material during 3D printing[49]) was removed by sonication of the microdevice in 10% SDS at 70°C for 2 hours. The microdevice was then rinsed with water and placed in an oven at 70°C for 30 minutes. If the wax was not completely removed, it seeped out after the heating.

5.3.5.2 Droplet injection

The experimental setup for droplet injection employing "Design 5" (**Figure 5.23**) was similar to that of "Design 4.2" as described in **Section 5.3.4.2**. The only difference being that the PTFE membrane was placed in between the top and the bottom layer of the microdevice.

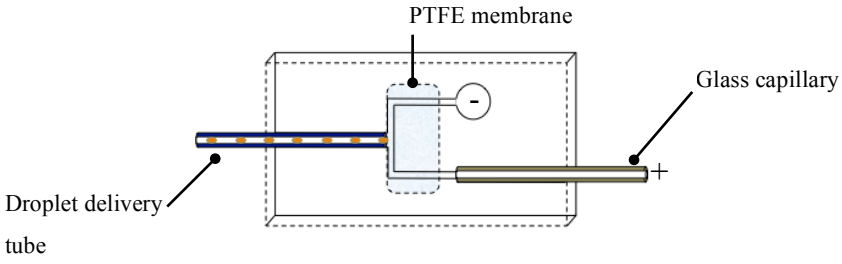

Figure 5.23: A schematic showing the experimental set up of droplet injection using the fifth generation interfacing microdevice developed from "Design 4.2". A PTFE membrane is cut into a small piece, folded and placed into the square hole of the bottom layer prior to being assembled with the top layer. A droplet delivery tube is inserted into the enlarged channel at the middle of the U-shaped channel, while a glass capillary is inserted into the other enlarged channel. A cathode is placed at a buffer reservoir, while an anode is placed at a buffer waste reservoir, which is a microcentrifuge tube (not shown) for the application of an electric field.

5.3.5.3 Results and Discussion

The fifth generation of interfacing microdevice ("Design 5") was developed from "Design 4.2". The major improvements of the fifth design are the robustness of the microdevice and more convenient alignment of the top and bottom layers. Other advantages of "Design 5" are the same as those described for "Design 4.2" and are mentioned in **Section 5.3.4.3**. In principle, droplet injection using "Design 5" works in the same manner as that of "Design 4.2" and is described in detail in **Section 5.3.4.2**.

(a) **(b)**

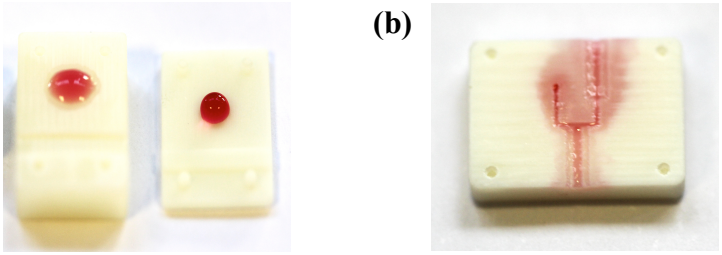

Figure 5.24: Images showing hydrophilic testing on the surface of 3D-printed pieces of microdevices (a) Red food dye was dropped onto the surface of each 3D-printed piece. Before (right) and after (left) surface treatment with 10% SDS at 70°C for 2 hours; (b) Red food dye filled up the entire channel of the microdevice.

Due to the shortage of alternative materials for 3D-printing, ABS was the only option at the time experiments were conducted. The contact angle, which is the angle measuring between the liquid and solid surface, indicates the degree of wetting. High wettability has large contact angle (more than 90°), while low wettability has low contact angle (less than 90°)[50]. It was found from experiment that before the ABS 3D-printed microdevice was treated with 10% SDS at 70°C for 2 hours, the contact angle of the droplet in **Figure 5.24a** (right) was large. The surface of the microdevice (**Figure 5.24a** (right)) was therefore considered to be hydrophobic. However, the surface of the 3D-printed microdevice became more hydrophilic (indicated by a smaller water contact angle) after the surface treatment as shown in **Figure 5.24a** (left). The entire channel of the treated 3D-printed microdevice was easily filled with red food dye from the buffer reservoir as shown in **Figure 5.24b**. The microdevice was flushed with water and dried prior to being

refilled with red dye again. This process was repeated every 15 minutes for 1.5 hours. It was found that the hydrophilicity of the microdevice gradually decreased, making it difficult for the liquid to penetrate along the entire channel. The other problem with the 3D-printed microdevice was the opacity of the ABS material, which made it impossible for droplet injection to be observed. Due to the hydrophobicity and the opacity of the ABS 3D-printed microdevice, it was not further used for droplet injection experiments.

5.3.6 Design 6

5.3.6.1 Schematics of designs and fabrication

The entire microdevice of the sixth design is illustrated in **Figure 5.25a**. The top layer of the microdevice consists of a single channel (100 μm wide and 100 μm deep) with a buffer reservoir (I.D. = 4 mm) and an enlarged channel at each end (**Figure 5.25bi**). The bottom layer is a flat PDMS sheet with the thickness of 0.15 – 0.3 mm (**Figure 5.25bii**).

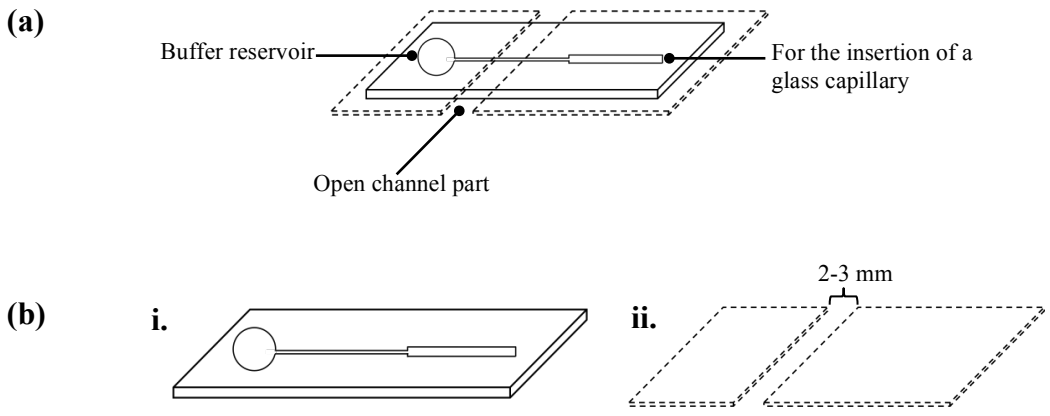

Figure 5.25: Schematics depicting the structure of the sixth design of interfacing microdevices. (a) A schematic of the entire microdevice consisting of a top (solid lines) and a bottom (dashed lines) layer of PDMS; (b) Schematics showing the separated top and bottom PDMS layers: (i) The top layer consisting of a straight channel connected to a buffer reservoir at one end and an enlarged channel for the insertion of a glass capillary at the other end, (ii) The 2-3 mm separated PDMS bottom layer after plasma treatment.

The fabrication of "Design 6" was as described for "Design 2". Briefly, the plasma-treated bottom layer was cut, separated by 2-3 mm (**Figure 5.25bii**) and bonded to the plasma-treated top layer. The cut bottom layer created the open part of the channel in which droplet contents would be injected into a glass capillary.

5.3.6.2 Droplet injection

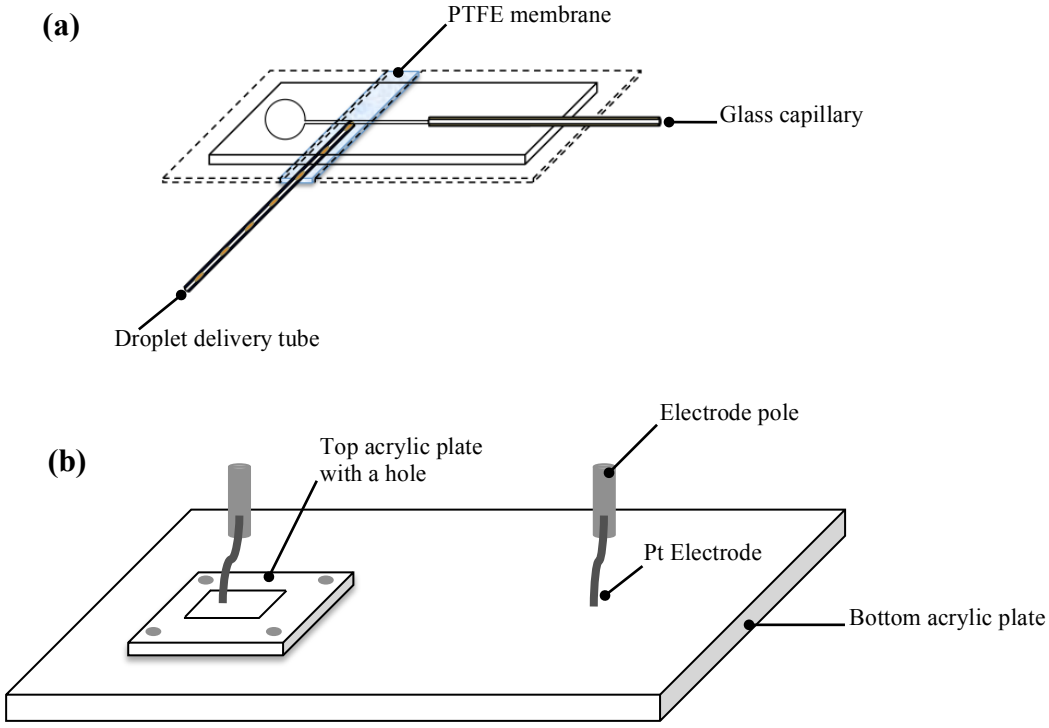

Figure 5.26: Schematics showing the experimental setup of droplet injection experiment using the sixth design of the interfacing microdevices. (a) A droplet delivery tube cut a 30° angle at one end was placed onto a PTFE membrane, while the other end of the tube was connected to a syringe pump. The microdevice with an inserted glass capillary was then placed on the tube by aligning the PDMS channel onto the mouth of the tube; (b) An acrylic platform used to hold the microdevice consisting of two plates. The microdevice along with the tube, the glass capillary and the PTFE membrane is placed on the bottom plate of the platform. The top plate is then put on the microdevice to secure everything in place. One Pt electrode is immersed into a buffer reservoir through a square cavity on the top acrylic plate, while the other Pt electrode is immersed into a buffer waste reservoir (a microcentrifuge tube which is not shown) placed at the end of the capillary.

A 5-cm long glass capillary was prepared by removing 4-cm of the polyimide coating to create a detection window as described in **Section 5.3.3.2**. The glass capillary was rinsed with 1 M HCl for 5 minutes and was then filled with 6% PEO (100 kDa) in 0.05 M TRIS-CHES, 0.1% SDS, pH 8.5. The capillary was inserted into an enlarged end of the microdevice that was already filled with 0.1% SDS. Meanwhile, a droplet delivery tube containing fluorescein droplets was cut a 30° angle at one end and placed onto a PTFE membrane, which was situated on a platform (**Figure 5.26b**). The open channel of the microdevice was then aligned onto the 30° cut mouth of the tube. Subsequently, the microdevice and tube were covered by the top acrylic plate. Droplets were delivered from the tube towards the open channel of the microdevice, while an electric field was applied using two Pt electrodes. At the junction, oil surrounding droplets were absorbed into the PTFE membrane, whilst droplet contents were injected into the PDMS channel in which they migrated under the electric field prior to detection.

5.3.6.3 Results and Discussion

The sixth generation of interfacing microdevices was fabricated based on the microdevice described by *Niu* and co-workers[33] in **Section 5.1** (**Figure 5.4ci**). The principle of droplet injection when using microdevice "Design 6" is the same as that of "Design 2". However, the design of the sixth generation is different from that of the second generation. The microdevice "Design 2" is made of PDMS; therefore, droplet contents are injected and separated in the entire PDMS channel. The microdevice "Design 6", however, consists of a PDMS part and a glass capillary part in which droplet contents are injected into the PDMS part and separated inside the glass capillary.

The key features of "Design 6" are that the design is simple, easy to fabricate and trivial to parallelize for high-throughput analysis. Oil depletion occurs passively by employing a PTFE membrane as an oil depletion unit. Moreover, either viscous or non-viscous buffer solutions can be used with this design without the leakage of buffer at an open channel. Moreover, this design prevents the microdevice from breaking due to the insertion of a droplet delivery tube as described for both "Design 4.1" and "Design 4.2".

Droplet injection performed using "Design 6" occurs in the same manner as that for "Design 2" and is described in detail in **Section 5.3.2.2**. The only difference being that after injection, separation and detection were performed in a PDMS channel for "Design 2" and in a glass capillary for "Design 6". The use of a glass capillary afforded several advantages. First, the buffer solution used in the PDMS part and in the capillary part did not have to be the same. This allowed a non-viscous buffer to be used in the PDMS part and more viscous buffer (i.e. gel based buffer) to be used in the glass capillary. By doing this, the non-viscous buffer solution in the PDMS part did not leak out at the open channel and the viscous buffer solution could be filled into the capillary without causing breakage of the microdevice. Second, EOF in the glass capillary was more controllable than that in the PDMS channel due to the well-characterized glass capillary surface. Finally, the glass capillary was easy to prepare and replace in case it was blocked or damaged.

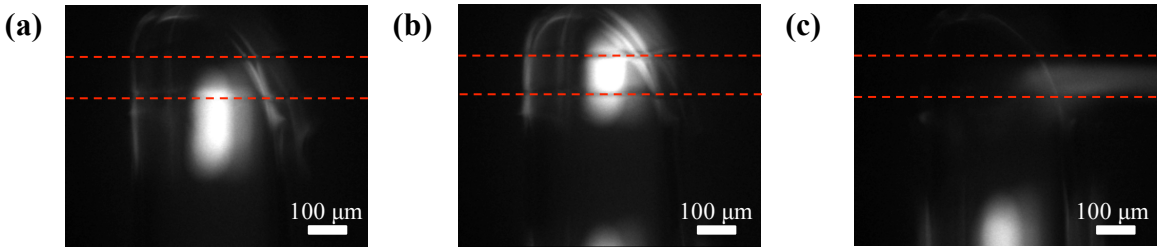

Figure 5.27: Images showing the injection of a fluorescein droplet. (a) A fluorescein droplet moves towards the mouth of the tube at the flow rate of 0.3 µl/min; (b) The oil surrounding the droplet is absorbed into a PTFE membrane, whilst fluorescein released from the droplet forms a spherical shape at the mouth of the tube; (c) Fluorescein is successfully injected into the PDMS channel (red dashed lines) and migrates under an electric field (333.33 V/cm) towards an anode.

Figure 5.27 shows the injection of a fluorescein droplet employing the "Design 6" microdevice. The fluorescein droplet forms a spherical shape at the mouth of the tube cut at 30° (to facilitate the droplet injection) whilst the oil surrounding the droplet was absorbed into the PTFE membrane (**Figure 5.27b**). The droplet contents were then injected into the open PDMS channel and moved further into the glass capillary to be

separated and/or detected (**Figure 5.27c**). The current during the experiment was found to be stable and the electric field was equally distributed all over the microdevice. Although successful droplet injection was achieved using "Design 6", the same problem as that occurred in "Design 2" still remained. Put simply, the inconvenience of the experimental setup (i.e. the alignment of the mouth of the tube and the PDMS channel) meant that experiments were time-consuming.

5.4 Conclusion

Six generations of interfacing microdevices were designed, fabricated and evaluated for use in the droplet-based separation of proteins (**Table 5.1)**. All microdevices incorporated passive oil depletion using a PTFE membrane as the oil depletion unit. The fabrication process for most of the designs was simple, except for "Design 1", "Design 4.1" and "Design 4.2" in which the connection between the top and the bottom layer of the microdevices required extremely precise alignment to ensure reproducible droplet injection.

All designs consisted of two parts for droplet injection and droplet content separation. Both parts needed to be transparent to visible light, to ensure that droplet injection could be observed and that the separated analytes could be detected on-line. All but one of the microdevices (excluding "Design 5") employed PDMS as the substrate material in the droplet injection part because of its transparency, durability, flexibility, ease of fabrication and ability to be rapidly prototyped. For "Design 5", droplet injection could not be observed since ABS was employed as the substrate material. For the separation part, PDMS was used in "Design 1" and "Design 2", with the remaining designs utilizing a glass capillary. Since PDMS was used in both parts of "Design 1" and "Design 2", the entire microdevice was entirely made of PDMS as depicted in **Figure 5.5a** and **Figure 5.9a**, respectively. Wholly PDMS microdevices encountered problems when using viscous buffer solutions. Filling up the PDMS microdevices with a viscous buffer solution caused not only the leakage of the buffer solution at the open channel but also the breakage of the microdevices due to the need for high pressures. Accordingly,

"Design 1" and "Design 2" were not used as interfacing microdevices. For the other designs using PDMS in the droplet injection part and a glass capillary as a separation channel, a non-viscous buffer solution could fill up in the PDMS part, while a viscous buffer solution could be filled up in the glass capillary without any operational issues.

It was found that the measured current was stable during the experiments for all microdevices except "Design 5", which was not tested. The electric field was also equally distributed across the entire microdevice for most of the designs except for "Design 3.1" and "Design 3.2" as previously discussed (**Section 5.3.3.3)**. As a result, "Design 3.1" and "Design 3.2" were discarded at viable options for the interfacing microdevice.

According to the results obtained from the evaluation of six designs of interfacing microdevices (**Table 5.1**), "Design 6" was deemed the most promising design for an interfacing microdevice for droplet-based separations of proteins. Although "Design 6" provided for many advantages over the other designs, the experimental setup was still problematic. Consequently, the microdevice "Design 6" needed further investigation and refinement. This process is discussed in detail in **Chapter 6.**

Table 5.1: Showing the summary of properties used as criteria to choose one out of six interfacing microdevices to be further used.

Design / **Properties**	**1**	**2**	**3.1 and 3.2**	**4.1 and 4.2**	**5**	**6**
1. Ease of fabrication (alignment/ bonding)	No	Yes	Yes	No	Yes	Yes
2. Materials used in the system	PDMS	PDMS	PDMS/ Glass capillary	PDMS/ Glass capillary	ABS/ Glass capillary	PDMS/ Glass capillary
3. Robustness	No	No with viscous buffer	No. Tubing can break the sealing.	No. Tubing can break the sealing.	Yes	Yes
4. Stable separation current	Yes	Yes	Yes	Yes	N/A	Yes
5. Uniform electric field distribution	Yes	Yes	No	Yes	N/A	Yes
6. Compatibility with buffer solution (viscous or non-viscous buffer)	Non- viscous	Non-viscous	Non-viscous or viscous	Non-viscous or viscous	Non-viscous or viscous	Non-viscous or viscous
7. Ease of manipulation	Yes	No	Yes	Yes	No	No
8. Oil depletion mechanism	Passive	Passive	Passive	Passive	Passive	Passive
9. Successful droplet injection	Yes	Yes	Yes	Yes	N/A	Yes

5.5 References

1. Evans, C. R. & Jorgenson, J. W. Multidimensional LC-LC and LC-CE for high-resolution separations of biological molecules. *Anal. Bioanal. Chem.* **378,** 1952–61 (2004).

2. Yang, C., Liu, H., Yang, Q., Zhang, L., Zhang, W. & Zhang, Y. On-line hyphenation of capillary isoelectric focusing and capillary gel electrophoresis by a dialysis interface. *Anal. Chem.* **75,** 215–218 (2003).

3. Liu, H., Zhang, L., Zhu, G., Zhang, W. & Zhang, Y. An etched porous interface for on-line capillary electrophoresis-based two-dimensional separation system. *Anal. Chem.* **76,** 6506–6512 (2004).

4. Wang, T., Ma, J., Wu, S., Sun, L., Yuan, H., Zhang, L., Liang, Z. & Zhang, Y. On-line combination of monolithic immobilized pH gradient-based capillary isoelectric focusing and capillary zone electrophoresis via a partially etched porous interface for protein analysis. *J. Chromatogr. B Anal. Technol. Biomed. Life Sci.* **879,** 804–810 (2011).

5. Zhang, Z. X., Zhang, M. Z. & Zhang, S. S. Online preconcentration and two-dimensional separation of cationic compounds via hyphenation of capillary zone electrophoresis with cyclodextrin-modified micellar electrokinetic capillary chromatography. *Electrophoresis* **30,** 1958–1966 (2009).

6. Lemmo, A. V & Jorgenson, J. Transverse flow gating interface for the coupling of microcolumn LC with CZE in a comprehensive two-dimensional system. *Anal. Chem.* **65,** 1576–1561 (1993).

7. Schoenherr, R. M., Ye, M., Vannatta, M. & Dovichi, N. J. CE-microreactor-CE-MS/MS for protein analysis. *Anal. Chem.* **79,** 2230–2238 (2007).

8. Flaherty, R. J., Huge, B. J., Bruce, S. M., Dada, O. O. & Dovichi, N. J. Nicked-sleeve interface for two-dimensional capillary electrophoresis. *Analyst* **138,** 3621–3625 (2013).

9. Zhang, J., Hu, H., Gao, M., Yang, P. & Zhang, X. Comprehensive two-dimensional chromatography and capillary electrophoresis coupled with tandem time-of-flight mass spectrometry for high-speed proteome analysis. *Electrophoresis* **25,** 2374–2383 (2004).

10. Kohl, F. J., Sánchez-Hernández, L. & Neusüß, C. Capillary electrophoresis in two-dimensional separation systems: Techniques and applications. *Electrophoresis* **36,** 144–158 (2015).

11. Rocklin, R. D., Ramsey, R. S. & Ramsey, J. M. A microfabricated fluidic device for performing two-dimensional liquid-phase separations. *Anal. Chem.* **72,** 5244–9 (2000).

12. Ramsey, J. D., Jacobson, S. C., Culbertson, C. T. & Ramsey, J. M. High-Efficiency, Two-Dimensional Separations of Protein Digests on Microfluidic Devices. *Anal. Chem.* **75,** 3758–3764 (2003).

13. Shadpour, H. & Soper, S. a. Two-dimensional electrophoretic separation of proteins using poly(methyl methacrylate) microchips. *Anal. Chem.* **78,** 3519–27 (2006).

14. Osiri, J. K., Shadpour, H., Park, S., Snowden, B. C., Chen, Z. Y. & Soper, S. A. Generating high peak capacity 2-D maps of complex proteomes using PMMA microchip electrophoresis. *Electrophoresis* **29,** 4984–4992 (2008).

15. Osiri, J. K., Shadpour, H. & Soper, S. a. Ultra-fast two-dimensional microchip electrophoresis using SDS μ-CGE and microemulsion electrokinetic chromatography for protein separations. *Anal. Bioanal. Chem.* **398,** 489–498 (2010).

16. Herr, A. E., Molho, J. I., Drouvalakis, K. A., Mikkelsen, J. C., Utz, P. J., Santiago, J. G. & Kenny, T. W. On-chip coupling of isoelectric focusing and free solution electrophoresis for multidimensional separations. *Electrophoresis* **75,** 1180–1187 (2003).

17. Cong, Y., Zhang, L., Tao, D., Liang, Y., Zhang, W. & Zhang, Y. Miniaturized two-dimensional capillary electrophoresis on a microchip for analysis of the tryptic digest of proteins. *J. Sep. Sci.* **31,** 588–594 (2008).

18. Gottschlich, N., Jacobson, S. C., Culbertson, C. T. & Ramsey, J. M. Two-dimensional electrochromatography/capillary electrophoresis on a microchip. *Anal. Chem.* **73,** 2669–74 (2001).

19. Ross, D., Shackman, J. G., Kralj, J. G. & Atencia, J. 2D separations on a 1D chip: gradient elution moving boundary electrophoresis-chiral capillary zone electrophoresis. *Lab Chip* **10,** 3139–48 (2010).

20. Chen, X., Wu, H., Mao, C. & Whitesides, G. M. A prototype two-dimensional capillary electrophoresis system fabricated in poly(dimethylsiloxane). *Anal. Chem.* **74,** 1772–8 (2002).

21. Li, Y., Buch, J. S., Rosenberger, F., Devoe, D. L. & Lee, C. S. Integration of isoelectric focusing with parallel sodium dodecyl sulfate gel electrophoresis for multidimensional protein separations in a plastic microfluidic network. **76,** 742–748 (2004).

22. Wang, Y.-C., Choi, M. H. & Han, J. Two-dimensional protein separation with advanced sample and buffer isolation using microfluidic valves. *Anal. Chem.* **76,** 4426–31 (2004).

23. Liu, J., Chen, C.-F., Yang, S., Chang, C.-C. & Devoe, D. L. Mixed-mode electrokinetic and chromatographic peptide separations in a microvalve-integrated polymer chip. *Lab Chip* **10,** 2122–2129 (2010).

24. Das, C., Zhang, J., Denslow, N. D. & Fan, Z. H. Integration of isoelectric focusing with multi-channel gel electrophoresis by using microfluidic pseudo-valves. *Lab Chip* **7,** 1806–1812 (2007).

25. Liu, J., Yang, S., Lee, C. S. & DeVoe, D. L. Polyacrylamide gel plugs enabling 2-D microfluidic protein separations via isoelectric focusing and multiplexed sodium dodecyl sulfate gel electrophoresis. *Electrophoresis* **29,** 2241–2250 (2008).

26. Das, C., Fredrickson, C. K., Xia, Z. & Fan, Z. H. Device fabrication and integration with photodefinable microvalves for protein separation. *Sensors Actuators, A Phys.* **134,** 271–277 (2007).

27. Yang, S., Liu, J., Lee, C. S. & Devoe, D. L. Microfluidic 2-D PAGE using multifunctional in situ polyacrylamide gels and discontinuous buffers. *Lab Chip* **9,** 592–599 (2009).

28. Emrich, C., Medintz, I., Chu, W. & Mathies, R. Microfabricated two-dimensional electrophoresis device for differential protein expression profiling. *Anal. Chem.* **79,** 7360–7366 (2007).

29. Griebel, A., Rund, S., Schönfeld, F., Dörner, W., Konrad, R. & Hardt, S. Integrated polymer chip for two-dimensional capillary gel electrophoresis. *Lab Chip* **4,** 18–23 (2004).

30. Kleparnik, K., Garner, M. & Bocek, P. Injection bias of DNA fragments in capillary electrophoresis with sieving. *J. Chromatogr. A* **698,** 375–383 (1995).

31. Niu, X. Z., Zhang, B., Marszalek, R. T., Ces, O., Edel, J. B., Klug, D. R. & deMello, A. J. Droplet-based compartmentalization of chemically separated components in two-dimensional separations. *Chem. Commun. (Camb).* 6159–61 (2009).

32. Pereira, F., Niu, X. & deMello, A. J. A Nano LC-MALDI mass spectrometry droplet interface for the analysis of complex protein samples. *PLoS One* **8,** (2013).

33. Niu, X., Pereira, F., Edel, J. B. & De Mello, A. J. Droplet-interfaced microchip and capillary electrophoretic separations. *Anal. Chem.* **85,** 8654–8660 (2013).

34. Edgar, J. S., Milne, G., Zhao, Y., Pabbati, C. P., Lim, D. S. W. & Chiu, D. T. Compartmentalization of chemically separated components into droplets. *Angew. Chemie* **121,** 2757–2760 (2009).

35. Draper, M. C., Niu, X., Cho, S., James, D. I. & Edel, J. B. Compartmentalization of electrophoretically separated analytes in a multiphase microfluidic platform. *Anal. Chem.* **84,** 5801–5808 (2012).

36. Edgar, J. S., Pabbati, C. P., Lorenz, R. M., He, M., Fiorini, G. S. & Chiu, D. T. Capillary electrophoresis separation in the presence of an immiscible boundary for droplet analysis. *Anal. Chem.* **78,** 6948–54 (2006).

37. Roman, G. T., Wang, M., Shultz, K. N., Jennings, C. & Kennedy, R. T. Sampling and electrophoretic analysis of segmented flow streams using virtual walls in a microfluidic device. *Anal. Chem.* **80,** 8231–8238 (2008).

38. Pei, J., Nie, J. & Kennedy, R. T. Parallel electrophoretic analysis of segmented samples on chip for high-throughput determination of enzyme activities. *Anal. Chem.* **82,** 9261–9267 (2010).

39. Wang, M., Roman, G. T., Perry, M. L. & Kennedy, R. T. Microfluidic chip for high efficiency electrophoretic analysis of segmented flow from a microdialysis probe and in vivo chemical monitoring. *Anal. Chem.* **81,** 9072–9078 (2009).

40. Kelly, R. T., Page, J. S., Marginean, I., Tang, K. & Smith, R. D. Dilution-free analysis from picoliter droplets by nano-electrospray ionization mass spectrometry. *Angew. Chemie - Int. Ed.* **48,** 6832–6835 (2009).

41. Ji, J., Nie, L., Qiao, L., Li, Y., Guo, L., Liu, B., Yang, P. & Girault, H. H. Proteolysis in microfluidic droplets: an approach to interface protein separation and peptide mass spectrometry. *Lab Chip* **12,** 2625 (2012).

42. Li, Q., Pei, J., Song, P. & Kennedy, R. T. Fraction collection from capillary liquid chromatography and off-line electrospray ionization mass spectrometry using oil segmented flow. *Anal. Chem.* **82,** 5260–5267 (2010).

43. Gielen, F., Vliet, L. V., Koprowski, B. T., Devenish, S. R. A., Fischlechner, M., Edel, J. B., Niu, X., deMello, A. J. & Hollfelder, F. A fully unsupervised compartment-on-demand platform for precise nanoliter assays of time-dependent steady-state enzyme kinetics and inhibition. *Anal. Chem.* **85,** 4761–4769 (2013).

44. Bao, N., Xu, J., Zhang, Q., Hang, J. & Chen, H. Electroosmotic flow in poly (dimethylsiloxane) microchannels. *J. Chromatogr. A.* **1099,** 203–206 (2005).

45. Muck, A. & Svatos, A. Chemical modification of polymeric microchip devices. *Talanta* **74,** 333–41 (2007).

46. Liu, J. & Lee, M. L. Permanent surface modification of polymeric capillary electrophoresis microchips for protein and peptide analysis. *Electrophoresis* **27,** 3533–46 (2006).

47. Friend, J. & Yeo, L. Fabrication of microfluidic devices using polydimethylsiloxane. *Biomicrofluidics* **4,** 1–5 (2010).

48. Anderson, J. R. Chiu, D. T., Jackman, R. J., Cherniavskaya, O., McDonald, J. C., Wu, H., Whitesides, S. H. & Whitesides, G. M. Fabrication of topologically complex three-dimensional microfluidic systems in PDMS by rapid prototyping. *Anal. Chem.* **72,** 3158–3164 (2000).

49. Martino, C., Berger, S., Wootton, R. C. R. & deMello, A. J. A 3D-printed microcapillary assembly for facile double emulsion generation. *Lab Chip* **14,** 4178–82 (2014).

50. Bracco, G. & Holst, B. Surface science techniques. *Springer Ser. Surf. Sci.* **51,** (2013).

Chapter VI

Interfacing droplet-based microdevice for protein separations

6.1 Introduction

Three components central to achieving successful droplet-based separation of proteins were investigated in previous chapters. These included a buffer for rapid and high-resolution protein separation (**Chapter 3**), a fluorescently labeled protein mixture (**Chapter 4**) and an interfacing microdevice (**Chapter 5**). The fluorescently labeled protein mixture used as a representative of proteins separated from the first separation dimension was the commercial benchmark fluorescent protein standard 11-155 kDa (Thermo Fisher Scientific, UK) as other laboratory-labeled protein mixtures studied in **Chapter 4** presented several challenges as detailed in **Section 4.3**. The promising buffer for capillary gel electrophoresis of proteins chosen from the investigation in **Chapter 3** was 6% PEO 100 kDa in 0.05 M TRIS-CHES, 0.1% SDS, pH 8.5 buffer since it reached the requirements mentioned in **Section 3.4** and significantly it could separate the benchmark fluorescent protein standard (11-155 kDa) reproducibly. For the interfacing microdevice, "Design 6" was chosen due to the advantages it provided over other designs discussed in **Chapter 5**. In this chapter, all three crucial and functional elements will be integrated, tested and assessed. The performance of the entire system as one unit will be examined to determine if it can be applied to successful and robust droplet-based protein separation.

6.2 Experimental

6.2.1 Droplet-based separation experiment

6.2.1.1 Droplet generation

Droplets of the following samples were generated according to **Section 2.3**. A stock solution of fluorescein (4.5 mM) prepared according to **Section 3.2.2** was diluted 300x and 1000x in 0.1x TBE buffer to achieve 4.5 μM and 15 μM fluorescein solution. BSA-FITC was dissolved in 0.2% SDS to achieve a concentration of 0.5 mg/ml and then heated at 95 °C for 5 minutes. Benchmark fluorescent protein standard (11-155 kDa, Thermo Fisher Scientific, UK) was diluted by adding 1.2 μl of 4.5 μM fluorescein and 18.8 μl DI water to achieve 0.33x fluorescent protein standard.

6.2.1.2 Experimental setup for droplet injection and separation

6.2.1.2.1 One-piece and Two-piece droplet delivery tubes

The generated droplets were directly collected in the tube (100 µm I.D. and 30 cm long) used to withdraw the sample during droplet generation. One end of the droplet collecting tube was detached from the robotic droplet generator, while the other end remained connecting to the glass syringe. This tube could be used as a single-piece or dual-piece droplet delivery tube that transferred droplets to the interfacing microdevice. In the case of the single-piece droplet delivery tube, the tube was cut at a 30° angle at the free end using a blade and could be directly placed underneath the open channel of the interfacing microdevice (**Figure 6.1a**).

The dual-piece droplet delivery tube, the droplet collecting tube was cut straight at the free end. The other tube (100 µm I.D. and 2 cm long) was cut a 30° angle at one end and cut straight at the other end. The two straight-cut ends of these two tubes were joined using a 0.38 mm I.D. tube (polyethylene tube, Smiths Medical, UK) as a sleeve. Each end of the sleeve was melted using a wax pen (Max Wax, USA) and squeezed to fix both tubes (**Figure 6.1b**).

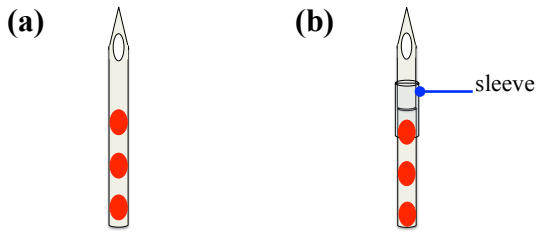

Figure 6.1: Illustrations of (a) one-piece and (b) two-piece droplet delivery tube.

6.2.1.2.2 Assembly of the interfacing droplet-based separation unit

Two platforms were employed for the assembly of the interfacing droplet-based separation unit. Herein, the utilization of the old platform is described, while the use of the new platform is described in detail in **Section 6.3.4**.

The droplet delivery tube (either one-piece or two-piece tube) cut a 30° angle at one end was placed onto a PTFE membrane, which was situated on the old platform (**Figure 6.2 and Figure 5.25b**) and secured by adhesive tape. The interfacing PDMS microdevice "Design 6" was filled with 0.1% SDS or 0.005 M TRIS-CHES, 0.1% SDS, pH 8.5 and cut open at the enlarged end for the insertion of a glass capillary (5 cm or 7 cm long) prepared according to **Section 5.2.6.2** and filled with 6% PEO 100 kDa in 0.05 M TRIS-CHES, 0.1% SDS, pH 8.5. The open channel (100 µm wide and 200-300 µm long) of the PDMS microdevice was then aligned above the 30° cut mouth of the tube. Subsequently, the microdevice and the tube were covered by the top acrylic plate. The entire platform was then fixed onto the microscope stage.

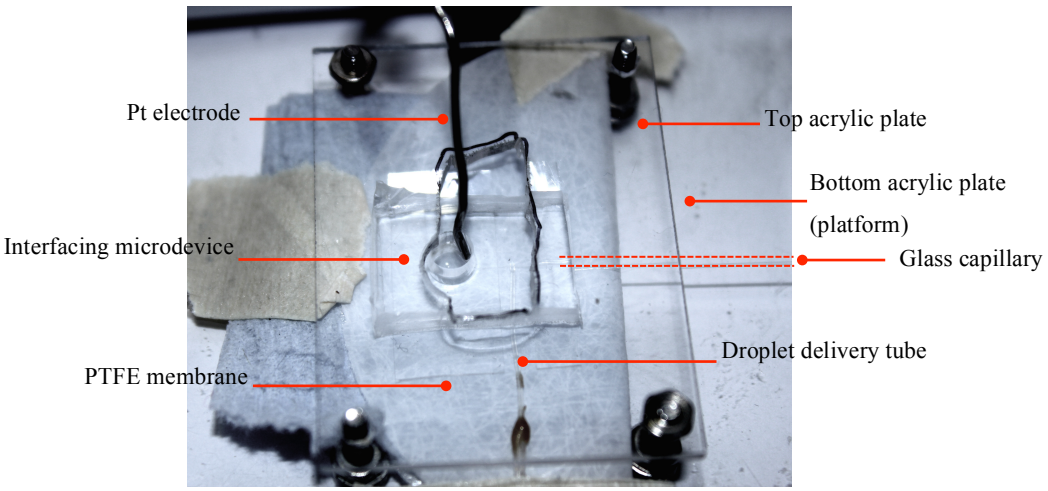

Figure 6.2: A photograph showing the assembly of the interfacing droplet-based microdevice on the old platform.

6.2.1.3 Droplet injection and separation

Droplets were delivered from the tube towards the open channel of the microdevice, while an electric field was applied using two platinum electrodes. At the junction, oil surrounding the droplets was absorbed into the PTFE membrane, whilst droplet contents were injected into the PDMS channel. Once the aqueous phase containing the sample fused with the aqueous phase within the separation channel, the samples migrated under the electric field down the length of the separation channel prior to detection.

6.2.2 Buffer testing using a cross-piece PDMS microdevice coupled to a glass capillary

The testing of the buffer to be used in the interfacing PDMS microdevice was performed in a cross-piece PDMS microdevice coupled to a glass capillary (**Figure 3.1b**) for the convenient experimental setup. The glass capillary was filled with 6% PEO 100 kDa in 0.05 M TRIS-CHES, 0.1% SDS, pH 8.5 buffer, while the cross-piece PDMS microdevice was filled with various buffers, which were 0.1% SDS; 0.1x TBE buffer; 0.05 or 0.005 M TRIS-CHES, 0.1% SDS, pH 8.5 and 6% PEO buffer. 0.5 mg/ml BSA-FITC in 0.2% SDS was used as a sample to investigate the injection in the cross-piece microdevice.

6.3 Results and Discussion

Droplet-based separations of the commercially fluorescent protein ladder in the developed buffer employing the interfacing microdevice "Design 6" were performed. The experiment can be divided into three main steps, which were droplet generation using the robotic droplet generator, the assembly of the interfacing droplet-based microdevice and droplet injection and separation. **Figure 6.3** shows what caused the problems at each step of the experiment. The problems and the solutions are discussed in detail in the following sections.

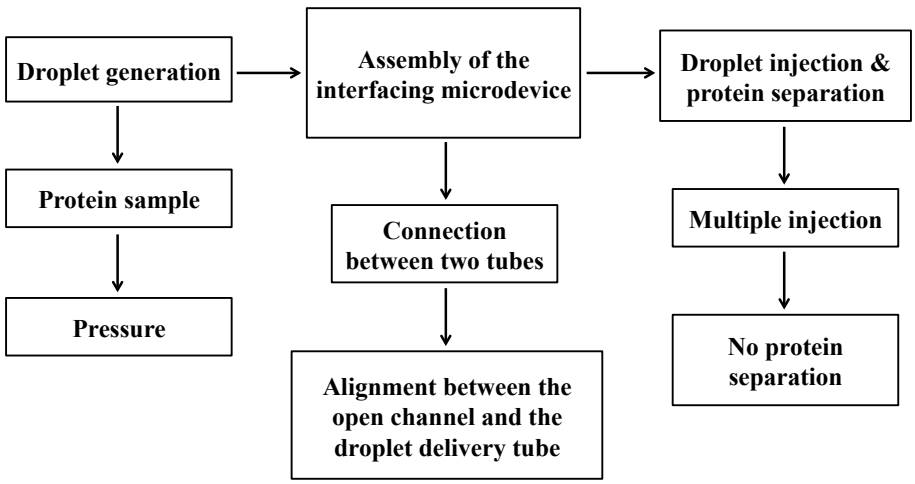

Figure 6.3: Diagram showing the problems occurred in each part of the experiment.

6.3.1 Droplet generation

All droplets used in this chapter were generated using the robotic droplet generator as described in detail in **Section 2.3.** This is because droplet size and interdroplet spacing were more conveniently controlled than using T-junction microdevices as mentioned earlier in **Section 5.2.2**. Among the samples used to generate droplets in this work, protein samples were the most challenging and lead to several problems. It was found that during droplet generation using the robot, vibration caused by the motion of the carousel would on occasion result in the formation of small bubbles within the suspended SDS-protein samples. The presence of proteins and surfactant lowered the surface tension between the liquid air interface resulting in conditions where bubble under minor vibration was significantly higher. These bubbles were often drawn in together with the protein sample resulting in droplets containing both analytes and air bubbles. Other problems with protein samples, especially the commercially available fluorescently labeled protein ladder, were the high viscosity and high cost. The high viscosity of the commercial protein ladder that contained glycerol restricted the use of the "low refilled flow rate" setting to withdraw protein samples into the tube, which in turn affected the control of droplet size. Due to the high cost of the commercial fluorescently labeled protein ladder, the sample volume for droplet generation was used as low as possible for each experiment. However, there was a minimum volume, at least 20 µl for a sample[1]. This is to ensure that the aqueous phase created a significant layer above the oil phase within the bottomless PCR vial in the robotic droplet generator. Consequently, a balance needed to be achieved in the sample preparation, where the protein sample concentration, the viscosity of samples and the sample volume all had to be within a specific range to permit the experiment to work. The commercial protein ladder was diluted to decrease the viscosity of the sample. Dilution was achieved by the addition of a very dilute fluorescein solution. Fluorescein was also used as a marker. Dilution reduces the viscosity but also has the effect of reducing protein sample concentration and consequently the intensity of the fluorescence signal.

Consistency of droplet size was required to ensure the same behavior of droplet injection during the entire experiment and additionally, so that the injection volume is consistent and results may be compared. Droplet size was mostly affected by the pressure in the

system during droplet generation. The three parameters that control droplet size and necessary to achieve stable pressure were the size of the tube for droplet collection, the number of generated droplets and the stabilized pressure prior to droplet generation. The size of the tube (i.e. small diameter and long tube) and the large amount of number of generated droplets could cause the backpressure leading to inconsistency of both droplet size and interdroplet spacing. The optimum size of the tube and the number of droplets, which minimized backpressure, were 100 μm I.D. and 30-cm long tube and 100-150 droplets. The last factor for achieving consistent droplet size was to stabilize the pressure by running the syringe pump at the required refilled flow rate for 5-10 minutes before starting droplet generation.

6.3.2 Assembly of the interfacing droplet-based separation unit

The interfacing droplet-based microdevice, a droplet delivery tube, a prepared glass capillary and a PTFE membrane were assembled for droplet-based separations on a platform as described in detail in **Section 5.2.6.2**. The set-up is tedious and requires all components to be ready and stable prior to interfacing. Furthermore, the assembly process can be time-consuming. Each aspect of the assembled platform and the challenges in hyphenating and solutions to these challenges are described below.

6.3.2.1 One-piece and two-piece droplet delivery tubes

It was found that the utilization of the two-piece droplet delivery tubes resulted in two advantages. First, the droplet collecting tube could be reused several times since the length of the tube remained the same (uncut). The mouth of the 2-cm long tube cut at 30° angle, which was aligned underneath the open channel of the microdevice, did not have to be removed when a new droplet collecting tube was changed. However, a significant disadvantage was the leakage of droplets at the junction between two tubes and between the tubes and the sleeve. This occurred when the two tubes were imperfectly joined as illustrated in **Figure 6.4a**. From the observation, there were two circumstances of leakage. First, a whole droplet leaked. Second, a part of a droplet leaked resulting in the deformed shape of the droplet (**Figure 6.4b**). Furthermore, it was time-consuming to join

the two tubes with a perfect connection that prevent droplets from leaking. Consequently, one-piece droplet delivery tube was employed instead although the tube needed to be changed more frequently.

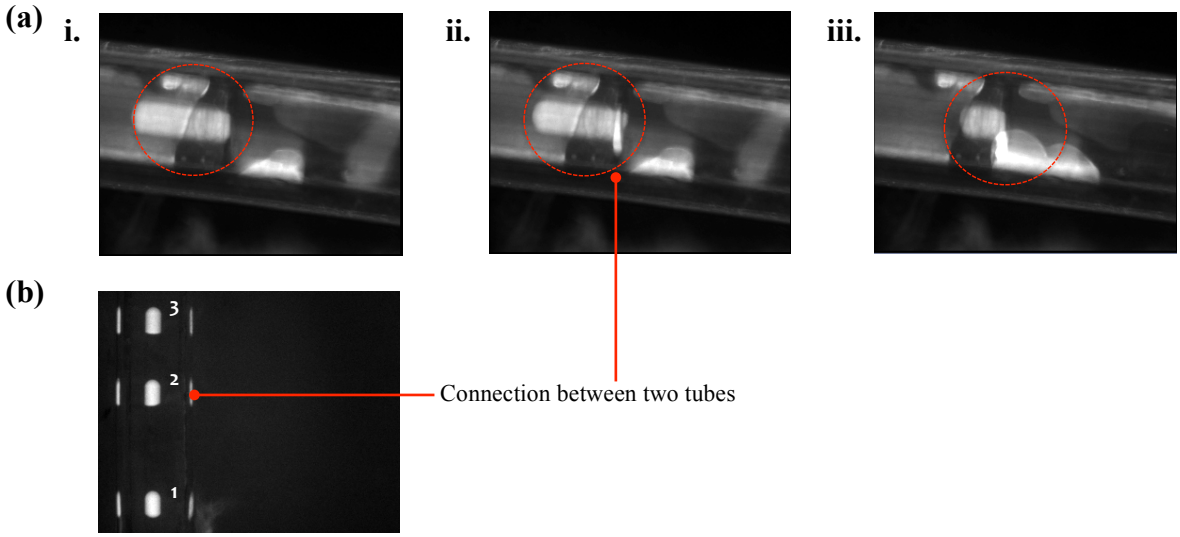

Figure 6.4: Images showing the leakage of a droplet due to the imperfect joining of two tubes (a) The leakage of a whole droplet (i) A droplet reaches the connection between two tubes, (ii) The droplet starts to leak into the sleeve, (iii) The rest of the droplet is leaking out; (b) The leakage of a part of a droplet. The droplet designated as "1" has the normal shape, while the shape of droplets designated as "2" and "3" is deformed after they pass the connection between two tubes.

6.3.2.2 Alignment between the droplet delivery tube and the open channel of the microdevice

The open channel of the microdevice (100 µm width and 100 µm depth) was aligned onto the mouth of the tube (100 µm I.D.), which was placed onto the PTFE membrane situated on the platform. The alignment of the microdevice and the tube was always done prior to fixing the platform to the microscope stage for the detection. This means that every time any component on the platform (i.e. the microdevice, the capillary, the PTFE membrane and the droplet delivery tube) needs replacement, the platform has to be detached from the microscope stage and the microdevice along with the capillary is removed from its well-aligned position and will be realigned after the replacement of any component is accomplished. Due to the extremely small size of the microchannel and the tube, it was

found to be difficult to achieve the precise alignment that allowed successful droplet injection.

6.3.3 Droplet injection and separation in single and parallel separation channel

6.3.3.1 Injection of fluorescein droplets in single separation channel

The mechanism of droplet injection using the interfacing microdevice "Design 6" was as the same as that of "Design 2", which was described in detail in **Section 5.3.2.3**. **Figure 6.5a** shows an electropherogram of injections of nine fluorescein droplets in which each droplet was injected as a whole droplet (single injection). The volume of successfully injected droplets in this experiment was 2.13 ± 0.15 nl (n = 30). The average electrophoretic mobility of nine fluorescein peaks was found to be 7.29×10^{-9} $m^2/V \cdot s$. In this experiment, the droplet was injected every ~ 22 seconds and detected at around 1 cm measured from the injection point to the detection point.

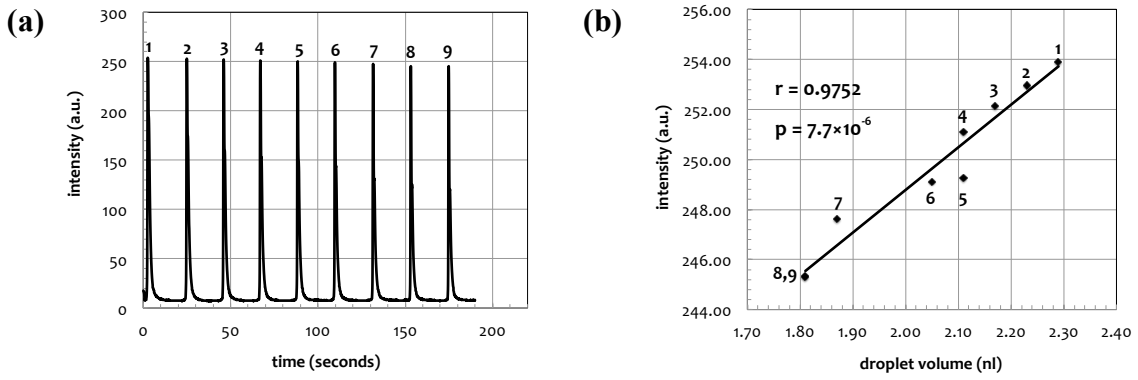

Figure 6.5: The injection of nine fluorescein droplets using "Design 6" interfacing microdevice. (a) An electropherogram of nine injected fluorescein droplets (designated from 1 to 9). In this experiment, the droplets were delivered to the mouth of the tube at the flow rate of 0.3 µl/min and injected to the open channel containing 0.1% SDS. Fluorescein released from droplets migrated into the 5-cm long glass capillary containing 6% PEO 100 kDa in 0.05 M TRIS-CHES, 0.1% SDS, pH 8.5. The applied electric field during this experiment was 333.33 V/cm. The detection was performed at 1 cm from the injection point; (b) A scatterplot between the droplet volume and the fluorescence intensity of nine injected droplets with the correlation coefficient (r) of 0.9752 and the p-value of 7.7×10^{-6}.

It was also found that the decrease in the fluorescence intensity of the injected droplets (**Figure 6.5a**) was as a result of the systematic decrease of the droplet volume during droplet generation using the robotic droplet generator. This could be due to the fact that the optical detection volume is larger than the droplets probed. **Figure 6.5b** shows the scatter plot and the data analyzed using Pearson's product-moment correlation, which indicated that the fluorescence intensity was significantly positively correlated with the droplet volume, $r = 0.9752$ and $p = 7.7\times10^{-6}$ ($p < 0.05$).

6.3.3.2 Injection of BSA-FITC droplets and the investigation of the buffer used in the interfacing PDMS microdevice

The injection of BSA-FITC droplets was also investigated. It was found that once BSA-FITC denatured in 0.2% SDS was released from a droplet into 0.1% SDS buffer in the interfacing PDMS microdevice, BSA-FITC migrated towards an anode for a short distance before it migrated backward to a cathode. This might be due to high EOF in the PDMS part of the channel. Therefore, the buffer in the PDMS part that could be used in conjunction with the glass capillary filled with 6% PEO buffer was investigated by testing various buffers using a cross-piece PDMS microdevice coupled to a glass capillary as described in **Section 6.2.2**. From the experiment, turbulence was observed and BSA-FITC was not accumulated in the cross piece filled with 0.1% SDS or 0.1x TBE when an electric field was applied during injection step. This indicated the presence of EOF. In case 6% PEO buffer was filled up both the cross-piece PDMS microdevice and the glass capillary, BSA-FITC could be successfully injected into the glass capillary. However, 6% PEO buffer could not be filled up the interfacing PDMS microdevice since this buffer was viscous and would leak from the open channel. Only base buffer (0.05 M TRIS-CHES, 0.1% SDS, pH 8.5) of 6% PEO buffer was therefore tested in the cross-piece PDMS part. Although EOF was not observed, the current was too high (> 100 μA) leading to buffer boiling. When 10x dilution of the base buffer (0.005 M TRIS-CHES, 0.1% SDS, pH 8.5) was employed, BSA-FITC could be successfully injected and the current was not high. Consequently, 0.005 M TRIS-CHES, 0.1% SDS, pH 8.5 buffer was chosen for the interfacing PDMS microdevice.

The injection and detection of BSA-FITC droplets using the interfacing microdevice "Design 6", which filled with 0.005 M TRIS-CHES, 0.1% SDS, pH 8.5 in the PDMS part, was shown in the electropherogram (**Figure 6.6**). Seven BSA-FITC droplets having an average volume of 2.05 ± 0.07 nl (n = 10) were injected every ~ 33 seconds and detected at 1 cm. The average electrophoretic mobility of seven BSA-FITC peaks was found to be 3.11×10^{-9} $m^2/V \cdot s$. According to the electropherogram (**Figure 6.6**), there was an intense band at the tail of each BSA-FITC peak. The bright band was as a result of a stacking effect. When the analyte migrated from the dilute to the concentrated background electrolyte (~10x difference in concentration)[1], the velocity of the analyte decreased resulting in more concentrated analyte and hence shorter analyte zone[2].

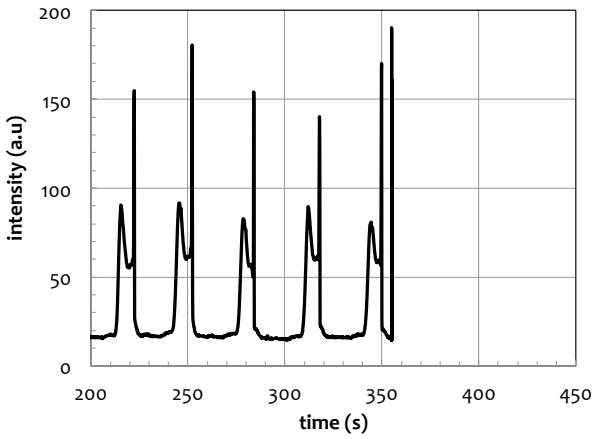

Figure 6.6: An electropherogram obtained from the injection of BSA-FITC droplets using "Design 6" interfacing microdevice. In this experiment, the droplets were delivered to the mouth of the tube at the flow rate of 0.3 µl/min and injected to the open channel containing 0.005 M TRIS-CHES, 0.1% SDS, pH 8.5. BSA-FITC released from droplets migrated into the 5-cm long glass capillary containing 6% PEO 100 kDa in 0.05 M TRIS-CHES, 0.1% SDS, pH 8.5. The applied electric field during this experiment was 333.33 V/cm. The detection was performed at 1 cm from the injection point.

6.3.3.3 Injection and separation of benchmark fluorescent protein standard (11-155 kDa)

Droplets of fluorescent protein standard (11-155 kDa) mixed with fluorescein were injected into the interfacing microdevice containing 0.005 M TRIS-CHES, 0.1% SDS, pH

8.5, separated and detected in the glass capillary containing 6% PEO buffer. It was found that proteins in the ladder were not separated. Although the detection was placed at longer distance varied from 0.5 to 5.0 cm, no separation of proteins was observed (data not shown).

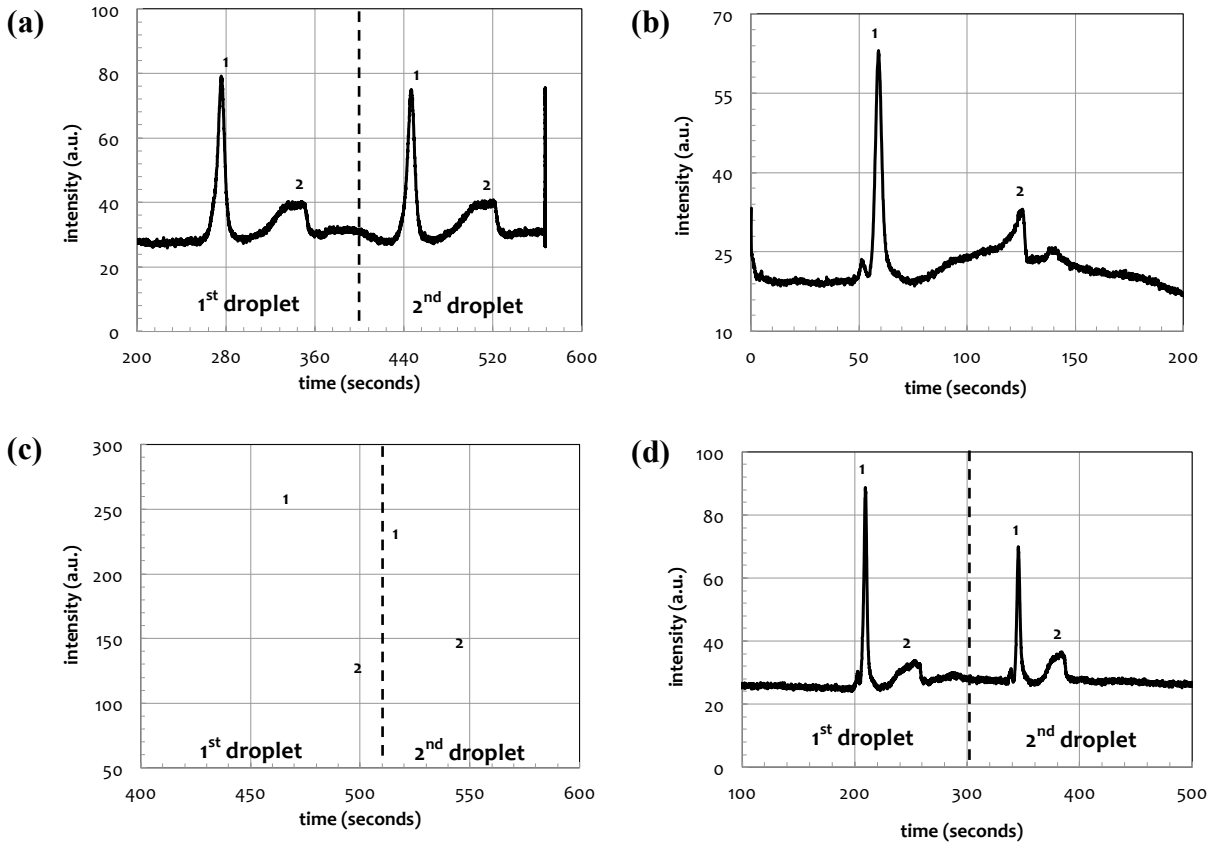

Figure 6.7: Electropherograms showing fluorescent protein standard (11-155 kDa) mixed with 0.18 μM fluorescein separated in 6% PEO 100 kDa in 0.05 M TRIS-CHES, 0.1% SDS, pH 8.5 using the interfacing droplet-based microdevice "Design 6". The droplets were delivered to the interfacing PDMS microdevice containing 0.005 M TRIS-CHES, 0.1% SDS, pH 8.5 at the flow rate of 0.08 μl/min. The detection was around 2.5 cm from the injection point, while the total length of the system was 8.0 cm. The applied separation fields were (a) 81.25 V/cm; (b) 118.75 V/cm; (c) 125 V/cm and (d) 150 V/cm. Fluorescein peak was designated as (1) and protein ladder was designated as (2).

- It was also found that too long of a detecting distance caused band broadening and required longer analysis time, as a result, the detecting distance was limited to be between 2.0-3.0 cm.

- Another reason might be that the frequency of droplet injection was so high that there was not enough time for proteins from each droplet to be separated properly. The frequency of droplet injection was therefore decreased by increasing the interdroplet spacing and decreasing the flow rate of droplet delivery to the interfacing microdevice. The interdroplet spacing could be increased by decreasing the frequency of droplet generation or by increasing the refilled flow rate during droplet generation. Although droplets were injected at lower frequency and the time between each injected droplet was longer (~170 seconds), proteins were still not separated (**Figure 6.7a**).
- The other parameter that was varied was the separation field strength. It was found that fluorescein was separated from protein ladder; however, proteins in the ladder were not separated as shown in **Figure 6.7**.
- Another reason behind this might be due to the loss of resolving power of the gel buffer when several droplets pass through. The gel buffer in the glass capillary was not frequently replaced during the experiment since it required the detachment of the whole setup, i.e. the detachment of the platform from the stage and the capillary from the interfacing PDMS microdevice, which was time-consuming.

Although there were many attempts, droplet-based separations of proteins were not achieved.

6.3.4 Platform improvement to hold the chip and capillary

According to the problems mentioned in **Section 6.3.2**, a new platform was fabricated as described in **Section 2.2** to facilitate the assembly of the interfacing droplet-based separation unit. The new platform consisted of the main acrylic plate as the base, the microdevice holding plate and the microdevice cover plate as illustrated in **Figure 6.8**. A PTFE membrane was placed on the main plate and was properly secured in place by the microdevice holding plate, while the membrane was secured using only adhesive tape in the previous platform. A droplet delivery tube already cut a 30° angle at one end was inserted into an aluminium tube used to hold the droplet delivery tube more tightly. The mouth of the tube was placed in the middle of the microdevice holding plate (~ 0.6 cm

measured from the inner edge of the holding plate), which would be the same place where the open channel would be situated. The interfacing PDMS microdevice along with the inserted glass capillary was then placed onto the mouth of the tube without significant alignment since the PDMS microdevice was cut to fit the holding space (1.2 cm width and 1.8 cm length). Consequently, whenever the microdevice was placed into the holding space, the open channel would always align onto the mouth of the tube. The microdevice was secured by the cover plate, which was also used to determine the distance between the open channel and the mouth of the tube by loosening or tightening the screws. This cover plate was cut open to allow an electrode to be immersed into the buffer reservoir. The entire platform was then fixed to the microscope stage.

There were four major advantages of the new platform over the previous one. First, the oil depletion unit (PTFE membrane) was properly secured in place; while still being easily replaced. Second, the alignment between the open channel and the mouth of the droplet delivery tube was more convenient leading to the third advantage was that the gel buffer could be replaced more often. Finally, the overall experimental setup was less time-consuming.

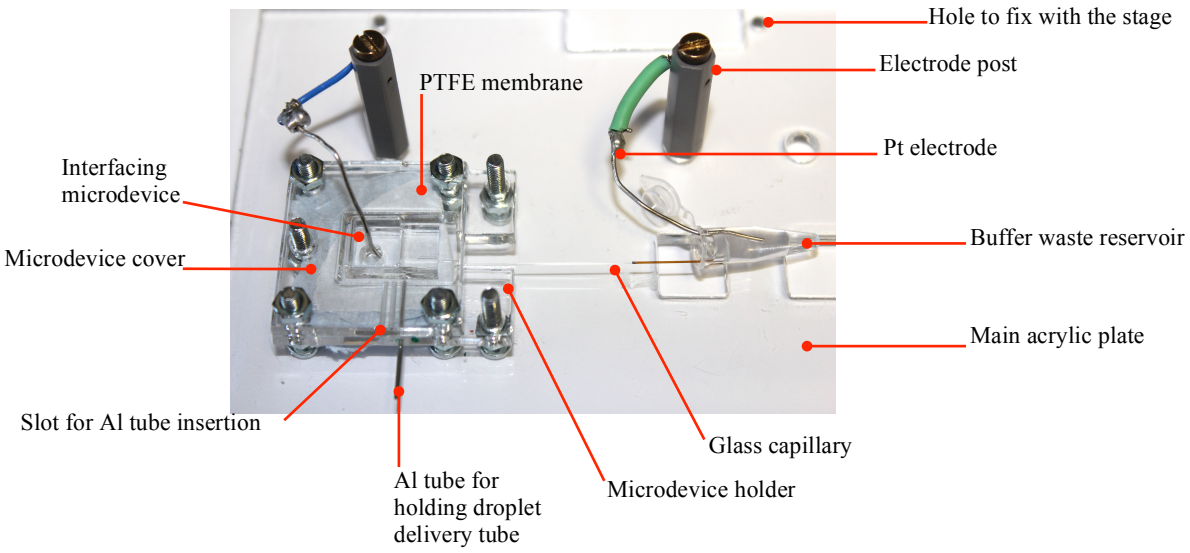

Figure 6.8: A photograph showing the new platform to facilitate the assembly of interfacing droplet-based separation unit. Note: the PDMS microdevice shown in the photo was not the actual size used in the experiment.

6.3.5 Injection of fluorescein droplets in parallel separation channel

The interfacing droplet-based microdevice "Design 6" could also be parallelized to achieve high-throughput separation. This was demonstrated by the injection of fluorescein droplets into two-parallel channels of the interfacing microdevice "Design 6" in which the experiment was performed using the new platform described in **Section 6.3.4** and the results were shown in the electropherograms (**Figure 6.9**). The volume of successfully injected droplets in the above channel was 2.02 ± 0.11 nl (n = 10) and in the below channel was 1.97 ± 0.05 nl (n = 10). The average electrophoretic mobilities of fluorescein peaks were found to be 1.35×10^{-8} $m^2/V\cdot s$ and 2.21×10^{-8} $m^2/V\cdot s$ for the above and below channel, respectively. The difference in the mobilities is most likely due to differences in the surface chemistry of the parallel channels resulting in difference in the driving EOF.

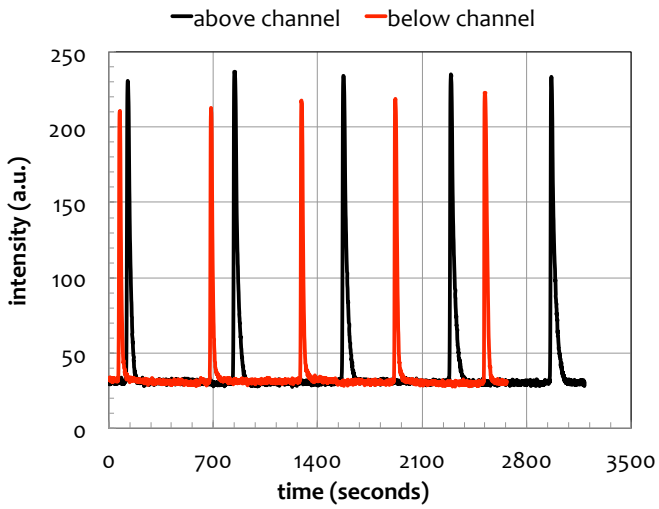

Figure 6.9: The overlay of electropherograms of fluorescein droplets injected in parallel channels of the interfacing droplet-based microdevice "Design 6". Fluorescein peaks obtained from the above channel and from the below channel were illustrated as black line and red line, respectively. The droplets were delivered to the interfacing PDMS microdevice containing 0.005 M TRIS-CHES, 0.1% SDS, pH 8.5 at the flow rate of 0.1 µl/min. The detection was around 1.3 cm from the injection point, while the total length of the system was 6.0 cm. The applied electric field was ~ 217 V/cm. The detection was performed at 1.3 cm from the injection point.

6.4 Conclusion

Here, both the fluorescent dye and protein droplets were successfully injected into the interfacing microdevice "Design 6" and were detected in the glass capillary during gel electrophoresis. To achieve this separation using the droplet injection format required that all three main parts of this experiment - droplet generation, device assembly and droplet injection and separation had to be independently and seamlessly prepared for and interfaced.

For each experimental part, challenges were met and addressed. For droplet generation, protein samples and the pressure changing in the system caused problems. SDS-protein samples used in this work, especially the commercial fluorescent protein ladder, were viscous and expensive. High viscosity protein samples limited the use of "low refilled" flow rate, which affected the control of droplet size. Therefore, the protein samples were diluted to reduce the effect of viscosity and to allow the small volume of expensive protein samples to be used. In addition to these complications, the SDS necessary for in protein sample preparation could easily cause bubble formation in the presence of vibration; hence, very careful handling was required. To prevent pressure changing during droplet generation, the size of the droplet collecting tube (100 μm I.D. and 30 cm long), the number of droplets (100-150 droplets) and the stabilized pressure prior to droplet generation (running the pump at the required flow rate for 5-10 min) were optimized.

Two foremost challenges that inconvenienced experimental setup making them time-consuming were the connection between the droplet collecting tube and the droplet transferring tube and the alignment between the droplet delivery tube and the open channel of the microdevice. The imperfect joining of the two tubes resulted in the leakage of droplets at the tubing connection. This challenge was addressed by replacing the two-piece delivery tubing with a one-piece droplet delivery tube. The other problem required the redesign of the chip-holder platform.

Additionally, maintaining stable injection conditions was difficult and although single injection of droplets was achieved, often droplets merged or split causing multiple

injections. This problem has been discussed in detail in **Section 5.3.2.3**. Furthermore, another problem that occurred during protein droplet injection was the presence of high EOF. This prevented proteins from migrating to the anode and therefore be detected. Several buffers were then tested to determine the most suitable buffer to be used in the PDMS section of the device to minimize the EOF in this section. Here, a cross-piece PDMS microdevice coupled to a glass capillary was used to perform the tests, where the capillary was filled with 6% PEO buffer. Following the screen, a 0.005 M TRIS-CHES, 0.1% SDS, pH 8.5 buffer (10x dilution of the base buffer of 6% PEO buffer) was employed. However, even with this buffer a stacking effect was observed when used in conjunction with the 6% PEO buffer in the glass capillary. Although droplet contents were successfully transferred into the capillary and several parameters (e.g. detecting distance, frequency of droplet injection and separation field strength) were varied, protein separation was not achieved. This might be due to the loss of resolving power of the gel buffer.

Finally, a new platform was designed and fabricated to alleviate the problems in the experimental setup. The new platform was tested in the injection of fluorescein droplets into a parallel separation channel using the adapted interfacing microdevice "Design 6". Not only did this experiment show the ability of "Design 6" to be parallelized, but also the advantages of the new platform. The oil depletion unit was properly secured when the new platform was utilized. Furthermore, the alignment between the droplet delivery tube and the open channel of the microdevice was more convenient. This allowed the gel buffer in the capillary to be replaced more often, which might improve the separation of proteins. Future experiments should explore the use of this optimized platform for the droplet injection and separation of proteins.

6.5 References

1. Gielen, F., Vliet, L. V., Koprowski, B. T., Devenish, S. R. A., Fischlechner, M., Edel, J. B., Niu, X., deMello, A. J. & Hollfelder, F. A fully unsupervised compartment-on-demand platform for precise nanoliter assays of time-dependent steady-state enzyme kinetics and inhibition. *Anal. Chem.* **85,** 4761–4769 (2013).

2. Friedberg, M. a., Hinsdale, M. & Shihabi, Z. K. Effect of pH and ions in the sample on stacking in capillary electrophoresis. *J. Chromatogr. A* **781,** 35–42 (1997).

3. Malá, Z., Křivánková, L., Gebauer, P. & Boček, P. Contemporary sample stacking in CE: A sophisticated tool based on simple principles. *Electrophoresis* **28,** 243–253 (2007).

Chapter VII

Conclusions and future work

7.1 Conclusions and Future work

Protein separation is a key process in proteomics, having undoubted importance in medical and pharmaceutical research. Proteins are normally separated using multiple dimensional separation methods, which provide for high-resolution analysis of complex protein mixtures. Unfortunately, during the transfer of proteins between dimensions, issues related to dead volumes, analytes dispersion (and loss) and resolution degradation are common.

In this work, a droplet-based microfluidic device was employed as an interface for transferring separated proteins between dimensions, with the aim of alleviating the aforementioned problems. Briefly, a fluorescently labeled protein mixture was used to represent proteins separated within a first separation dimension. This sample was compartmentalised into droplets (as a segmented flow) using a robotic droplet generator. The formed droplets were then transferred to the developed interfacing microdevice and subsequently separated via capillary gel electrophoresis, which was chosen as a representative second separation dimension. The buffer used for protein separation, the reaction between proteins and fluorescent labels and the nature of the interfacing microdevice, were considered to be crucial in the overall process, and as such were investigated in detail.

A novel buffer for protein separations using the droplet-based microfluidic system was developed to allow for high-speed and high-resolution separations of proteins and to ensure compatibility with the microfluidic substrates (i.e. PDMS and glass capillaries). Initially, both commercial and laboratory-made buffers were screened using a commercial CE instrument prior to testing within PDMS microdevices. Interestingly, it was found that the commercial "Beckman buffer" provided for high-resolution separation of protein mixtures using the commercial CE instrument. However, it was incompatible with the PDMS microdevice due to excessive Joule heating occurred and poor heat dissipation within the PDMS. Since the recipe of Beckman buffer remains proprietry, it was difficult to modify Beckman buffer to allow compatibility with the PDMS microdevice. Accordingly, in-house buffers based on PEO and dextran were assessed. Extensive

experimentation demonstrated that a 5% PEO 100 kDa in 0.1 M TRIS-CHES, 0.1% SDS, pH 8.7 buffer provided for compromised resolution and analysis time. By decreasing the concentration of background electrolyte and the pH was successful in reducing Joule heating and EOF. Although a 5% PEO 100 kDa in 0.05 M TRIS-CHES, 0.1% SDS, pH 8.5 buffer allowed the successful separation of protein ladders (11-155 kDa) within the PDMS microdevice, an increase in PEO concentration to 6% was found to provide for similar resolution over shorter separation lengths and using lower separation fields. Additionally, proteins could be separated using the 6% PEO buffer in a cross-piece PDMS microdevice coupled to a glass capillary. As a result, the 6% PEO 100 kDa in 0.05 M TRIS-CHES, 0.1% SDS, pH 8.5 buffer was used for subsequent protein separations in the interfacing droplet-based microfluidic format.

To avoid the necessity of using expensive (commercially) fluorescently labeled protein mixtures and improve operational flexibility, three fluorescent dyes were investigated with respect to protein labeling. FITC and NHS-Fluorescein exhibited similar problems related to inefficient labeling chemistry. This included the incomplete removal of unbound dye, which could further react with components in the separation buffer, reduced labeling efficiencies and unbound dye in the conjugate samples compromising absorbance measurements. Accordingly, NanoOrange was employed to address such problems. Unfortunately, the use of NanoOrange raised other problems including the binding of NanoOrange with SDS micelles, the precipitation of protein samples in the presence of NanoOrange and low fluorescence intensities from droplets containing protein conjugates. Related problems were observed for all laboratory-conjugated proteins studied, and as a result, it was decided that commercially labeled proteins samples were best suited to act as benchmarks for the droplet-based separation of proteins.

Six interfacing microdevice constructs were designed, fabricated and evaluated for use in the droplet-based separation of proteins. All designs employed a PTFE membrane as an oil depletion unit in which oil removal occurred passively. Herein, the ease of fabrication, robustness, stability of separation currents, uniformity of the electric field distribution, compatibility with buffer solutions, ease of manipulation and successful droplet injection were evaluated as key figures of merit. Based on these metrics, “Design 6”, consisting of

an interfacing PDMS microdevice coupled to a glass capillary, was chosen as the most appropriate design as it provided for superior performance despite its more involved operation. Accordingly, further investigations and refinement of "Design 6" were performed and described in **Chapter 6**.

The developed buffer, the commercial protein mixture and the chosen interfacing microdevice were then integrated to perform droplet-based separations of proteins. Several challenges were observed from each part of the experiment and were in the large part successfully addressed. For droplet generation, protein samples and unstable pressure were the major issues. Protein samples used in gel electrophoresis (unlike nucleic acid samples) contained SDS for denaturation, which could often cause bubble formation; the handling of protein samples during droplet generation was therefore critical. In addition, the commercially sourced fluorescent protein ladder was diluted to reduce the viscosity, which allowed the use of lower refill flow rates and in turn allowed generation of smaller droplets. Pressure variations during droplet generation were addressed by optimizing the size of the droplet collection tubing (100 μm I.D. and 30 cm long), the number of droplets (100-150 droplets) and the stabilized pressure prior to droplet generation (i.e. by running the pump at the required flow rate for 5-10 minutes prior to use). For the assembly of the interfacing droplet-based separation unit, a one-piece droplet delivery tube was employed to address the imperfect join between two tubes. During protein droplet injection, significant EOF was present, which prevented proteins from migrating to the anode for detection. Accordingly, 0.005 M TRIS-CHES, 0.1% SDS, pH 8.5 was employed in the PDMS part instead of 0.1% SDS to minimize EOF. However, when using this buffer in conjunction with the 6% PEO buffer in the capillary, stacking effects were observed. The successful single injection of each protein droplet was achieved; however, protein ladder was still not perfectly separated. This is likely to be a result of the loss of resolving power of the gel buffer.

Finally, the new platform was fabricated and used to perform the injections of fluorescein droplets into parallel channels. The new platform allowed the oil depletion unit and the droplet delivery tube to be properly secured. In addition, the alignment between the open channel of the interfacing microdevice and the droplet delivery tube could be achieved

quickly and easily, which allowed for more frequent changes of the gel buffer in the glass capillary.

It is expected that future studies will assess the use of this optimized platform for droplet injection and the separation of protein mixtures. Moreover, droplet docking could be added between droplet generation and the interface to store droplets containing separated analytes from the first dimension in a sequential manner prior to further analysis. By doing so, droplets entering the interface microdevice could be better controlled. In addition, the developed interfacing microdevice could be integrated to several downstream processes such as other separation dimensions (based on IEF, CZE, MEKC and nano LC for example), on-chip sample preparation or microreactors. The developed interfacing microdevice along with the optimized platform has also demonstrated potential for parallelization, which would undoubtedly afford high-throughput analysis of more complex biological samples. This would save much time in the study of real-world protein samples.